Signals from the underground and their interplay with plant immunity

Ioannis Stringlis

Signals from the underground and their interplay with plant immunity

PhD thesis

Ioannis Stringlis, January 2018

Utrecht University | Plant-Microbe Interactions

This thesis was accomplished with financial support from the ERC Advanced Grant number 269072 of the European Research Council.

ISBN 978-90-393-6920-3

Cover: Iliana Boshoven-Gkini | www.AgileColor.com
Layout: Iliana Boshoven-Gkini | www.AgileColor.com
Printing: Ridderprint BV | www.ridderprint.nl

Signals from the underground and their interplay with plant immunity

Signalen uit de bodem en
hun interactie met het afweersysteem van planten

(met een samenvatting in het Nederlands)

Proefschrift

ter verkrijging van de graad van doctor aan de Universiteit Utrecht
op gezag van de rector magnificus, prof.dr. G.J. van der Zwaan,
ingevolge het besluit van het college voor promoties in
het openbaar te verdedigen op
vrijdag 19 januari 2018 des ochtends te 10.30 uur

door

Ioannis Stringlis

geboren op 15 mei 1985
te Pyrgos, Griekenland

Promotor: Prof. dr. ir. C.M.J. Pieterse

To my family

῾Εν οἶδα ὅτι οὐδὲν οἶδα
Σωκράτης (469-399 π.Χ.)

The only true wisdom is in knowing you know nothing
Socrates (469-399 B.C.)

Contents

CHAPTER 1

General introduction
Game of biomes: plant roots versus their interacting microbiome

Ioannis A. Stringlis[1] and Corné M. J. Pieterse[1]

[1] Plant-Microbe Interactions, Department of Biology, Faculty of Science, Utrecht University, P.O. Box 800.56, 3508 TB, Utrecht, The Netherlands

Abstract

Plants are sessile organisms that provide diverse classes of microbes with niches, where they can colonize, acquire nutrients and proliferate. Photosynthesis-derived or stress-induced exudation through plant roots is responsible for the formation of highly diverse microbial communities in the thin soil layer surrounding roots, known as the rhizosphere. The vast diversity of microbes in the rhizosphere, called the microbiome, can strongly influence plant health either by promoting growth, facilitating nutrient or water uptake and suppressing diseases caused by soil-inhabiting pathogenic microbes. Selected members of the microbiome, including bacteria of the genus *Pseudomonas*, are also capable of enhancing the defense capacity of foliar tissues upon successful colonization of roots. Key steps of this induced systemic resistance (ISR) are already elucidated and the function of specific components, such as transcription factor MYB72, is highlighted. The early molecular dialogue between microbes and roots that results in the establishment of beneficial associations remains largely unknown. Here, we review the current knowledge on the role of root exudation in shaping the root microbiome composition and on how members of the rhizosphere microbiome interact with the host immune system to promote plant health in a cost-efficient manner.

Root microbiome

Roots and their surrounding soil constitute one of the most rich and diverse ecosystems on Earth. Apart from dealing with numerous environmental challenges, plants need also to interact with an astonishing diversity of root-associated microbes, ranging from bacteria and viruses to protists and fungi, to successfully fulfil their sessile lifestyle (Zamioudis and Pieterse, 2012; Bulgarelli et al., 2013). The soil layer accommodating these diverse communities is strongly affected by root exudation and is known as the rhizosphere, while the totality of microbes residing there is known as the microbiome (Bais et al., 2006; Berendsen et al., 2012). The maintenance of a balance between plant health and accommodation of this plethora of microbes in the root rhizosphere requires a coordination of complex processes in the rhizosphere where both partners benefit (Zamioudis and Pieterse, 2012). From the one side, plants exude up to 20% of the photosynthetically fixed carbon through their roots, therewith providing the soil-borne microbes that reside in mostly low-nutrient soils with an important food source (Bais et al., 2006; Jones et al., 2009). On the other side, the root microbiome acts as an intermediate between the plant and the nutrients in the soil. The root microbiome aids the host in nutrient uptake while at the same time components of these microbiomes can increase host tolerance against different stresses (Hacquard et al., 2015).

Recent advances in next-generation sequencing allowed the characterization of the microbiome in healthy plants in a culture-independent manner, not only in the rhizosphere but also in the root interior (endosphere). Analysis at phylum level revealed that the microbiome of healthy *Arabidopsis thaliana* (hereafter Arabidopsis) plants originates from the more diverse soil communities, and is dominated by the phyla Proteobacteria, Actinobacteria, Bacteroidetes and less by Firmicutes (Bulgarelli et al., 2012; Lundberg et al., 2012). Similarly, the root microbiome of closely related species belonging to the Brassicaceae family (*Cardamine hirsute*, *Arabidopsis halleri*, *Arabidopsis lyrata* and *Arabis alpina*) display quite similar root microbiome assemblages (Schlaeppi et al., 2014; Dombrowski et al., 2017). Interestingly, in plant species not related to Arabidopsis, such as barley, rice and *Lotus japonicus,* the phyla Proteobacteria, Actinobacteria, Bacteroidetes and Firmicutes constitute the highest proportion among the identified bacteria (Bulgarelli et al., 2015; Edwards et al., 2015; Zgadzaj et al., 2016). The ability of these phyla to be highly represented in roots and rhizospheres of different hosts suggests that members of these phyla constitute competitive and adaptable colonizers under various soil types and locations (Muller et al., 2016). Recently, sequencing of microbiome DNA and RNA from the rhizosphere and the root of *Brassica napus* and stable isotope probing of plant fixed carbon demonstrated that the phyla Proteobacteria, Actinobacteria and Bacteroidetes are really active in these two compartments and assimilate most of the carbon released by the roots (Gkarmiri et al., 2017).

Effect of root exudation on root-associated microbiome

Root-derived exudates, apart from supporting microbial proliferation in the rhizosphere, are also responsible for the formation of distinct microbiome assemblages between soil and rhizosphere, a phenomenon described as the "rhizosphere effect" (Hiltner, 1904; Berendsen et al., 2012; Bulgarelli et al., 2013). The age and developmental stage of the plant has influence on exudation and subsequently on the microbiome

assembled. Exudates of Arabidopsis plants collected at different plant age varied in sugar levels which affected accordingly microbial functions related with sugar and secondary metabolism (Chaparro et al., 2013), while Beta-proteobacteria populations fluctuated at different life stages of potato due to altered exudation profiles (Inceoglu et al., 2010). Chaparro and coworkers (2014) also found that Arabidopsis plants during the early and late stage of their development can influence the abundance of Actinobacteria, Bacteroidetes and Cyanobacteria and microbial activity as well. Functions aligning with pathogens were more represented at early developmental stages while later developmental stages were dominated by functions related with antibiosis and chemotaxis and aligned to beneficial microbes, suggesting a selective pressure during plant aging towards microbes that provide their hosts with important services.

Rhizodeposits are quite diverse and include organic acids, amino acids, sugars, products of secondary metabolism and even the release of dying root cap border cells (Dakora and Phillips, 2002; Bais et al., 2006; Driouich et al., 2013). Different rhizodeposits display differential effects on the microbiome as well. Combinations of exudates collected from Arabidopsis plants growing in vitro and applied in soil in the absence of plants revealed differential effects of phenolic compounds on the abundance of bacterial taxa (Badri et al., 2013). More specifically, phenolics seemed to have the biggest effect on the growth and attraction of bacterial operational taxonomic units (OTUs), followed by amino acids and sugars. A role of phenolics in affecting soil microbial diversity was also demonstrated with an Arabidopsis ABC transporter mutant (*abcg30*) which releases more phenolics but shows a reduced export of sugars (Badri et al., 2009b). In soil in which *abcg30* plants was grown, an increased abundance of plant growth-promoting rhizobacteria (PGPR) or bacteria involved in heavy metal remediation was observed compared to wild type Col-0 plants, suggesting a role for phenolics in attracting beneficial microbes. In another study, different organic acid profiles identified in the exudates of two hosts (cucumber, banana) could explain the colonization specificity of two rhizobacteria, due to an exudate-specific effect on chemotaxis and biofilm formation (Zhang et al., 2014). Other naturally occurring exudates, like flavonoids and strigolactones, act as signaling compounds for the establishment of well-characterized symbiotic interactions of plant hosts with rhizobia and mycorrhizal fungi (Akiyama et al., 2005; Subramanian et al., 2007). Moreover, border cells and border-like cells that are forming an extra root layer between the root tip and soil have been shown to affect a group of soilborne bacteria, because of proteins synthesized and released through them (Driouich et al., 2013). Arabinogalactan proteins were identified among the secreted molecules and were found to regulate *Rhizobium* and *Agrobacterium* attachment on roots (Gaspar et al., 2004; Vicre et al., 2005; Xie et al., 2012). In that direction, a recent breakthrough methodology based on a microfluidics setup allowed the visualization of the preferential colonization of *Bacillus subtilis* at the elongation zone of Arabidopsis roots (Massalha et al., 2017). The authors of that study found that this root part exhibited increased secretion of compounds acting as chemoattractants for *B. subtilis*. Such studies provide strong evidence that naturally occurring compounds in exudates of healthy plants can influence the abundance of members of the root microbiome and even orientate their growth on different root parts.

Activation of immunity and microbiome assemblage

Rhizodeposition is not constant and exudation profiles can dramatically change due to nutrient deficiencies, pathogen challenge and their interplay, which in turn can modify the composition and the functions of the microbiome. When plants deal with pathogens or insects, two plant hormones have a key role in regulating immune responses to fight back these challenges, salicylic acid (SA) and jasmonic acid (JA) (Pieterse et al., 2012). Several studies have shown the role of these plant defense-related hormones in shaping the root microbiome. Plants either compromised in SA biosynthesis and signaling or hyperimmune displayed modified bacterial communities compared to wild type Arabidopsis plants, mostly on the phyla Actinobacteria and Proteobacteria. Families with pronounced abundance differences were Rhizobiaceae, Bulkholderiaceae, Pseudomonadaceae, Enterobacteriaceae, Xanthomonadaceae and Sinobacteraceae (Lebeis et al., 2015). Upon activation of JA signaling, following application of methyl jasmonate (MeJA), different rhizosphere communities were observed, with treated plants displaying less diverse bacterial populations compared to control plants, suggesting a selective role of JA-dependent exudation on the microbiome (Carvalhais et al., 2013). Research from the same group observed differential root exudation in vitro from the mutants *myc2* and *med25* defective in JA signaling compared to wild type Arabidopsis that was translated in distinct bacterial and archaeal communities in their rhizospheres, mostly affecting the phyla of Actinobacteria, Firmicutes and Proteobacteria (Carvalhais et al., 2015). Recently, the effect of JA in a compartment-dependent manner was demonstrated in barley, where microbial diversity in the endophytic tissues was reduced compared to the rhizosphere, with a profound selection for microbes suppressing pathogens (Liu et al., 2017). Moreover, pathogen-induced changes in the abundance of specific exudates can also have a role in the selection occurring in the rhizosphere. In Arabidopsis, leaf infection with the bacterial pathogen *Pseudomonas syringae* increased malic acid in root exudates that resulted in the attraction of the ISR-inducing rhizobacterium *B. subtilis* FB17 (Lakshmanan et al., 2012). Additionally, recent data by Berendsen et al (2017) show that foliar defense activation by the downy mildew pathogen *Hyaloperonospora arabidopsidis* promotes the recruitment of bacterial genera in the rhizosphere. Importantly, when these bacteria were isolated and used in combination to colonize Arabidopsis they could promote plant growth and induce systemic immunity. Except foliar pathogen-/defense hormone-induced exudation, also the presence of the pathogen itself in the rhizosphere can lead to altered exudation or microbiome shifts. Exudates of sweet basil roots treated with fungal elicitors were enriched in rosmarinic acid, which exhibited in vitro antimicrobial activity against a range of soil-borne microorganisms (Bais et al., 2002). A recent study revealed that biofilm formation by *Phytophthora parasitica* on tomato roots reversed the abundance of Proteobacteria and Bacteroidetes phyla between healthy and infected roots while specific *Pseudomonas* spp. were found to associate with the pathogen in order to gain access to plant carbon sources (Larousse et al., 2017). Another study focusing on the citrus microbiome after infection by the causal agent of the Hunglongbing disease, employed both metagenomic and metatranscriptomic methodologies to unravel changes in community composition and functions enriched between the rhizosphere and the rhizoplane (root surface) (Zhang et al., 2017). The disease negatively affected the abundance of rhizoplane-enriched genera compared to healthy plants and also the activity of genes involved in secretion systems. On the other hand, around 40 of the rhizoplane-depleted genera were significantly increased

after disease compared to healthy plants. Additionally, the rhizoplane microbiome was found to be more "active" compared to the rhizosphere microbiome in terms of bacterial chemotaxis, motility, carbohydrate metabolism and sugar uptake from roots. Interestingly, citrus inoculation with two strains of *Burkholderia*, the most abundant rhizoplane genus in this study, resulted in SA-mediated ISR (Zhang et al., 2017). Studies like these can help in understanding how the composition and the activity of the microbiome change in response to pathogens and in a next step identify functions or even microbes that could be used as a measure to control these diseases.

Interplay of nutrient deficiency, immunity and microbial attraction

In nature, plants growing in nutrient-limited soils display altered plant performance and physiology. Root exudation is among the physiological aspects of plant growth that is affected by nutrient deficiencies, which subsequently affects soil chemistry and microbial processes (Bais et al., 2006). When different plant hosts experience nitrogen (N) and/or phosphate (P) deficiency, there is increased production of strigolactones that act as attractants for arbuscular mycorrhizal fungi (AMF) (Akiyama et al., 2005; Yoneyama et al., 2007; Yoneyama et al., 2012). Eventually, AMF form a symbiotic interaction that results in facilitating P uptake for the plant and supply of carbohydrates and fatty acids for the fungus (Parniske, 2008; Jiang et al., 2017). Besides strigolactones, another class of compounds, coumarins, are also released during P stress (Ziegler et al., 2016; Tsai and Schmidt, 2017). Coumarins are fluorescent phenolic compounds produced via the phenylpropanoid pathway and function in facilitating iron uptake from the rhizosphere since plants defected in their production cannot grow normally under iron-limited conditions (Jin et al., 2007; Rodriguez-Celma et al., 2013; Fourcroy et al., 2014; Schmid et al., 2014). Recently, Arabidopsis mutants *phr1* (accumulate less free phosphate than wild type) and *spx1;spx2* (hyper accumulate phosphate) developed different root-associated microbial communities compared to wild type plants when grown in soil (Castrillo et al., 2017). This may be caused by the contribution of different exudation profiles that are displayed by plants with different tolerance to P stress (Ziegler et al., 2016).

The interplay between nutrient status and immunity could be a factor determining microbial composition inside and on the roots. This was demonstrated in the study of Hiruma and colleagues (2016) where the endophytic fungus *Colletotrichum tofieldiae* could support plant growth and P transfer in Arabidopsis when P was limited, but in concert with an intact plant immune system. More evidence towards this direction was provided by studies where plants impaired in ISR showed altered exudation patterns of fluorescent phenolic compounds compared to wild type plants under iron (Fe) limitation (Zamioudis et al., 2014). Previously, manipulation of the plant iron nutrition status via a foliar spray on barley plants grown in an iron deficient soil, significantly influenced the composition of the microbial community in the rhizosphere (Yang and Crowley, 2000). The microbiome itself or selected microbiota members can contribute to iron acquisition, either through the activity of iron-chelating siderophores or the production of volatile organic compounds (VOCs) that can activate iron uptake mechanisms in plants. Growth of plants in sterile soil (maize, sunflower, clover) resulted in decreased growth and Fe uptake compared to non-sterile soils (Masalha et al., 2000; Jin et al., 2006), while application of bacterial siderophores in hydroponic cultures of tomato and barley

increased photosynthesis, iron uptake and growth (Duijff et al., 1994; Nagata et al., 2013). Several studies have shown that iron-stressed plants, possibly through exudation, can select microbes present in their rhizosphere and attract more siderophore-producing microbes than plants growing with iron supply (Jin et al., 2006; Jin et al., 2010). VOCs produced by ISR-inducing microbes have also been found to contribute to stress amelioration when plants were grown in vitro under iron deficiency (Zhang et al., 2009; Zamioudis et al., 2015; Martinez-Medina et al., 2017). Both siderophores and VOCs are recognized as determinants for the elicitation of ISR (Meziane et al., 2005; Zamioudis et al., 2015; Martinez-Medina et al., 2017), so the interplay between exudation under nutrient deficiency, microbial attraction in the rhizosphere, and elicitation of ISR could be a possible scenario for the establishment of mutually beneficial plant-microbe relationships.

Disease suppression and microbiome

The microbes selected by the plants to inhabit either the root interior or proliferate in the rhizospheres can provide their hosts with valuable services for their health and fitness. Disease suppressiveness is a phenomenon observed when low disease levels are observed despite the presence of a pathogen in the plant growth environment. This action is attributed to the microbiome when specific groups of bacteria are enriched in the rhizosphere of plants growing under the pressure of soilborne pathogens but can also occur due to the natural properties of a soil (Weller et al., 2002; Berendsen et al., 2012). While soil-derived suppressiveness has an effect on various pathogens, suppressiveness induced by the presence of a pathogen can develop when plants are grown in monoculture for a long time period and can be specific for a plant-pathogen interaction (Berendsen et al., 2012). Several studies have aimed to elucidate the composition of the microbiome in suppressive or conducive soils to different diseases including *Thielaviopsis basicola*, *Streptomyces* spp., *Fusarium oxysporum*, *Rhizoctonia solani* and *Gaeumannomyces graminis* var. *tritici* (Kyselkova et al., 2009; Mazurier et al., 2009; Sanguin et al., 2009; Mendes et al., 2011; Rosenzweig et al., 2012). Those studies focused mostly on bacterial communities and demonstrated that depending on the pathogen suppression, not only pseudomonads but also other bacterial genera (eg. *Azospirillum*, *Burkholderia*, *Comamonas*) or phyla such as Acidobacteria, Planctomycetes, Chloroflexi, Alpha-proteobacteria, Beta-proteobacteria, Gamma-proteobacteria and Firmicutes can be enriched in suppressive soils. Presence of a pathogen in a soil is not affecting solely bacterial community composition, but also the functions of enriched bacteria. In fact, a recent study revealed the elevated expression of secretion systems for virulence factors or extracellular lytic enzymes and expression of stress-sensing mechanisms in the most abundant bacterial families when the pathogenic fungus was present (Chapelle et al., 2016).

Modulation of immunity by the microbiome

The effect of the beneficial microbes in the rhizosphere is not restricted in directly targeting and suppressing the pathogens. Selected members of the microbiome can also trigger a form of plant immunity that is expressed in the systemic aerial tissues. This phenomenon is known as ISR and is effective against a broad

set of foliar pathogens and pests (Pieterse et al., 2014). Rhizobacteria-mediated ISR and pathogen-induced systemic acquired resistance (SAR), that is also effective against a broad range of pathogens, were initially thought to be functioning similarly. However, while SAR is typically activated upon pathogen infection and dependent on the plant hormone salicylic acid (SA), ISR is a defense mechanism activated by beneficial bacterial and fungal species, and is often dependent on the plant hormones jasmonic acid (JA) and ethylene (ET) (Pieterse et al., 2014). Pioneer studies on ISR triggered by *Pseudomonas fluorescens* WCS417 and *Pseudomonas putida* WCS358 (recently renamed as *Pseudomonas simiae* WCS417 and *Pseudomonas capeferrum* WCS358 respectively; Berendsen et al., 2015) on radish and Arabidopsis demonstrated that ISR development doesn't coincide with accumulation of pathogenesis-related (PR) proteins, typical of SAR (Hoffland et al., 1995; Pieterse et al., 1996; Van Wees et al., 1997a). The fact that ISR is established without requiring SA signaling was also observed for other PGPR such as *Serratia marcescens* 90-166, *Bacillus pumilus* strain SE34, *Pseudomonas protegens* CHA0, *P. fluorescens* Q2-87, *P. putida* LSW17S and *Pseudomonas* sp. Ps14 (Iavicoli et al., 2003; Ryu et al., 2004; Ahn et al., 2007; Weller et al., 2012; Alizadeh et al., 2013). Similarly, ISR triggered by plant growth-promoting fungi (PGPF) such as *Piriformospora indica*, *Penicillium* sp. GP16-2, *Trichoderma harzianum* T-39 and *T. harzianum* T-78 also requires intact JA and ET signaling (Hossain et al., 2008; Korolev et al., 2008; Stein et al., 2008; Martinez-Medina et al., 2017). Although ISR is generally regulated through JA- and ET-signaling, there are examples of PGPRs that can induce an SA-dependent ISR such as *Paenibacillus alvei* K165, *P. fluorescens* SS101 and *Bacillus cereus* AR156 (Tjamos et al., 2005; Van de Mortel et al., 2012; Niu et al., 2016). From the presented examples, it becomes apparent that the phyla of Proteobacteria and Firmicutes and fungal orders of Sebacinales and Hypocreales constitute pools for ISR-inducing PGPR and PGPF.

Another mechanism of immune modulation by the microbiome, independent of ISR, was observed recently in the study by Castrillo and colleagues (2017). In that case, a synthetic community of microbes isolated from roots of Brassicaceae and natural soil activated marker genes of the phosphate starvation response (PSR) and suppressed defense transcriptional changes in Arabidopsis. This transcriptional response was found to be controlled by Myb-CC family transcription factor PHR1, the master regulator of phosphate starvation response (PSR) (Bustos et al., 2010). Interestingly, the repressed defense transcriptome was overrepresented by SA-responsive genes, highlighting once more the role of hormones such as SA in the interplay between plant immunity and root microbiome assemblage (Lebeis et al., 2015; Castrillo et al., 2017).

Role of MYB72 in ISR

Most of the current understanding on the molecular steps underlying the establishment of ISR is derived from studies on the interaction between Arabidopsis and the PGPR *P. simiae* WCS417. Employment of JA and ET response mutants revealed the dependency of ISR on JA and ET signaling (Pieterse et al., 1998). Moreover, systemic tissues of WCS417-colonized plants were sensitized for enhanced JA/ET–responsive gene expression upon leaf infection by the bacterial pathogen *Pseudomonas syringae* pv. *tomato* DC3000 or herbivory by larvae of the generalist insect *Spodoptera exigua* (Van Wees et al., 1999; Verhagen et al., 2004; Van Oosten et al., 2008). This quick activation of plant defenses in response to a pathogen or insect

attack following PGPR or PGPF colonization is called "priming" and results in potentiated stress resistance (Martinez-Medina et al., 2016). While transcriptomic changes in leaves of Arabidopsis plants colonized by *P. simiae* WCS417 are not profound, roots respond extensively to colonization and one of the genes affected is the root-specific transcription factor gene *MYB72* (Verhagen et al., 2004). Reporter line *MYB72*$_{pro}$*:GFP-GUS* elucidated the tissue-specific expression pattern of *MYB72* upon root colonization by WCS417 in epidermal and cortical cells of Arabidopsis roots (Zamioudis et al., 2015). Induction of *MYB72* is also achieved after root colonization by ISR-inducing bacteria and fungi such as *P. capeferrum* WCS358, *Trichoderma harzianum* T-78 and *Trichoderma asperellum* T-34, but not by the non-ISR inducer in Arabidopsis *Pseudomonas defensor* WCS374 (previously *P. fluorescens* WCS374) (Zamioudis et al., 2015; Martinez-Medina et al., 2017). The importance of MYB72 in the onset of ISR was shown with *myb72* knockout mutants that were unable to establish ISR following root colonization by either *P. simiae* WCS417 or *T. asperellum* T-34. These findings highlight the conserved role of MYB72 in the onset of ISR triggered by different types of beneficial microbes (Van der Ent et al., 2008; Segarra et al., 2009).

MYB72 and the link of ISR with iron deficiency

The role of the root-specific transcription factor MYB72 in plant performance is not restricted to the onset of ISR. When plants experience iron limitation, *MYB72* gene expression is induced in the roots, while together with its closest homologue MYB10 it is important for plant survival (Colangelo and Guerinot, 2004; Buckhout et al., 2009; Palmer et al., 2013). Interestingly, colonization of Arabidopsis roots or plant exposure to VOCs of the ISR–inducing PGPR WCS417 upregulated the expression of *MYB72* and iron deficiency marker genes *IRT1* and *FRO2* (Zamioudis et al., 2015). Additionally, a significant proportion of the transcriptomic response of roots colonized by WCS417 overlaps with that of roots experiencing iron limitation, providing a link between plant iron status and onset of ISR (Dinneny et al., 2008; Zamioudis et al., 2015). The ability of ISR–inducing microbes to trigger iron deficiency is supported likewise by studies where VOCs produced by beneficial microbes *B. subtilis* GB03 and *Trichoderma* spp. can induce both ISR and the expression of key iron deficiency molecular players *FIT, IRT1* and *FRO2* in Arabidopsis roots, even in plants growing under iron-sufficient conditions (Ryu et al., 2004; Zhang et al., 2009; Martinez-Medina et al., 2017).

As mentioned earlier, the secretion of fluorescent phenolic compounds is a mechanism employed by plants to mobilize iron from the rhizosphere (Jin et al., 2007; Rodriguez-Celma et al., 2013; Fourcroy et al., 2016). Fluorescent phenolics are products of the phenylpropanoid pathway, in which MYB transcription factors have a central regulatory function (Dubos et al., 2010; Liu et al., 2015a). Accordingly, MYB72 was found to regulate the biosynthesis of fluorescent phenolics under iron-deprived conditions and the MYB72-regulated β-glucosidase BGLU42, a novel ISR component, to affect their release into the rhizosphere (Zamioudis et al., 2014). Production of fluorescent phenolic compounds is also observed following root colonization by the plant growth-promoting rhizobacteria *P. fluorescens* SS101 and *Paenibacillus polymyxa* BFKC01 (Van de Mortel et al., 2012; Zhou et al., 2016). Several of these fluorescent phenolic compounds, such as the coumarin phytoalexin scopoletin, accumulate at infection sites and display antimicrobial

activity (Kai et al., 2006; El Oirdi et al., 2010; Vogt, 2010; Sun et al., 2014). For that, secretion of such compounds following stimulation by specific members of the root-associated microbiota may be part of the selection process responsible for the assembly of the rhizosphere microbial community. In that case, microbes that induce iron deficiency responses in roots are less sensitive to the phenolics accumulated and secreted in the rhizosphere compared to other soil-inhabiting microbes. Subsequently, these microbes take a share of plants sugar-containing exudates, while plants benefit by selecting microbes that can boost their defense capacity through ISR. However, we should not exclude the possibility that accumulation of these compounds within roots could allow plants to also control extensive colonization by their beneficial partners that could otherwise result in opposite effects, as was suggested for the association of endophyte *C. tofieldiae* and Arabidopsis (Hiruma et al., 2016).

Microbiome and root immunity

Plant immunity

Soil-borne microbes providing plants with positive services for their health and fitness, either directly or indirectly, need to colonize successfully and sufficiently either the rhizosphere or the endophytic tissues of roots. Soil microbial populations constitute of a mix of beneficial and pathogenic microbes. Hence, plants need to successfully recognize them and subsequently reprogram their defense strategies to allow or block their colonization (Zamioudis and Pieterse, 2012). To effectively and timely perceive microbial signals, plants have evolved a multilayered detection system that leads, depending on the trigger, to the activation of downstream defense responses (Dodds and Rathjen, 2010). The first step of microbial recognition is mediated by surface-localized pattern recognition receptors (PRRs) specialized in the perception of conserved microbe-derived molecules, called microbe-associated molecular patterns (MAMPs). Plants PRRs are categorized as receptor-like kinases (RLKs) or receptor-like proteins (RLPs), with the latter lacking the intracellular kinase domain of RLKs. The ectodomains of PRRs can be composed either by leucine-rich repeat proteins (LRR), lysine motifs (LysMs) or lectin motifs. In Arabidopsis, some MAMP/PRR pairs are well defined (Couto and Zipfel, 2016). Bacterial flagellin is perceived by receptor kinase FLAGELLIN-SENSING 2 (FLS2) (Gomez-Gomez and Boller, 2000), while ELONGATION FACTOR TU RECEPTOR (EFR) recognizes bacterial elongation factor Tu (Kunze et al., 2004). Additionally, CHITIN ELICITOR RECEPTOR KINASE 1 (CERK1) and Lysin Motif Containing Receptor-Like Kinase 5 (Lyk5) recognize hepta- or octamers of fungal elicitor chitin (Miya et al., 2007; Cao et al., 2014). Moreover, LRR-composed PRRs can identify "self" molecules known as host-derived damage-associated molecular patterns (DAMPs). The recognition of a MAMP leads to the induction of immune responses in the host plant that constitute the first layer of defense referred to as MAMP-triggered immunity (MTI). Based on their timing, the activated immune responses range from instant (medium alkalization, oxidative burst, protein phosphorylation) and early (ethylene biosynthesis, defense gene activation) to late (callose deposition and growth inhibition) (Boller and Felix, 2009). All these processes aim to halt further growth of a microbe on/in plant tissues. However, there are microbes adapted to overcoming this first immune layer through the secretion of effector molecules that suppress PTI and allow the pathogen to cause disease, a phenomenon known as effector-triggered susceptibility (ETS). In

turn, during their co-evolution with microbes, plants have developed intracellular receptors for effectors called nucleotide-binding (NB) LRR (NLR) proteins that when activated lead to strong hypersensitive response (HR) that stops pathogen ingress. This immunity layer is termed effector triggered immunity (ETI) (Dodds and Rathjen, 2010). Most of these steps are elucidated by the extensive study of pathogen perception in the aerial plant tissues. However, evidence is accumulating that roots can perceive MAMPs and generate MAMP-specific responses in a similar manner (Millet et al., 2010; Jacobs et al., 2011; Wyrsch et al., 2015; Poncini et al., 2017).

MAMPs, symbiotic signals and root responses

Early detection and discrimination of diverse microbial signals derived from the microbe-rich root surroundings is crucial for plant health and fitness. The evidence that there is an active interface between plant roots and microbial derived-molecules originates from studies on beneficial symbiotic and nonsymbiotic microbes. Elicitors isolated from PGPR *P. simiae* WCS417 (LPS), *P. capeferrum* WCS358 (LPS and flagella) and *B. cereus* AR156 (extracellular polysaccharides - EPS) could trigger ISR in Arabidopsis against *P. syringae* (Meziane et al., 2005; Van Wees et al., 2008; Jiang et al., 2016), while cell wall extracts of these fluorescent pseudomonads could trigger MTI responses in tobacco suspension cells (Van Loon et al., 2008). In a breakthrough study, Millet and colleagues (2010) observed that Arabidopsis roots could sense bacterial (flg22, PGNs; peptidoglycans) and fungal (chitin) elicitors and activate tissue-specific responses (callose deposition, camalexin biosynthesis, expression of defense-related genes) that resembled MTI generated in leaves. Similarly, inoculation of Arabidopsis roots with heat-killed *P. simiae* WCS417 bacteria could trigger responses typical of MTI, due to the involvement of MAMPs. Additionally, Jacobs and associates (2011) suggested a role of MAMPs in the recognition of beneficial fungus *P. indica*, since colonization of the fungus was increased in *cerk1* plants that are impaired in chitin perception. Border-like cells in the root tips of Arabidopsis and flax are also sensitized by MAMPs (flg22 and PGN) and consequently induce defense reactions such as ROS production, callose deposition and higher expression of genes with a role in plant immunity (Plancot et al., 2013). Another study (Trda et al., 2014) showed that the magnitude of responses triggered by the flg22 peptide of the PGPR *Burkholderia phytofirmans* differs between Arabidopsis and grapevine, since weaker immune responses were observed in the latter. The authors of this study suggested that this difference was explained by the co-evolution of the endosymbiont with the host, which led to changes in flagellin to evade recognition by the grapevine FLS2 receptor. The adaptation of microbes to their host is also evidenced on a larger scale. Only a small fraction of the genomes of the culturable microbiome of Arabidopsis (3-6%) contains genes coding for flg22 or elf18 peptides, while the peptide cold shock protein 22 (csp22) recognized by Solanaceae and not by Arabidopsis is present in 25% of the isolated Arabidopsis-associated microbes (Wang et al., 2016; Hacquard et al., 2017). This suggests that the presence of PRRs in roots exerts a selective pressure on the root-associated microbes that need to develop mechanisms to mask the presence of their MAMPs and achieve colonization.

The complexity of signals in the rhizosphere ranges from immune-eliciting MAMPs to molecules produced by symbiotic microbes aiming to initiate symbiosis (Zamioudis and Pieterse, 2012). Symbiotic signals like rhizobial Nod factors when released by N_2-fixing bacteria are able to trigger developmental processes and

nodule formation in host roots (Oldroyd, 2013), while lipochitooligosaccharides (LCOs) secreted by AM fungus *Rhizophagus irregularis* (previously *Glomus intraradices*) facilitate formation of endosymbiosis with different plant species (Maillet et al., 2011; Sun et al., 2015). In another study, EPS produced by *Mesorhizobium loti* and perceived by EPS receptor EPR3 in its compatible legume host *L. japonicus* was critical for the successful infection of root cortex and nodule primordia (Kawaharada et al., 2017). In rice, perception of chito-tetraose or fungal exudates from AM *Gigaspora margarita* by *Os*CERK1 receptor was required to trigger nuclear calcium (Ca^{2+}) spiking, a key process during early root colonization by AMF (Carotenuto et al., 2017). Interestingly, it was previously shown that *Os*CERK1 has a dual function, not only in controlling pathogen perception but also in the establishment of symbiosis. More specifically plants with impaired *OsCERK1* were more susceptible to the rice pathogen *Magnaporthe oryzae* and supported less colonization by the AMF *R. irregularis* (Zhang et al., 2015a). However, recent evidence indicates that leguminous plants have acquired specialized receptors discriminating between symbiotic and pathogenic signals (Kelly et al., 2017). For instance, LysM PRRs of *L. japonicus* and *Medicago truncatula* are specialized in perceiving immunogenic chitin and activate defense responses, but mutant plants for these PRRs display increased susceptibility to pathogens, while nodulation and mycorrhization are not affected (Bozsoki et al., 2017). From the abovementioned studies, it is evident that there is an intricate interplay between molecules produced by symbiotic and nonsymbiotic beneficial microbes and the surveillance system of the plant that defines the fate of the subsequent relationship.

Presence and activation of PRRs is not restricted to aboveground tissues, since expression of these receptors and triggering of defense responses is also observed in roots (Gomez-Gomez and Boller, 2000; Robatzek et al., 2006; Millet et al., 2010; Jacobs et al., 2011; Beck et al., 2014; Cao et al., 2014; Wyrsch et al., 2015). Constitutive activation of PRRs in microbe- and elicitor-enriched environments like roots and the surrounding rhizosphere could result in unnecessary MTI that in turn could result in growth and yield inhibition of plants (Gomez-Gomez et al., 1999; Vos et al., 2013). Thus, plants need to use their receptor repertoire, to discriminate whether a detected signal is derived from a pathogen or from a beneficial microbe and in a next step it needs to regulate downstream responses either to allow or block their entry and accommodation (Antolin-Llovera et al., 2014). Recent studies aimed to define the involvement of different plant organs in flg22 perception by its receptor FLS2 (Beck et al., 2014) and the contribution of different root tissues in the induction of MTI upon flg22 elicitation (Wyrsch et al., 2015). By generating reporter lines of Arabidopsis expressing the *GUS* gene under the control of the *FLS2* promoter, Beck and associates (2014) determined that the receptor of flagellin is expressed at basal levels in tissues usually targeted by invading microbes, such as stomata and hydathodes of leaves and in the vascular cylinder of roots. Expression of *FLS2* was also observed in emerging lateral roots, which constitute another potential entry site of bacterial pathogens (Vasse et al., 2000; Cooley et al., 2003).

Roots are plant organs characterized by radial organization where each concentric layer corresponds to a different tissue (Wachsman et al., 2015). Generation of Arabidopsis transgenic lines expressing *FLS2* under the control of tissue-specific promoters (in *fls2* background) allowed Wyrsch and colleagues (2015) to observe that each root tissue can detect flg22, however the amplitude of MTI responses induced upon *FLS2* activation differed between different tissues. Interestingly, inner tissues showed higher expression

of the receptor and stronger MAMP responses (ROS production, MAP kinase activation, induction of defense genes) compared to epidermal tissues. This observation together with the low representation of genes encoding flg22 peptides in the culturable microbiome of Arabidopsis (Hacquard et al., 2017) could explain why there is no constitutive activation of immune responses in Arabidopsis roots. Intracellular Ca^{2+} elevations are among the earliest responses to a stress and generation of Arabidopsis lines expressing the calcium intensity sensor R-GECO allowed the monitoring of the spatial pattern of Ca^{2+} dynamics in roots in response to MAMPs flg22 and chitin (Keinath et al., 2015; Stanley et al., 2017). When MAMPs were applied homogeneously on the roots in a microfluidic platform then the maximum and first Ca^{2+} signal observations were localized in the elongation zone and later spread towards the root tip (Keinath et al., 2015). In another microfluidic device allowing for asymmetric treatment with flg22 (only on the one side of the root), the Ca^{2+} signal could travel from the epidermis to the vasculature but couldn't reach the untreated side of the root (Stanley et al., 2017), highlighting in that case the previously observed contribution of different root tissues on the MTI following MAMP perception (Wyrsch et al., 2015). Regarding the elongation zone, Millet et al. (2010) have previously shown increased callose deposition and defense gene expression in that root part in response to flg22, while in a microfluidic setup *B. subtilis* accumulated strongly in this root zone within 6 hours following root inoculation (Massalha et al., 2017). All these studies, suggest the important role of different root tissues in root-microbe interactions and indicate the elusive role of the elongation zone, since it can display increased defense potential and at the same time be a niche for preferential bacterial colonization. In this context, it remains to be answered how beneficial microbes are perceived by different root tissues, what are the early responses following recognition, and how are these responses translated to effective colonization and subsequent beneficial effects for the plant.

Suppression of root responses

Since plant "patrol" systems are able to detect microbial presence in the root vicinity, beneficial microbes alike pathogens need to find ways to overcome their recognition and establish a fruitful interaction (Zamioudis and Pieterse, 2012). Associations of mycorrhizal fungi and PGPF with plant hosts provide examples of mechanisms that are employed for a symbiotic outcome. *R. irregularis* is an AMF with ISR-inducing potential. It secretes effector SP7 to suppress ERF transcription factor ERF19 that controls ET-dependent defense responses in roots, therewith promoting AMF colonization (Kloppholz et al., 2011). The mutualism effector MiSSP7 of the ectomycorrhizal fungus *Laccaria bicolor* was shown to contribute in the establishment of symbiosis by stabilizing JAZ6 and consequently repress downstream JA-dependent defense signaling (Plett et al., 2011; Plett et al., 2014b), which together with ET restricts symbiosis between poplar roots and the fungus (Plett et al., 2014a). In contrast, the endophytic fungus *P. indica* requires intact JA signaling to suppress defense responses activated by its MAMPs (Jacobs et al., 2011). During later colonization steps this fungus modulates the endoplasmic reticulum (ER) and induces cell death to promote root invasion (Qiang et al., 2012). More recently, *P. indica* effector PIIN_08944 was found to play role in the early colonization steps of Arabidopsis roots by suppressing MTI and SA-dependent responses (Akum et al., 2015). PGPF *Trichoderma* spp. also seem to upregulate JA signaling in order to suppress immune responses activation during early colonization (Brotman et al., 2013). Several PGPF-derived proteins with

a function in the modulation of the host immune response have been described. Swollenin secreted by *Trichoderma asperellum* facilitates colonization of cucumber roots (Brotman et al., 2008). Additionally, the effector protein TVHYDII1 of *T. virens* has a dual role in Arabidopsis colonization and antagonism against *R. solani* (Guzman-Guzman et al., 2017).

Beneficial bacteria, symbiotic or not, provide also examples of host manipulation to accomplish colonization. Heat-killed *P. simiae* WCS417 are inducing MTI in roots, yet alive bacteria suppress these responses (Millet et al., 2010). Similarly, *B. subtilis* FB17 represses a part of root defense responses when colonizing Arabidopsis (Lakshmanan et al., 2013). In *M. truncatula* there are two transcriptional profiles observed following colonization by *Sinorhizobium meliloti*, one where defense responses are down-regulated and a second where processes related to the formation and activity of nodules are overrepresented (Maunoury et al., 2010). More detailed studies in rhizobia-legume interaction revealed the significance of the Type III secretion system (T3SS) in the establishment of symbiosis (Zamioudis and Pieterse, 2012). The T3SS is a multicomponent apparatus that Gram negative bacteria, mostly pathogenic, use to secrete effector molecules into host cells aiming to restrict the defense responses mounted due to their recognition and achieve host colonization (Galan and Collmer, 1999). *Sinorhizobium fredii* HH103 with defective T3SS is unable to suppress SA-dependent defenses and subsequently fails to promote nodulation on its legume host (Jimenez-Guerrero et al., 2015). Interestingly, the T3SS in some cases can even trigger nodulation when rhizobia cannot secrete Nod factors (Okazaki et al., 2013; Okazaki et al., 2016a). PGPR non-symbiotic rhizobacteria such as *P. fluorescens* SBW25, *P. fluorescens* Q8r1-96, *P. simiae* WCS417 and other root-associated pseudomonads, are also found to possess a T3SS, but its role in root colonization is not defined (Preston et al., 2001; Mavrodi et al., 2011; Loper et al., 2012; Berendsen et al., 2015). Studies with a focus on the microbial community level revealed an enrichment of functions that provide plant-microbe and microbe-microbe competence in the root/rhizosphere microbiome compared to soil microbiome. In rhizospheres of plants with an established AM symbiosis, the microbiome is enriched in fluorescent pseudomonads harboring a T3SS compared to rhizospheres of non-mycorrhizal plants (Viollet et al., 2011). More recently, Bulgarelli and associates (2015) demonstrated the significant enrichment of secretion systems (T3SS, T6SS), adhesion, iron mobilization and sugar transport in bacteria present in root and rhizosphere of barley. Interestingly, Hacquard et al. (2017) provide evidence that in the genomes of the culturable microbiome of Arabidopsis, previously isolated by Bai et al. (2015), only members of the Proteobacteria phylum possess genes coding for T3SS components. These data indicate that microbes such as those belonging to Proteobacteria, need to have the molecular potential to confront either with other microbes or with the root immune system in order to proliferate in the nutrient-rich root niches.

Concluding remarks

Roots have a crucial role in the maintenance of plant health, considering the mesmerizing diversity of health-promoting microbes surrounding them in soil. The existence of an immune system locally in the roots (Millet et al., 2010) and the differential activity of PRRs in different root tissues (Beck et al., 2014; Wyrsch et al., 2015) suggest that plants need to adaptively respond to various triggers and to avoid

unnecessary defense activation that halts plant growth (Huot et al., 2014). Exudates released by roots under different biotic and abiotic stresses can exert a selective pressure on the microbes enriched in the rhizosphere. Successful microbes need to be recognized as friends or avoid recognition by the host to achieve colonization (Bardoel et al., 2011; Hiruma et al., 2016). Microbiome studies have revealed that well-adapted rhizosphere microbes either lack traditional MAMPs or display increased activity of secretion systems delivering effectors (Bulgarelli et al., 2015; Hacquard et al., 2017). It remains unclear though how the plant deals with symbiotic or beneficial microbes that employ common signaling components to achieve colonization (Wang et al., 2012; Zhang et al., 2015a). Recent data suggest that plants may have evolved more receptors to differentially recognize a pathogen from a beneficial microbe (Bozsoki et al., 2017). Additionally, ETS and ETI are well studied in leaves, but their role in root-microbe interactions remains elusive.

In order to get a deeper understanding of how plants discriminate between friends and foes in rhizosphere, research is needed to understand what are the root targets of the effector repertoire characterized in various pathogenic and beneficial soil-inhabiting microbes. Additionally, detailed transcriptomic and metabolomic studies both on the microbial and plant side can reveal specific pathogenic or beneficial "signatures" that will allow the understanding of the mechanisms and functions involved in root colonization. Microbiome analysis in roots infected by pathogenic fungi/bacteria or developing symbiosis by AMF or rhizobia could also unearth the contribution of pathogen- or symbiont-associated microbes in the success of the interaction, and could provide microbial targets either to dampen disease or enhance symbiosis. Finally, studying the interplay between immunity, nutrient deficiencies and microbiome assembly could provide us with pools of beneficial microbes successfully adapted to hijack the nutrient status of the plant to potentiate its defense capacity and increase its growth.

Acknowledgements

The authors would like to thank Ke Yu and dr. Ronnie de Jonge for their comments on the general introduction.

Thesis outline

Roots anchor plants in fixed positions and expose the plant to the microbe-rich soil environment where beneficial microbiota help to sustain plant well-being. One of the main tasks of plant roots is to timely discriminate between those microbes providing beneficial services and those causing disease. Among them there are selected soil-inhabiting bacteria and fungi that can promote growth and activate ISR. Recent findings demonstrate that microbes triggering ISR can also activate iron deficiency responses in roots. The root-specific transcription factor MYB72 emerged as a key player in both processes. However, early recognition of ISR-eliciting microbes as well as the ISR-dependent chemical dialogue between roots and their interacting partners remains uncharacterized. In this thesis, our goal was to explore early events observed locally in roots following recognition of an ISR-inducing bacterium and in a next step characterize

the metabolomics response of roots following *MYB72* activation and study the role of these compounds on root-microbe interactions and the assembly of the root microbiome.

In Chapter 2, we employed time series RNA-sequencing technology to unravel the early root transcriptional changes in response to the plant growth-promoting and ISR-eliciting rhizobacterium *Pseudomonas simiae* WCS417, its MAMP flg22^{417}, and the pathogen-associated MAMPs flg22^{Pa} and chitin. We discovered that the beneficial root-associated rhizobacterium actively suppresses a large sector of the MAMP-triggered transcriptional network in Arabidopsis roots. Detailed comparative analysis of the transcriptomes of rhizobacteria and MAMP-treated roots uncovered a transcriptional signature that pointed to a role for auxin signaling in the adaptation of plant roots to the beneficial effects of the root-associated microbes, which we subsequently validated using auxin signaling mutants.

Previously, Millet et al. (2010) observed that live WCS417 bacteria can suppress root immune responses. Because, genes coding for type III secretion system (T3SS) proteins were formerly found in the genomes of *P. simiae* WCS417 and *P. defensor* WCS374 (Berendsen et al., 2015), we further characterized the T3SS gene clusters of WCS417 and WCS374 in terms of function and genomic organization in Chapter 3. Additionally, the phylogenetic similarity of the T3SS components encoded by the WCS417 and WCS374 genomes was studied and compared to those of other beneficial and pathogenic *Pseudomonas* spp. strains. Moreover, we bioinformatically analyzed the WCS417 and WCS374 genomes for putative effector genes and performed a preliminary test for effector delivery in leaves of tobacco.

Previous findings suggested that the root-specific transcription factor MYB72 and its downstream target BGLU42 are not only required for the onset of ISR, but also for the production and secretion of iron-mobilizing fluorescent compounds (Zamioudis et al., 2014). In Chapter 4, we studied in detail the metabolomes of roots and root exudates of wild-type Col-0 and mutant *myb72* and *bglu42* plants by performing untargeted metabolomics. We found that production of the fluorescent and iron-mobilizing coumarins scopolin, scopoletin, esculin and esculetin is largely regulated by MYB72. Moreover, we show that the β-glucosidase BGLU42 is involved in the deglycosylation of scopolin and the subsequent release of scopoletin into the rhizosphere. Scopoletin is the most abundant compound exuded by Col-0 roots, but is depleted in *myb72* and *bglu42* exudates. Scopoletin displayed antimicrobial activity against soilborne fungi but didn't affect growth of ISR-inducing bacteria WCS417 and WCS358. Hence, we further explored the role of coumarins in the assembly of the root microbiome by performing shotgun metagenomic sequencing of the rhizospheres of Col-0, *myb72* and scopoletin biosynthesis mutant *f6'h1* mutant. This revealed a role for scopoletin in the assembly of the microbial community in the rhizosphere. The results of Chapter 4 point to a scenario in which plants and beneficial rhizobacteria join forces to trigger MYB72- and BGLU42-dependent scopoletin production and excretion to outcompete scopoletin-sensitive microbes in the rhizosphere and to prime plant immunity.

In Chapter 5, we initiated a forward genetic screen aiming to find novel components of the ISR or iron deficiency signaling pathway with a role in the activation of *MYB72*. We performed EMS mutagenesis on the transgenic reporter line of *MYB72$_{pro}$:GFP-GUS*, previously used to study the cell type-specific expression of *MYB72* in response to ISR-inducing rhizobacteria and iron starvation (Zamioudis et al., 2015). Putative

mutants were selected based on decreased GFP activity under fluorescence stereomicroscopy, indicating defected or no *MYB72* expression in roots. Rescreening by qRT-PCR confirmed the lack of *MYB72* expression in a number of putants. None of the putants possessed a mutation in the *MYB72* gene suggesting that these mutants are impaired in one or more genes that play a role in the activation of *MYB72*, providing a basis for future studies.

In Chapter 6, the results presented in this thesis are discussed according to the current knowledge on root-microbe/microbiome interactions.

CHAPTER 2

Root transcriptional dynamics induced by beneficial rhizobacteria and microbial immune elicitors reveal signatures of adaptation to mutualists

Ioannis A. Stringlis[1,#], Silvia Proietti[1,2,#], Richard Hickman[1], Marcel C. Van Verk[1,3], Christos Zamioudis[1,4] and Corné M.J. Pieterse[1]

[1] Plant-Microbe Interactions, Department of Biology, Faculty of Science Utrecht University, P.O. Box 800.56, 3508 TB, Utrecht, the Netherlands
[2] Present address: Department of Ecological and Biological Sciences, University of Tuscia, Viterbo, Italy
[3] Present address: Keygene N.V., P.O. Box 216, 6700 AE Wageningen, The Netherlands
[4] Present address: Rijk Zwaan Breeding B.V., P.O. Box 40, 2678 ZG De Lier, The Netherlands

[#] These authors contributed equally

The Plant Journal (DOI: 10.1111/tpj.13741) (2017)

Abstract

Belowground, microbe-associated molecular patterns (MAMPs) of root-associated microbiota can trigger costly defenses at the expense of plant growth. However, beneficial rhizobacteria, such as *Pseudomonas simiae* WCS417 (WCS417), promote plant growth and induce systemic resistance without being warded off by local root immune responses. To investigate early root responses that facilitate WCS417 to exert its plant-beneficial functions, we performed time-series RNA-Seq of Arabidopsis roots in response to live WCS417 and compared it to MAMPs flg22^{417} (from WCS417), flg22^{Pa} (from pathogenic *Pseudomonas aeruginosa*), and fungal chitin. The MAMP transcriptional responses differed in timing, but displayed a large overlap in gene identity. MAMP-upregulated genes are enriched for genes with functions in immunity, while downregulated genes are enriched for genes related to growth and development. Although 74% of the transcriptional changes inflicted by live WCS417 overlapped with the flg22^{417} profile, WCS417 actively suppressed more than half of the MAMP-triggered transcriptional responses, possibly to allow the establishment of a mutually beneficial interaction with the host root. Interestingly, the sector of the flg22^{417}-repressed transcriptional network that is not affected by WCS417 has a strong auxin signature. Using auxin response mutant *tir1afb2afb3*, we demonstrate a dual role for auxin signaling in finely balancing growth-promoting and defense eliciting activities of beneficial microbes in plant roots.

Introduction

Through photosynthesis, plants have the ability to convert sunlight into chemical energy and provide other organisms with food and oxygen, both aboveground and belowground. Belowground, roots interact with an astonishing number of microbiota, also called the rhizosphere microbiome (Berendsen et al., 2012; Bulgarelli et al., 2013). Via root exudations, plants invest up to 20% of the photosynthetically-fixed carbon sources in the preservation of these rhizosphere microbiota (Bais et al., 2006; Philippot et al., 2013). In return, beneficial rhizosphere microbiota improve root architecture, enhance nutrient uptake, and stimulate the plant's immune system (Lugtenberg and Kamilova, 2009; Berendsen et al., 2012; Pieterse et al., 2016; Venturi and Keel, 2016). Classical examples of such beneficial microbes are mycorrhizal fungi, *Rhizobium* bacteria and plant growth–promoting rhizobacteria (PGPR) and fungi (PGPF) (Zamioudis and Pieterse, 2012).

In the past two decades, the interaction between the PGPR *Pseudomonas simiae* WCS417 (WCS417; formerly known as *Pseudomonas fluorescens* WCS417; Berendsen et al., 2015) and the model plant *Arabidopsis thaliana* (Arabidopsis) was intensively studied to elucidate the molecular mechanisms underlying plant-beneficial effects of this PGPR on plant growth and immunity (Pieterse et al., 2014). Colonization of Arabidopsis roots by WCS417 promotes plant growth by driving auxin-dependent developmental changes in root architecture, resulting in the stimulation of lateral root emergence and root hair formation (Zamioudis et al., 2013). Colonization of Arabidopsis roots by WCS417 also triggers an induced systemic resistance (ISR) that is effective against a broad spectrum of pathogens (Pieterse et al., 2014). WCS417-ISR is not associated with the direct activation of costly defenses, but with a phenomenon called defense priming (Martinez-Medina et al., 2016). WCS417-primed plants display an accelerated defense response upon pathogen or insect attack, but in the absence of an invader, costly defenses are not expressed. The ability of PGPRs to simultaneously promote growth and immunity, without the antagonistic features that are typically associated with growth-defense tradeoffs (Huot et al., 2014), make these beneficial soil microbes ideal for the development of biological control agents.

Although generally beneficial for plants, PGPR and PGPF possess microbe-associated molecular patterns (MAMPs), that, like MAMPs of pathogens, can be recognized by pattern recognition receptors (PRRs) of the plant immune system (Jones and Dangl, 2006; Dodds and Rathjen, 2010). Well-characterized MAMPs are flagellin, the principle component of bacterial flagella, which is recognized by the PRR FLAGELLIN-SENSITIVE2 (FLS2) (Gomez-Gomez et al., 1999; Boller and Felix, 2009), and the fungal cell wall component chitin, which is recognized by the PRR CHITIN ELICITOR RECEPTOR KINASE1 (CERK1) (Miya et al., 2007). MAMP recognition by PRRs results in the induction of a coordinated set of defense responses, called MAMP-triggered immunity (MTI). MTI forms a first line of defense against pathogen invasion (Macho and Zipfel, 2014). Purified flagellin from PGPR strains *P. simiae* WCS417, *Pseudomonas capeferrum* WCS358, and *Pseudomonas defensor* WCS374 (previously known as *Pseudomonas putida* WCS358 and *Pseudomonas fluorescens* WCS374, respectively; Berendsen et al., 2015) elicited typical MTI responses in tobacco suspension cells, such as generation of active oxygen species, extracellular medium alkalization, and activation of defense-related gene expression (Van Loon et al., 2008). In Arabidopsis roots, heat-killed

P. simiae WCS417 bacteria activated the expression of the MTI marker gene *CYP71A12* and triggered the deposition of callose in exposed root cells to the same extent as did the 22-amino acid defense elicitor-active epitope flg22^{Pa} from the opportunistic pathogen *Pseudomonas aeruginosa* PO1 (Millet et al., 2010). Similarly, flg22^{PsJN} derived from flagellin of the endophytic PGPR *Burkholderia phytoformans* PsJN induced MTI responses in grapevine and Arabidopsis (Trda et al., 2014). Also, MAMPs of the PGPF *Piriformospora indica* activated strong MTI responses in Arabidopsis roots (Jacobs et al., 2011), indicating that both PGPR and PGPF in the rhizosphere are potential activators of local root immune responses. As a result of the activation of energy-costly defense mechanisms, exposure to MAMPs typically has a negative effect on plant growth (Gomez-Gomez et al., 1999; Pel and Pieterse, 2013). Nevertheless, PGPR and PGPF, which abundantly interact with plant roots, promote plant growth rather than suppressing it. Hence, beneficial microbes must have evolved strategies to reduce stimulation of local host immune responses or to actively suppress MTI (Van Wees et al., 2008; Zamioudis and Pieterse, 2012; Trda et al., 2015).

In this study, we used time-series RNA-Seq to investigate the early transcriptional responses of Arabidopsis roots to living plant growth-promoting and ISR-inducing WCS417 bacteria in comparison to its MAMP flg22^{417}. We show that the root response to flg22^{417} is highly similar to that of flg22^{Pa} of the pathogen *P. aeruginosa* and that of fungal chitin. Transcriptional changes inflicted by living WCS417 overlap largely with those mediated by the MAMPs, but about half of the MAMP-induced transcriptional changes are suppressed by living WCS417 cells. The MAMP-repressed genes that are not affected by WCS417 have a strong auxin signature. We provide evidence that points to a dual role for auxin in finely balancing root growth and defense responses to plant growth-promoting rhizobacteria.

Results

Time-series RNA-Seq reveals kinetics of transcriptional changes to live WCS417 and MAMPs

Colonization of Arabidopsis roots by WCS417 bacteria typically stimulates plant growth (Zamioudis et al., 2013; Pieterse et al., 2014). By contrast, when plant roots are exposed to purified MAMPs, such as flagellin, plant growth is severely inhibited (Gomez-Gomez et al., 1999). We reasoned that a comparison between early transcriptional root responses to live WCS417 and its MAMP flg22^{417} would provide insight into how WCS417 is able to bypass growth-defense tradeoffs. To this end, we analyzed whole transcriptome changes in roots of 22-d-old Arabidopsis Col-0 plants at 0.5, 1, 3, and 6 h after elicitation with live WCS417 cells or its MAMP flg22^{417}. The well-characterized MAMPs flg22^{Pa} of *P. aeruginosa* (containing 5 amino acid differences in comparison to flg22^{417}; Supplemental Figure S1) and fungal chitin were included in the study as well. First, we verified the expression pattern of the root MTI marker genes *MYB51* and *CYP71A12* (Denoux et al., 2008; Millet et al., 2010) in the harvested root material (Figure 1).

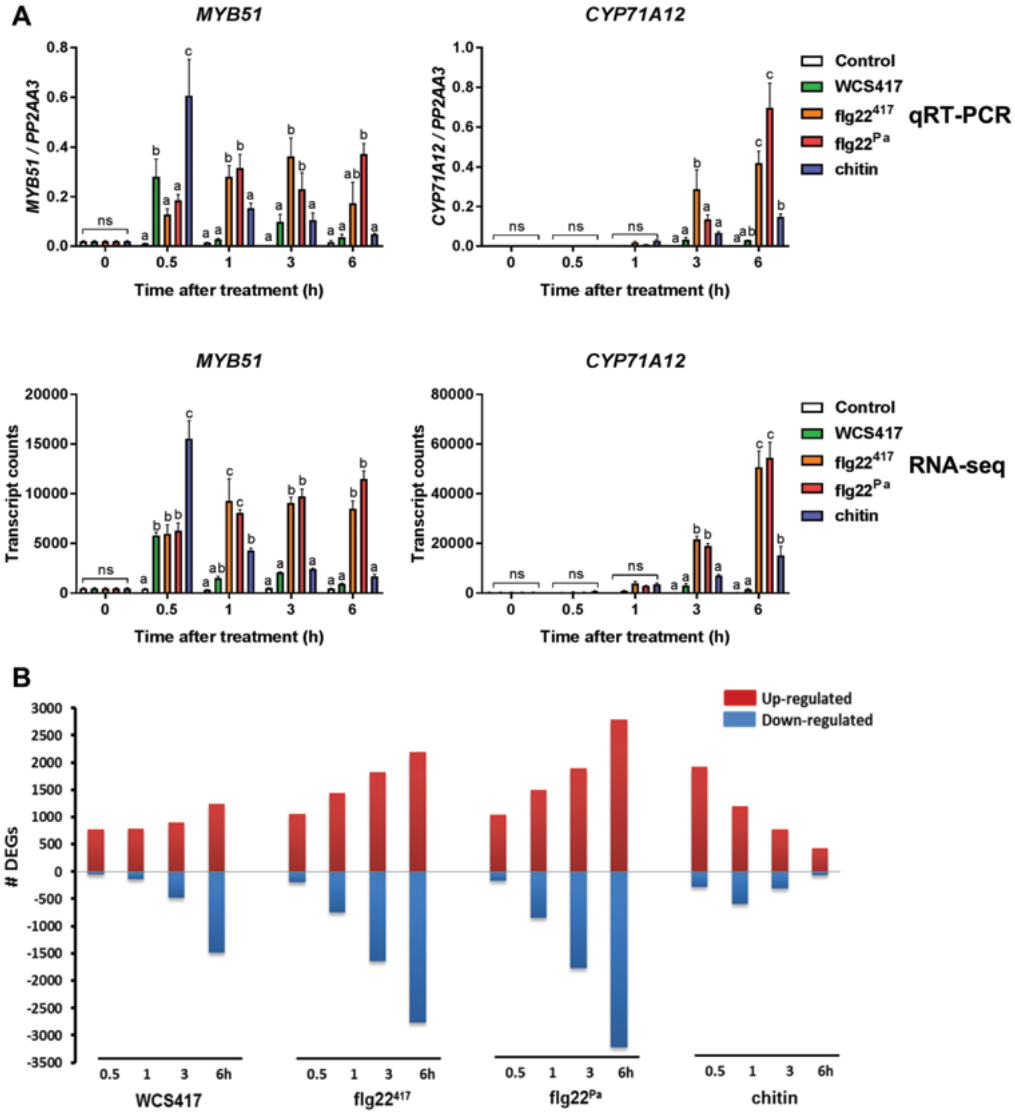

FIGURE 1. Expression profiles of MTI marker genes *MYB51* and *CYP71A12*, and number of DEGs in roots in response to WCS417, flg22^{417}, flg22^{Pa}, and chitin.

(A) Gene expression profiles of *MYB51* and *CYP71A12* in WCS417-, flg22^{417}-, flg22^{Pa}-, and chitin-treated Arabidopsis Col-0 roots quantified by qRT-PCR (top) and RNA-Seq (bottom). For qRT-PCR, transcript levels were normalized to that of reference gene *PP2AA3* (At1g13320). Data are means of 3 biological replicates. Error bars represent SE. Different letters represent statistically significant differences between treatments (Two-way ANOVA, Tukey's test; $P < 0.05$; ns, not significant). **(B)** Number of induced (red bars) and repressed (blue bars) differentially expressed genes (DEGs) from RNA-Seq analysis of WCS417-, flg22^{417}-, flg22^{Pa}-, and chitin-treated Arabidopsis Col-0 roots at indicated time points after treatment (FDR <0.05; >2-fold).

The MAMPs flg22^{417}, flg22^{Pa} and chitin significantly activated both marker genes in the 6-h time window tested, albeit with different timing and amplitude. At 0.5 h after treatment, live WCS417 cells activated *MYB51* expression significantly compared to control, after which it quickly returned to basal levels. *CYP71A12* transcript levels remained unchanged after WCS417 treatment. Because the MTI marker genes were significantly activated in response to MAMP treatment, we pursued with the RNA-Seq analysis. Per treatment and time point, 3 biological replicates were subjected to RNA-Seq. Each biological replicate consisted of 8 roots that were pooled to form one sample. RNA-Illumina sequencing yielded on average 30 million reads per sample of which >90% aligned to the Arabidopsis genome after quality filtering (Van Verk et al., 2013; Hickman et al., 2017). The expression profiles of *MYB51* and *CYP71A12* quantified by RNA-Seq were highly similar to those quantified by quantitative reverse transcriptase PCR (qRT-PCR) (Figure 1A), confirming that the RNA-Seq analysis was performed correctly.

Magnitude and timing of early root transcriptional responses

Differentially expressed genes (DEGs) were selected from each treatment and time point according to their significance in fold change expression (false discovery rate (FDR) <0.05) and an additional threshold level of at least 2-fold change (-1> $\log_2$ >1) in comparison to the untreated controls that were harvested at the same time as the treated samples (Supplemental Dataset S1). RNA-Seq results revealed that the number of genes that are significantly activated or repressed during the different treatments differs over time (Figure 1B). Within the first 0.5 h, live WCS417 cells predominantly activated the expression of genes. In terms of numbers of DEGs, a similar pattern was observed for flg22^{417} and flg22^{Pa}. At later time points, the number of DEGs gradually increased for both the up- and the down-regulated genes, although this was notably milder in response to WCS417 (accumulating to a total of 3559 unique DEGs) than in response to flg22^{417} and flg22^{Pa} (accumulating to a total of 5934 and 6955 unique DEGs, respectively). The root response to chitin showed a different pattern. The number of DEGs peaked already at 0.5 h after chitin treatment, after which the number of predominantly upregulated DEGs gradually decreased. With a total number of 3342 unique DEGs, the response to chitin was milder than that of the flg22 MAMPs.

FIGURE 2. Dynamics and comparative analysis of the root transcriptome in response to live WCS417 cells and the MAMPs flg22^{417}, flg22^{Pa} and chitin.

(A) Dynamics of the expression patterns of the 3559 WCS417-, 5934 flg22^{417}-, 6955 flg22^{Pa}-, and 3342 chitin-responsive DEGs in Arabidopsis Col-0 roots**.** Gene expression is plotted in yellow–blue color scale with yellow indicating up-regulation and blue indicating down-regulation in comparison to controls at the same time point. DEGs were clustered using SplineCluster. **(B)** Venn diagrams showing the pairwise overlap between the up-regulated and down-regulated DEGs of the indicated treatments. Enriched GO terms associated with the core sets of up-regulated (1307) and down-regulated (437) DEGs in all treatments are shown with *P*-values indicated on X-axes (Full data in Supporting Dataset 3). **(C)** Venn diagrams showing the overlap between the up-regulated and the down-regulated genes of the indicated treatments. Percentages indicate the percentage of the smallest group of genes that is shared with the other group of genes in the comparison. Color of circles in Venn diagrams in 2C are as follows: Green = WCS417; orange = flg22^{417}; red = flg22^{Pa}; blue = chitin.

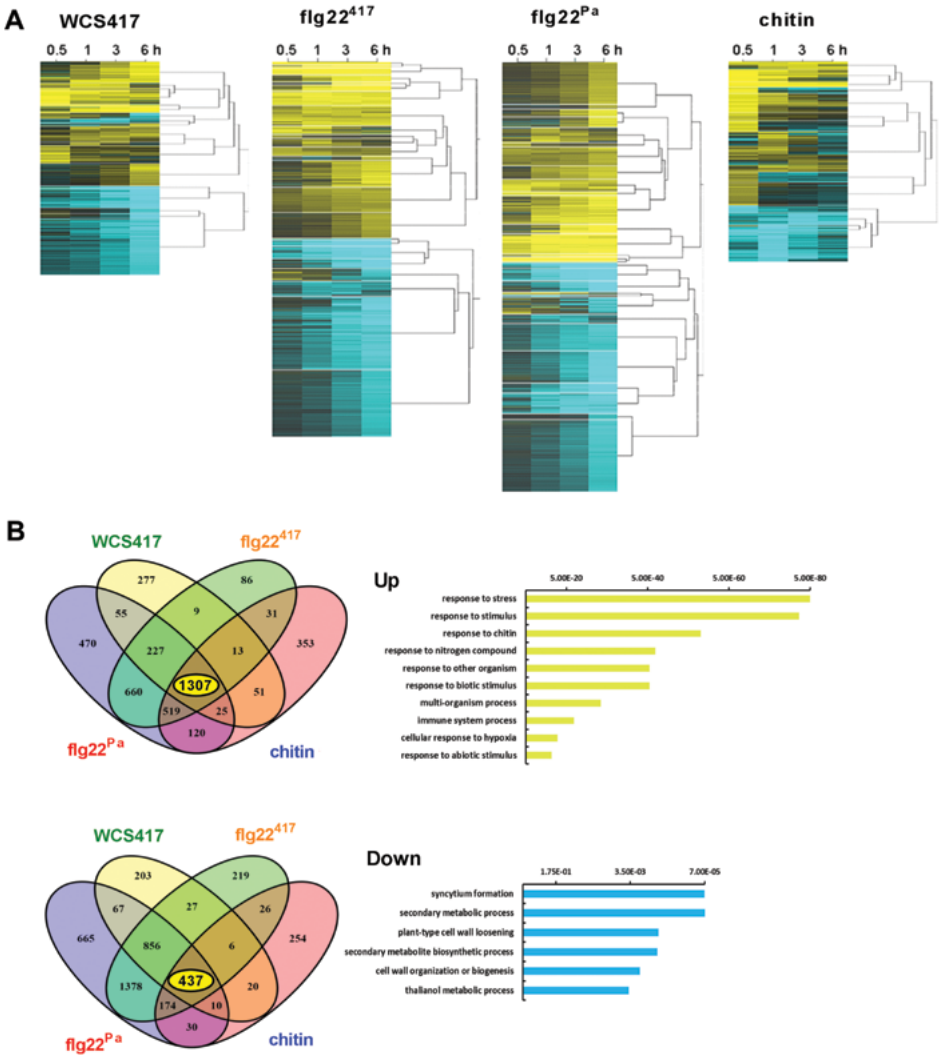
A
WCS417
flg22417
flg22Pa
chitin
0.5 1 3 6 h
B
WCS417
flg22417
flg22Pa
chitin
277
86
55
9
31
470
227
13
353
1307
660
51
519
25
120
Up
5.00E-20
5.00E-40
5.00E-60
5.00E-80
response to stress
response to stimulus
response to chitin
response to nitrogen compound
response to other organism
response to biotic stimulus
multi-organism process
immune system process
cellular response to hypoxia
response to abiotic stimulus
203
219
67
27
26
665
856
6
254
437
1378
20
174
10
30
Down
1.75E-01
3.50E-03
7.00E-05
syncytium formation
secondary metabolic process
plant-type cell wall loosening
secondary metabolite biosynthetic process
cell wall organization or biogenesis
thallanol metabolic process
C
WCS417 – flg22417
up
down
408
1556
(79%)
1296
300
1326
(81%)
1797
(74%)
flg22Pa – chitin
up
down
1412
1971
(81%)
448
2966
651
(76%)
306
(81%)
flg22417 – flg22Pa
up
down
139
2713
(95%)
670
278
2845
(91%)
772
(93%)

To investigate to what extent the root transcriptional responses to flg22^{Pa} and chitin in our study relate to previous microarray studies in which the response to these MAMPs were analyzed in Arabidopsis roots (Wan et al., 2008; Beck et al., 2014) or seedlings (Zipfel et al., 2004), we selected DEGs from the 0.5 h time point of our flg22^{Pa} and chitin RNA-Seq datasets. This time point was selected because it overlapped with that used in the published microarray studies. DEGs whose probe sets were not present on the used microarrays were excluded from the selection (Supplemental Dataset S2).

Venn diagrams in Supplemental Figure S2 show that of the 357 DEGs responding within 0.5 h to flg22^{Pa} in roots of Arabidopsis accession Landsberg *erecta* (L*er*-0) (Beck et al.(2014); Supplemental Dataset S2), 75% was also present in our set of flg22^{Pa}-responding DEGs. For the 932 DEGs responding within 0.5 h to flg22^{Pa} in whole L*er*-0 seedlings (Zipfel et al.(2004); Supplemental Dataset S2), the overlap with our set of flg22^{Pa}-responding DEGs in roots was 48%. Of the 878 DEGs responding within 0.5 h in Col-0 roots to the chitin octamer chitooctaose (Wan et al.(2008); Supplemental Dataset S2), 66% was also present in our set of chitin-responding DEGs. In this study, we significantly expanded the MAMP-responsive dataset of roots by generating an information-rich time series of gene expression profiles that allow analysis of the dynamics of co-expressed gene clusters in the triggered gene transcriptional networks.

Nature and timing of core root responses to WCS417, flg22^{417}, flg22^{Pa} and chitin

To investigate to what extent genes and biological processes are shared between the four treatments, we compared their DEGs. Figure 2 shows heatmaps of the clustered expression profiles of the DEGs at 0.5, 1, 3 and 6 h after treatment of the roots with WCS417, flg22^{417}, flg22^{Pa} or chitin. Figure 2B shows the overlap in DEGs in the up- and down-regulated gene sets. Of the union of 4203 upregulated genes, a core set of 1307 genes are upregulated, whereas of the union of 4372 downregulated genes, a core set of 437 are downregulated in response to all 4 treatments. Among the core sets of shared DEGs are several well-characterized MAMP-responsive marker genes, including *CYP71A12* (At2g30750), *FRK1* (At2g19190), *PROPEP2* (At5g64890) and *MPK11* (At1g01560). Gene Ontology (GO) analysis (Boyle et al., 2004) of overrepresented biological processes in the core set of DEGs shows that the upregulated DEGs are predominantly associated with stress and defense, while the core set of downregulated genes are predominantly related to growth and development (Supplemental Dataset S3). A similar pattern can be observed in the significance analysis of the GO terms that are enriched in each treatment over time (Figure 3). GO terms related to responses to stress elicitors are clearly most significantly enriched in the upregulated set of DEGs, while GO terms related to cell wall biogenesis and root development are most prominently enriched in the downregulated set of DEGs.

WCS417 versus flg22^{417}. In a more detailed analysis, we performed pairwise comparisons between the sets of up- and downregulated DEGs of the 4 treatments. Figure 2C shows that there is a large overlap between the DEGs of the WCS417 and flg22^{417} treatment. Of the 1964 WCS417-induced genes, 79% is also activated in response to flg22^{417} treatment. For the 1626 downregulated genes this percentage is similarly high (81%). When comparing the significance of the enriched GO terms in the up- and down-regulated sets of DEGs of both treatments over time (Figure 3), the nature of the root response to live WCS417 cells

and flg22^{417} is rather similar. However, while many of the GO terms in the upregulated set of DEGs remain significantly overrepresented in the flg22^{417}-treated roots over time, they disappear at later time points in the WCS417-induced set of DEGs. Interestingly, a large proportion of the 5934 DEGs responding to flg22^{417} treatment (50%) were not responding to WCS417 treatment, suggesting that the flg22^{417}-responsiveness of these DEGs is suppressed by live WCS417 bacteria. The nature of the differential root response to live WCS417 cells and flg22^{417} is analyzed in more detail below.

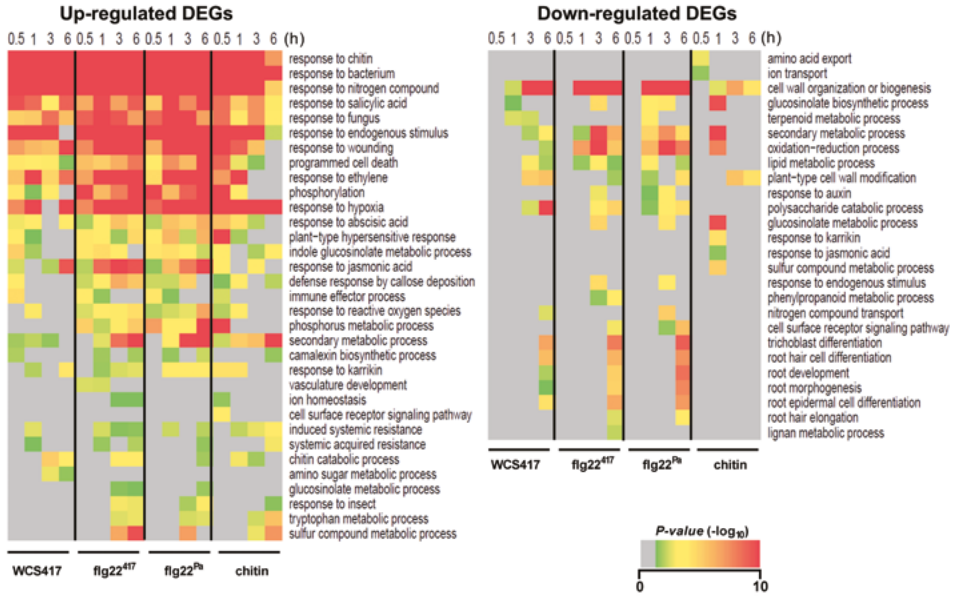

FIGURE 3. Time-course GO term enrichment analysis of the WCS417, flg22^{417}, flg22^{Pa} and chitin DEGs sets. Heatmaps represent the *P*-values of GO term overrepresentation of up- or down-regulated DEGs (corresponding to DEGs provided in Supplemental Dataset 1) in response to treatment of the Arabidopsis roots with WCS417, flg22^{417}, flg22^{Pa} or chitin at given time points. On the right, overrepresented GO terms. The significance was plotted in grey-red color scale with grey indicating no significance and red high significance.

flg22^{417} versus flg22^{Pa}. The sequence of the 22-amino acid flg22 peptides of the mutualist *P. simiae* WCS417 and the pathogen *P. aeruginosa* PAO1 differs at 5 of the 22 positions (Supplemental Figure S1). Previous studies have shown that replacement of specific amino acids in the flg22 sequence of *P. aeruginosa* or other bacterial phytopathogens (black and red arrows, Supplemental Figure S1) can dramatically affect immune elicitation in tomato and Arabidopsis, and growth inhibition in the latter (Felix et al., 1999; Sun et al., 2006; Naito et al., 2008). One of these amino acids (red arrow, Supplemental Figure S1) was different in the sequence of flg22^{417} compared to flg22^{Pa}. Nevertheless, the set of DEGs in Arabidopsis roots responding to flg22^{417} and flg22^{Pa} show a very high overall overlap, both in numbers and in gene identity (Figure 2C; 95% overlap in the upregulated DEGs, 91% overlap in the downregulated DEGs, 93% overall overlap). When comparing the significance of the enriched GO terms in the up- and down-regulated sets of DEGs of both treatments over time (Figure 3), it is clear that the nature as well as the timing of the root response to flg22^{417} and flg22^{Pa} is highly similar.

flg22^{Pa} versus chitin. A plethora of soil microbiota possess either flagellin or chitin. Hence plant roots must be abundantly exposed to both MAMPs. Pairwise comparison of the genes that are significantly affected in response to exposure of Arabidopsis roots to flg22^{Pa} or chitin revealed that, although the overall number of DEGs in response to the chitin treatment is considerably lower (3342 DEGs for chitin versus 6955 DEGs for flg22^{Pa}), a substantial part of the chitin-responsive genes is also responsive to flg22^{Pa} (Figure 2C; 81% in the upregulated DEGs, 76% in the downregulated DEGs, 81% overall). Comparison of the enriched GO terms in the sets of DEGs of both treatments over time (Figure 3), shows that the nature of the upregulated responses is very similar, although in general they seem to dampen off over time in the chitin treated roots. The number of downregulated genes in the chitin set of DEGs is much lower than in the flg22^{Pa} set of DEGs (987 versus 3647). The GO term analysis (Figure 3) suggests that processes related to root development are downregulated by flg22^{Pa}, while they remain unaffected in response to chitin.

Suppression of MAMP responses by live WCS417 cells

Figure 2 shows that the genes that become up- or downregulated in roots responding to live WCS417 cells are overall similarly responsive to its MAMP flg22^{417}, suggesting that the root response to colonization by WCS417 is largely MAMP-mediated. Besides flagellin, WCS417 bacteria produce more MAMPs, including elongation factor Tu (EF-Tu; Kunze et al. (2004)) and lipopolysaccharides (LPS; Zeidler et al. (2004)), which are likely to elicit partly similar MAMP responses in the roots as flagellin does. To investigate whether the observed WCS417 root transcriptional response is flagellin-specific or merely mediated by the concerted action of multiple WCS417 MAMPs, we selected two genes (*WRKY30* and *JAZ8*) from our RNA-Seq dataset that were similarly responsive to WCS417 and the flg22 peptides flg22^{417} and flg22^{Pa}, two WCS417-specific genes (*SRO4* and *SAD6*) that were induced by WCS417 but not by the flg22 peptides, and two MAMP-responsive genes (*MYB51* and *CYP71A12*) that were strongly induced by the flg22 peptides, but are suppressed by live WCS417 cells (Figure 1A and Figure 4).

To test whether the expression patterns of the selected genes were flagellin-specific or not, we monitored their expression pattern in roots of wild-type Col-0 and flagellin receptor mutant *fls2* over time by qRT-PCR. Figure 4B shows that the WCS417-specific genes *SRO4* and *SAD6* were induced by WCS417 in both Col-0 and *fls2* mutant but not by flg22^{417} and flg22^{Pa}, confirming that the roots responded to WCS417. As expected, the flg22-specific genes *MYB51* and *CYP71A12* followed a FLS2-dependent expression pattern and were not induced by live WCS417 cells. The WCS417- and flg22-responsive genes *WRKY30* and *JAZ8* were induced in Col-0 roots by WCS417 and both flg22 peptides. WCS417 induced these genes also in the *fls2* mutant, while the flg22 peptides did not, indicating that these MAMP-responsive genes can also be induced by other WCS417 MAMPs. These results highlight that WCS417-mediated root transcriptional responses are not flagellin-specific but are likely caused by the concerted action of multiple WCS417 MAMPs.

Although the root transcriptional response to live WCS417 bacteria largely overlaps with the root response to its MAMP flg22^{417}, more than 50% of the 5934 flg22^{417}-responsive genes are not responsive to WCS417, suggesting that live cells actively suppress a significant part of the MAMP response. GO term analysis of the set of flg22^{417}-responsive genes that are not responsive to WCS417 (Figure 5) are predominantly associated

with defense, suggesting that live WCS417 cells actively suppress a significant portion of the defense-related genes that are potentially activated by its MAMPs. Interestingly, the flg22^{417}-downregulated set of genes that are not downregulated by live WCS417 cells represents GO terms related to cell wall organization, plant growth and development (Figure 5), suggesting that live WCS417 cells actively prevent the MAMP-mediated suppression of genes that are associated with plant growth. Indeed, treatment of Arabidopsis Col-0 seedlings with flg22^{417} or flg22^{Pa} strongly reduced shoot fresh weight, lateral root formation and root length (Figure 6). Mutant *fls2* did not display these flg22-mediated growth retardations confirming that this is a flg22-mediated response. Chitin, which in contrast to flg22^{417} and flg22^{Pa} did not downregulate GO terms related to growth and development (Figure 5), also did not reduce shoot fresh weight, lateral root formation and root length (Figure 6A). Interestingly, in both Col-0 and *fls2,* treatment of the roots with live WCS417 cells increased shoot fresh weight and the number of lateral roots formed, while mildly reducing primary root length (Figure 6B and 6C). These results suggest that the suppression of the flg22^{417}-mediated transcriptional response by live WCS417 cells is partially directed towards bypassing the plant growth-repressing effects of MAMP recognition.

Auxin signature in early root response to WCS417

The positive effects on plant growth and root architecture mediated by colonization of the roots by WCS417 (Figure 6B and 6C) was previously shown to be regulated by auxin, as WCS417 colonization resulted in the activation of the *DR5::YFP* reporter gene in roots, and the auxin response triple mutant *tir1afb2afb3* did not display these growth responses upon treatment with WCS417 (Zamioudis et al., 2013). Also, the GO term analysis of the set of DEGs that were suppressed by flg22^{417} but not by live WCS417 cells yielded a number of significantly enriched GO terms related to growth, development while this gene set contained a considerable number of genes involved in auxin-related processes (Figure 5; Supplemental Dataset S4). To investigate whether this role of auxin in WCS417-mediated root responses was also apparent in the WCS417-triggered root transcriptome, we compared the WCS417-responsive set of DEGs (all 4 time points) with genes from the study of Chaiwanon and Wang (2015), in which transcriptome changes were analyzed in Arabidopsis roots 4 h after treatment with the auxin analog indole-3-acetic acid (IAA) (Figure 7; Supplemental Dataset S5). This comparison revealed that 44% of the WCS417-responsive DEGs (1561 genes) are also responsive to auxin. GO term analysis of the shared set of DEGs showed that this gene set is associated with cell organization, growth and secondary metabolism (Supplemental Dataset S5). This finding confirms that the early root response to live WCS417 bacteria has a strong auxin signature, which may contribute to the growth-promoting effect of WCS417.

A

Gene name	0.5 h			1 h			3 h			6 h			Induced by:
	WCS417	flg22^{417}	flg22^{Pa}	WCS417	flg22^{417}	flg22^{Pa}	WCS417	flg22^{417}	flg22^{Pa}	WCS417	flg22^{417}	flg22^{Pa}	
SRO4	-0.46	-3.09	-2.82	3.96	-2.57	-1.07	4.78	-0.76	-0.70	6.85	0.45	0.94	WCS417
SAD6	-0.01	-2.04	-0.97	2.21	-2.16	-1.10	2.81	-0.66	-0.39	3.33	-1.47	-0.36	WCS417
JAZ8	1.22	0.72	0.31	2.25	5.04	4.28	3.36	5.32	5.11	5.78	6.13	7.50	WCS417 + flg22
WRKY30	6.89	7.96	8.12	5.50	7.41	7.94	5.38	6.37	6.49	3.25	4.82	3.78	WCS417 + flg22
CYP71A12	1.45	2.17	1.78	2.26	4.33	3.95	4.17	6.98	6.78	2.56	7.66	7.76	flg22
MYB51	3.73	3.77	3.84	2.14	4.76	4.56	2.06	4.18	4.28	1.02	4.19	4.62	flg22

B

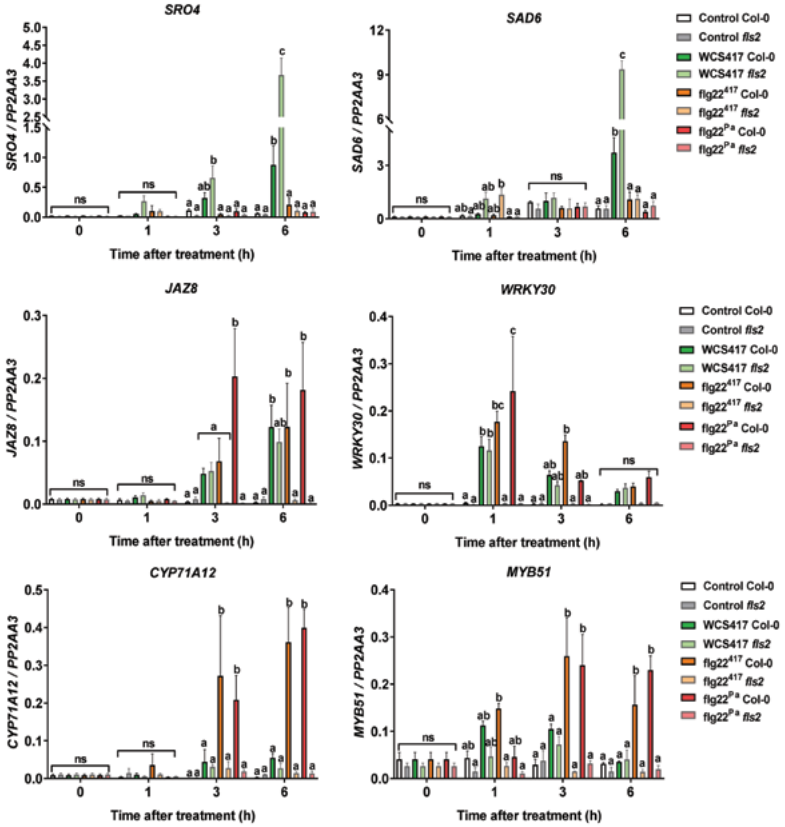

FIGURE 4. Expression profile of selected genes responsive to WCS417, flg22^{417} and flg22^{Pa} treatments.
(A) Expression profile of *SRO4*, *SAD6*, *JAZ8*, *WRKY30*, *CYP71A12* and *MYB51* in Col-0 roots by RNA-Seq analysis. Heatmap showing the expression profile in Col-0 roots at indicated time points after treatment with live WCS417 cells, flg22^{417}, or flg22^{Pa} as obtained by RNA-Seq analysis. Gene expression was plotted in blue–yellow color scale with blue indicating down-regulation or low expression and yellow indicating high expression. Gene expression was calculated relative to mock ($\log_2$-fold change). **(B)** Expression profile of *SRO4*, *SAD6*, *JAZ8*, *WRKY30*, *CYP71A12* and *MYB51* in Col-0 and *fls2* roots by qRT-PCR. Graphs show gene expression levels in Col-0 or *fls2* roots at indicated time points after treatment with live WCS417, flg22^{417}, or flg22^{Pa}, as quantified by RT-qPCR. Gene expression was normalized to the expression level of reference gene *At1g13320,* using the $2^{-\Delta Ct}$ method. The shown data are means of 3 replicates. Error bars represent SE. Different letters represent statistically significant differences between treatments (Two-way ANOVA, Tukey's test; $P < 0.05$; ns, not-significant).

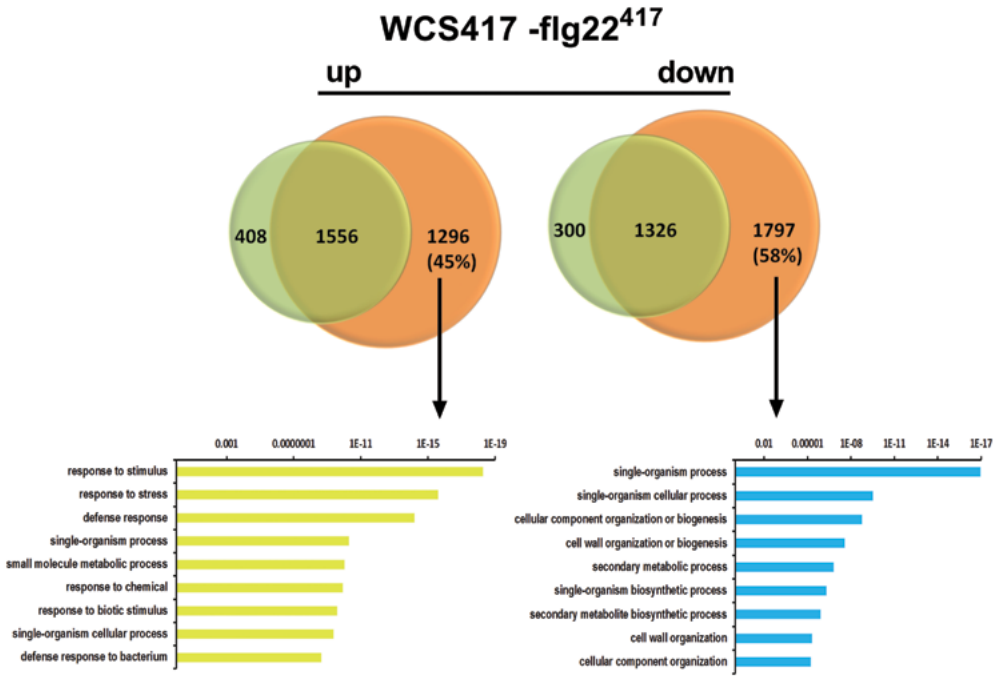

FIGURE 5. Comparative analysis of the root transcriptome to live WCS417 and flg22^{417}.
Venn diagrams showing the overlap between the genes up-regulated and down-regulated upon treatment with WCS417 and flg22^{417}. The bottom section shows the most highly enriched GO terms associated with the sets of DEGs that are specifically up- or down-regulated after root exposure to flg22^{417} but not upon colonization of the roots by live WCS417 bacteria. *P*-values are indicated on the X-axes.

Besides promoting plant growth, WCS417 is also a potent elicitor of ISR. Recently, it was demonstrated that the onset of ISR in Arabidopsis and tomato coincides with the activation of the iron deficiency response in colonized roots (Zamioudis et al., 2015; Martinez-Medina et al., 2017). The onset of both ISR and the iron deficiency response by ISR-inducing rhizobacteria is marked by the activation of the root-specific transcription factor gene *MYB72* and the high-affinity iron transporter gene *IRON-REGULATED TRANSPORTER1* (*IRT1*) (Van der Ent et al., 2008; Zamioudis et al., 2015). Because previously auxin has been shown to be essential for the activation of the iron deficiency response in Arabidopsis roots (Chen et al., 2010), we reasoned that the WCS417-induced auxin response in Arabidopsis roots observed in this study might be at the basis of the activation of the iron deficiency response that is required for the onset of ISR. To test this, we assessed the expression of *MYB72* and *IRT1* in roots of wild-type Col-0 and the auxin response triple mutant *tir1afb2afb3,* 48 h after treatment of the roots with WCS417. As controls we also tested the expression of the well-characterized auxin-responsive gene *GH3.3*, and the auxin-independent WCS417-responsive gene *SAD6* (Figure 7B). As expected, the auxin-independent gene *SAD6* was induced by WCS417 in both Col-0 and the triple mutant, indicating that the WCS417 treatment worked correctly. Furthermore, the ISR and iron deficiency response marker genes *MYB72* and *IRT1,* and the auxin-responsive marker gene *GH3.3* were significantly upregulated in Col-0 roots upon colonization by WCS417. By contrast, their expression was not affected by WCS417 in the roots of the auxin response mutant *tir1afb2afb3* (Figure 7B).

Together, these findings suggest an important role for auxin signaling in early root responses to beneficial WCS417 rhizobacteria that are associated with the promotion of plant growth and the onset of ISR.

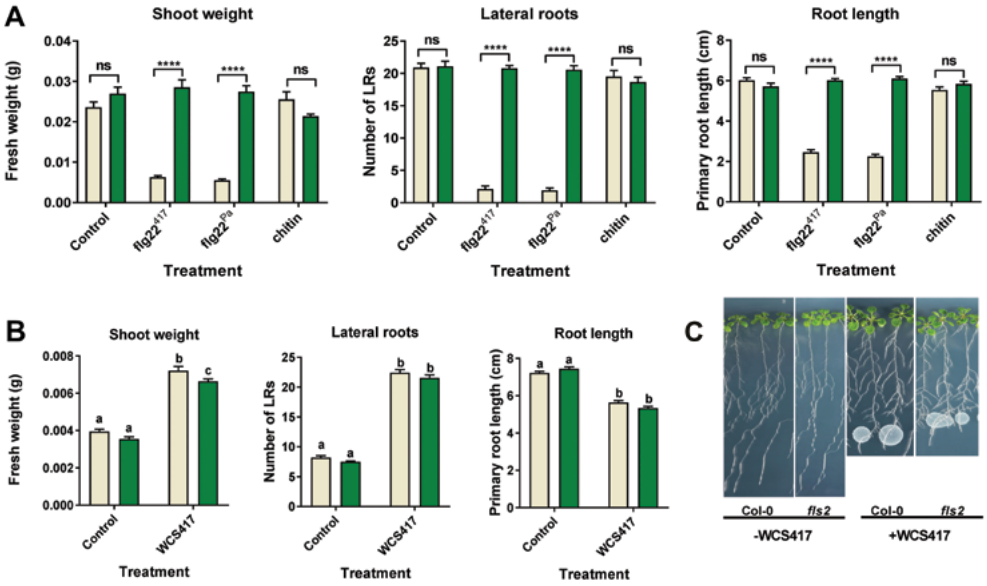

FIGURE 6. Effect of WCS417, flg22^{417}, flg22^{Pa} and chitin on shoot and root growth in Col-0 and the *fls2* mutant.
(A) Effect of flg22^{417}, flg22^{Pa} and chitin on shoot and root growth of Col-0 and *fls2* seedlings. Seven-day-old Arabidopsis seedlings were cultivated for 7 days in liquid MS medium with 0.5% sucrose, supplemented with or without 500 nM flg22^{417} or flg22^{Pa} or 500 µg ml^{-1} chitin, after which shoot fresh weight, number of lateral roots formed, and primary root length were measured. **(B** and **C)** Effect of live WCS417 bacteria on shoot and root growth of Col-0 and *fls2*. Three-day-old Arabidopsis seedlings were cultivated for 7 days on agar-solidified MS medium with 0.5% sucrose and inoculated with a 10-µl suspension containing 2 x 10^6 CFU of WCS417 cells or not inoculated (Control) right below the root tip of each seedling, resulting in rapid colonization of the whole root system. Error bars indicate SE (n=24). Different letters indicate statistically significant differences between Col-0 and *fls2* after control and WCS417 treatment (Two-way ANOVA, Tukey's test; $P < 0.05$) and asterisks indicate significant difference between Col-0 and *fls2* plants treated with the same elicitor (Two-way ANOVA, Sidak's test; ****$P < 0.0001$; ns, not significant).

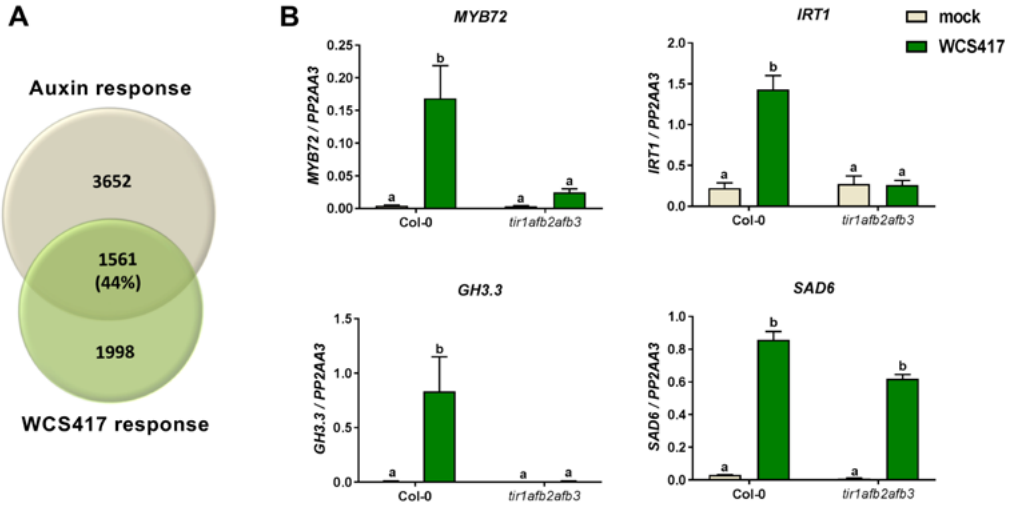

FIGURE 7. Auxin signatures in the early transcriptome of WCS417-colonized roots and auxin signaling-dependent induction of the ISR markers *MYB72* and *IRT1*.
(A) Venn diagram showing the overlap between genes responding to IAA (auxin) and WCS417 in Arabidopsis roots. The effect of auxin was tested 4 h after treatment of the roots with 5 μM IAA (dataset from Chaiwanon and Wang (2015)), while the effect of WCS417 was tested at all time points after application of the rhizobacteria. **(B)** Expression levels of *MYB72, IRT1, GH3.3* and *SAD6* as quantified by qRT-PCR. Expression was tested in roots of 14 d-old Col-0 and *tir1afb2afb3* seedlings at 48 h after inoculation with WCS417. Gene expression levels were normalized to that of reference gene *At1g13320* using the $2^{-\Delta Ct}$ method. The shown data are means of 3 biological replicates. Error bars represent SE. Different letters represent statistically significant differences between treatments (Two-way ANOVA, Tukey's test; $P < 0.05$).

Discussion

Roots are essential plant organs responsible for the uptake of nutrients and water, stable anchorage in the soil, and support of shoot growth. Mutualistic and pathogenic interactions of roots with microbiota members in the rhizosphere strongly influences both plant growth and immunity (Berendsen et al., 2012). To safeguard their fitness, plant roots need to effectively ward off pathogens and at the same time exploit the profitable functions that are provided by beneficial microbes. Plant roots are continuously exposed to an astonishing number and complexity of microbes, most of which possess MAMPs that potentially activate growth retarding immune responses in plant roots (Hacquard et al., 2017). Yet, in general plants profit from their root-associated microbiota by simultaneously displaying enhanced growth and primed systemic immunity. To investigate the mechanisms behind this phenomenon, we compared the early root response of Arabidopsis to colonization by the plant growth-promoting and ISR-eliciting rhizobacterium *P. simiae* WCS417 with those of the purified MAMP elicitors flg22^{417}, flg22^{Pa} and chitin. Using time-series RNA-Seq, we monitored the dynamics of the Arabidopsis root response to live WCS417 cells and the three MAMPs, yielding gene expression profiles that markedly expand those previously obtained that only analyzed one or two time points (Verhagen et al., 2004; Pozo et al., 2008; Wan et al., 2008; Beck et al., 2014).

Intriguingly, the transcriptional root response to flg22^{417} of beneficial WCS417 rhizobacteria was essentially similar to flg22^{Pa} of the bacterial pathogen *P. aeruginosa* PAO1 (93% overlap; Figure 2), even though the 22-amino acid sequence of the flg22 peptides differed at 5 positions (Supplemental Figure S1). The root response to fungal chitin was markedly milder, although the overlap with flg22-triggered transcriptional changes in both gene identity (81% overlap; Figure 2) and GO term enrichment (Figure 3) was very high. This observation is consistent with previous findings in leaves and roots where different MAMPs/pathogens could activate common components of defense signaling pathway and/or affect a significant proportion of the transcriptome in a similar manner (Asai et al., 2002; Zipfel et al., 2006; Denoux et al., 2008; Wan et al., 2008; Millet et al., 2010).

When comparing the WCS417-responsive set of DEGs with that of its flagellin epitope flg22^{417} (Figure 2), we discovered that 74% of the 3559 genes that significantly respond in the roots to WCS417 also respond to flg22^{417}. This indicates that the root response to this beneficial rhizobacterium is largely mediated by flagellin or one or more of its other MAMPs, which are likely to activate largely overlapping gene sets in a redundant manner (Figure 4). On the other hand, half of the 5934 genes that significantly respond to flg22^{417} were not responsive to live WCS417 cells, suggesting that WCS417 actively suppresses the initiation of a large portion of transcriptional changes that are inflicted by its MAMPs. The set of flg22^{417}-upregulated genes that is suppressed by live WCS417 cells represents GO terms that are predominantly associated with defense (Figure 5), indicating that WCS417 actively suppresses the activation of local immune responses that are potentially activated by its MAMPs. Previously, Millet et al. (2010) demonstrated that inoculation of Arabidopsis roots with WCS417 prior to treatment of the roots with flg22^{Pa} prevented the activation of the flg22^{Pa}-responsive genes *MYB51* and *CYP71A12,* supporting the notion that beneficial WCS417 bacteria are able to prevent the activation of MAMP-responsive genes. Also in our study, both *MYB51* and *CYP71A12* were strongly activated by flg22^{417} and flg22^{Pa} (Figure 1), but in response to WCS417 they were either not induced at all (*CYP71A12*), or only activated at 0.5 h after colonization and rapidly downregulated afterwards to basal levels (*MYB51*). Because MAMP-induced responses can result in the inhibition of plant growth (Figure 6; (Gomez-Gomez et al., 1999; Pel and Pieterse, 2013)), significantly tempering of this response by WCS417 may minimize the growth-retarding effect of MAMP recognition by plant roots. Moreover, suppression of local MAMP-triggered immune responses may facilitate colonization of root tissues by the beneficial microbes that suppress it, as was demonstrated for the beneficial fungus *Piriformospora indica* (Jacobs et al., 2011).

The set of flg22^{417}-downregulated genes that are not downregulated by WCS417 largely represents GO terms associated with plant growth and development (Figure 5). Hence, downregulation of this sector of the flg22-responsive transcriptome may reflect the growth-inhibiting effect of flg22-recognition on Arabidopsis seedlings (Figure 6; (Gomez-Gomez et al., 1999; Pel and Pieterse, 2013; Beck et al., 2014)). By preventing MAMP-mediated suppression of this sector of the root transcriptome, live WCS417 cells may further contribute to the promotion of plant growth. This is supported by the observation that Arabidopsis seedlings of which the roots were treated with flg22^{417} or flg22^{Pa} showed a strong FLS2-dependent growth reduction, while treatment of the roots with live WCS417 cells promoted plant growth in an FLS2-independent manner (Figure 6).

Of the 3559 WCS417-responsive genes, 44% was also identified as responsive to auxin in the roots of Arabidopsis (Figure 7A; Chaiwanon and Wang (2015)). This auxin signature in the WCS417-triggered root transcriptome corroborates with previous findings that showed that WCS417 induced the auxin-responsive reporter *DR5::YFP* in Arabidopsis roots and that the WCS417-mediated plant growth-promoting effect was blocked in the auxin response mutant *tir1afb2afb3* (Zamioudis et al., 2013). Together, these findings demonstrate that auxin-dependent responses in the roots are key to the growth-promoting effect of WCS417. We further tested whether auxin signaling may also contribute to the onset of early root responses that have been shown to be essential for the development of broad-spectrum ISR. The onset of WCS417-induced ISR is associated with by the activation of the ISR marker gene *MYB72* and the iron uptake marker gene *IRT1* in the roots (Van der Ent et al., 2008; Zamioudis et al., 2015). We showed that activation of both genes by WCS417 is blocked in the triple mutant *tir1afb2afb3* (Figure 7), suggesting that auxin signaling is indeed important in the early stages of ISR initiation in the Arabidopsis root.

In sum, our analysis of the early root transcriptional changes inflicted by live beneficial WCS417 bacteria and purified MAMPs, showed that 1) the early root response to live WCS417 bacteria is largely driven by its MAMPs, 2) WCS417 actively suppresses about half of the MAMP-triggered transcriptional changes, 3) the root response to the flagellin epitopes flg22^{417} of beneficial WCS417 rhizobacteria and flg22^{Pa} of pathogenic *P. aeruginosa* PAO1 bacteria (differing in 5 amino acids) are essentially similar, and 4) auxin plays a dual role in finely balancing the growth-promoting and systemic immunity-eliciting activity of this beneficial rhizobacterium. Evasion of MAMP-responsive transcriptional changes emerged as a major component of the early root response of Arabidopsis to colonization by beneficial WCS417 bacteria. Hence, future research will be directed towards elucidating the bacterial determinant(s) that are responsible for this phenomenon. Detailed knowledge on how beneficial members of the root microbiota simultaneously promote plant growth and immunity will be essential to ultimately utilize their properties in sustainable strategies for crop improvement and crop protection.

Materials and methods

Plant material and growth conditions

Arabidopsis thaliana accession Col-0 and the mutants *fls2* and *tir1afb2afb3* (in Col-0 background) were used in this study. For all experiments, seeds were surface sterilized (Van Wees et al., 2013) and sown on agar-solidified 1x Murashige and Skoog (MS) medium supplemented with 0.5% sucrose (Murashige and Skoog, 1962). After 2 d of stratification at 4°C, the Petri dishes were positioned vertically and transferred to a growth chamber (22°C; 10 h light, 14 h dark; light intensity 100 µmol m^{-2} s^{-1}).

For testing effects of live WCS417 cells and the MAMPs flg22^{417}, flg22^{Pa} and chitin on gene expression, uniform 12-d-old seedlings were transferred from MS agar plates to 6-well plates (ø 35 mm per well) containing liquid 1x MS with 0.5% sucrose after which they were cultured for 10 more days under the same growth conditions. The day before treatment with WCS417 or MAMP elicitors, the medium of each well was replaced with fresh 1x MS medium with 0.5% sucrose. Plants were treated when 22 d old. At this age, the

plants possessed a well-developed root system which reproducibly responded to the elicitors and yielded sufficient RNA for the RNA-Seq gene expression analysis.

For testing the effect of live WCS417 cells and the MAMPs flg22^{417}, flg22^{Pa} and chitin on plant growth parameters, uniform 7-d-old seedlings were transferred from MS agar plates to 6-well plates containing 1x MS with 0.5% sucrose (in case of MAMP treatment), or to a fresh 1x MS agar plate with 0.5% sucrose (in case of treatment with live WCS417 cells). Seedlings were treated when 9 days old. Effects on growth parameters were measured 7 d later.

For testing the role of auxin signaling in WCS417-mediated expression of ISR marker genes locally in the roots, uniform 10-d-old seedlings were transferred from MS plates to square plates (120 x 120 x 17 mm) containing modified agar-solidified Hoagland medium containing 5 mM KNO_3, 2 mM $MgSO_4$, 2 mM $Ca(NO_3)_2$, 2.5 mM KH_2PO_4, 70 µM H_3BO_3, 14 µM $MnCl_2$, 1 µM $ZnSO_4$, 0.5 µM $CuSO_4$, 10 µM NaCl, 0.2 µM Na_2MoO_4, 4.7 mM MES, 43 mM sucrose and 50 µM Fe-EDTA (Rodriguez-Celma et al., 2013). The pH was adjusted to 5.5. Seedlings were cultivated for 2 d before treatment with WCS417.

Cultivation of *Pseudomonas simiae* WCS417 and treatment

Pseudomonas simiae WCS417 was cultured at 28°C on King's medium B (KB) agar plates (King et al., 1954) supplemented with 50 µg ml^{-1} of rifampicin. After 24 h of growth, cells were collected in 10 mM $MgSO_4$, washed twice with 10 mM $MgSO_4$ by centrifugation for 5 min at 5000 *g,* and finally resuspended in 10 mM $MgSO_4$. For RNA-Seq and qRT-PCR gene expression analysis, bacteria were added in each well to a final optical density of 0.1 at 600 nm (OD_{600}; 10^8 colony-forming units (CFU) ml^{-1}). For measurements of the effect of WCS417 on root and shoot growth, 9-day-old Col-0 and *fls2* seedlings growing on MS agar plates were inoculated by placing a 10-µl suspension of WCS417 at an OD_{600} of 0.002 (2 x 10^6 CFU ml^{-1}) right below the root tip of each seedling. For studying gene expression in roots of Col-0 and *tir1afb2afb3* seedlings growing on Hoagland agar medium, a 10-µl bacterial suspension at OD_{600} = 0.1 was added below the hypocotyl of each seedling.

Chemical treatments

For RNA-Seq and qRT-PCR analysis of gene expression in Arabidopsis roots in response to MAMPs, defense elicitors were added to the liquid growth medium at the following final concentrations: 1 µM for flg22^{417} and flg22^{Pa}, and 1 mg ml^{-1} for chitin (Sigma-Aldrich, St. Louis, MO, USA). For the analysis of the effects of MAMPs on plant growth, the following final concentrations were used: 500 nM for flg22^{417} and flg22^{Pa}, and 500 µg ml^{-1} for chitin. The flg22 peptides were added to the liquid MS medium from a 100 µM stock in water. Chitin was added to the MS medium from a 10 mg.ml^{-1} stock that was prepared as described (Millet et al., 2010). Control plants remained untreated. The amino acid sequence of flg22^{417} was derived from the flagellin-encoding gene "flagellin" (PS417_19850 - WP_029529076.1) that was extracted from the whole-genome sequence of WCS417 (Berendsen et al., 2015). The flg22^{417} and flg22^{Pa} peptides were synthesized by Proteogenix (Schiltigheim, France) and GenScript (Piscataway, NJ, USA), respectively (purity > 95%).

Measurement of plant biomass and parameters of root architecture

Col-0 and *fls2* seedlings were germinated on 1x MS agar plates with 0.5% sucrose. 7-d-old seedlings were transferred to liquid MS medium with 0.5% sucrose, with or without flg22^{417}, flg22^{Pa} or chitin. For treatment with live WCS417 cells, 7-d-old Col-0 and *fls2* seedlings were transferred to new agar-solidified 1x MS plates with 0.5% sucrose. 2 d later, roots were treated with WCS417 by applying 10 µl of a bacterial suspension (OD_{600} = 0.002) right below the root tip of each seedling. Seven d after the start of the treatments, shoot fresh weight, primary root length, and number of lateral roots (LRs) were determined essentially as described (Zamioudis et al., 2013).

RNA sequencing

For RNA-Seq analysis of root transcriptional profiles, roots of Col-0 seedlings were collected in triplicate at 0, 0.5, 1, 3 and 6 h after treatment with live WCS417 cells or after treatment with the elicitors flg22^{417}, flg22^{Pa}, or chitin. Roots of untreated Col-0 seedlings were collected at the same time points. Each of the three biological replicates per treatment and time point consisted of 8 pooled root systems harvested from 8 similarly-treated plants. After harvest, root samples were snap frozen in liquid nitrogen and stored at -80ºC.

Arabidopsis roots were homogenized using a mixer mill (Retsch) set to 30 Hz for 45 sec. RNA extraction, library preparation, and RNA-Seq were performed essentially as described (Coolen et al., 2016). Samples were sequenced by an Illumina NextSeq 500 platform using 6 sequencing runs. Within each run, samples were randomly assigned to 7 lanes of the Illumina flow cells. In total 12 randomized samples were loaded per lane of a NextSeq 500 V3 flow cell. To account for technical variation, each mix of 12 samples was sequenced in 4 different lanes over different flow cells. Three biological replicates of the 5 time points were sequenced in 4 technical replicates, resulting in ~30 million reads per sample with a read length of 75 bp single end. The raw RNA-Seq read data are deposited in the Short Read Archive (http://www.ncbi.nlm.nih.gov/sra/; BioProject ID: PRJNA412447).

Processing of raw sequencing data, alignment of the RNA-Seq data to the Arabidopsis genome, and downstream processing was performed as described (Van Verk et al., 2013; Coolen et al., 2016; Hickman et al., 2017). RNA-Seq reads were aligned to the TAIR version 10 version of the Arabidopsis genome using TopHat v2.0.4 (Trapnell et al., 2009) with parameters: 'transcriptome-mismatches 3', 'N 3', 'bowtie1', 'no-novel-juncs', 'genome-read-mismatches 3', 'read-mismatches 3', 'G', 'min-intron-length 40', 'max-intron-length 2000'. Gene expression levels were calculated by counting the number of mapped reads per annotated gene model using HTSeq-count v0.5.3p9 (Anders et al., 2015). DESeq2 was used to calculated differential gene expression in the treatments relative to the respective control treatments (Love et al., 2014). For downstream analyses, raw read counts were normalized for between sample differences in sequencing depth (Love et al., 2014).

Gene ontology analysis

Enriched gene ontology (GO)-terms in the different sets of DEGs were identified using 'GO Term Finder' (Boyle et al., 2004). This method tests for over-representation of GO categories using the hypergeometric distribution and false discovery rate for multiple testing (*P*-value ≤ 0.05). Heatmaps of *P*-values were generated using R (version 3.2.1).

Analysis of differentially expressed gene sets

Differentially expressed genes were processed with Virtual Plant web tool (http://virtualplant.bio.nyu.edu/cgi-bin/vpweb/virtualplant.cgi) in order to perform comparisons presented with Venn diagrams and identify overlapping gene sets between different treatments and treatment-specific DEGs (Katari et al., 2010).

Clustering of gene expression profiles.

Clustering of DEGs was performed with SplineCluster (Heard et al., 2006) using $\log_2$-fold change differences in expression between the live WCS417 or elicitor-treated samples and their respective controls.

Quantitative real-time PCR analysis

Total RNA extraction for qRT-PCR gene expression analysis was performed as described previously (Hickman et al., 2017). Transcript levels were calculated relative to the reference gene *At1g13320* (Czechowski et al., 2005) using the $2^{-\Delta Ct}$ method (Livak and Schmittgen, 2001; Schmittgen and Livak, 2008). The primers used for qRT-PCR are provided in Supplemental Table S1.

Accession numbers

Arabidopsis gene names and identifiers referred to in the RNA-Seq analysis are listed in Supplementary Dataset S1 (Sheet "AGI"). Arabidopsis gene names and identifiers referred to in qRT-PCR analyses are listed in Supplementary Table S1.

Acknowledgements

This work was supported by ERC Advanced Grant no. 269072 of the European Research Council (to CMJP), FP7-PEOPLE-2012-IEF Marie Curie Fellowship no. 327282 (to SP), and the Netherlands Organization for Scientific Research (NWO) through the Dutch Technology Foundation (STW) VENI Grant no. 13682 (to RH).

Supplemental data

SUPPLEMENTAL TABLE S1. List of primers used in this study

Primer name	Primer sequence (5'→3')
*PP2AA3*_Fw	TAACGTGGCCAAAATGATGC
*PP2AA3*_Rev	GTTCTCCACAACCGCTTGGT
*CYP71A12*_Fw	GATTATCACCTCGGTTCCT
*CYP71A12*_Rev	CCACTAATACTTCCCAGATTA
*MYB51*_Fw	ACAAATGGTCTGCTATAGCT
*MYB51*_Rev	CTTGTGTGTAACTGGATCAA
*SRO4*_Fw	TTGGAGCACACACATGAACA
*SRO4*_Rev	CCAAGGAGATTTCGGGTTTT
*SAD6*_Fw	TCTTCTCAAACCCGTTGACC
*SAD6*_Rev	CTTTCCCTCAGCTCACGAAC
*JAZ8*_Fw	TGTGTTTTTCTTCAGATGTTACCC
*JAZ8*_Rev	TCTCTGCTTGCGATCGATATT
*WRKY30*_Fw	AGAGCGATGATTCCGATCAAG
*WRKY30*_Rev	CATCGTCCAGCGTTCTATCAA
*MYB72*_Fw	ACGAGATCAAAAACGTGTGGAAC
*MYB72*_Rev	TCATGATCTGCTTTTGTGCTTTG
*IRT1*_Fw	ACCCGTGCGTCAACAAAGCTAAAG
*IRT1*_Rev	TCCCGGAGGCGAAACACTTAATGA
*GH3.3*_Fw	CATCACAGAGTTCCTCACAAGC
*GH3.3*_Rev	GTCGGTCCATGTCTTCATCA

SUPPLEMENTAL FIGURE S1. **Alignment of flg22 peptides from flagellin of *P. simiae* WCS417 (flg22^{417}) and *P. aeruginosa* PO1 (flg22^{Pa}).** Arrows indicate the amino acids previously shown (Felix et al., 1999) to be required for the induction of immune responses in tomato. Alignment is created using the sequence alignment tool of CLC Main Workbench 6.9.

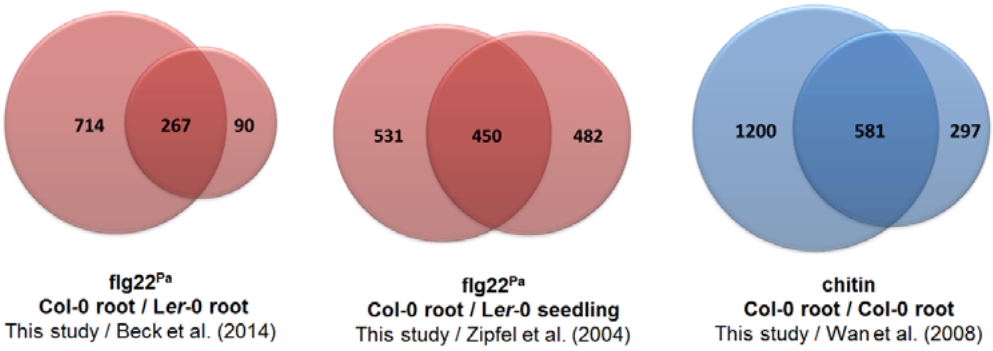

SUPPLEMENTAL FIGURE S2. Venn diagrams of DEGs shared between Arabidopsis responses to flg22^{Pa} or chitin in different studies.

Venn diagrams show the overlap between DEGs responding to **(A)** flg22^{Pa}, 0.5 h after treatment of Col-0 roots (RNA-Seq data of this study) or L*er*-0 roots (Beck et al., 2014), **(B)** flg22^{Pa}, 0.5 h after treatment of Col-0 roots (RNA-Seq data of this study) or L*er*-0 seedlings (Zipfel et al., 2004), and **(C)** chitin, 0.5 h after treatment of Col-0 roots (RNA-Seq data of this study versus Wan et al., 2008). In the study of Beck et al. (2014), L*er*-0 roots were treated with 10 mM flg22^{Pa}. In the study of Zipfel et al. (2004), whole L*er*-0 seedlings were treated with 10 mM flg22^{Pa}. In the study of Wan et al. (2008), Col-0 roots were treated with 1 mM chitooctaose. In all cases, DEGs were selected based on FDR <0.05 and $\log_2$-fold change >1.

Supplemental Datasets S1-S5 are available upon request.

CHAPTER 3

Type III secretion system of beneficial rhizobacteria *Pseudomonas simiae* WCS417 and *Pseudomonas defensor* WCS374

Ioannis A. Stringlis[1], Christos Zamioudis[1,2], Roeland L. Berendsen[1], Peter A.H.M. Bakker[1] and Corné M.J. Pieterse[1]

[1] Plant-Microbe Interactions, Department of Biology, Faculty of Science, Utrecht University, P.O. Box 800.56, 3508 TB, Utrecht, the Netherlands
[2] Present address: Rijk Zwaan Breeding B.V., P.O. Box 40, 2678 ZG De Lier, The Netherlands

Partly adapted from:

Berendsen, R. L , Van Verk, M. C., Stringlis, I. A., Zamioudis, C., Tomassen, J., Pieterse, C. M. J., and Bakker, P. A. H. M. Unearthing the genomes of plant-beneficial *Pseudomonas* model strains WCS358, WCS374 and WCS417

***BMC Genomics 6:* 539 (2015)**

Abstract

Plants roots host a mesmerizing variety of microbes, some of which enhance the defense potential of their host through the activation of a broad-spectrum immune response in leaves, known as induced systemic resistance (ISR). However, establishment of such a mutualistic interaction requires active suppression of local root immune responses to allow successful colonization. To facilitate colonization of their host, phytopathogenic bacteria secrete immune-suppressive effectors into host cells via the type III secretion system (T3SS). Here, we analyzed the genomes of the ISR-inducing rhizobacteria *Pseudomonas simiae* WCS417, *Pseudomonas defensor* WCS374, and *Pseudomonas capeferrum* WCS358 for the presence of a T3SS. We identified the components for a putatively functional T3SS in the genomes of WCS417 and WCS374, displaying strong similarity in genomic organization, but not in the genome of WCS358. Phylogenetic and gene cluster alignment analysis grouped the T3SS of WCS417 and WCS374 in a clade that is enriched for beneficial rhizobacteria. A bioinformatic search for effectors in the genomes of WCS417 and WCS374 yielded 11 putative effectors for WCS417 and 15 putative effectors for WCS374. However, initial tests for WCS417 or WCS374 effector recognition in tobacco did not yield signs of a hypersensitive response (HR). Our results suggest that the beneficial rhizobacteria WCS417 and WCS374 possess a T3SS and effectors. However, future T3SS mutant studies and heterologous expression of effector proteins should shed more light on their putative role in plant-beneficial microbe interactions in the rhizosphere.

Introduction

Plants roots secrete significant amounts of carbon-rich compounds into the soil surrounding their roots, known as the rhizosphere, therewith shaping the microbial composition on their root system (Berendsen et al., 2012). In turn, these root microbiota can influence plant fitness and longevity either in a negative or a positive manner (Zamioudis and Pieterse, 2012). Beneficial members of the root microbiome provide the plant with important services, such as growth promotion, water and nutrient uptake, and protection against pathogens. *Pseudomonas* spp. bacteria are among the beneficial microbes that are strongly enriched in the rhizosphere in comparison to the bulk soil (Lugtenberg et al., 2001; Bakker et al., 2013). Members of this genus have been found to promote growth and nutrient uptake of their hosts, to compete with pathogens in the rhizosphere via antibiosis, and to trigger a systemic form of plant immunity, called induced systemic resistance (ISR) (Lugtenberg and Kamilova, 2009; Pieterse et al., 2014). To provide these benefits to their hosts, beneficial microbes need to colonize host roots, thereby outcompeting other microbes that aim to colonize the same niches and use the same carbon sources (Raaijmakers et al., 1995; Venturi and Keel, 2016). Like pathogenic *Pseudomonas* spp., beneficial *Pseudomonas* spp. need to cope with plant defense mechanisms in order to efficiently colonize their host (Pieterse et al., 2012; Zamioudis and Pieterse, 2012). For that, effective interference with local host immune responses is a prerequisite.

During coevolution with their hosts, animal- and plant-pathogenic *Pseudomonas* spp. have developed mechanisms that allow them to suppress or evade host defense responses and overcome basal immune responses (Jones and Dangl, 2006; Bardoel et al., 2011; Pel and Pieterse, 2013). The type III-secretion system (T3SS) that delivers immune-suppressive effector molecules into the host cell, emerged as a conserved mechanism in Gram-negative bacteria employed for effective colonization of their host (Alfano and Collmer, 2004; Deslandes and Rivas, 2012). The T3SS is a protein secretion nanomachine composed of approximately 30 proteins. Electron microscopy has elucidated the three-dimensional structure of the T3SS, a needle complex consisting of a base that is composed of several rings and is anchored in the bacterial membrane, and a needle extension that is projected from the bacterial surface (Galan et al., 2014). Bacterial effector proteins that need to be secreted pass through the needle to become directly injected into the host cell. The proteins of the base and the ring structures that form the basal body of the secretion apparatus are conserved among different bacteria (Tampakaki et al., 2004) and can thus be easily identified in the genomes of Gram-negative bacteria of interest. Although the effector molecules that are secreted via the T3SS are not conserved, they contain molecular features that allows their identification in genome searches. Many effector-encoding genes from the bacterial leaf pathogen *Pseudomonas syringae* are characterized by the existence of a sequence in their promoter region, known as the "hrp box". This motif is recognized by HrpL, a transcription (sigma) factor that regulates the expression of genes in the hrp operon (Chatterjee et al., 2002). Additional features reside in the N-terminal region of the effector protein sequence, such as the abundance of serine and polar amino acid residues, abundance of acidic amino acid residues in the first 12 amino acids, and an aliphatic amino acid in position 3 or 4 (Guttman et al., 2002; Petnicki-Ocwieja et al., 2002).

The existence of T3SS is not restricted to pathogenic bacteria. Also mutualistic root-associated bacteria, such as rhizobia and non-symbiotic plant growth-promoting rhizobacteria (PGPR) have been shown to possess a

functional T3SS (Zamioudis and Pieterse, 2012). In rhizobia, effectors delivered via the T3SS are thought to assist in the suppression of host immunity, to determine host specificity, and to play a role in nodulation (Okazaki et al., 2013; Gourion et al., 2015; Okazaki et al., 2016b). In the case of PGPR, Rainey (1999) described a T3SS for the PGPR *Pseudomonas fluorescens* SBW25 and since then the T3SS of other fluorescent pseudomonads was studied (Preston et al., 2001; Rezzonico et al., 2005; Mavrodi et al., 2011). Despite the discovery of T3SSs in the genomes of a number of root-associated *Pseudomonas* spp. (Loper et al., 2012; Berendsen et al., 2015), the role of this secretion machinery and the effectors it delivers remained elusive (Zamioudis and Pieterse, 2012).

Since the beginning of 1990's, three *Pseudomonas* spp. strains have been extensively studied as ISR-inducing PGPR in different plant hosts: *Pseudomonas putida* WCS358, *P. fluorescens* WCS374 and *P. fluorescens* WCS417 (Pieterse et al., 2014). Although WCS358, WCS374 and WCS417 are all capable of eliciting ISR, they show host specificity in terms of their ability to induce ISR in different plant species. For instance, in radish, WCS374 and WCS417 are potent elicitors of ISR, whereas WCS358 is not (Leeman et al., 1996). Conversely, in *Arabidopsis thaliana* (hereafter Arabidopsis), WCS417 and WCS358 are able to trigger ISR, whereas WCS374 is not (Van Wees et al., 1997b). Moreover, Arabidopsis possesses natural genetic variation for the ability to express WCS417-mediated ISR, a trait that could be mapped to a single genetic locus in the Arabidopsis genome, indicating that recognition of ISR-inducing rhizobacteria is genetically determined (Ton et al., 1999; Ton et al., 2001). Recently, the genomes of WCS358, WCS374 and WCS417 were described and based on their taxonomy the strains were renamed into *Pseudomonas capeferrum* WCS358, *Pseudomonas defensor* WCS374, and *Pseudomonas simiae* WCS417, respectively (Berendsen et al., 2015). Interestingly, Millet et al. (2010) found that live WCS417 can actively suppress host immune responses in Arabidopsis roots, suggesting a role for *Pseudomonas*-excreted molecules in host immune suppression.

With the ultimate goal to investigate the role of T3SSs and effectors of WCS358, WCS374 and WCS417 in beneficial host-microbe interactions, we searched the genomes of WCS358, WCS374 and WCS417 for T3SS components and effectors and found that WCS374 and WCS417 possess a T3SS and several putative effectors, while WCS358 does not (Berendsen et al., 2015). Here we describe the characterization of the T3SSs of these beneficial root-associated rhizobacteria.

Results

Characterization of T3SS components in bacterial genomes

To identify components of the T3SS in the genome sequences of *P. simiae* WCS417, *P. defensor* WCS374, and *P. capeferrum* WCS358, we performed a BlastP search for homology to genes encoding protein sequences of the canonical T3SS cluster of *P. aeruginosa* (Yahr and Wolfgang, 2006). The search yielded genes corresponding to T3SS components for WCS417 and WCS374, while no T3SS sequences could be identified in the genome of WCS358 (Berendsen et al., 2015). For the naming of the detected T3SS genes, we followed the nomenclature proposed by Preston et al. (2001) for *P. fluorescens* SBW25 T3SS genes and proteins. In this nomenclature system, genes involved in the structure and regulation of the T3SS are named *rsp* (rhizosphere-expressed secretion protein) or *rsc* (rsp conserved), whereas type III effector genes are named *rop* (rhizosphere-expressed outer protein) (Figure 1A).

A

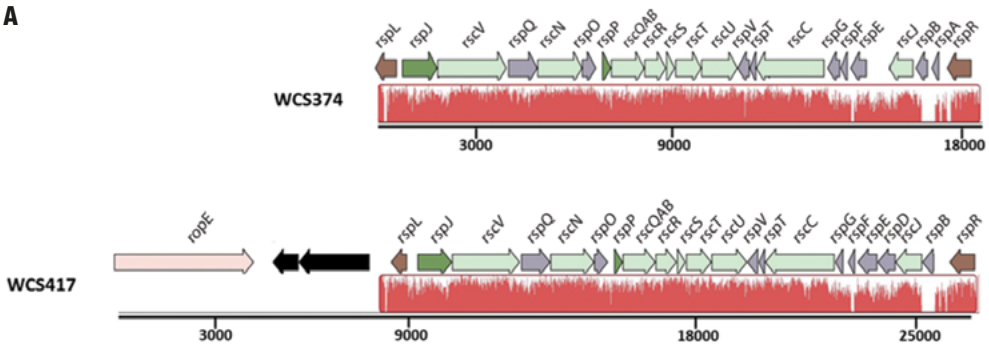

B

Color code	Structure/Function	WCS374	WCS417	Genes that code for proteins with role in structure or function of T3SS
	Exported	–	1	***ropE***
	Transcriptional regulators	2	2	***rspL, rspR***
	Secretion regulators	2	2	***rspJ, rspP***
	Non-conserved core components	9	9	***rspQ, rspO, rspV, rspT, rspG, rspF, rspE, rspD, rspB, rspA***
	Conserved core components	9	9	***rscV, rscN, rscQAB, rscR, rscS, rscT, rscU, rscC, rscJ***
	Unknown	–	2	

FIGURE 1. Genetic organization of the T3SS gene clusters of WCS347 and WCS417.
(A) Orientation and organization of the genes in the T3SS clusters recognized in the genomic sequence of *P. defensor* WCS374 (WCS374) and *P. simiae* WCS417 (WCS417). The red color below the genes indicate regions similar between the two clusters, and the height of the peaks the degree of similarity. **(B)** Each gene in the cluster in Figure 1A is given a color based on the role its encoding protein has either in the structure or the function of the T3SS apparatus. The color code, the putative role of the protein encoded by each gene, number of genes encoding for proteins with specific role and their names are presented. Green letters indicate gene presence only in the WCS417 cluster, while red letters indicate gene presence only in the WCS374 cluster.

The genes coding for components of the T3SS in WCS417 and WCS374 reside in a 26-kb and 18-kb region, respectively (Figure 1A) and they exhibit strong similarity in arrangement and orientation. Protein blast searches revealed that the genes of the WCS374 and WCS417 T3SS clusters encode proteins that are highly similar to components of T3SS systems described in other beneficial bacteria (Supplemental Figures S1 and S2). As shown in Figure 1, the T3SS gene clusters of WCS374 and WCS417 contain two regulatory proteins that are important for the expression of T3SS associated genes, *rspL* and *rspR* (Preston et al., 2001; Jackson et al., 2005), and nine genes representing core structural components of T3SS systems, *rscV, rscN, rcsQAB, rscR, rscS, rscT, rscU, rscC* and *rscJ* (Tampakaki et al., 2004). In addition to the regulatory and structural T3SS genes, the WCS417 gene cluster contains a gene that shares 79% identity to *ropE,* which codes for a putative effector protein in *P. fluorescens* SBW25 and has similarity with the AvrE effector of the bacterial pathogen *P. syringae* pv. *tomato* DC3000 (Preston et al., 2001; Mudgett, 2005). The WCS374 T3SS gene cluster does not contain this putative effector gene. Comparison of T3SS components of WCS374 and WCS417 gene clusters at protein level using BlastP and comparing components with the same function suggests that most of their components share a degree of similarity ranging from 30-97% (Supplemental Figure S3).

A number of methodologies including microscopy, crystallography and modelling have allowed the visualization of the structure of the T3SS in high resolution (Cornelis, 2010; Worrall et al., 2011). In Figure 2, we placed the proteins encoded by the identified conserved T3SS components of WCS374 and WCS417 as part of the T3SS injectisome, based on their homology with characterized components of this bacterial apparatus in *P. syringae* (Galan et al., 2014). It becomes apparent that the conserved components responsible for the outer ring structure (RscC), inner ring structure (RscJ) and the base of the T3SS apparatus (RscR, RscS,RscU, RscT, RscV) are present in both WCS374 and WCS417. Other conserved components such as the cytosolic ATPase (RscN) and sorting platform component (RscQAB), which are responsible for substrate recognition and initial formation of the apparatus, are also present in both T3SS gene clusters. The only differences between WCS374 and WCS417 are the presence of genes coding for the putative effector RopE and the cytoplasmic protein RspD in WCS417, and the needle filament component RspA (Galan et al., 2014), which is present in WCS374, but not in WCS417. In neither WCS417 nor WCS374, components involved in effector translocation such as RspZ were detected. Other non-conserved genes with a role in T3SS apparatus that could be identified in both bacterial T3SS clusters are *rspF*, *rspT*, *rspB*, *rspQ*, *rspO* and *rspE*. RspB is a component of the inner rod that connects the needle with the apparatus base, while RspQ is a component of the inner ring of the base. The function of RspO is uknown but is expected to function in the cytoplasm, together with RspE that functions in linking ATP to RscQAB. Finally, RspT interacts with RscC in the formation of the outer ring structure and RspF is involved in pore formation in the cell membrane of the host (Tampakaki et al., 2010; Galan et al., 2014).

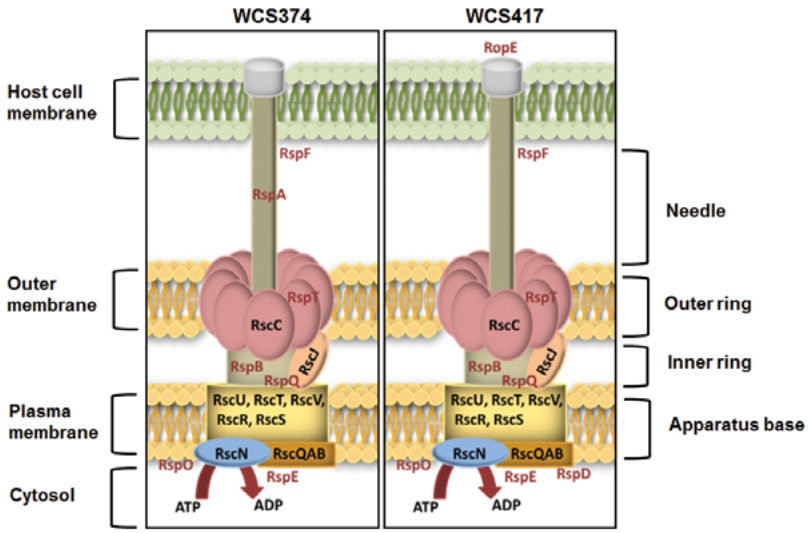

FIGURE 2. Schematic overview of T3SS-injection machineries of WCS347 and WCS417.
Conserved and non-conserved components of the T3SS-body were identified by BlastP and the encoded proteins are placed as parts of the T3SS injectisome, based on their *P. syringae* homologues (Galán et al., 2014). On the right of the figure the basic parts of T3SS body are indicated (apparatus base, inner ring, outer ring and needle). On the left, the cell compartments where the T3SS is spanning from including the bacterial cytosol, plasma membrane and outer membrane and the cell membrane of the host. Conserved components are indicated with black letters, and non-conserved with red letters.

Both WCS374 and WCS417 possess a *rspL* and a *rspR* gene in their T3SS gene cluster. In *P. fluorescens* SW25, RspL and RspR have a regulatory role in the expression of other genes present in a T3SS cluster (Preston et al., 2001). In the T3SS gene cluster of the pathogen *P. syringae,* comprised of the *hrp/hrc* genes, the RspR homologue HrpR and HrpS (no homologue found in WCS417 and WCS374) activate the expression of the *rspL* homologue *hrpL*, after which HrpL activates the expression of the *hrp*, *hrc* genes and the effector-encoding *avr* genes by binding to a conserved promoter motif, the "hrp box" (GGAACC-N15/16-CCACNNA), present in the promoter region of these genes (Tampakaki et al., 2010). The presence of this motif is a good indication for regulation of T3SS-related genes within a genome (Greenberg and Vinatzer, 2003). Manual examination of the WCS417 and WCS374 T3SS gene clusters revealed the existence of hrp box promoter elements upstream of *ropE*, *rspJ* and *rspG* in WCS417 and upstream of *rspJ* and *rspA* in WCS374 (Figure 3).

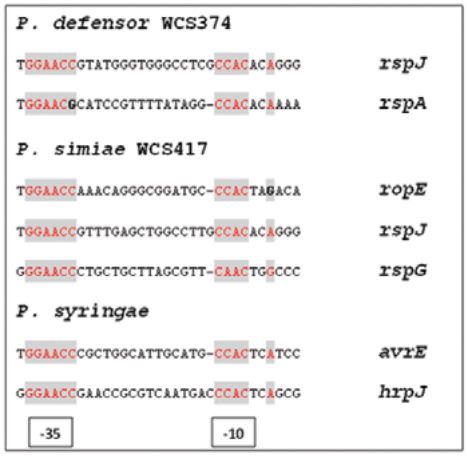

FIGURE 3. Structure and position of putative hrp boxes identified in WCS374 and WCS417 gene clusters.
Putative RspL- binding sites in genes present in the T3SS gene clusters of WCS417 and WCS374 found after manual examination in the promoter region upstream of the indicated genes. Conserved nucleotides are indicated with red letters and divergent nucleotides with bold letters. The box motif upstream of *ropE*, similarly to *avrE*, have a shorter spacer region of 15 nucleotides between the -35 and -10 sites.

Phylogenetic relationship of WCS374 and WCS417 T3SS with those of other beneficial and pathogenic *Pseudomonas* spp.

In order to investigate the relationship of WCS358, WCS374, and WCS417 with other *Pseudomonas* spp. strains, the concatenated sequences of the housekeeping genes 16*S rRNA, gyrB, rpoB,* and *rpoD* were compared to those of 107 *Pseudomonas* sp. type strains (Berendsen et al., 2015). On the basis of this analysis WCS358 was placed in the *P. putida* group, whereas WCS374 and WCS417 were placed in the *P. fluorescens* group of the phylogenetic tree of the *Pseudomonas* genus (Mulet et al., 2010). To analyze the phylogenetic relationship of the T3SS gene clusters of WCS374 and WCS417, we first built a phylogenetic tree based on the *16S rRNA* genomic sequence of WCS417 and WCS374 and those of the plant-beneficial *P. fluorescens* group species *simiae* R81, *P. fluorescens* SBW25, *P. defensor* SS101, *P. defensor* A506, *P. brassicacearum* F11, and *P. brassicacearum* Q8r1-96, and the phytopathogenic *P. syringae* group species *P. syringae* pv. *syringae* B728a, *P. syringae* pv. *phaseolicola* 1448a, and *P. syringae* pv. *tomato* DC3000. Neighbor-Joining (NJ) phylogeny was used to construct a tree depicting evolutionary distance between the different species, using the *16S rRNA* sequence from *Cellvibrio japonicus* strain Ueda 107 as an outgroup for our analysis (Figure 4). The resulting NJ phylogenetic tree contained a clade for the outgroup *C. japonicus*, a

clade with the pathogenic *P. syringae* species, and three clades with plant-beneficial *Pseudomonas* spp., i.e. *P. brassicacearum* spp., *P. simiae* and *P. fluorescens* spp., and *P. defensor* species, respectively (Figure 4A). In this analysis, the *P. brassicacearum* spp. are more closely related to pathogenic *P. syringae* spp. than to the other plant-beneficial *Pseudomonas* spp., confirming previous findings (Berendsen et al., 2015).

Next, we performed a similar phylogenetic analysis using the protein sequences of the conserved T3SS component HrcC (RscC in beneficial rhizobacteria) and the conserved effector AvrE (RopE in beneficial rhizobacteria). The NJ phylogenetic tree built with the conserved HrcC sequence revealed that there is a considerable evolutionary distance between the beneficial *Pseudomonas* species related to WCS374 and WCS417 and pathogenic *P. syringae* species (Figure 4B). Conversely, the HrcC sequence of the *P. brassicacearum* species is more closely related to those of the phytopathogenic *P. syringae* species (Figure 4B). The protein sequences of homologs of RopE could only be retrieved for the beneficial *Pseudomonas* spp. *P. fluorescens* SW25 and *P. simiae* WCS417 and R81. However, the evolutionary distance between the RopE sequences of the beneficial and pathogenic *Pseudomonas* spp. was similarly large as that for HrcC/RscC (Figure 4C).

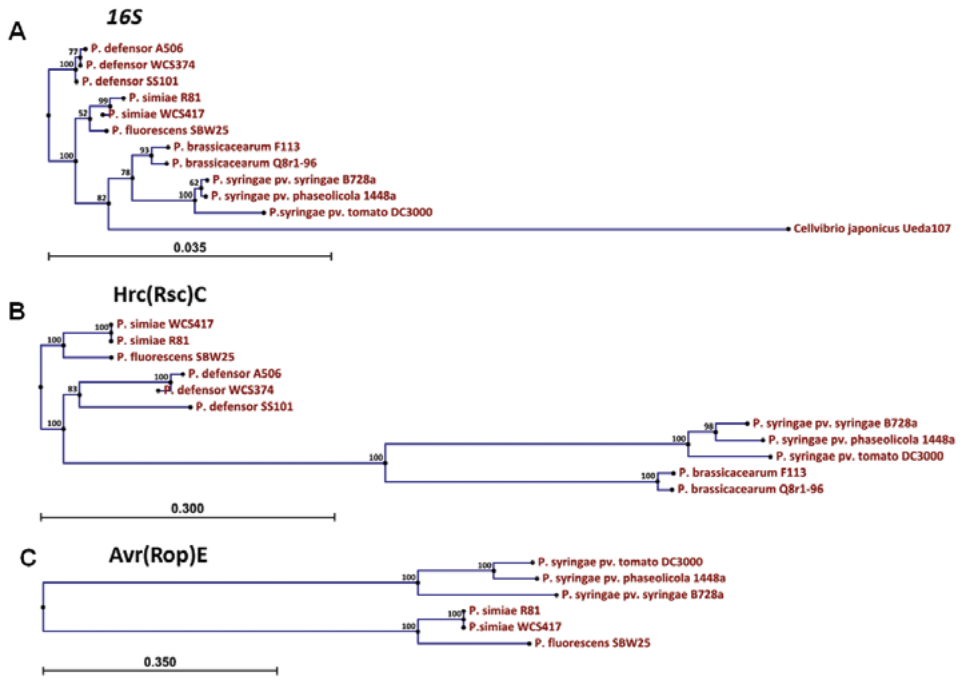

FIGURE 4. Phylogenetic relationship of WCS417 and WCS374 T3SS components with other beneficial and phytopathogenic *Pseudomonas* spp.

Neighbor-joining phylogenetic trees for aligned nucleotide sequence of *16S rRNA* **(A)** and protein sequences of Hrsc(Rsc)C **(B)** and Avr(Rop)E **(C)**. In the case of *16S rRNA* the evolutionary distance was calculated with Kimura 80 model, while evolutionary distance between protein sequences was estimated with Jukes-Cantor model. Numbers on nodes are calculated with bootstrap test using 1000 replicates. The length of branches is corresponding to the amount of changes in the time of evolution.

Then, we aligned the genome sequences of the whole T3SS gene clusters of the beneficial *Pseudomonas* spp. strains and that of the pathogen *P. syringae* pv. *tomato* DC3000 using Progressive Mauve (Figure 5). The color coding in this alignment indicates similarity between T3SS components of the clusters and the height of the peaks the level of similarity. Figure 5 shows that the T3SS gene clusters of the beneficial *Pseudomonas* spp. strains display a high degree of similarity, the degree of which is in line with the phylogenetic clustering displayed in Figure 4. The T3SS gene clusters of *P. defensor* strains WCS374, A506, and SS101 are highly similar. The same holds true for the T3SS gene clusters of the *P. simiae* strains WCS417 and R81. The T3SS gene cluster of *P. fluorescens* SBW25 differentiates from those of the *P. defensor* and *P. simiae* strains, but this is largely due to the presence of *ropE* at the beginning of the cluster (absent in the *P. defensor* strains), and the absence of a number of components that are present in the *P. defensor* and *simiae* strains (green region). Like *P. fluorescens* SBW25, the two *P. simiae* species (R81 and WCS417) contain the genomic region encoding *ropE* (purple region located in the first 4000 bp). This genomic region in the T3SS clusters of WCS417 and R81 is followed by a genomic region of ~4000 bp that is not present in the other species (light blue region). The remaining part of the T3SS gene cluster of WCS417 and R81 is quite similar to that of the *P. defensor* strains WCS374, SS101 and A506. We included *P. brassicacearum* species in this analysis due to their intermediate phylogenetic distance between the *defensor* and *simiae* strains and the phytopathogenic ones (Berendsen et al., 2015). Only some parts of the T3SS gene clusters found in the *P. brassicacearum* species F113 and Q8r1-96 aligned with the other beneficial *Pseudomonas* spp. strains. These clusters contain regions (first 7000 bp, 14500-16000 bp, 18000-20500 bp, 26000-29000 bp) that are not detected in the other beneficial *Pseudomonas* spp. strains. The T3SS gene cluster of *P. syringae* pv. *tomato* DC3000 is significantly longer than those of the beneficial *Pseudomonas* spp. strains and only few genomic regions aligned with the T3SS gene clusters of the beneficial *Pseudomonas* spp. (Figure 5).

FIGURE 5. Similarity of WCS417 and WCS374 T3SS gene clusters with other beneficial and phytopathogenic *Pseudomonas* spp.
Gene clusters were identified in available sequenced genomes of beneficial and phytopathogenic *Pseudomonas* spp. Progressive Mauve was used to align the clusters and find regions exhibiting high similarity. Similar colors correspond to similar genomic regions in a cluster. The height of peaks in each cluster depicts the degree of similarity in regions present in T3SS clusters of different *Pseudomonas.* spp.

Identification of putative effector proteins in WCS417 and WCS374

From the computational analysis presented above, *ropE* was identified in the WCS417 T3SS gene cluster as a gene encoding a putative secreted effector. However, genes encoding secreted effector proteins are not always in the genomic proximity of the T3SS gene cluster and can be scattered around the genome (Peters et al., 2007). A common method to identify type III effectors in bacterial genomes is by searching for genes that have conserved Hrp(Rsp) "box motifs" in their promoter regions (Figure 6). This hrp box is defined by the following sequence: xGGAACx[$N_{15\text{-}16}$]CCACxxAG and the space between the motif and the regulated gene varies from 30 -300 bp (Zwiesler-Vollick et al., 2002). By screening the genomes of WCS374 and WCS417 for such hrp box motifs, we identified 62 and 73 genes encoding putative secreted effector proteins, respectively. In a next step, we analyzed their N-terminal protein sequence for characteristics typical of T3SS-secreted proteins (i.e., abundance of Ser and polar residues, one acidic residue in the first 12 positions, and an aliphatic amino acid in position 3 or 4; Guttman et al., 2002; Petnicki-Ocwieja et al., 2002). This extra step resulted in a final list of 15 putative effectors for WCS374 and 11 putative effectors for WCS417 (Figure 7).

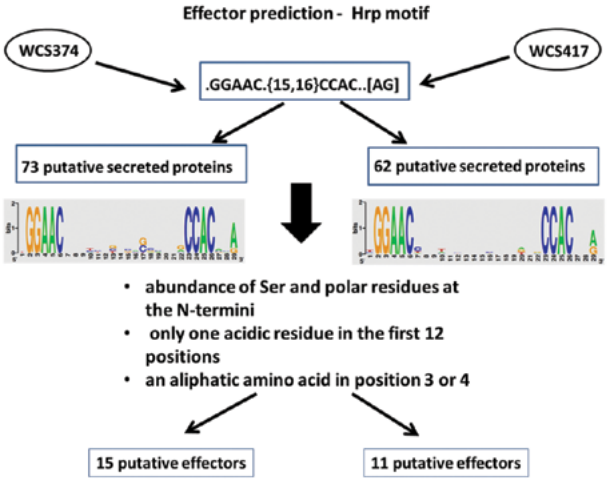

FIGURE 6. Workflow for the identification of putative effectors in the genome of WCS417 and WCS374.
Genomes of WCS374 and WCS417 were searched for the presence of hrp box motif in gene promoter regions. The candidates found by the hrp box search were further screened for characteristics of their protein, typical of T3SS-effectors. These characteristics were searched in the first 50 aa of the N-terminal region.

A BlastP search with the protein sequences of these putative effectors (Figure 7) revealed that the putative effectors of WCS374 were quite similar with previously identified effectors of *P. defensor* A506 (Loper et al., 2012), while putative effectors of WCS417 displayed high homology with proteins identified in *P. simiae* R81. Among the identified putative effectors are proteins previously characterized as T3SS-secreted effectors such as RopE (Preston et al., 2001), ExoU and HopJ. ExoU is a type III-delivered toxin of *P. aeruginosa* associated with bacterial spreading and lung injury in humans and animals (Finck-Barbancon et al., 1997). HopJ is a T3SS-secreted effector with high degree of conservation among beneficial and pathogenic *Pseudomonas* spp. (Lindeberg et al., 2005; Trantas et al., 2015). However, the majority of the WCS417 and WCS374 effectors show no homology to previously identified effectors.

A. *P. defensor* WCS374

Locus tag	Gene name	% G+C	Hrp box			Protein length (aa)	N-terminal residues			
			Presence	position	sequence		Serines	Acidic	Polar	Aliphatic
PD374_10455		57.4	Yes	-72	A**GGAACT**GATTCCGACGCAAAA**CCAC**ACA	339	9	1	27	yes
PD374_10460		63.1	Yes	-211	A**GGAACG**AATTACGCCCATTTG**CCAC**AGA	55	3	1	21	yes
PD374_10465		59.4	Yes	-97	C**GGAACT**GCCGAGTTCCTCCAA**CCAC**ACA	305	8	1	25	yes
PD374_12660		56.8	Yes	-223	T**GGAACC**ACAGGGCGAGTGGCGA**CCAC**GCA	97	2	2	25	no
PD374_06830		57	Yes	-67	T**GGAACC**ATCTTCATTCGTACG**CCAC**AGA	78	7	0	22	yes
PD374_06915		51.3	Yes	-84	G**GGAACC**TTTTTTTCAGGCTTG**CCAC**AGA	79	6	0	21	yes
PD374_25750	ExoU	60.2	No			639	8	1	25	yes
PD374_26065		63.4	Yes	-380	A**GGAACT**GGTGTCCGCGGCTT**CCAC**CAA	496	8	1	23	no
PD374_20980		55.2	Yes	-44	T**GGAACG**CCCAACGCCCCTTGCG**CCAC**GCA	365	7	1	24	yes
PD374_23045	HopJ	58.7	No			112	2	1	22	yes
PD374_21415		62.2	Yes	-924	A**GGAACA**GTTCGCCGCCCAGGC**CCAC**GGA	177	7	0	19	no
PD374_17010		54.6	Yes	-98	A**GGAACT**TTTCCGACCGCCTGG**CCAC**GCA	376	5	0	26	no
PD374_23880		51.7	Yes	-158	T**GGAACT**TTACCTACAGCATCA**CCAC**TCA	949	3	3	24	no
PD374_10035		53.5	Yes	-36	A**GGAACG**GCCTCCACCCGTAACA**CCAC**ATA	575	6	1	30	no
PD374_10025		51.5	Yes	-36	C**GGAACG**GTTTCGTCAGGCCCG**CCAC**ATA	499	7	0	23	no

B. *P. simiae* WCS417

Locus tag	Gene name	% G+C	Hrp box			Protein length (aa)	N-terminal residues			
			Presence	position	sequence		Serines	Acidic	Polar	Aliphatic
PS417_09765		54.3	Yes	-94	C**GGAACC**GTTGTTTCCTGTGCA**CCAC**TCA	303	4	0	22	yes
PS417_12720		55.2	Yes	-76	T**GGAACC**TTACGAAGTGCCAAG**CCAC**TTA	2133	4	0	28	yes
PS417_12770		56.8	Yes	-52	A**GGAACC**CCACTCCACAAGAGG**CCAC**ACA	94	2	1	27	no
PS417_13220		67.1	Yes	-373	T**GGAACC**CGCGCCTGCACGCC**CCAC**GGG	239	4	0	21	yes
PS417_20780		55.8	Yes	-684	C**GGAACT**GGTTGGCCGAGAAA**CCAC**GGG	155	2	0	21	yes
PS417_03420	ropE	59.9	Yes	-34	T**GGAACC**AAACAGGGCGGATGC**CCAC**TAG	1432	3	1	25	no
PS417_06035		55.4	Yes	-60	C**GGAACC**GGCCGGGTGCGCTCA**CCAC**AGA	114	5	0	22	yes
PS417_06040		51.8	Yes	-32	T**GGAACC**GCTTTGACTTAAATG**CCAC**ATA	64	0	1	25	yes
PS417_07390		58.7	Yes	-67	T**GGAACC**TTTTTTCAAGGGGCT**CCAC**GCA	1169	4	0	19	yes
PS417_26495	ExoU	60	No			643	2	0	25	yes
PS417_23510	HopJ	60.8	No			112	2	2	23	yes

FIGURE 7. Lists of putative type III secreted effectors found in WCS374 (A) and WCS417 (B).
Putative T3SS effectors identified in the genomes of WCS417 and WCS374 after searching for the presence of hrp box motif in their promoter region and N-terminal characteristics typical of T3SS-effectors (abundance of Ser and polar residues, one acidic residue in the first 12 positions, and an aliphatic amino acid in position 3 or 4). Putative effectors were also identified with BlastP, based on their similarity with previously characterized bacterial effectors (i.e ExoU, HopJ). The figure contains information for each putative T3SS effector such as locus tag, gene name, % G+C, presence, position and sequence of the putative Hrp box and characteristics of N-terminal residues.

WCS374 and WCS417 do not trigger an HR in tobacco

Previously Preston et al. (2001) tested whether *P. fluorescens* SBW25 could elicit HR upon infiltration in leaves of different plant hosts. In a first test to study whether the T3SSs of WCS374 and WCS417 secrete functional effector proteins, we infiltrated these rhizobacteria in the leaves of *Nicotiana tabacum* and *Nicotiana benthamiana*. In case an *R* gene is present in tobacco plants that could recognize effector molecules of these bacteria, then an hypersensitive response (HR) could be observed. To test this, we grew our bacteria in the presence or absence of exudates aiming to induce the activation of T3SS (Anderson et al., 2014). In a next step, we infiltrated *N. benthamiana* and *N. tabacum* leaves with two bacterial concentrations (OD_{600}: 0.1 and 1) and tested for HR symptoms after 2 d.

As shown in Figure 8, the beneficial rhizobacteria didn't elicit HR symptoms, unlike DC3000 which induced a visible and clear HR in all plants and concentrations tested. From this experiment, it seems that either none of WCS374/WCS417 effectors are recognized by these plants or that the system is not specific for root-inhabiting microbes. Further studies, employing T3SS mutants and heterologous expression systems could demonstrate the functionality of these secretion machineries.

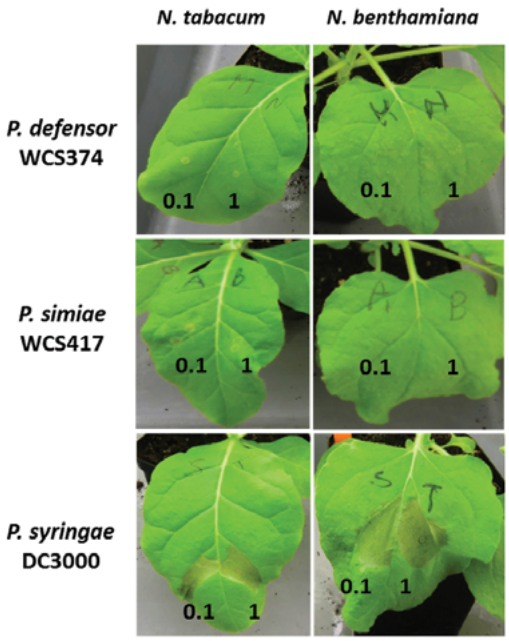

FIGURE 8. WCS374 and WCS417 are unable to elicit HR symptoms in tobacco leaves.
Leaves of *N. tabacum* (left side) and *N. benthamiana* (right side) were infiltrated with a bacterial suspension at OD_{600}: 0.1 and 1, using a 1-ml blunt-ended syringe. Bacteria were grown in MS with exudates, MS without exudates, $MgSO_4$ with exudates and $MgSO_4$. In the pictures, infiltrations are shown which were performed with bacteria grown in MS with exudates (all other growth media gave similar results). *P. syringae* DC3000 was used as a positive control. Photographs of symptoms were taken at 2 d after infiltration.

Discussion

Selected root-inhabiting microbes are known to provide their plant hosts with benefits such as growth promotion, facilitation of nutrient uptake, and biological control of root-infecting pathogens (Zamioudis and Pieterse, 2012). Among these beneficial microbes, specific *Pseudomonas* species are extensively studied for their ability to trigger broad-spectrum ISR (Pieterse et al., 2014). The establishment of this plant defense mechanism requires colonization of plant roots by ISR-triggering microbes in high population densities (Raaijmakers et al., 1995). Additionally, the ability of beneficial *Pseudomonas* spp. to trigger ISR is host specific (Leeman et al., 1996; Berendsen et al., 2015). These characteristics of ISR suggest that specific microbial functions contribute to the suppression of host immunity, allowing the beneficial microbe to colonize its host in a host-microbe genotype specific manner. Since the T3SS-secreted effectors of phytopathogenic bacteria provide such host-selective microbial functions (Alfano and Collmer, 2004), we aimed at investigating the T3SSs of the three well-studied ISR-inducers *P. simiae* WCS417, *P. defensor* WCS374 and *P. capeferrum* WCS358 (Pieterse et al., 2014). The recent genomic elucidation of these strains by Berendsen and associates (2015) showed that WCS374 and WCS417 contain a T3SS in their genome, whereas WCS358 does not. In the present study, we show that the genomes of WCS417 and WCS374 possess most of the components of a functional T3SS. The T3SS genes of WCS417 and WCS374 reside in clusters of 26 and 18 kb, respectively, and share strong similarities in their organization and orientation (Figure 1). The T3SS gene clusters of these rhizobacteria contain each more than 20 genes, encoding structural and regulatory proteins of T3SS (Supplemental Figures S1 and S2). The first T3SS in a beneficial *Pseudomonas* spp. was described for *P. fluorescens* SBW25 (Preston et al., 2001), which was present in a 20-kb genomic region. Since then, several other T3SS gene clusters of saprophytic plant-associated *Pseudomonas* spp. have been identified, all located in a genomic region ranging between 18 and 28 kb (Loper et al., 2012). In phytopathogenic *Pseudomonas* spp., HrpR and HrpS proteins regulate the expression of *hrpL,* encoding alternative sigma factor HrpL, which is required for the activation of genes encoding components of the T3SS (Xiao et al., 1994; Jovanovic et al., 2011). The T3SS clusters of WCS417 and WCS374 both possess the *hrpL* and *hrpR* homologues *rspL* and *rspR*, but, like *P. fluorescens* SBW25 (Preston et al., 2001), lack a homologue of *hspS* (Figure 1). HrpL recognizes a specific hrp box sequence present in the promoter region of the genes it regulates (Tampakaki et al., 2010). Our analysis of the WCS374 and WCS417 genomes revealed the existence of such motifs upstream of genes present in the T3SS clusters of both bacteria, suggesting RspL-dependent regulation of T3SS components (Figure 3), as was already suggested for SBW25 (Jackson et al., 2005) and *P. syringae* (Xiao and Hutcheson, 1994). Most of the components identified in the T3SS clusters in this study correspond to proteins responsible for the formation of intracellular parts of the T3SS-injection machinery as well as for the formation of the ring structures (Figure 2). In other plant-beneficial *Pseudomonas* spp., such as *P. brassicacearum* Q8r1-96 and *P. fluorescens* 2P24, additional proteins responsible for pilus and pore formation were identified in the T3SS cluster (Mavrodi et al., 2011; Liu et al., 2015b). Proteins responsible for needle formation were detected only in the case of WCS374 (RspA) but not in WCS417, while no proteins associated with effector translocation could be found in the T3SS clusters of WCS374 and WCS417 (Figure 2). All these findings together suggest that both WCS417 and WCS374 have T3SS gene clusters containing all components for its activation but also for the formation of an apparatus that could potentially deliver effector molecules.

Phylogenetic analysis using the highly conserved T3SS protein sequence RscC revealed that the T3SS of WCS417 and WCS374 are evolutionary different from those of the plant-beneficial bacterium *P. brassicacearum* Q8r1-96 (Mavrodi et al., 2011) and phytopathogenic *Pseudomonas* species (Figure 4). Neighbor joining phylogeny of the conserved T3SS component RscC and RopE effector protein placed WCS417 in the same clade with its close relative *P. simiae* R81 and *P. fluorescens* SBW25, while RscC phylogeny placed WCS374 in a different clade together with *P. defensor* A506 and *P. defensor* SS101 (Figure 4). These phylogenetic relationships are in line with those obtained by Berendsen et al. (2015) who aligned the concatenated sequences of the housekeeping genes *16S rRNA*, *gyrB*, *rpoB*, *rpoD*. Moreover, alignment of whole T3SS clusters with Progressive Mauve (Figure 5) further supported the phylogenetic observations. In that case not only one gene but the whole cluster was compared in terms of homology and organization and it became apparent that WCS417 possesses a cluster representative of *simiae* species, while WCS374 a cluster representative of *defensor* species. On the other hand, the phylogenetically distant *brassicacearum* species (Q8r1-96 and F113) have larger clusters resembling more the T3SS of *Pst* DC3000 than those of the other beneficial *Pseudomonas* spp.

In a next step, we looked whether putative effectors could be identified in the genomes of WCS417 and WCS374, following the workflow presented in Figure 6. This methodology allowed us to predict the existence of 15 and 11 putative effectors in WCS374 and WCS417, respectively (Figure 7). In other beneficial *Pseudomonas* spp., the number of putative effectors following prediction ranged between 4 to 16 (Loper et al., 2012). Most of the proteins identified in this study are novel and couldn't be linked to known effector families (Figure 7). One exception is the prediction of RopE in WCS417, which resides in the T3SS gene cluster of WCS417 next to rspL transcriptional regulator and shares similarity with T3SS secreted protein AvrE from *P. syringae* (Preston et al., 2001). AvrE proteins are major virulence factors in plant pathogenic bacteria, and they have been found to target salicylic-acid mediated defense responses in plants, facilitating like that infection of the host (DebRoy et al., 2004; Ham et al., 2009). Moreover, proteins ExoU and HopJ were found in both bacteria and are known to be T3SS-secreted in other systems (Finck-Barbancon et al., 1997; Lindeberg et al., 2005). The activity of T3SS and the effector molecules delivered via this secretion machinery could have various roles either in microbe-microbe or plant-microbe interactions. Both pathogenic and beneficial microbes need to modulate host defense responses to establish an interaction with their host (Zamioudis and Pieterse, 2012). In PGPR *P. fluorescens* SBW25, expression of conserved T3SS components like *rscC* gene was observed in the rhizosphere of sugar beet plants (Rainey, 1999). Nodulation in some legume species can happen independently of rhizobial Nod-factors, but through the activity of T3SS (Okazaki et al., 2013; Okazaki et al., 2016b). The role of T3SS is also demonstrated in mycorrhization, since T3SS-harboring bacteria (among them *P. fluorescens* species) are enriched in the rhizospheres of plants forming symbiosis either with ectomycorrhizal fungus (EMF) *Laccaria proxima* or arbuscular mycorrhizal fungi (AMF) (Warmink and Van Elsas, 2008; Viollet et al., 2011). More recently, Viollet *et al.* (2017) demonstrated that a T3SS mutant of *P. fluorescens* C7R12 couldn't promote root colonization of *Medicago truncatula* by AMF. Additionally, effectors of PGRP *P. brassicacearum* Q8r1-96 can suppress plant immune response when injected in tobacco leaves (Mavrodi et al., 2011). The presence of T3SS in rhizosphere-inhabiting bacteria suggests their possible involvement in local suppression of root immune responses facilitating like that root colonization by the PGPR or its interacting partner (AMF).

Finally, we aimed to test whether both rhizobacteria could trigger local immune responses in leaves of tobacco following their infiltration. Hypersensitive response (HR) is an indication of activated plant resistance locally at the site of the infection, due to the recognition of effector molecules delivered by bacterial pathogens (Mur et al., 2008). However, no visible HR symptoms were observed in leaves of both *N. benthamiana* and *N. tabacum* (Figure 8). Similar observations were made in other beneficial Pseudomonas strains (Preston et al., 2001; Liu et al., 2015b). The explanation in this case could be that either the system of study is not optimal, since we infiltrated leaves with rhizosphere-specific microbes and expression of T3SS is lower, or that the secreted molecules are not recognized by the hosts tested (Preston et al., 2001). Additionally, the role of T3SS present in PGPR bacteria could have a role before plant colonization, when bacteria need to compete with other bacterial or fungal species for the same niches (Rezzonico et al., 2005) or in suppressing local root immune responses (Millet et al., 2010; Mavrodi et al., 2011). Elucidation of the role of T3SS and putative effector molecules found in WCS417 and WCS374 could be achieved either by generating bacteria defective in T3SS activation or by employing heterologous systems for effector delivery (Mavrodi et al., 2011; Liu et al., 2015b).

To sum up, our data confirm the presence of T3SS gene clusters in the beneficial PGPR rhizobacteria *P. simiae* WCS417 and *P. defensor* WCS374, but no genes corresponding to T3SS function were found in *P. capeferrum* WCS358. Moreover, components of the T3SS gene clusters from WCS417 and WCS374 exhibit high phylogenetic similarity with other beneficial rhizobacteria, but are distinct compared to phytopathogenic *P. syringae*. Identification of putative effector molecules was possible in WCS417 and WCS374, but further study could explain the role of T3SS clusters and T3SS-secreted proteins in these beneficial rhizobacteria and their involvement in ISR-host specificity and rhizosphere competence.

Materials and methods

Bioinformatic analysis

For the bioinformatics analyses, we used the genomes of *P. simiae* WCS417, *P. defensor* WCS374 and *P. capeferrum* WCS358 described previously (Berendsen et al., 2015). To locate the T3SS gene clusters, we performed BlastP search in the predicted proteome of WCS417, WCS374 and WCS358, using protein sequences of T3SS conserved components previously identified in the T3SS gene cluster of *P. aeruginosa* (Yahr and Wolfgang, 2006). To identify the functions of T3SS components we searched in National Center of Biotechnology Information (NCBI) database for protein sequences with the highest similarity. Alignments and phylogenetic trees were created with CLC main Workbench 6.9 (CLCbio, Aarhus, Denmark) using the neighbor joining algorithm and 1000 bootstrap replicates. T3SS cluster alignments and comparison was performed with progressive MAUVE 2.4.0 (Darling et al., 2010).

Collection of root exudates

A. thaliana accession Col-0 seeds were surface sterilized and sown on agar-solidified 1x Murashige and Skoog (MS) medium supplemented with 0.5% sucrose (Murashige and Skoog, 1962). After 2 d of stratification at 4°C, the Petri dishes were positioned vertically and transferred to a growth chamber (22°C; 10 h light: 14 h dark; light intensity: 100 μmol m^{-2} s^{-1}). Five days after germination, seedlings were transferred to 6-well plates containing 1x MS supplemented with 0.5% sucrose and kept growing for 7 d. When 12 d old, plants were removed and the remaining growth medium containing the root exudates was filtered (0.22 μM) and stored at −20°C.

Cultivation of bacteria and leaf infiltration assay

P. simiae WCS417 and *P. defensor* WCS374 were cultured at 28°C on King's medium B (KB; (King et al., 1954)) agar plates supplemented with 50 μg ml^{-1} of rifampicin. After 24 h of growth, cells were collected in 10 mM $MgSO_4$, washed twice by centrifugation for 5 min at 5000 *g* and finally resuspended in 10 mM $MgSO_4$. Next, overnight bacterial cultures were initiated with a starting density of OD_{600} = 0.5 (5 x10^8 colony-forming units (cfu) per mL) in MS with root exudates (1:1), MS without root exudates (1:1), $MgSO_4$ with root exudates (1:1) and $MgSO_4$ without root exudates (1:1). The next day, growth of bacteria in these substrates was determined and bacterial densities were adjusted to OD_{600} = 0.1 and 1, after resuspension in 10 mM $MgSO_4$. Subsequently, bacterial suspensions were infiltrated in leaves of 5-week-old *N. tabacum* and *N. benthamiana* plants using a 1-ml syringe without a needle. Leaves were visually checked for symptoms of an hypersensitive response (HR) 2 d after infiltration. As a positive control for HR induction, tobacco leaves were infiltrated with *P. syringae* pv. *tomato* DC3000.

Acknowledgements

This work was supported by ERC Advanced Grant no. 269072 of the European Research Council (to CMJP).

Supplemental data

Gene name	Function	Position	Protein length (aa)	e-value	Closest protein
PS417_03420	ropE	784645…788943	1432	0	putative type III secreted protein [*P. fluorescens* SBW25] - AvrE
PS417_03430	methyltransferase type 11	789520…790326	666	0	type 11 methyltransferase [*Pseudomonas* sp. R81]
PS417_03435	cytochrome P450	790323...792323	25	0	cytochrome P450 [*Pseudomonas* sp. R81]
PS417_03450	rspL	793158...793709	183	3.00E-113	sigma factor [*P. fluorescens* SBW25]
PS417_03455	rspJ	793973...795037	354	2.00E-156	type III secretion regulator RspJ [*P. fluorescens* A506]
PS417_03460	rscV	795034...797127	697	0	type III secretion protein RscV [*Pseudomonas* sp. R81]
PS417_03465	rspQ	797162...798061	299	5.00E-151	type III secretion protein RspQ [*P. fluorescens*]
PS417_03470	rscN	798058...799416	452	0	type III secretion ATP synthase RscN [*P. fluorescens* A506]
PS417_03475	rspO	799403...799831	142	2.00E-60	rspO - nodulation-related hypothetical protein [*P. fluorescens* SBW25]
PS417_03480	rspP	799828...800286	152	3.00E-46	rspP - nodulation-related hypothetical protein [*P. fluorescens* SBW25]
PS417_03485	rscQAB	800283...801296	337	0	rscQ - putative type III secretion protein [*P. fluorescens* SBW25]
PS417_03490	rscR	801293...801946	217	4.00E-135	type III secretion protein HrcR [*P. fluorescens* BBc6R8]
PS417_03495	rscS	801954...802217	87	8.00E-51	type III secretion protein RscS [*Pseudomonas* sp. R81]
PS417_03500	rscT	802228...803016	262	1.00E-152	type III secretion system rscT [*P. fluorescens* WH6]
PS417_03505	rscU	803013...804110	365	0	RscU [*P. fluorescens*]
PS417_03510	rspV	804111...804449	112	3.00E-73	type III secretion system negative regulatory protein RspV [*P. fluorescens*]
PS417_03515	rspT	804461...804664	67	1.00E-35	putative type III secretion lipoprotein [*P. poae* RE*1-1-14]
PS417_03520	rscC	804661...806802	713	0	RscC [*P. fluorescens*]
PS417_03525	rspG	806817...807209	130	3.00E-24	type III secretion protein RspG [*P. synxantha* BG33R]
PS417_03530	rspF	807211...807429	72	1.00E-45	hypothetical protein O204_03835 [P. fluorescens EGD-AQ6]
PS417_03535	rspE	807504...808115	203	5.00E-143	type III secretion apparatus protein RspE [*Pseudomonas* sp. R81]
PS417_03540	rspD	808118...808675	185	4.00E-130	type III secretion protein [*P. fluorescens* EGD-AQ6]
PS417_03545	rscJ	808668...809489	273	5.00E-63	type III secretion apparatus lipoprotein RscJ [*Pseudomonas* sp. R81]
PS417_03550	rspB	809496...809858	120	2.00E-79	putative type III secretion protein [*Pseudomonas* sp. R81]
PS417_03555	rspR	810332...811258	308	2.00E-138	putative type III secretion system, regulatory protein [*Pseudomonas* sp. Ag1]

Supplemental Figure S1. Components of T3SS in the genome of *P. simiae* WCS417.
Genes of WCS417 encoding a T3SS protein were identified based on their BlastP similarity with T3SS components of *P. aeruginosa*. For these genes putative function, their position in the genome, the length of the protein they encode and the e-value of their similarity with their closest protein match are presented.

Gene name	Function	Position	Protein length (aa)	e-value	Closest protein
EL30_03545	rspL	827057…827608	183	1.00E-132	RNA polymerase sigma factor RspL [*P. fluorescens* A506]
EL30_03550	rspJ	827873…828937	354	0	Type III secretion regulator RspJ [*P. fluorescens* A506]
EL30_03555	rscV	828934…831027	697	0	type III secretion protein RscV [*P. fluorescens* A506]
EL30_03560	rspQ	831065…831964	299	0	type III secretion apparatus protein, YscD/HrpQ family [Pseudomonas sp. CF150]
EL30_03565	rscN	831961…833319	452	0	type III secretion ATP synthase RscN [*P. fluorescens* A506]
EL30_03570	rspO	833306…833734	142	6.00E-88	type III secretion protein RspO [*P. fluorescens* A506]
EL30_03575	rspP	833731…834189	152	2.00E-100	type III secretion protein RspP [*P. fluorescens* A506]
EL30_03580	rscQ	834186…835199	337	0	putative type III secretion protein [Pseudomonas sp. CF150]
EL30_03585	rscR	836196…835849	217	8.00E-149	type III secretion protein RscR [*P. fluorescens* A506]
EL30_03590	rscS	835857…836120	87	2.00E-50	type III secretion protein RscS [*P. fluorescens* A506]
EL30_03595	rscT	836131…836919	262	0	type III secretion protein SpaR/YscT/HrcT [Pseudomonas sp. CF150]
EL30_03600	rscU	836916…838013	365	0	putative type III secretion protein [Pseudomonas sp. CF150]
EL30_03605	rspV	838014…838364	116	3.00E-77	type III secretion system negative regulatory protein RspV [*P. fluorescens* A506]
EL30_03615	rscC	838576…840717	713	0	type III secretion outer membrane protein RscC [*P. fluorescens* A506]
EL30_03620	rspG	840732…841124	130	3.00E-86	type III secretion protein RspG [*P. fluorescens* A506]
EL30_03625	rspF	841125…841340	71	3.00E-43	type III secretion protein RspF [*P. fluorescens* A506]
EL30_03630	rspE	841431…842024	197	1.00E-139	type III secretion apparatus protein RspE [*P. fluorescens* A506]
EL30_03635	rscJ	842597…843397	266	0	type III secretion apparatus lipoprotein RscJ [*P. fluorescens* A506]
EL30_03640	rspB	843400…843765	121	1.00E-83	type III secretion apparatus protein RspB [*P. fluorescens* A506]
EL30_03645	rspA	843883…844107	74	3.00E-44	type III secretion apparatus protein RspA [*P. fluorescens* A506]
EL30_03650	rspS	844351…845274	307	0	type III secretion system transcriptional regulator RspS [*P. fluorescens* A506]

Supplemental Figure S2. Components of T3SS in the genome of *P. defensor* WCS374.
Genes of WCS374 encoding a T3SS protein were identified based on their BlastP similarity with T3SS components of *P. aeruginosa*. For these genes putative function, their position in the genome, the length of the protein they encode and the e-value of their similarity with their closest protein match are presented.

WCS417			WCS374			BlastP	
Gene name	**Function**	**Protein length (aa)**	**Gene name**	**Function**	**Protein length**	**e-value**	**Identities**
PS417_03420	ropE	1432					
PS417_03430	methyltransferase type 11	666					
PS417_03435	cytochrome P450	25					
PS417_03450	rspL	183	EL30_03545	rspL	183	2.00E-78	62%
PS417_03455	rspJ	354	EL30_03550	rspJ	354	8.00E-166	69%
PS417_03460	rscV	697	EL30_03555	rscV	697	0	91%
PS417_03465	rspQ	299	EL30_03560	rspQ	299	4.00E-157	76%
PS417_03470	rscN	452	EL30_03565	rscN	452	0	94%
PS417_03475	rspO	142	EL30_03570	rspO	142	5.00E-71	77%
PS417_03480	rspP	152	EL30_03575	rspP	152	2.00E-72	68%
PS417_03485	rscQAB	337	EL30_03580	rscQ	337	0	73%
PS417_03490	rscR	217	EL30_03585	rscR	217	1.00E-136	89%
PS417_03495	rscS	87	EL30_03590	rscS	87	8.00E-59	97%
PS417_03500	rscT	262	EL30_03595	rscT	262	3.00E-152	83%
PS417_03505	rscU	365	EL30_03600	rscU	365	0	86%
PS417_03510	rspV	112	EL30_03605	rspV	116	4.00E-36	55%
PS417_03515	rspT	67					
PS417_03520	rscC	713	EL30_03615	rscC	713	0	54%
PS417_03525	rspG	130	EL30_03620	rspG	130	7.00E-12	35%
PS417_03530	rspF	72	EL30_03625	rspF	71		
PS417_03535	rspE	203	EL30_03630	rspE	197	1.00E-20	31%
PS417_03540	rspD	185					
PS417_03545	rscJ	273	EL30_03635	rscJ	266	6.00E-45	35%
PS417_03550	rspB	120	EL30_03640	rspB	121	4.00E-01	80%
			EL30_03645	rspA	74		
PS417_03555	rspR	308	EL30_03650	rspR	307	4.00E-77	43%

Supplemental Figure S3. BlastP similarity between T3SS components of WCS417 and WCS374.
Genes of WCS417 and WCS374 as detected based on their BlastP similarity withT3SS components of *P. aeruginosa*. For these genes putative function, the length of the protein they encode and the e-value of their similarity and the percentage of matching are presented.

CHAPTER 4

The role of MYB72-dependent root exudation of coumarins in microbiome assembly

Ioannis A. Stringlis[1,#], Ke Yu[1,#], Kirstin Feussner[2,#], Ronnie de Jonge[1,3,4], Sietske Van Bentum[1], Marcel C. Van Verk[1], Roeland L. Berendsen[1], Peter A.H.M. Bakker[1], Ivo Feussner[2,5], and Corné M.J. Pieterse[1]

[1] Plant-Microbe Interactions, Department of Biology, Faculty of Science, Utrecht University, 3508 TB Utrecht, the Netherlands
[2] Department of Plant Biochemistry, Albrecht-von-Haller-Institute for Plant Sciences, University of Goettingen, 37077 Goettingen, Germany
[3] Department of Plant Systems Biology, VIB, Technologiepark 927, 9052 Ghent, Belgium
[4] Department of Plant Biotechnology and Bioinformatics, Ghent University, Technologiepark 927, 9052 Ghent, Belgium
[5] Department of Plant Biochemistry, Goettingen Center for Molecular Biosciences (GZMB), University of Goettingen, 37077 Goettingen, Germany

[#] These authors contributed equally

Abstract

Plant roots nurture a tremendous diversity of microbes via exudation of photosynthetically fixed carbon sources into the rhizosphere. In turn, beneficial members of the root microbiome promote plant growth and protect the host plant against pathogen and insect attack. In the *Arabidopsis thaliana-Pseudomonas simiae* WCS417 model system, the root-specific transcription factor MYB72 and the MYB72-controlled β-glucosidase BGLU42 emerged as important regulators of rhizobacteria-induced systemic resistance (ISR) and iron uptake responses. Under conditions of iron limitation, MYB72 regulates the biosynthesis of iron-mobilizing fluorescent phenolic compounds after which the activity of BGLU42 is required for their excretion into the rhizosphere. Using metabolite fingerprinting by UPLC-ESI-TOF-MS, we identified the antimicrobial coumarin scopoletin as a dominant metabolite that is produced in the roots and excreted into the rhizosphere in a MYB72- and BGLU42-dependent manner. We show that scopoletin impacts the performance of the soil-borne fungal pathogens *Fusarium oxysporum* and *Verticillium dahliae*, while the ISR-inducing rhizobacterial strains *P. simiae* WCS417 and *Pseudomonas capeferrum* WCS358 are highly tolerant. Shotgun-metagenome sequencing of root-associated microbiota of Col-0, *myb72,* and the scopoletin biosynthesis mutant *f6'h1* revealed that scopoletin significantly impacts the assembly of the microbial community in the rhizosphere. Collectively, our results point to a scenario in which plants and beneficial rhizobacteria join forces to trigger MYB72- and BGLU42-dependent scopoletin production and excretion to outcompete scopoletin-sensitive microbes in the rhizosphere and to prime plant immunity.

Introduction

Plant roots exude a significant proportion of their photosynthetically fixed carbon into the rhizosphere (Bais et al., 2006). As a result, the rhizosphere constitutes one of the richest environments on Earth, containing up to 10^{11} microbial cells per gram of root (Mendes et al., 2011; Berendsen et al., 2012). The microbial community that inhabits the root-soil interface is called the root microbiome. Root exudates greatly influence the composition of the root microbiome, which is typically different from that in bulk soil, a phenomenon called the rhizosphere effect (Hiltner, 1904; Berendsen et al., 2012; Bulgarelli et al., 2013). Besides detrimental pathogens, the root microbiome also harbors beneficial members that promote plant growth or stimulate plant health (Berendsen et al., 2012; Raaijmakers and Mazzola, 2016; Hacquard et al., 2017). Such mutualistic microbes can serve plants in acquiring water and nutrients, in fixing nitrogen, in suppressing soil-borne pathogens, or in stimulating plant immunity (Berendsen et al., 2012; Bulgarelli et al., 2013; Pieterse et al., 2016).

Selected plant growth-promoting rhizobacteria (PGPR) can trigger an induced systemic resistance (ISR) that is effective against a broad range of foliar pathogens and even insect herbivores (Pieterse et al., 2014). ISR is well-studied in the interaction between *Arabidopsis thaliana* (Arabidopsis) and the PGPR *Pseudomonas simiae* WCS417 (formerly known as *P. fluorescens* WCS417; (Berendsen et al., 2015)). WCS417-ISR in Arabidopsis functions independently of the defense hormone salicylic acid (SA), but instead requires a functional response to the plant hormones ethylene and jasmonic acid (JA) (Pieterse et al., 1998; Pieterse et al., 2014). In the absence of a pathogen, WCS417-ISR-expressing leaves do not display abundant transcriptional changes (Verhagen et al., 2004). However, upon pathogen or insect attack, ISR-expressing leaves develop an accelerated, primed defense response that is associated with enhanced resistance (Verhagen et al., 2004; Pozo et al., 2008; Van Oosten et al., 2008; Martinez-Medina et al., 2016). In contrast to foliar tissues, WCS417-colonized roots show abundant transcriptional changes (Verhagen et al., 2004; Pozo et al., 2008; Zamioudis et al., 2014; Stringlis et al., 2017). Amongst the WCS417-induced genes, the root-specific R2R3-type MYB transcription factor gene *MYB72* emerged as a central regulator for the onset of ISR (Verhagen et al., 2004; Van der Ent et al., 2008). *MYB72* is also induced in Arabidopsis roots in response to colonization by the ISR-inducing fungi *Trichoderma asperellum* T-34 and *Trichoderma harzianum* T-78 (Martinez-Medina et al., 2017). Knockout *myb72* mutants are unable to mount ISR upon colonization of the roots by WCS417 or *T. asperellum* T-34 (Van der Ent et al., 2008; Segarra et al., 2009), suggesting that MYB72 plays a central role in the regulation of ISR triggered by different root-associated microbes. Downstream of MYB72 action in Arabidopsis roots, the β-glucosidase BGLU42 was identified as an important player in the onset of ISR. Constitutive overexpression of *BGLU42* resulted in enhanced systemic disease resistance against *Botrytis cinerea, Pseudomonas syringae,* and *Hyaloperonospora arabidopsidis*, while mutant *bglu42* was blocked in the ability to mount WCS417-ISR (Zamioudis et al., 2014).

Besides being essential for the onset of ISR, MYB72 emerged as an integral part of the plant's adaptive strategy to iron deficiency. Together with its closest paralog MYB10, MYB72 is essential for plant survival in alkaline soils where iron availability is largely restricted (Palmer et al., 2013). Under iron-limiting conditions, *MYB72* is strongly induced in the roots of Arabidopsis as part of a set of coordinated responses

that is collectively referred to as the Strategy I iron deficiency response, which boosts iron mobilization and uptake from the soil environment (Colangelo and Guerinot, 2004; Buckhout et al., 2009; Kobayashi and Nishizawa, 2012). The core of the Strategy I response consists of acidification of the rhizosphere by the activity of the H^+-ATPase AHA2 (Santi and Schmidt, 2009), which increases the concentration of soluble ferric iron (Fe^{3+}). Fe^{3+} is subsequently reduced to ferrous iron (Fe^{2+}) by FERRIC REDUCTION OXIDASE2 (FRO2), after which it is transported from the soil environment into root cells via IRON-REGULATED TRANSPORTER1 (IRT1) (Eide et al., 1996; Robinson et al., 1999). The basic helix-loop-helix transcription factor FIT (FER-LIKE IRON DEFICIENCY TRANSCRIPTION FACTOR) is a central regulator of the iron uptake response (Colangelo and Guerinot, 2004) and also regulates the expression of *MYB72* (Zamioudis et al., 2015).

During iron deprivation, plant roots also exude a whole suite of secondary metabolites into the rhizosphere that aids in the mobilization and uptake of iron. These metabolites include phenolics, organic acids, flavins, and flavonoids (Rodriguez-Celma et al., 2013; Fourcroy et al., 2014; Schmid et al., 2014). In Arabidopsis roots, MYB72 is required for the biosynthesis of iron mobilizing fluorescent phenolic compounds, while the β-glucosidase BGLU42 is important for their subsequent excretion into the rhizosphere (Zamioudis et al., 2014). These so-called coumarins are synthesized via FERULOYL-COA 6 -HYDROXYLASE1 (F6'H1) in the phenylpropanoid pathway and are excreted from Arabidopsis roots by the iron deficiency–regulated ABC transporter PLEIOTROPIC DRUG RESISTANCE9 (PDR9) (Rodriguez-Celma et al., 2013; Fourcroy et al., 2014; Schmid et al., 2014; Fourcroy et al., 2016). Knockout mutants *myb72* and *bglu42* are both impaired in the excretion of iron-mobilizing coumarins and in the ability to mount rhizobacteria-mediated ISR, suggesting a mechanistic link between the iron deficiency response and plant immunity (Zamioudis et al., 2014; Verbon et al., 2017).

Interplay between plant immunity and plant responses to nutrient deficiencies was also demonstrated for the phosphate starvation response (PSR) (Hiruma et al., 2016; Castrillo et al., 2017). Interestingly, phosphate-starved plants release metabolites into the rhizosphere that are also exuded during conditions of iron deficiency (Ziegler et al., 2016; Tsai and Schmidt, 2017). Plants responding to changes in their biotic or abiotic environment, show changes in root exudation patterns (Dakora and Phillips, 2002; Carvalhais et al., 2013), which in turn affects the composition of the root-associated microbiome (Bais et al., 2006; Reinhold-Hurek et al., 2015). Mutations in the SA-, JA- or phosphate starvation signaling pathways also significantly impact the composition of the root-associated microbial community (Carvalhais et al., 2015; Lebeis et al., 2015; Castrillo et al., 2017). Hence, the picture is emerging that components of the plant immune system and the plant's adaptive response to nutrient starvation are interlinked in influencing the assembly of the root-associated microbiome and vice versa. However, the molecular mechanisms and ecological and evolutionary advantage of this apparent relationship are largely unknown.

In this study, we aimed to gain detailed insight into the interplay between the exudation of MYB72-dependent metabolites into the rhizosphere and the root-associated microbiome. We performed a metabolite fingerprinting analysis (UPLC-ESI-TOF MS) of root extracts and exudates of wild-type Col-0 and mutant *myb72* and *bglu42* plants. We identified the coumarin scopoletin as a major metabolite that in response to iron deficiency is produced and excreted into the rhizosphere in a MYB72-BGLU42-dependent

manner. Scopoletin possesses antimicrobial activity (Valle et al., 1997; Chong et al., 2002) and was previously linked to disease resistance in different plant species (Kim et al., 2000; Shimizu et al., 2000; El Oirdi et al., 2010; Sun et al., 2014). We show that scopoletin inhibits growth of two soil-borne fungal pathogens in vitro, but has little or no effect on growth of two beneficial ISR-inducing rhizobacteria. Metagenome analysis of microbiota associated with roots of Col-0 plants and roots of the scopoletin biosynthesis mutant *f6'h1* shows that this antimicrobial and iron-mobilizing coumarin plays a role in the assembly of the root-associated microbiome. Collectively, our results suggest that MYB72-BGLU42-mediated production and excretion of scopoletin is part of a positive feed forward loop that favors the interaction between plant roots and beneficial members of the root microbiome.

Results

Metabolite fingerprinting of root exudates

In Arabidopsis roots, MYB72 is required for the biosynthesis of iron mobilizing fluorescent phenolic compounds, while BGLU42 has a role in their subsequent excretion into the rhizosphere (Zamioudis et al., 2014). Under iron starvation conditions, Col-0 roots exuded high quantities of fluorescent phenolic compounds (Figure 1A) and activated the iron deficiency marker genes *FRO2, IRT1, MYB72,* and *F6'H1* (Figure 1B). Mutant *myb72* did not exude detectable levels of the fluorescent compounds, while in *bglu42* their exudation was significantly impaired, confirming previous findings (Zamioudis et al., 2014). To identify the metabolites that were synthesized and secreted from Arabidopsis roots in a MYB72- and BGLU42-dependent manner, we analyzed the metabolome of root exudates of wild-type Col-0 and mutant *myb72* and *bglu42* plants. Therefore, plants were grown under iron-sufficient and iron-deficient conditions and the root exudates were analyzed by metabolite fingerprinting UPLC-ESI-TOF-MS (Supplemental Data S1). Principal component analysis (PCA) of the exudate profiles of 722 high-quality metabolite features (false discovery rate (FDR) <0.001) indicates that the metabolite pattern in the exudates of the different genotypes grown under iron-sufficient conditions are largely similar (Figure 1C). In contrast, the metabolite patterns in root exudates of iron-starved plants were clearly different from those of iron-sufficient plants. The root exudate profiles of iron-starved *myb72* clearly separated from those of iron-starved Col-0 and *bglu42*, indicating that the metabolite profile of *myb72* root exudates is markedly different from that of Col-0 and *bglu42*.

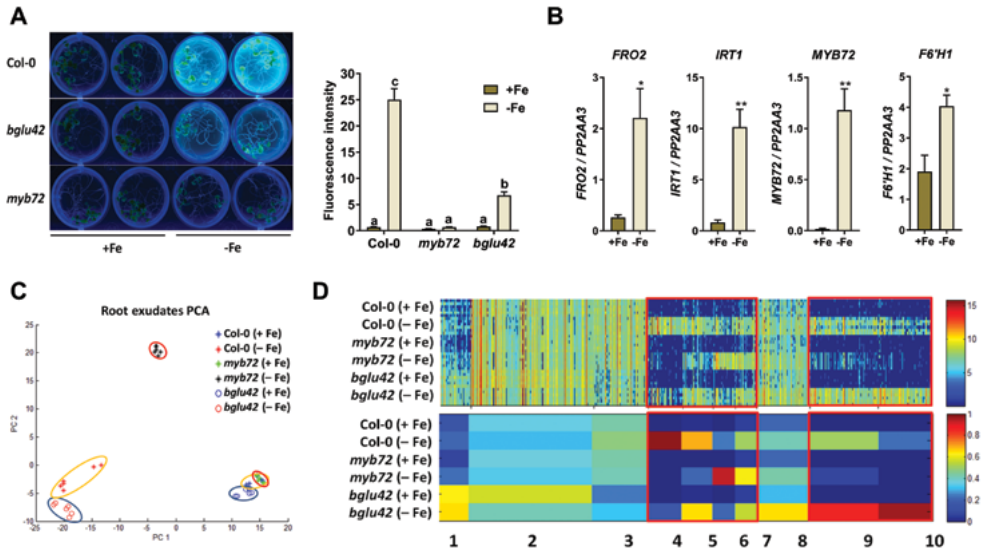

FIGURE 1. Iron deficiency-induced changes and metabolite fingerprinting of root exudates of Col-0, *myb72* and *bglu42* grown under iron sufficient and iron starvation conditions.

(A) Accumulation and secretion of fluorescent phenolic compounds of 20-d-old Col-0, *myb72* and *bglu42* plants grown in Hoagland medium with (+Fe) or without (-Fe) iron. Visualization of fluorescence was achieved under UV light (365 nm). Fluorescence intensity was quantified in a 96-well microplate reader (excitation: 360nm; emission: 528 nm) after removal of the seedlings from the growth medium. Different letters indicate statistically significant differences (Two-way ANOVA, Tukey's test, $P < 0.05$). **(B)** Gene expression profiles of the iron-deficiency marker genes *FRO2, IRT1, MYB72,* and *F6'H1* in roots of 20-d-old Col-0 plants grown in Hoagland medium with (+Fe) or without (-Fe) iron, quantified by qRT-PCR. Transcript levels were normalized to that of reference gene *PP2AA3* (At1g13320). Data are means of 3 biological replicates. Error bars represent SE. Asterisks indicate statistically significant differences between treatments (Student's *t*-test,$^{**}P < 0.001$;$^{*}P < 0.05$). **(C)** PCA plot of root exudates of 20-d-old Col-0 (encircled in yellow), *myb72* (encircled in red) and *bglu42* (encircled in blue) plants grown in Hoagland medium with (+Fe) or without (-Fe). Data were obtained by metabolite fingerprinting (UPLC-ESI-TOF-MS analysis in positive and negative ionization mode). **(D)** 1D-SOM clustering and prototype assignment of 722 high-quality metabolite features (FDR <0.001) derived from positive as well as negative ionization mode of the metabolite fingerprinting analysis. The number of features assigned to one prototype determines its width. The raw intensity of individual features (top panel) and prototypes (bottom panel) mostly affected by iron deficiency are highlighted in the red box. Heatmaps correspond to the intensity of each individual feature (top panel) and the average intensity of each cluster/prototype (bottom panel). Color key reflects range of signal intensities. Three biological replicates per treatment were used for analysis.

To obtain a global overview of the metabolite features and their relative abundances in the root exudates, we clustered the profiles of the 722 high-quality metabolite features by one-dimensional self-organizing maps (1D-SOMs; (Kaever et al., 2009; Kaever et al., 2015)), which organized the intensity profiles in 10 clusters (prototypes) (Figure 1D). Analogous to the PCA plot, the intensity profiles of the metabolite features of Col-0, *myb72* and *bglu42* grown under iron-sufficient conditions are highly similar. For all three genotypes, the iron starvation treatment changed the metabolome of root exudates, which resulted in increased signal intensities, most strikingly visible in clusters 4-7 and 9-10. Clusters 1-3 and 8 represent features with a rather indifferent intensity profile or with only a weak accumulation in the *bglu42* mutants. Cluster 4 represents features that highly accumulated in exudates of Col-0 plants, while cluster 6 and 10 show features mainly enriched in *myb72* or *bgu42* exudates, respectively. The metabolite features of clusters 5 and 9 show clearly lower intensities for iron-starved *myb72* than for iron-starved Col-0 and *blgu42*. Collectively, these results indicate that MYB72 affects the composition of the root exudate metabolite profile under conditions in which the iron deficiency response is activated.

Exudation of MYB72- and BGLU42-dependent metabolites under iron deficiency

To determine the identity of the MYB72- and BGLU42-dependent metabolites in the root exudates of iron-starved Arabidopsis plants, we generated a subset of metabolome data from root exudates of iron-deprived Col-0, *myb72,* and *bglu42* plants (Supplemental Data S2) with 311 high-quality metabolite features (FDR<0.001). The intensity profiles of these 311 features were clustered by means of 1D-SOMs and organized into five prototypes (Figure 2A). Metabolite features in clusters 1, 2 and 5 showed clearly lower intensities in *myb72* than in Col-0, suggesting that during iron deficiency the abundance of the corresponding metabolites increased in Col-0 root exudates in a MYB72-dependent manner. Of these MYB72-dependent clusters, the metabolite features of prototype 1 were also depleted in *bglu42,* suggesting that the corresponding MYB72-dependent metabolites are excreted in a BGLU42-dependent manner.

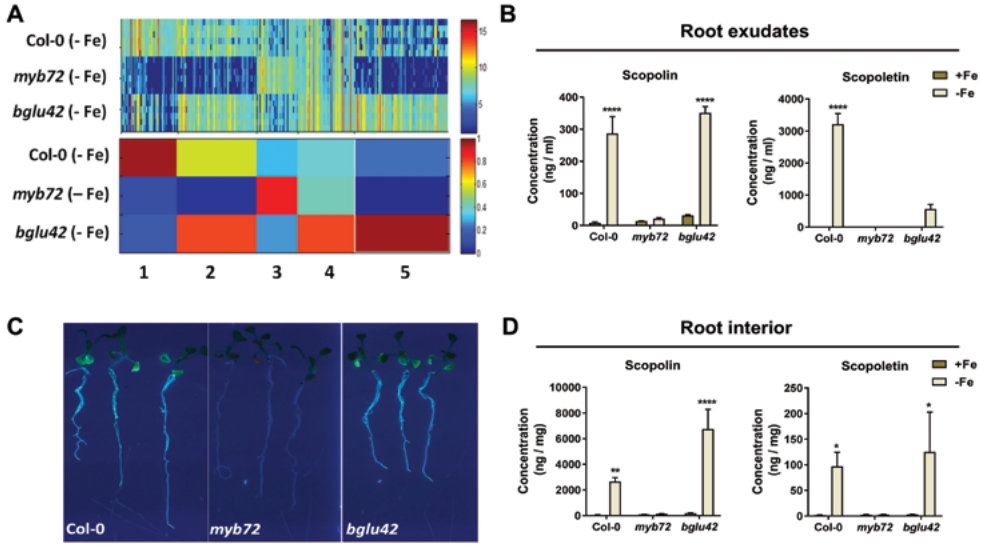

FIGURE 2. MYB72- and BGLU42-dependent metabolites in exudates and roots of iron-starved Col-0, *myb72,* and *bglu42* plants.

(A) 1D-SOM clustering and prototype assignment of 311 high-quality metabolite features (FDR <0.001) in root exudates of iron-starved Col-0, *myb72,* and *bglu42* plants. The number of features assigned to one prototype determine its width. Heatmaps correspond to the intensity of each individual feature (top panel) and the average intensity of each cluster/prototype (bottom panel). Color key reflects range of signal intensities. For details on metabolite features see Supplementary Table S2. **(B)** HPLC quantification of scopolin and scopoletin in root exudates of Col-0, *myb72* and *bglu42* grown under iron-sufficient (+Fe) and iron-starved (-Fe) conditions. The shown data are means of 3 replicates of the pooled root exudates of 50-60 plants per replicate. Error bars represent SE. Asterisks indicate statistically significant differences between the iron conditions within a genotype (Two-way ANOVA, Sidak's test; $****P < 0.0001$; $**P < 0.01$; $*P < 0.05$). **(C)** Photographs of iron-starved Col-0, *myb72,* and *bglu42* plants that had been grown in 12-well plates with liquid Hoagland medium without iron. Visualization of fluorescent phenolic compounds was achieved under UV light (365 nm). **(D)** HPLC quantification of scopolin and scopoletin in the root interior of Col-0, *myb72* and *bglu42* grown under iron-sufficient and iron-starved conditions. The shown data are means of 3 replicates of the pooled root extracts of 130 plants per replicate. Error bars represent SE. Asterisks indicate statistically significant differences between the iron conditions within a genotype (Two-way ANOVA, Sidak's test; $****P < 0.0001$; $**P < 0.01$; $*P < 0.05$).

Amongst the MYB72-dependent metabolite features that are depleted in the root exudates of iron-starved *myb72*, we identified features matching with coumarins that were previously found to play a role in iron

mobilization and uptake from alkaline substrates (Rodriguez-Celma et al., 2013; Fourcroy et al., 2014; Schmid et al., 2014). The intensity profiles of the coumarins scopolin, scopoletin, esculin, esculetin and isofraxidin (Supplemental Figure S1) show that they all strongly increase in root exudates of iron-starved Col-0 (with scopoletin being the most abundant one), while they are depleted in root exudates of iron-starved *myb72*. High-resolution MS/MS analysis confirmed the identity of the coumarins (Supplemental Figure S2). Of these MYB72-dependent coumarins, only scopoletin levels were reduced in the root exudates of iron-starved *bglu42* plants.

Quantification of scopolin and its aglycone scopoletin by HPLC confirmed the pattern of the non-targeted metabolite fingerprinting approach (Figure 2B). Scopoletin was significantly increased in abundance in root exudates of iron-starved Col-0 plants, while it was undetectable or strongly reduced in root exudates of the *myb72* and *bglu42,* respectively. Figure 2B shows that also the glycosylated form of scopoletin, scopolin, accumulated in a MYB72-dependent manner in the exudates of iron-starved roots, albeit at 10-fold lower levels than scopoletin (note: compare scales of Y-axes). However, the *bglu42* mutation had no effect on the iron-starvation-induced levels of scopolin. Collectively, these results show that scopoletin is the major MYB72- and BGLU42-dependent metabolite that is secreted by roots of iron-starved Arabidopsis plants.

Besides coumarins, also the coumarin precursor phenylalanine and the citric acid cycle-related organic acids citrate, malate and succinate increased in abundance in root exudates of iron-starved Col-0 plants (Supplemental Figures S1 and S2), confirming previous findings (Fourcroy et al., 2014; Schmidt et al., 2014). However, their excretion was not dependent on MYB72 and BGLU42, so they were not further analyzed in this study.

Role of BGLU42 in excretion of scopoletin

BGLU42 encodes a β-glucosidase that belongs to glycoside hydrolase (GH) family 1 (Xu et al., 2004). Previously, it was shown that GH family 1 members BGLU21, BGLU22 and BGLU23 can hydrolyze scopolin, resulting in the production of scopoletin (Ahn et al., 2010). Glycosylation and deglycosylation can change phenylpropanoid solubility, stability and toxic potential, as well as influence their compartmentalization and biological activity (Le Roy et al., 2016). While *myb72* plants are blocked in the ability to produce fluorescent phenolic compounds in their roots, iron-starved *bglu42* roots still accumulate significant amounts (Figure 2C). Hence, we hypothesized that if BGLU42 activity facilitates the excretion of scopoletin, then iron-starved *bglu42* mutant plants should accumulate high levels of the glycosylated form scopolin within their roots. To test this, we characterized the metabolic profiles of the polar and non-polar extractions of the root interior of Col-0, *myb72* and *bglu42* plants grown under iron-sufficient and iron-starved conditions by UPLC-ESI-TOF-MS (Supplemental Data S3 and S4). Similar to what was observed for the root exudates, the polar fraction of the extracts of the root interior of Col-0, *myb72,* and *bglu42* plants grown under iron-sufficient and iron-starved conditions showed distinct metabolome profiles in terms of iron treatment and plant genotype (Supplemental Figure S3A). Like observed in the root exudates, metabolite features related to iron-mobilizing coumarins were abundantly present in the polar extracts of the root interior, with scopolin, scopoletin and esculin being the most abundant ones (Supplemental Figure S3, and Supplemental Figure S4). Scopolin, scopoletin and esculin were produced within the roots in a MYB72-dependent manner, while

BGLU42 did not negatively impact their abundance in the root interior (Figure 2D and Supplemental Figure S3C). Scopolin even increased to higher levels in the root interior of iron-starved *bglu42* plants compared to Col-0, supporting the notion that BGLU42-mediated deglycosylation of scopolin and the subsequent excretion of scopoletin is impaired in this mutant. As opposed to root exudates of iron-starved Col-0 plants, where scopoletin levels were 10-fold higher than that of scopolin (Figure 2B), within the root interior of iron-starved Col-0 plants scopoletin levels were 25-fold lower than those of scopolin (Figure 2D). Collectively, these results indicate that roots of iron-starved Col-0 plants produce the coumarins scopolin and scopoletin in a MYB72-dependent manner and that BGLU42 activity is important for deglycosylation of scopolin and subsequent excretion of the aglycone scopoletin into the rhizosphere.

In addition to the polar fraction, we also analyzed the non-polar fraction of the extracts of the root interior of Col-0, *myb72,* and *bglu42* plants grown under iron-sufficient or iron-starved conditions (Supplemental Data S4). However, this analysis didn't yield any further information regarding the roles of MYB72 and BGLU42 in the production of coumarins via the phenylpropanoid pathway (Supplemental Figure S3B) and will not be further discussed. Moreover, analysis of the metabolome profiles of roots and root exudates of Col-0, *myb72,* and *bglu42* yielded multiple additional metabolites that were produced or excreted in either a MYB72 or a BGLU42-dependent manner, but because they were not clearly impaired in both the *myb72* and the *bglu42* mutant background, they are not further described in this study.

Differential antimicrobial effect of scopoletin on soil-borne microbes

Induction of *MYB72, BGLU42* and genes of the coumarin biosynthesis pathway is also associated with the onset of rhizobacteria-mediated ISR in Arabidopsis roots (Zamioudis et al., 2014; Zamioudis et al., 2015). Hence, we wondered what would be the role of coumarin excretion for the beneficial interaction between ISR-inducing PGPR and the plant. Previously, scopoletin was shown to possess antimicrobial activity, so we first tested its effect on the growth of the ISR-inducing PGPR *P. simiae* WCS417 and *P. capeferrum* WCS358 (Berendsen et al., 2015). To this end, we tested the effect of scopoletin on in vitro growth of WCS417 and WCS358, using a range of scopoletin concentrations (Sun et al., (2014)) and the antibiotic tetracyclin as a positive control (Figure 3A and 3B). While tetracyclin prevented growth of both WCS417 and WCS358, scopoletin had no (WCS417) or very limited (WCS358) effect on growth of both PGPR. Additionally, we tested the effect of scopoletin on growth of the soil-borne fungal pathogens *Fusarium oxysporum* f.sp. *raphani* and *Verticillium dahliae* JR2, using the fungicide Delvo®Cid as a positive control (Figure 3C and 3D). Scopoletin concentrations of 500 μM and higher inhibited growth of both fungi in vitro. Since we detected scopoletin concentrations of up to 3000 $ng.ml^{-1}$ (~15 μM) in the growth medium of iron-starved Col-0 (Figure 2B), it is realistic that in the much more concentrated root exudates scopoletin reaches concentrations of over 500 μM. Together, these results indicate that scopoletin has a differential antimicrobial effect to which the tested soil-borne fungal pathogens *F. oxysporum* f.sp. *raphani* and *V. dahliae* JR2 are sensitive, while the PGPR *P. simiae* WCS417 and *P. capeferrum* WCS358 are not.

To further investigate the activity of scopoletin on fungal physiology and growth, we assessed the effect of 500 μM scopoletin on *F. oxysporum* f.sp. *raphani* radial growth on PDA plates. Scopoletin reduced radial growth of the fungus (Figure 3E). Moreover, scopoletin inhibited the formation of pigment in the mycelial

mat (Figure 3E). Metabolites involved in fungal pigmentation can be associated with protection against abiotic stresses or competition with other microbes (Medentsev et al., 2005; Son et al., 2008), indicating that scopoletin potentially exerts its effect on multiple determinants of fungal performance.

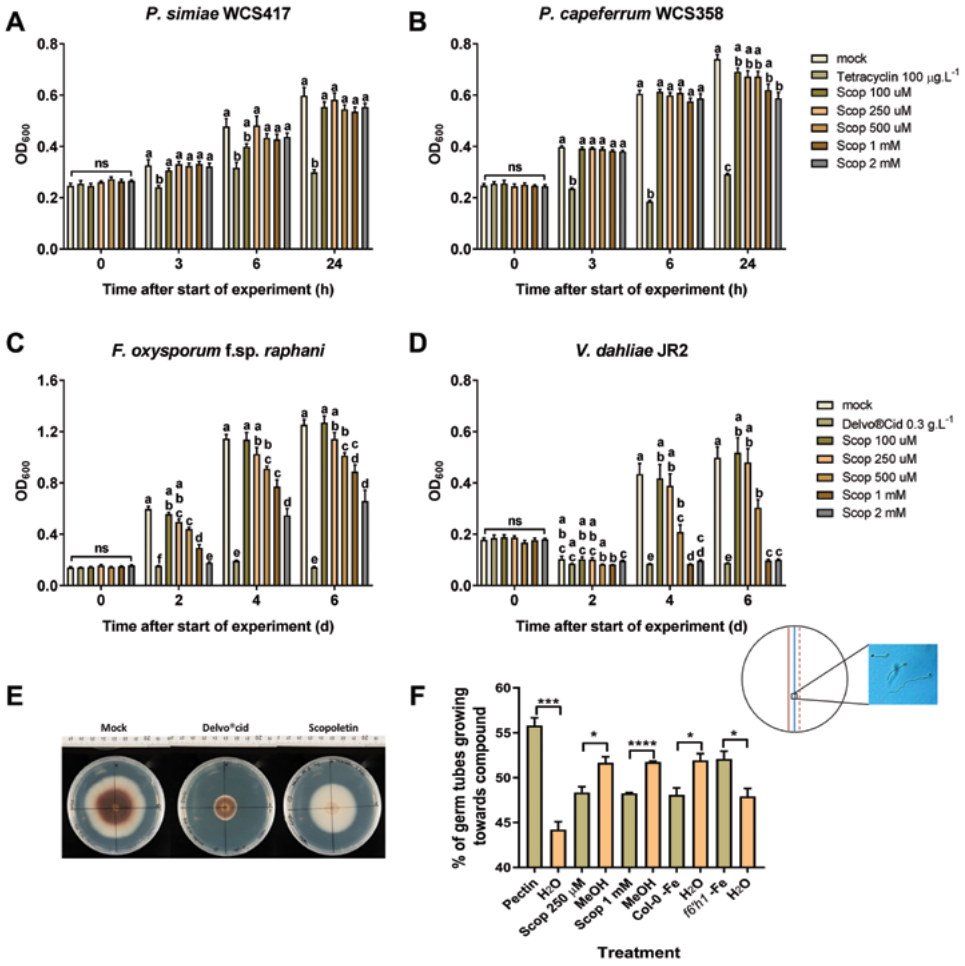

FIGURE 3. Differential effect of scopoletin on bacterial and fungal growth.
Graphs show growth (OD_{600}) of *P. simiae* WCS417 (**A**), *P. capeferrum* WCS358 (**B**), *F. oxysporum* f.sp. *raphani* (**C**) and *V. dahliae* JR2 (**D**) under different scopoletin (Scop) concentrations. Tetracyclin and Delvo®Cid were used as positive controls for bacteria and fungi, respectively. Growth measurements were performed over a period of 24 h (bacteria) or 6 d (fungi). The shown data are means of 8-10 replicates. Error bars represent SE. Different letters represent statistically significant differences between treatments (Two-way ANOVA, Tukey's test; $P < 0.05$). (**E**) Growth of *F. oxysporum* f.sp. *raphani* mycelium on PDA plates supplemented with 0.2 $g.L^{-1}$ of the fungicide Delvo®cid or 500 µM of scopoletin. Pictures were taken of representative plates after 7 d of fungal growth at 28°C. (**F**) Chemotropism of *F. oxysporum* f.sp. *raphani* spores towards pectin (1 % (w/v)), scopoletin (250 µM and 1 mM) and root exudates of iron-starved Col-0 and *f6'h1* plants. Chemotropism was evaluated as percentage of the germinating spores growing towards the tested compound or its solvent. Pectin was used as a positive control. Shown are the mean percentages of three replicates per treatment, each based on hyphal orientation counts of ca. 900 conidia. Error bars represent the standard error of the mean. Asterisks indicate statistically significant differences between treatments (Student's *t*-test, $****P < 0.0001$; $***P < 0.001$; $*P < 0.05$). The inset provides a representation of the chemotropism test of Turra et al. (2015), in which the orientation of hyphal growth was tested on the blue, middle line, with the solvent on the red line and the test compound on the dashed line. The photo is a representative image of germinating *Fusarium* spores at the moment of scoring.

To investigate the effect of scopoletin in root exudates on *F. oxysporum* f.sp. *raphani* hyphal growth, we performed a chemotropism assay (Turrà et al., (2015) with root exudates of iron-starved Col-0 and scopoletin biosynthesis mutant *f6'h1* plants (Kai et al., 2008; Schmid et al., 2014), increasing concentrations of scopoletin, and pectin as a positive control. Figure 3F shows that fungal hyphae from germinating conidia are chemotropically attracted towards pectin, confirming previous findings (Turrà et al., 2015). Both concentrations of scopoletin deterred the fungal hyphae, which preferentially grew away from scopoletin. Root exudates of iron-starved Col-0 plants, which exude large amounts of scopoletin (Figure 1), similarly deterred the fungal hyphae. Conversely, root exudates of iron-starved *f6'h1* plants significantly attracted the fungal hyphae. Together, these results indicate that scopoletin in root exudates can have a multifaceted negative effect on the performance of scopoletin-sensitive microbes in the rhizosphere.

Shotgun metagenome analysis of the root microbiomes of Col-0, *myb72* and *f6'h1*

In Arabidopsis roots, beneficial rhizobacteria such as *P. simiae* WCS417 and *P. capeferrum* WCS358 induce *MYB72* (Zamioudis et al., 2015), which in turn leads to the activation of coumarin biosynthesis genes (Zamioudis et al., 2014). On the one hand, this benefits the host plant because activation of the MYB72 gene regulatory module in the roots systemically stimulates host immunity. On the other hand, it may benefit scopoletin-insensitive microbes because MYB72-dependent production and exudation of scopoletin can suppress other microbes that compete for the same niche in the rhizosphere. To investigate the role of scopoletin in the assembly of the root microbiome, we analysed the metagenomes of the root-associated microbiomes of Col-0, *myb72,* and the scopoletin biosynthesis mutant *f6'h1,* which does not produce fluorescent phenolic compounds upon colonization of the roots by WCS417 (Figure 4A). Arabidopsis seedlings were first grown in vitro under iron-sufficient or iron-starved conditions to verify their coumarin-exudation status at the start of the experiment. As expected, iron-starved Col-0 seedlings exuded large amounts of fluorescent phenolic compounds, while *myb72* and *f6'h1* seedlings did not (Figure 4B). Subsequently, the plants were transplanted into natural Reijerscamp soil (Berendsen et al., 2017) that was limed to maintain iron limitation. At the moment of transplanting, *MYB72, FRO2* and *IRT1* were strongly induced in the roots of iron-starved seedlings. Their induced expression levelled off over time, but was still detectable at day 3 after transplanting (Figure 4C). To verify the speed by which the roots become colonized in the limed Reijerscamp soil, we mixed WCS417 bacteria through a separate batch of soil and monitored WCS417 colonization of Col-0 roots over time (Figure 4D). Already within one day, the density of WCS417 bacteria in the rhizosphere increased 10-fold in comparison to that in unplanted bulk soil. This 10-fold increase in WCS417 abundance was similar for the rhizospheres of the iron-sufficient and the iron-starved seedlings and was maintained for the 7-d period of monitoring. Together, these results show that the roots of the transplanted Arabidopsis seedlings expressed the iron deficiency response during the first days of growth in the Reijerscamp soil, and that the roots were rapidly colonized by soil-borne microbes. No difference was observed in the level of colonization of WCS417 on roots of coumarin-producing (iron-starved) and non-producing (iron-sufficient) Col-0 seedlings, supporting the notion that WCS417 is insensitive to the growth-inhibiting effect of coumarins, also in the rhizosphere.

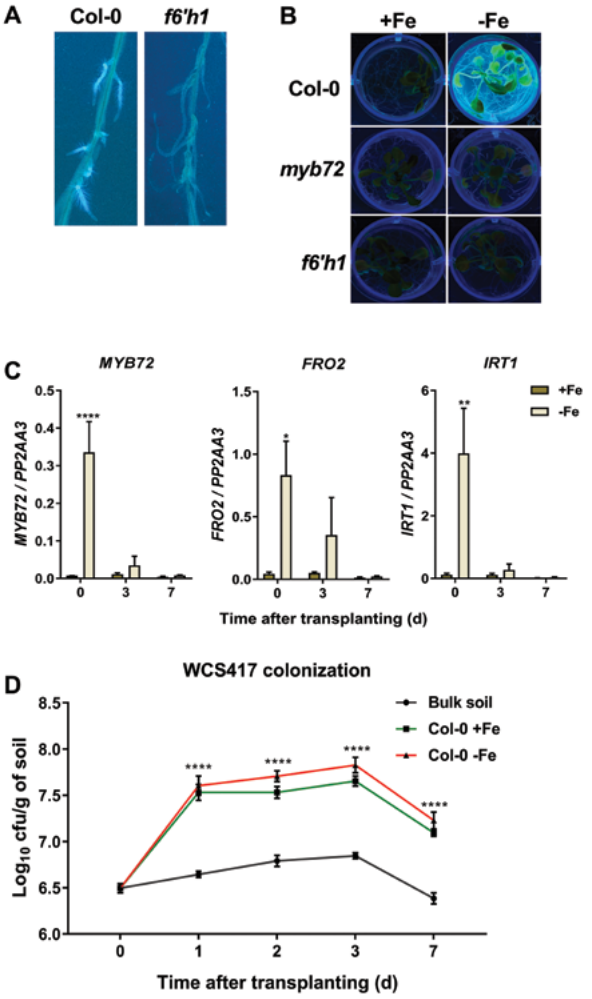

FIGURE 4. Effect of scopoletin on WCS417 colonization.

(A) Visualization of fluorescent phenolic compounds produced in roots of Col-0 and scopoletin biosynthesis mutant *f6'h1,* colonized by *P. simiae* WCS417. Visualization of fluorescent phenolic compounds was achieved under UV light (365 nm). Photographs were taken from roots of 20-d-old in vitro-grown Arabidopsis plants, 7 d after colonization by the rhizobacteria. **(B)** Excretion of fluorescent phenolic compounds by 26-d-old Col-0, *myb72* and *f6'h1* plants grown in Hoagland medium with (+Fe) or without (-Fe) iron. Visualization of fluorescence was achieved under UV light (365 nm). **(C)** Gene expression profiles of *MYB72* and the iron-deficiency marker genes *FRO2* and *IRT1* in roots of Col-0 plants pre-grown for 14 days in Hoagland medium with (+Fe) or without (-Fe) iron and transplanted on day 0 to limed Reijerscamp soil. Gene expression was quantified by qRT-PCR. Transcript levels were normalized to that of reference gene *PP2AA3* (At1g13320). Data are means of 3 biological replicates. Error bars represent SE. Asterisks indicate statistically significant differences between treatments (Student's *t*-test, $****P < 0.0001$; $**P < 0.01$; $* P < 0.05$). **(D)** Number of *P. simiae* WCS417 bacteria recovered from rhizospheres of Col-0 grown in limed Reijerscamp soil that was amended with 10^5 cfu.g^{-1} WCS417 bacteria. Root colonization was determined at indicated days after transplanting the seedlings from iron-sufficient (+Fe) or iron-starved (-Fe) Hoagland growth medium into the WCS417-amended Reijerscamp soil. Values for each time point were calculated from 5 rhizosphere or bulk soil samples. Asterisks indicate statistically significant differences between bulk soil and colonized plants (Two-way ANOVA, Tukey's test, $****P < 0.0001$).

Next, we analyzed the microbiota associated with roots of iron-starved Col-0, *myb72,* and *f6'h1* plants that were grown in limed Reijerscamp soil for 3 d (without WCS417). As a control, we characterized the root microbiota of Col-0 plants that were pre-grown under iron-sufficient conditions. Day 3 after transplanting was chosen because enhanced expression levels of *MYB72, FRO2,* and *IRT1* were still detectable at that time point (Figure 4C), and because phenolics excreted by the roots can reside in the soil for several days (Mimmo et al., 2014). We postulated that during the first 3 d of root colonization, the differential excretion of coumarins by Col-0, *myb72,* and *f6'h1* would have had its impact on microbiome assembly. To analyse the effect of MYB72 and F6'H1 activity on the composition of the root microbiome, genomic DNA of the root-associated microbiota was subjected to shotgun metagenome sequencing. Illumina NextSeq 500 sequencing yielded a total of 1098.6 million (M) paired-end reads with a read length of 150 base pairs (bp) (Supplemental Table S2). For the analysis of the metagenomes we followed a classification-first approach using Kaiju, a program that estimates sequence similarity of metagenomic reads with reference prokaryotic and eukaryotic microbial protein databases (Menzel et al., 2016). For the root samples, Kaiju classified 28-32% of the reads at genus level to Arabidopsis and 32-38% of the reads to microbiota in the reference database (Supplemental Table S4). For the bulk soil samples, almost no reads were classified to Arabidopsis, while 65% matched with microbiota in the reference database. For all samples, around 35% of the reads couldn't be classified at genus level.

Taxonomic classification at the genus level resulted in 4,046 genera belonging to the domains of Bacteria, Eukaryota and Archaea (Supplemental Datasets S5 and S6). Bacteria were the most dominant domain in terms of relative abundance (RA), with Eukaryota being the second and Archaea representing only a small fraction of the microbial communities (Supplemental Figure S5A). Genus level classification and publicly available taxonomy databases (Federhen, 2012) allowed us to track shifts in higher taxonomic ranking between the root-associated microbial communities and those assembled in the unplanted soil (Supplemental Figure S5A). Interestingly, Bacteria displayed a significant decrease in the root samples of all genotypes compared to soil. In contrast, Eukaryota showed a significant increase in root samples compared to soil while RA of Archaea remained unaffected in both compartments (Supplemental Figure S5A). At phylum level, we focused on the most abundant phyla with RA over 0.5%. Proteobacteria were the most abundant (around 50% RA) with Actinobacteria, Firmicutes and Bacteroidetes being overrepresented as well but with lower RA (Figure 5A). For the phyla of Acidobacteria, Actinobacteria, Bacteroidetes and Firmicutes there were statistical significant changes in the RA between soil and all root/rhizosphere samples. For the phyla Chlorophyta, Mucoromycota, Planctomycetes, and Proteobacteria only a subset of the genotype-treatment combinations showed statistical significant changes in the RA in root/rhizosphere versus bulk soil samples (Figure 5A).

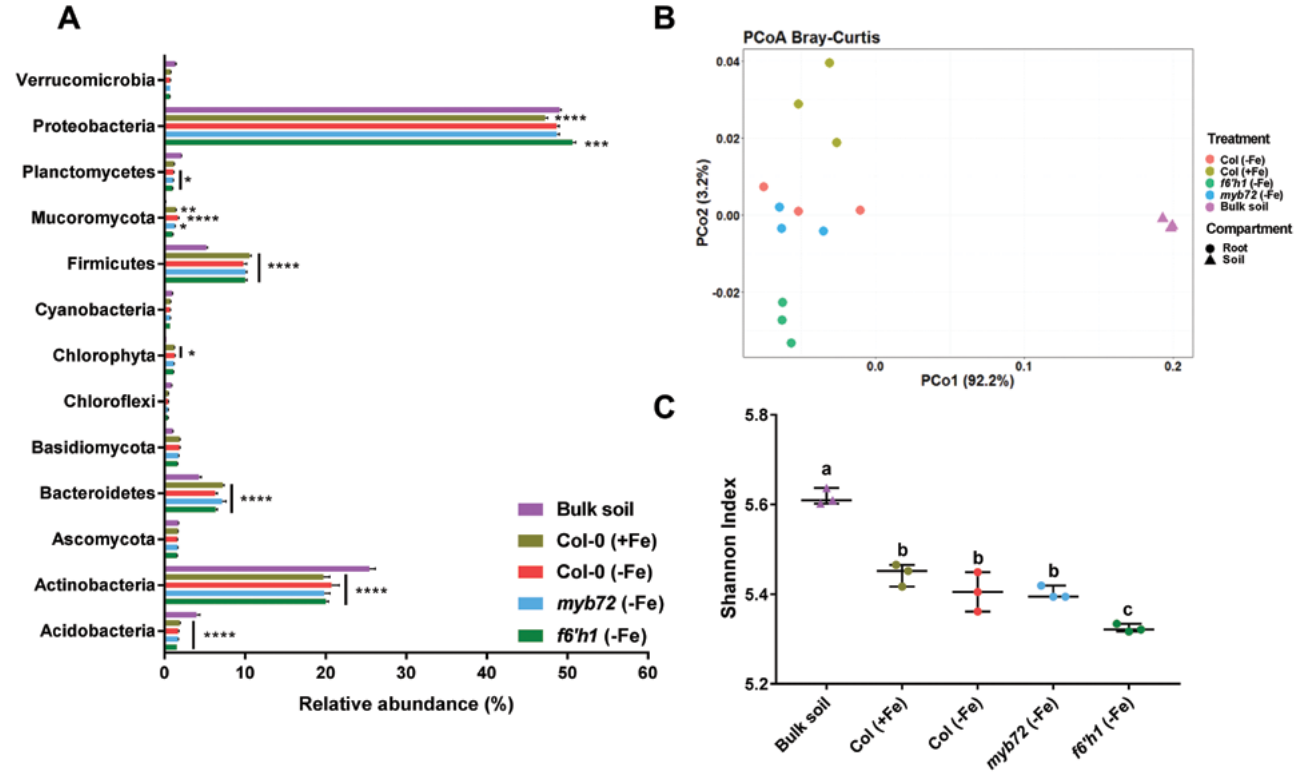

FIGURE 5. Metagenome analysis of bulk soil and root-associated microbiomes of Col-0, *myb72*, and *f6'h1* plants. (**A**) Average relative abundance (RA >0.5\%) of most-abundant phyla in bulk soil and root-associated microbial communities. Bars correspond to the average of 3 replicates and error bars represent the standard error of the mean. Asterisks indicate statistically significant differences of root samples compared to bulk soil (Two-way ANOVA, Tukey's test; ****$P < 0.0001$; ***$P < 0.001$; **$P < 0.01$; *$P < 0.05$). (**B**) Principal coordinates analysis (PCoA) using Bray-Curtis metrics display dissimilarity of microbial communities between soil (triangles) and root samples (circles) and between Col-0 pre-grown under iron-sufficient (+Fe) conditions (light brown), and Col-0 (red), *myb72* (light blue) and *f6'h1* (green) pre-growth under iron-starved conditions (–Fe). (**C**) Shannon's diversity index displaying the within-sample diversity of different treatments. Shapes with same color indicate samples of one treatment. Horizontal bars correspond to median and interquartile range of values. Different letters indicate statistically significant differences (One-way ANOVA, Tukey's test; $P < 0.05$).

Effect of scopoletin on rhizosphere microbiome assembly

To understand how diverse or rich the microbial communities are in the different samples, we performed β- and α-diversity analysis. Principal coordinate analysis (PCoA) using Bray-Curtis similarities revealed that the microbiome of bulk soil is separating from the root-associated communities of the different plant genotypes and treatments (Figure 5B), indicating a significant effect of the plant on microbiome assembly already at 3 d after transferring plants to soil. Along the second principal coordinate, there is also differentiation between the root-associated microbial communities of iron-sufficient (+Fe) and iron-starved (-Fe) Col-0 plants (Figure 5B), suggesting that root exudates produced during iron-starvation affected microbiome assembly. Interestingly, the microbial communities of iron-starved Col-0 and *myb72* both displayed intermediate separation from that of iron-sufficient Col-0, while the microbial community on the scopoletin biosynthesis mutant *f6'h1* diverged most distinctly.

To pinpoint genotype-mediated differences in the root-associated microbial communities, the microbial diversity within each sample (α-diversity) was calculated as Shannon index (Figure 5C), number of observed genera (Supplemental Figure S5B), and Chao1 index (Supplemental Figure S5C). The two latter indexes didn't suggest differences between the different genotypes and between bulk- and root-associated microbial communities. However, the Shannon index calculation showed that microbial communities in unplanted bulk soil are significantly more diverse and complex than the root-associated microbial communities (Figure 5C). Amongst the root-related samples, the Shannon index for the *f6'h1* root-associated microbiota was significantly lower than that for other genotypes. The observation that the scopoletin-biosynthesis mutant *f6'h1* clearly separates from the other genotypes both in between- and in within-samples diversity estimations, suggests that this coumarin affects root microbiome assembly.

To dissect the plant genotype-mediated differences in root microbiome structure on lower taxonomic ranking, we performed pairwise comparisons using DESeq2. Subsequently, we searched for genera with differential abundance on the roots of Col-0, *myb72* and *f6'h1* plants. Comparison between iron-starved Col-0 and *f6'h1* revealed the largest number (35) of genera with differential abundance patterns (Figure 6A). The genera enriched on Col-0 over *f6'h1* roots (=stimulated in a F6'H1/scopoletin-dependent manner) represent 7 phyla, with *Psychrobacillus* and *Paraclostridium* from the Firmicutes phylum, and *Rhizophagus*, a genus of mycorrhizal fungi, being amongst the most-strongly stimulated genera (Figure 6A). The genera enriched on *f6'h1* over Col-0 roots (=inhibited on Col-0 roots in a F6'H1-dependent manner) represent 4 phyla, with *Pontibacter*, *Rufibacter*, and *Adhaeribacter*, all belonging to Hymenobacteraceae family, being amongst the most-strongly affected genera.

Pairwise comparison between the root-associated microbiota of iron-sufficient and iron-starved Col-0 plants revealed 21 genera with differential abundance. The majority of them are enriched in the root microbiomes of iron-starved Col-0 plants and predominantly belong to the Proteobacteria and Firmicutes (Figure 6B). *Psychrobacillus*, *Stenotrophomonas*, and *Paeinisporosarcina* and *Dyella* were the genera with the highest differential abundance in the root-associated microbiomes of iron-starved Col-0, suggesting that these are promoted by the exudates of iron-starved Col-0 plants. *Adhaeribacter*, *Niastella*, and *Hymenobacter* were most- highly enriched on roots of iron-sufficient Col-0 plants, suggesting that their growth is inhibited by

exudates of iron-starved Col-0 plants. Interestingly, *Adhaeribacter* and *Hymenobacter* were also significantly more abundant in the root microbiomes of both iron-starved *f6'h1* (Figure 6A; underlined in green) and iron-sufficient Col-0 (Figure 6B; underlined in green) as opposed to the root microbiome of iron-starved Col-0 plants, suggesting that these genera are particularly sensitive to F6'H1-dependent metabolites, such as scopoletin, that are secreted under iron starvation.

Comparison between the root microbiomes of iron-starved Col-0 and *myb72* plants yielded only 3 genera (Figure 6C). However, the *myb72*-enriched genus *Psychromonas* was also significantly enriched in the root microbiome of *f6'h1* (Figure 6A and 6B, red underline). Together these results demonstrate that the MYB72- and F6'H1-dependent root exudation patterns, with the coumarin scopoletin as a major compound, can positively and negatively influence the abundance of specific genera in the root-associated microbiome of Arabidopsis, therewith impacting the assembly of the root microbiome.

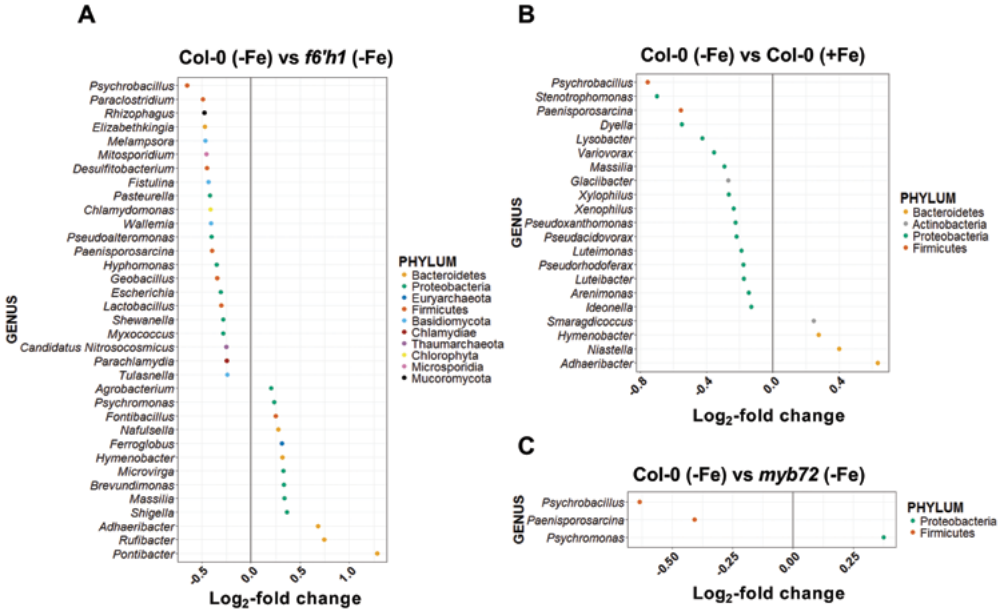

FIGURE 6. Genera showing differential abundance between genotypes with different scopoletin exudation. Differentially abundant bacteria and fungi between root samples of Col-0 (-Fe) and (**A**) *f6'h1* (-Fe), (**B**) Col-0 (+Fe) and (**C**) *myb72* (-Fe), as determined using DESeq2. Comparisons were performed at genus level using a false discovery rate (FDR) < 0.05 to select for significance. In all graphs, negative $\log_2$–fold change values relate to genera that are significantly enriched in iron-starved Col-0 (–Fe) root samples in comparison to the contrasting genotype/treatment combination. Different colors of the dots correspond to different Phyla.

Discussion

MYB72 is a regulator of coumarin biosynthesis during iron-starvation conditions

The rhizosphere microbiome is quite diverse and its interplay with roots has a marked influence on plant fitness. At the same time root exudates can strongly affect the composition and functions of the rhizosphere microbiome (Berendsen et al., 2012). Selected members of the microbiome, when enriched in the rhizosphere, can trigger ISR through the activity of the root-specific transcription factor MYB72 and the MYB72-regulated β-glucosidase BGLU42 (Van der Ent et al., 2008; Pieterse et al., 2014). MYB72 and BGLU42 have also a defined role in the production and excretion of iron-mobilizing fluorescent phenolic compounds when plants grow under conditions of iron starvation (Zamioudis et al., 2014). We used this knowledge to identify the metabolites that are produced and excreted by Arabidopsis roots in a MYB72- and BGLU42-dependent manner. Using untargeted UPLC-ESI-TOF-MS metabolomics analysis of root exudates and root extracts of iron-sufficient and iron-starved Col-0, *myb72,* and *bglu42* plants we identified coumarins as a major group of compounds whose production relies on MYB72 activity (Supplemental Figures S2 and S4; Supplemental Data S1 and S2). MYB transcription factors are known regulatory components of the phenylpropanoid pathway, a major biosynthesis route for many secondary metabolites, including coumarins (Liu et al., 2015a). To our knowledge, MYB72 is the first MYB transcription factor with an evidenced role in the production of fluorescent phenolic compounds under iron-starvation conditions in Arabidopsis. Coumarins, such as scopolin, scopoletin, esculin, esculetin, fraxetin, and isofraxidin, were previously found to be highly abundant in roots and exudates of Col-0 plants experiencing iron deficiency (Rodriguez-Celma et al., 2013; Fourcroy et al., 2014; Schmid et al., 2014), where they play a role in the mobilization and uptake of iron (Jin et al., 2007; Schmid et al., 2014; Fourcroy et al., 2016). The depletion of coumarins observed in root exudates and roots of mutant *myb72* (Figures 1, 2 and 3) resembled that of the coumarin biosynthetic mutant *f6'h1* (Schmid et al., 2014). *F6'H1* and *MYB72* genes are both upregulated during iron deficiency by the transcription factor FIT (Colangelo and Guerinot, 2004; Schmid et al., 2014). Our results suggest that MYB72 acts upstream or in parallel with F6'H1 in the biosynthesis of coumarins in iron-starved Arabidopsis roots.

BGLU42 is required for the excretion of scopoletin under iron-starvation conditions

Roots of mutant *bglu42* produced high levels of coumarins under iron-starvation conditions, but were specifically impaired in their excretion (Figure 2 and Supplemental Figures S1 and S3). This phenotype resembles that of the ABC transporter mutant *pdr9* t, which is defected in the exudation of fluorescent phenolic compounds that accumulate inside the roots during conditions of iron deficiency (Fourcroy et al., 2014). Analysis of the metabolome profile of root exudates and root extracts of iron-sufficient and iron-starved Col-0 and *bglu42* roots pointed to a role for BGLU42 in the excretion of the coumarin scopoletin (Figures 1 and 2). Scopolin accumulated to high levels in iron-starved *bglu42* roots, but the levels of its aglycone scopoletin in the roots and exudates were dramatically decreased. This finding suggests that BGLU42 functions in the hydrolysis of scopolin, and that this activity is required for the excretion of scopoletin into the rhizosphere. This is in line with previous findings in which the Arabidopsis β-glucosidases BGLU21, 22 and 23 were shown to specifically hydrolyze scopolin into scopoletin (Ahn et al., 2010). β-glucosidases can hydrolyze glycosidic bonds either between 2 carbohydrates or

between a carbohydrate and a non-carbohydrate (Morant et al., 2008). Plants accumulate and store compounds with potential toxicity in soluble, non-toxic forms within roots. Upon stress, β-glucosidases hydrolyze these inactive forms that are later released as bioactive forms (Jones and Vogt, 2001; Morant et al., 2008). The activity of BGLU42 seems to be specific for scopolin/scopoletin, since other coumarin pairs like esculin/esculetin were not affected by the absence of this β-glucosidase in *bglu42* (Supplemental Figure S1 and S3). We, thus, conclude that BGLU42 activity in iron-starved Arabidopsis roots plays an important role in the processing of scopolin to scopoletin, resulting in the excretion of scopoletin into the rhizosphere.

Differential antimicrobial activity of scopoletin

Our analysis revealed that scopoletin was the most abundant MYB72- and BGLU42-dependent coumarin in the root exudates of iron-starved Col-0 root exudates (Figure 2). Scopoletin and other fluorescent coumarins produced under iron deficiency play a role in the mobilization and uptake of Fe^{3+} (Schmid et al., 2014; Fourcroy et al., 2016). Besides its role in the iron uptake response, scopoletin was also shown to accumulate in leaves around infection sites, where it inhibited growth of the foliar fungal pathogens *Botrytis cinerea* and *Alternaria alternata* and the bacterial pathogen *P. syringae* (El Oirdi et al., 2010; Simon et al., 2010; Sun et al., 2014). Here, we show that scopoletin can also inhibit growth of the tested soil-borne pathogens *F. oxysporum* and *V. dahliae* (Figure 3). However, the plant-beneficial rhizobacterial strains *P. simiae* WCS417 and *P. capeferrum* WCS358 were insensitive to scopoletin (Figure 3). Interestingly, coumarins (including scopoletin) were among the metabolites with increased abundance in Arabidopsis roots after colonization by the ISR-inducing rhizobacteria *P. fluorescens* strain SS101 and *Paenibacillus polymyxa* BFKC01 (Van de Mortel et al., 2012; Zhou et al., 2016). Given the fact that beneficial ISR-inducing rhizobacteria, such as *P. simiae* WCS417 and *P. capeferrum* WCS358 activate the expression of *MYB72* in Arabidopsis roots, even under iron-sufficient conditions (Zamioudis et al., 2014; Zamioudis et al., 2015), that subsequently regulates the production of coumarins in Arabidopsis roots (Figure 4A), we hypothesized that rhizobacteria that provide plants with benefits have higher levels of tolerance towards scopoletin than harmful soil-borne microbes. Inducing the excretion of antimicrobial scopoletin may thus be a mechanism to outcompete other microbes in the same root niche. Previous studies have shown that coumarins can affect not only growth but also biofilm formation and virulence of pathogenic bacteria in different systems (Lee et al., 2014; Gutierrez-Barranquero et al., 2015). Biofilm formation allows root microbes to achieve high biomasses that provides them with competitiveness, since it makes them more tolerant to different stresses and predation and enhances the efficiency of the uptake of plant-derived carbon sources (Danhorn and Fuqua, 2007).

Besides inhibiting fungal growth, we showed that scopoletin also affected pigmentation of *F. oxysporum* when growing in plates containing scopoletin (Figure 3). A pigment responsible for the red color of hyphae is the polyketide bikaverin that is produced by various fungal species, including *Fusarium*. It has antibiotic activities against protozoa, fungi and oomycetes (Son et al., 2008; Limon et al., 2010). Pigment inhibition by scopoletin could, thus, render this soil-borne fungus less competitive and viable in the rhizosphere. Additionally, scopoletin in the root exudates also deterred germinating *F. oxysporum* spores (Figure 3). Collectively, our results indicate that some soil-borne microbes can be sensitive to the antimicrobial activity of scopoletin, while others are tolerant.

Scopoletin affects root microbiome assembly

Increased abundance of phenolic compounds in the rhizosphere of iron-stressed plants enhanced the abundance of siderophore-producing bacteria (Jin et al., 2010). Moreover, addition of exudates rich in phenolic compounds into the soil showed more pronounced effects on the microbial community than other classes of compounds (Badri et al., 2013). Exudation of coumarins is a response that is shared between the iron- and the phosphate-starvation response of plants (Ziegler et al., 2016; Tsai and Schmidt, 2017; Verbon et al., 2017). Interestingly, Castrillo et al. (2017) observed that phosphate uptake-deficient or phosphate hyperaccumulating Arabidopsis genotypes assembled significantly different root-associated microbiomes. To investigate the role of scopoletin in root microbiome assembly, we analyzed the microbial communities on the roots of Col-0, *myb72* and the scopoletin biosynthesis mutant *f6'h1* by shotgun metagenome sequencing. This approach allows for the identification of both prokaryotic and eukaryotic members of a microbiome (Quince et al., 2017), providing an advantage over the most-commonly used amplicon sequencing that targets either bacterial *16S rRNA* or fungal *ITS* (Siegwald et al., 2017). To characterize the communities assembled in our samples, we followed the phyloseq pipeline, commonly used in the analysis of metagenomic data (McMurdie and Holmes, 2013). The most abundant differences in microbiome composition were those between unplanted bulk soil and the root-associated microbiota (Figure 5 and Supplemental Figure S5), resembling the rhizosphere effect (Bakker et al., 2013). Between the bulk soil and root-rhizosphere samples, the RA of Archaea was unaffected while that of Bacteria was lower and that of Eukaryota higher in the rhizosphere, supporting previous findings in crop species (Turner et al., 2013). At the phylum level, the RA of Proteobacteria, Firmicutes, and Bacteroidetes was generally increased in root-rhizosphere samples compared to bulk soil, whereas the RA of Actinobacteria and Acidobacteria was decreased (Figure 5A). Such shifts in phylum level abundance were also observed in other rhizosphere microbiome studies of Arabidopsis, rice and barley plants growing for prolonged periods of in the soil (Bulgarelli et al., 2012; Lundberg et al., 2012; Bulgarelli et al., 2015; Edwards et al., 2015; Lebeis et al., 2015). Moreover, the α-diversity estimation with Shannon's index (Figure 5C) showed a diversity gradient from higher to lower between soil and rhizosphere samples, suggesting that microbial selection is occurring in the rhizosphere (Lundberg et al., 2012; Bulgarelli et al., 2015; Zgadzaj et al., 2016). In this study, we found that the foundation of the root microbiome community structure becomes already established within 3 d of root colonization.

Relative to the differences in microbiome composition between planted and unplanted soil, the plant genotype- and treatment-mediated differences were relatively small (Figure 5B). This is in line with previous findings (Peiffer et al., 2013; Lebeis et al., 2015; Castrillo et al., 2017; Zhang et al., 2017). Between the genotypes Col-0, *myb72* and *f6'h1,* the microbiomes assembled on the roots of iron-starved Col-0 and *f6'h1* displayed the largest differences, indicating that excretion of scopoletin affects the root microbiome assembly. Genus-level analysis with DESeq2 (Figure 6) revealed the differential abundance of bacterial and fungal genera between the rhizospheres of Col-0 plants growing under iron deficiency and those depleted in coumarins (*myb72* and *f6'h1*). Some of the enriched bacterial genera associated with roots of iron-starved Col-0 over *f6'h1* (i.e. *Stenotrophomonas*, *Lactobacillus*, *Psychrobacillus*, *Elizabethkingia*, *Chlamydomonas* and *Geobacillus*) were previously found to be able to hydrolyze different coumarins (Aliotta et al., 1999;

Nazina et al., 2001; Kim et al., 2005; Guan et al., 2008; Krishnamurthi et al., 2010). Interestingly, some of the most abundant genera in the root samples of iron-stressed Col-0 can promote plant growth (*Psychrobacillus*, *Variovorax*), facilitate metal uptake in plants (*Psychrobacillus*), have a role in nitrogen cycling in soil (*Candidatus* Nitrosocosmicus) or possess antimicrobial potential (*Pseudoalteromonas*) (De Nys and Steinberg, 2002; Han et al., 2011; Perez Rodriguez et al., 2014; Sauder et al., 2017). Hence, it is tempting to speculate that the production and excretion of coumarins, such as scopoletin, aid in the assembly of a plant-beneficial root microbiome. In this respect, another noteworthy observation was that two genera that represent mycorrhizal fungi, *Rhizophagus* and *Tulasnella*, were enriched in the root samples of Col-0 in comparison to that of *f6'h1,* which is in line with the observation that phenolic compounds stimulate growth and root colonization of arbuscular mycorrhizal fungi (Fries et al., 1997).

Coumarins are not present in the exudates of *myb72* (-Fe) and Col-0 (+Fe) (Supporting Figures S4 and S6) and *f6'h1* (-Fe) (Schmid et al., 2014). In the rhizosphere of Col-0 (+Fe) there was enrichment of the genus *Niastella*, that can control nitrous oxide flux in the soil following fertilization with organic amendments (Nishizawa et al., 2014). Both the rhizospheres of Col-0 (+Fe) and *f6'h1* (-Fe) were also enriched in genera belonging to the Hymenobacteriaceae family (previously Cytophagaceae) (Figure 6). More specifically, the genera of *Adhaeribacter* and *Hymenobacter* in Col-0 (+Fe) and *Adhaeribacter*, *Pontibacter*, *Rufibacter* and *Hymenobacter* in *f6'h1* (-Fe) displayed increased abundance compared to the rhizosphere of Col-0 (-Fe). Genera of this family can grow in poor substrates, can form strong biofilms and their motility is not based on flagellar movement (gliding motility), while *Pontibacter* species have been characterized for growth promotion in pea plants (McBride, 2001; Dastager et al., 2011; McBride et al., 2014; Srinivasan et al., 2015). Moreover, in the rhizosphere of *f6'h1* (-Fe) the genus *Nafulsella*, was previously found to be incapable of hydrolyzing the coumarin esculin (Zhang et al., 2013). The absence of coumarins suggest that in these rhizospheres there is enrichment of microbes that cannot use them as carbon sources and microbes with different motility strategies and abiotic stress tolerance.

Comparison of microbial abundance between *myb72* and *f6'h1* rhizospheres didn't yield any bacteria or fungi with statistically significant enrichment or decrease (data not shown), suggesting that similar exudation patterns are responsible for similarly enriched/depleted communities. Interestingly, comparison of root-associated communities of iron-starved Col-0 and *f6'h1* plants yielded more fungal and bacterial genera with differential abundance than that of Col-0 and *myb72* (Figure 6). This may be explained by the possibility that the striking differences observed in fluorescent phenolic compound exudation between iron-starved Col-0 and *myb72* observed in vitro (Figure 1) might be less-severe in soil due to soil properties and the microbial activity (Kuijken et al., 2015).

In sum, our study on the root metabolome and root microbiome under conditions that induce MYB72 activity revealed that 1) MYB72 is required for the production of coumarins, 2) BGLU42 activity plays a role in the deglycosylation of scopolin and the subsequent excretion of scopoletin into the rhizosphere, 3) scopoletin displays differential antimicrobial activity towards selected beneficial rhizobacteria and pathogenic soil-borne pathogens, 4) the "rhizosphere effect" is already detectable within 3 d after transplanting, and 5) scopoletin affects the assembly of the root microbiome. Future research will be focused on testing the hypothesis that the observed MYB72- and F6'H1-dependent differences in the root

microbiome are associated with enrichment for plant beneficial microbes. To this end, it will be important to isolate microbial strains from the genera that are differentially affected by MYB72- and F6'H1-activity in plant rhizospheres and test them for their effect on their potential to enhance plant immunity, promote plant growth, or ameliorate abiotic stresses of plants.

Materials and methods

Plant material and growth conditions

In this study, *Arabidopsis thaliana* accession Col-0 and the mutants *myb72* (Van der Ent et al., 2008), *bglu42* (Zamioudis et al., 2014) and *f6'h1* ((Kai et al., 2008); kindly provided by Prof. Jürgen Zeier) were used. For all experiments, seeds were surface sterilized (Van Wees et al., 2013) and sown on agar-solidified 1x Murashige and Skoog (MS) medium supplemented with 0.5% sucrose (Murashige and Skoog, 1962). After 2 d of stratification at 4°C, the Petri dishes were positioned vertically and transferred to a growth chamber (22°C; 10 h light, 14 h dark; light intensity 100 µmol m^{-2} s^{-1}). For growth under conditions with sufficient or limited iron, uniform 13-day-old seedlings were transferred to 12-well plates (2 seedlings per well) containing liquid Hoagland medium (5 mM KNO_3, 2 mM $MgSO_4$, 2 mM $Ca(NO_3)_2$, 2.5 mM KH_2PO_4, 70 µM H_3BO_3, 14 µM $MnCl_2$, 1 µM $ZnSO_4$, 0.5 µM $CuSO_4$, 10 µM NaCl, 0.2 µM Na_2MoO_4, 4.7 mM MES, 0.5% (w/v) sucrose; pH 5.5). For iron-sufficient growth conditions, Fe(III)EDTA was added to a final concentration of 50 µM, whereas for iron starvation conditions Fe(III)EDTA was added to a final concentration of 10 µM (medium-low iron condition) or left out of the growth medium (low iron condition).

For the metabolome analysis, roots and exudates were harvested from 20-d-old Col-0, *myb72* and *bglu42* plants that had been grown for 7 d in the media described above under low iron (no added Fe(III)EDTA) or sufficient iron (50 µM Fe(III)EDTA) conditions.

For the root microbiome analysis, 13-day-old Col-0, *myb72* and *f6'h1* seedlings were transferred to 12-well plates containing the medium described above, with 50 µM Fe(III)EDTA (sufficient iron) or 10 µM Fe(III)EDTA (medium-low iron). Six days later, the 19-d-old plants were transferred to new 12-well plates containing either 50 µM Fe(III)EDTA (sufficient iron) or 0 µM Fe(III)EDTA (low iron). After 1 week of growth under iron-sufficient or iron-starved conditions, 26-d-old plants were transferred to 60-ml pots containing a natural soil taken from a field in nature reserve the Reijerscamp (52°01'02.55'', 5°77'99.83''), where natural Arabidopsis populations grow. Before use, the Reijerskamp soil was prepared as described (Berendsen et al., 2017), after which the soil was limed with CaO (0.0025 $g.g^{-1}$ of soil) to make the soil alkaline (pH >7.5) and reduce iron availability.

To visualize production of the root fluorescence in response to colonization by WCS417, Col-0 and *f6'h1* plants were initially grown on MS medium supplemented with 0.5% sucrose. Seven-day-old seedlings were transferred to plates containing Hoagland medium with sufficient iron (50 µM Fe(III)EDTA). Six days later, plants were inoculated in the root-shoot junction with 5 µl of WCS417 bacteria cell suspension (OD_{600}=0.1) and after 1 week root fluorescence was monitored under UV light (365 nm).

Quantification of fluorescent phenolic compounds in root exudates

The production and secretion of fluorescent phenolic compounds by Arabidopsis roots was monitored under UV light (365 nm) as described (Zamioudis et al., 2014). In order to quantify the amount of fluorescent phenolic compounds in the root exudates, 200 µl of growth medium was transferred into a 96-well microplate. Fluorescence emitted by the root exudates (excitation at 360 nm; emission at 528 nm) was measured with a Synergy™ Multi-Mode Microplate Reader (BioTek, Winooski, VT, USA) as described (Zamioudis et al., 2014).

Quantitative real-time PCR analysis

Total RNA was extracted from Arabidopsis roots using a modified protocol of Oñate-Sánchez and Vicente-Carbajosa (2008), after which it was treated with DNase according to the manufacturer's instructions (Thermo Scientific, Waltham, MA USA). Subsequently, cDNA was synthesized using SuperScript III Reverse Transcriptase (Invitrogen, Waltham, MA, USA), according to the manufacturer's instructions. PCR reactions were performed in optical 384-well plates (Applied Biosystems, Foster City, CA, USA) with an ABI PRISM® 7900 HT sequence detection system, using SYBR® Green (Applied Biosystems) to monitor the synthesis of double-stranded DNA. A standard thermal profile was used: 50°C for 2 min, 95°C for 10 min, 40 cycles of 95°C for 15 s and 60°C for 1 min. Amplicon dissociation curves were recorded after cycle 40 by heating from 60 to 95°C with a ramp speed of 1.0°C min^{-1}. Transcript levels were calculated relative to the reference gene *At1g13320* (Czechowski et al., 2005) using the $2^{-\Delta Ct}$ method described previously (Livak and Schmittgen, 2001; Schmittgen and Livak, 2008). The expression levels of *IRT1, FRO2, MYB72, F6'H1,* and *At1g13320* were determined using the gene-specific primers that are listed in Supplemental Table S1.

Metabolite fingerprinting analysis

For metabolite fingerprinting of the root exudates, 200 µl exudates were extracted by two-phase-extraction with methyl-*tert*-butyl ether (MTBE) using a method described in Floerl et al. (2012) adapted from Matyash et al. (2008). Polar and non-polar phases of root exudates were combined, evaporated under a nitrogen stream and, resolved in 100 µl acetonitrile/methanol/water (1:1:12, *v/v/v*). After centrifugation 80 µl of the supernatant were transferred to a micro vial and used for analysis.

For metabolite fingerprinting of the root samples, 100 mg of homogenized root material were extracted by two-phase-extraction in MTBE using the protocol (Bruckhoff et al., 2016) adapted from Matyash et al. (2008). The polar extraction phase was dried under nitrogen stream and resuspended in methanol/acetonitrile/water (15:15:100, *v/v/v*), while the non-polar extraction phase was dried and resuspended in 100 µl of chloroform/methanol/water (60:30:4.5 (*v/v/v*).

The metabolite fingerprinting analysis was performed by Ultra Performance Liquid Chromatography (UPLC, ACQUITY UPLC System, Waters Corporation, Milford, USA) coupled with a photo diode array detector and an orthogonal time-of-flight mass spectrometer (TOF-MS, LCT Premier, Waters Corporation, Milford, USA) as described by König et al. (2014). Data acquisition was carried out by using the MassLynx software (MassLynx

V4.1 SCN779, Waters Corporation, Milford, USA) in centroid data format. For data deconvolution (peak picking and alignment) the software MarkerLynx (Waters Corporation, Milford, USA) was used. For further data processing like ranking and filtering of the data, adduct identification and correction, combining of the data sets of positive and negative ionisation as well as for clustering and visualization we used the toolbox MarVis (MarkerVisualization, http://marvis.gobics.de) (Kaever et al., 2009; Kaever et al., 2015).

For data analysis and visualization, the intensity pattern of the high-quality metabolite features were clustered by means of one-dimensional self-organizing-maps (1D-SOMs). After normalization, sample aggregation is performed on mean values and marker scaling by the Euclidean norm (2-norm). Clusters with intensity pattern of interest in the respective experimental condition were selected. Features represented by these clusters were putatively identified by an automated database search within a mass deviation of 5 mDa: AraCyc (http://www.arabidopsis.org), MetaCyc (http://metacyc.org) and KEGG (http:// www.genome.jp/kegg). The identity of the markers was confirmed by further methods as MS^2 fragmentation analysis, UV/VIS analysis or comparison of retention time with authentic standards.

Determination of scopolin and scopoletin in root exudates and extracts

Root extracts of Col-0, *myb72* and *bglu42* were extracted by a protocol adapted from Zum Felde et al. (2007). Homogenized root material (10 mg) was extracted with 1 ml 80% methanol in the presence of zirconia beads for 30 min at room temperature. After centrifugation for 10 min at 16.000 *g* the supernatant was transferred to a fresh vial and diluted 1:1 (*v/v*) in 80% methanol. Samples of Col-0 and *bglu42* grown without iron were diluted additionally 1:50 (*v/v*) in 80% methanol. Aliquots of 5 µl were injected into an Agilent 1100 HPLC system coupled with a fluorescence detector and equipped with a Nucleosil 120-5 C-18 column (EC250/2, Machery&Nagel, Germany). Separation was achieved using a flow rate of 0.3 ml/min, a solvent system of water with 0.1% formic acid (solvent A), acetonitrile with 0.1% formic acid (solvent B) and a linear gradient from 10 to 40% B within 20 min, followed by a washing step of 100% solvent B for 5 min and re-equilibrating the column for initial flow conditions for 5 min. Scopolin and scopoletin were detected by fluorescence analysis at 336 nm (excitation) and 438 nm (emission) as described by Schmid et al. (2014). For quantification purposes detector calibration (external calibration) was performed with a seven-point calibration curve of commercial available scopolin and scopoletin (Phytolab, Germany).

Root exudates were diluted 4:1 (*v/v*) in methanol. Exudates of Col-0 and *bglu42* grown without of iron were diluted in addition 1:20 (*v/v*) in 80 % methanol. Aliquots of 5 µl were directly used for HPLC-fluorescence analysis (see above).

Cultivation of microbes

V. dahliae isolate JR2 (Fradin et al., 2009; kindly provided by Prof. Bart Thomma) was grown on potato dextrose agar (PDA) at 21°C. *F. oxysporum* f.sp. *raphani* (Pieterse et al., 1996) was grown on PDA at 28°C.

For assessing the effect of scopoletin on fungal growth in 96-well plates, *F. oxysporum* and *V. dahliae* spores were prepared by growing the fungi in 100 ml liquid SSN medium (Sinha and Wood, 1968) in 250-ml

Erlenmeyer flasks at 28°C (*F. oxysporum*) or 23°C (*V. dahliae*) under continuous shaking at 120 rpm for one week. The fungal suspension was filtered through glass wool. The filtrate was centrifuged for 10 min at 900 *g*. The pellet was suspended with ddH2O to a final spore density of 10^5 conidia.ml^{-1}.

For the chemotropism assay, *F. oxysporum* spores was prepared by growing the fungus in 100 ml liquid SSN medium (Sinha and Wood, 1968) in a 250-ml Erlenmeyer flasks at 28°C under continuous shaking at 120 rpm for one week. The fungal suspension was filtered through glass wool. The filtrate was centrifuged for 10 min at 900 *g*. The pellet was suspended with ddH_2O to a final spore density of 2.5x10^9 conidia.ml^{-1}.

P. simiae WCS417 and *P. capeferrum* WCS358 (Berendsen et al., 2015) were cultured on King's medium B (KB) agar plates (King et al., 1954) supplemented with 50 µg/ml rifampicin at 28°C. After 24 h of growth, cells were collected in 10 mM $MgSO_4$, washed twice by centrifugation for 5 min at 5000 *g* and finally resuspended in 10 mM $MgSO_4$ to a final density of OD_{600}=0.2 (2x10^8 colony-forming units (cfu).ml^{-1}).

In vitro assay for antimicrobial effect of scopoletin

To quantify the effect of scopoletin on in vitro growth of the fungal soil-borne pathogens *F. oxysporum* f.sp. *raphani* and *V. dahliae* JR2, and on the PGPR *P. simiae* WCS417 and *P. capeferrum* WCS358, we designed a microplate assay based on Pryor et al. (2007). In brief, 96-well plates (flat bottom; Greiner Bio-One, Kremsmünster, Austria) were filled with 100 µl liquid potato dextrose broth (PDB) for the fungi or 100 µl liquid KB for the bacteria. The growth media were supplemented with different concentrations of scopoletin (Sigma-Aldrich, St. Louis, MO, USA) from a 50-mM stock in 80% methanol. The blank controls contained equal amounts of methanol (3.2%) without scopoletin. The antibiotics Delvo®Cid (0.3 g.L^{-1}; DSM, Heerlen, the Netherlands) and tetracyclin (100 µg.ml^{-1}) were used as positive controls for the inhibition of fungal and bacterial growth, respectively. At the start of the microbial growth curves, 100 µl of fungal spore or bacterial cell suspension was added to each well (final density 5x10^4 spores.ml^{-1} or 5x10^8 cfu.ml^{-1}, respectively). The 96-well plates were covered with sterile seals (Excel Scientific SealPlate film; Sigma-Aldrich) and wrapped in aluminium foil. Plates with *F. oxysporum* and the bacteria were incubated at 28°C, whereas plates with *V. dahliae* were kept at room temperature. Fungal and bacterial growth was quantified for 6 and 1 d of growth, respectively, by measuring the optical density of the cultures at OD_{600} using a SPECTROstar Nano Microplate Reader (BMG LabTech, Ortenberg, Germany).

The inhibition of *F. oxysporum* mycelial growth by scopoletin in vitro was tested in Petri dishes by subculturing a mycelium plug of 5 mm diameter on PDA containing 500 µM scopoletin for 6 d in the dark at 28°C. PDA supplemented with 1% methanol served as a negative control and PDA with 0.2 g.L^{-1} Delvo®Cid and 1% methanol as a positive control. The area of mycelium growth was recorded every 2 d.

Scopoletin chemotropism assay

To quantify the level of chemotropism in *F. oxysporum* in response to scopoletin, a chemotropism assay was used based on the method described by Turrà et al. (2015). Conidia of *F. oxysporum* f.sp. *raphani* were obtained from an SSN liquid culture at a density of 2.5.x10^9 conidia.ml^{-1} ddH_2O. The conidia suspension

was further diluted in 0.5% (w/v) water agar (Oxoid, Badhoevedorp, The Netherlands) to a final density of $2.5x10^7$ spores.ml^{-1}. A total volume of 4 ml of the water agar with conidia was poured into Petri dishes (Ø 94 mm with vents; Greiner Bio-One, Kremsmünster, Austria). The Petri dishes were marked on the bottom with three parallel lines crossing the width of the plate at a distance of 0.5 mm from each other. Two square wells were cut into the agar along the two outer marked lines, after which 50 µl of a test compound solution or its solvent were added to either well. Pectin (1% (w/v); Fluka Analytical, Buchs, Switzerland) dissolved in distilled water was used as a positive control (Turrà et al., 2015). Scopoletin (Sigma-Aldrich, Steinheim, Germany) was applied in concentrations of 250 µM and 1 mM. Root exudates of Col-0 and *f6'h1* plants, pre-grown under the iron-deficient conditions described above, collected 3 d after transferring the plants in MQ were tested as well. Plates were sealed with parafilm and wrapped in aluminium foil for overnight incubation at 28°C. After 12 h, the plates were moved to 4°C after which pictures were taken of germinating conidia using a Zeiss Axioskop 2 (100x magnification) with a Lumenera Inifinity 1 camera and the software Image-Pro Insight 9.1. Using Adobe Photoshop CS6 (Adobe Systems, San Jose, CA, USA), germinating conidia in each picture were assigned a direction of germination towards the solvent, towards the test compound or towards neither ('neutral'). Chemotropism was calculated as the percentage of germinating tubes growing towards the solvent or the test compound. Between 800 and 1100 hyphae from germinating conidia growing towards either the test compound or the solvent were assessed per treatment.

Root colonization by *P. simiae* WCS417

To assess root colonization by rifampicin-resistant *P. simiae* WCS417, 23-d-old Col-0 plants were transferred from the in vitro growth system to a sand:potting soil mixture to which WCS417 bacteria were added to a final density of 10^5 cfu.g^{-1} soil (Van Wees et al., 2013). Rhizosphere samples (roots with adhering soil) were harvested at 1, 2, 3 and 7 d after transplanting after which bacterial densities in the rhizosphere were determined. To this end, 0.1 g of rhizosphere sample or bulk soil (soil from unplanted pots) of five replicate pots per treatment were transferred into 2-ml Eppendorf tubes containing 1 ml of 10 mM $MgSO_4$ and shaken vigorously for 1 min. Aliquots of 100 µl of serial dilutions were plated onto KB agar plates containing 150 µg.ml^{-1} rifampicin and 0.2 g.L^{-1} Delvo®Cid. Plates were incubated overnight at 28°C after which WCS417 colonies were counted and densities in the rhizosphere and bulk soil samples were calculated.

Root microbiome analysis

Rhizosphere samples and bulk soil were harvested 3 d after transferring 26-day-old Col-0, *myb72* and *f6'h1* plants from the in vitro system into pots containing limed natural Reijerscamp soil. To this end, the total pot content was carefully removed and plant roots were gently shaken to remove loose soil particles. Roots together with adhering rhizosphere soil were transferred to 2-mL tubes, flash frozen in liquid nitrogen and stored at -80°C.

Genomic DNA isolation was performed by Vertis Biotechnologie AG (Freising, Germany). Briefly, the samples were ground with liquid nitrogen. From the tissue powders, genomic DNA was isolated using the RNA PowerSoil Total RNA Isolation Kit (MO BIO, Carlsbad, CA, USA.). The gDNA samples (approx. 20 ng

dsDNA each) were analyzed on a 0.8% agarose gel and the total RNA preparations were quality checked by capillary electrophoresis.

Library preparation was performed by Vertis Biotechnologie AG (Freising, Germany). The gDNA samples were treated with ultrasound (6 pulses of 30 s at 4°C). After end-repair, TruSeq sequencing adapters were ligated to the DNA fragments. Finally, the DNA was PCR-amplified to about 10-20 ng.μl^{-1} using a High-fidelity DNA polymerase. The amplified libraries in the size range of about 300 – 600 bp were then fractionated using a differential clean-up with the Agencourt AMPure kit (Beckman Coulter Brea, CA, USA). Aliquots of the size-fractionated libraries were quality checked by capillary electrophoresis.

Libraries were pooled and sequenced on an Illumina NextSeq 500 platform (Utrecht University DNA sequencing facility; USF), achieving on average 73 million paired-end reads sequencing depth per sample. Raw paired-end sequencing reads generated by Nextseq 500 were processed by the automated pipeline provided by USF for adapter removal, ambiguity, length and quality trimming.

Quality-filtered Illumina reads were taxonomically classified with Kaiju (Menzel et al., 2016). Kaiju translates metagenomic sequencing reads into amino acid sequences, and then compares amino acid sequences with protein sequences in NCBI BLAST nr + euk database. The reference database consisted of non-redundant protein sequences form bacteria, archaea, viruses, fungi, microbial eukaryotes and Arabidopsis, which are extracted from National Center for Biotechnology Information. Protein-level classification guarantees a higher sensitivity than nucleotide-based comparison. Running mode of Kaiju was set as the fastest MEM mode, with a default minimum match length as 11.

Statistical analyses were performed in R-studio (version Version 1.0.136) using R environment (R 2017, https://www.r-project.org version 3.3.3). Relative abundance data were normalized by the number of reads per sample replicate (total sum normalization) and α-diversity (Shannon and Chao1 index) and β-diversity (PCoA using Bray–Curtis dissimilarities) were calculated in the "phyloseq" package (version 1.19.1; McMurdie and Holmes, 2013). DESeq function of package DESeq2 (version 1.14.1) was used to perform two-class testing for differential RA of genera between different genotypes or genotypes under different iron treatment (Col-0) (Love et al., 2014). Genera were considered significantly differentially abundant between genotypes if their adjusted p-value was below 0.05 (corresponding to FDR <5% under the Benjamini-Hochberg correction). Package ggplot2 (version 2.2.1) was used to create plots and graphs of the microbiome analysis (Wickham, 2009).

Acknowledgements

This work was supported by ERC Advanced Grant no. 269072 of the European Research Council (to CMJP), China Scholarship Council (to KY), a postdoctoral fellowship of the Research Foundation Flanders (RJ) no. 12B8116N, and the Deutsche Forschungsgemeinschaft (ZUK 45/2010) (to IF). The authors would like to thank David Turrá for his suggestions on chemotropism assay, Bart Thomma for providing *Verticillium dahliae* JR2, Jürgen Zeier for *f6'h1* seeds, Richard Hickman for the discussion on the statistical analysis of the microbiome data and Hans Van Pelt for his essential technical assistance.

Supplemental data

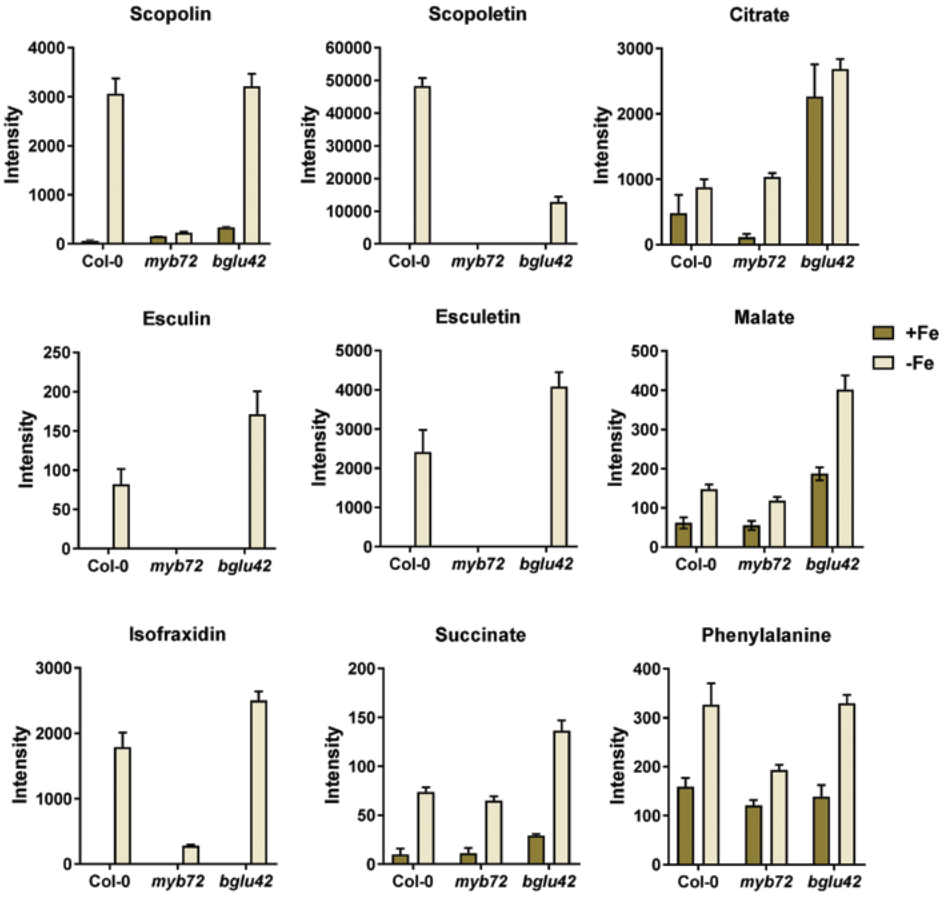

SUPPLEMENTAL FIGURE S1. Root exudation patterns of metabolite features corresponding to iron-starvation associated coumarins, TCA cycle intermediates, and phenylalanine.

Graphs represent the signal intensity of the metabolite features of the coumarins scopolin, scopoletin, esculin, esculetin and isofraxidin, the organic acids succinate, citrate, malate and the amino acid phenylalanine (precursor of coumarins) in root exudates of Col-0, *myb72,* and *bglu42* grown under iron sufficient (+Fe) or iron deficient (-Fe) conditions. The shown data are means of 3 replicates. Error bars represent SE.

#	RT (min)	Measured m/z	Molecular formula	Calculated mass (Da)	Error (mDa)	Name	MS^2 fragmentation
				coumarin derivatives			
1	3.06	355.101	$C_{16}H_{18}O_9$	354.095	-1.9	Scopolin	355.1005 [M+H]+, 193.049 [M-Glc+H]+, 178.0251, 133.0274
2	3.96	193.048	$C_{10}H_8O_4$	192.042	-1.4	Scopoletin	193.0482 [M+H]+ , 178.0255, 150.0303, 133.0278, 137.0593, 122.0357, 94.0412, 77.0386
3	2.78	341.085	$C_{15}H_{16}O_9$	340.079	-1.4	Esculin	341.085 [M+H]+, 179.0333 [M-Glc+H]+, 153.0906, 123.0409, 87.0441
4	3.15	179.032	$C_9H_6O_4$	178.027	-2	Esculetin	179.0319 [M+H]+, 151.039, 133.0273, 123.0433
5	4.23	223.059	$C_{11}H_{10}O_5$	222.053	-1.1	Isofraxidin	223.0589 [M+H]+, 207.0289, 190.0242, 179.032, 162.0299, 147.0424, 123.0428, 106.0378 (fragment of isofraxidin)
				Amino acids and TCA cycle intermediates			
6	0.78	191.020	$C_6H_8O_7$	192.027	0.5	Citrate	193.0303 [M+H]+, 157.0125, 139.0016, 129. , 111.0073, 87.0076, 68.997
7	0.59	133.016	$C_4H_6O_5$	134.022	1.9	Malate	133.0121 [M-H]-, 115.0023, 71.0131
8	0.97	119.033	$C_4H_6O_4$	118.027	-1.1	Succinate	117.0181 [M-H]-, 99.0074, 73.0287
9	1.99	166.085	$C_9H_{11}NO_2$	165.079	-1.8	Phenylalanine	166.0863 [M+H]+, 149.0676, 131.0482, 120.0808, 103.0546, 93.0698, 77.0386, 65.0387

SUPPLEMENTAL FIGURE S2. MS/MS confirmation of the identity of metabolite features corresponding to the selected coumarins, TCA cycle intermediates, and phenylalanine shown in Supplemental Figure S1.
Retention times (RT), exact mass-to-charge ratios (m/z), molecular formula, calculated mass (Da) and error (accuracy of single reading) of a selected group of compound standards. Identification was achieved with MS/MS fragmentation and related to their intensity changes in root exudates of Col-0, *myb72* and *bglu42* plants grown under iron-sufficient or iron-deficient conditions.

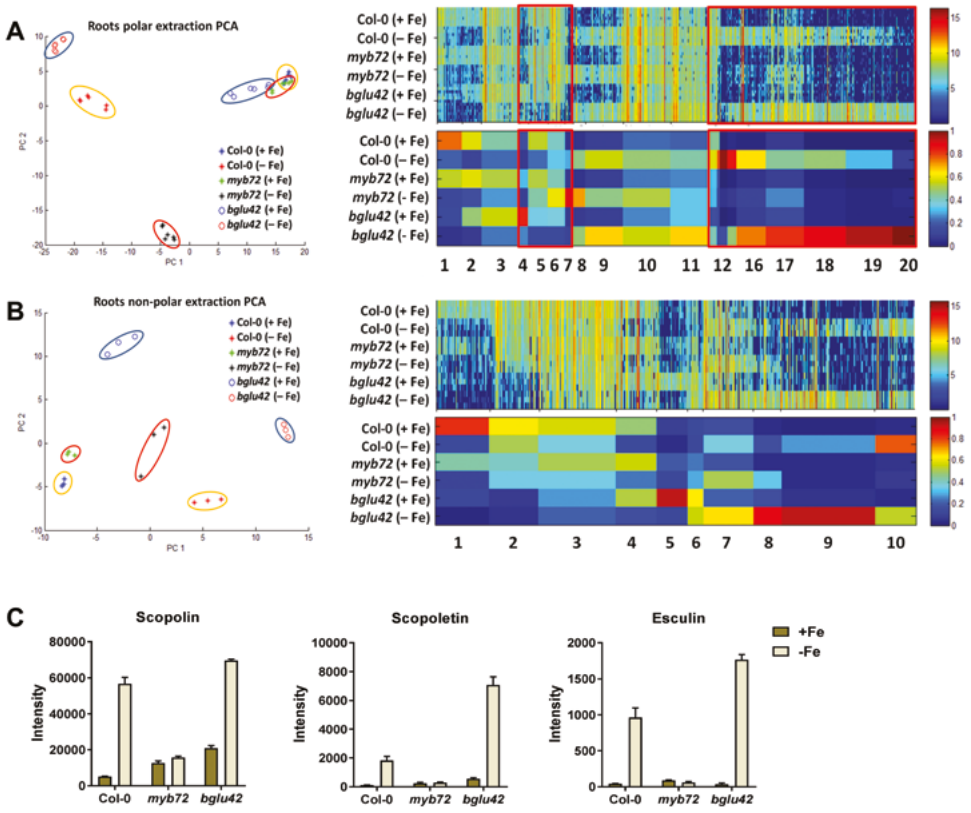

SUPPLEMENTAL FIGURE S3. Metabolite fingerprinting of features detected in the root interior of Col-0, *myb72* and *bglu42* grown under iron sufficient and iron starvation conditions.

(A) PCA plot of UPLC-ESI-TOF-MS metabolite profiles of polar compounds identified in the root interior of 20-d-old Col-0 (encircled in yellow), *myb72* (encircled in red) and *bglu42* (encircled in blue)plants grown in Hoagland medium with (+Fe) or without (-Fe). On the right, 1D-SOM clustering and prototype assignment of 1354 high-quality metabolite features (FDR $<10^{-8}$). Individual features (top panel) and prototypes (bottom panel) mostly affected by iron deficiency are highlighted in the red box. Heatmaps correspond to the intensity of each individual feature (top panel) and the average intensity of each cluster/prototype (bottom panel). **(B)** PCA plot of UPLC-ESI-TOF-MS metabolite profiles of non-polar compounds identified in the root interior of 20-d-old Col-0 (encircled in yellow), *myb72* (encircled in red) and *bglu42* (encircled in blue) plants grown in Hoagland medium with (+Fe) or without (-Fe). On the right, 1D-SOM clustering and prototype assignment of 554 high-quality metabolite features (FDR <0.001). Heatmaps correspond to the intensity of each individual feature (top panel) and the average intensity of each cluster/prototype (bottom panel). **(C)** Signal intensity of features related to scopolin, scopoletin and esculin in the root extracts of Col-0, *myb72* and *bglu42* plants grown under iron-sufficient (+Fe) or iron-deficient (-Fe) conditions. The shown data are means of 3 replicates. Error bars represent SE.

#	RT (min)	Measured m/z	Molecular formula	Calculated mass (Da)	Error (mDa)	Name	MS² fragmentation
				coumarin derivatives			
1	3.09	355.101	$C_{16}H_{18}O_9$	354.095	-1.3	Scopolin	355.1005 [M+H]+, 193.049 [M-Glc+H]+, 178.0251, 133.0274
2	3.98	193.048	$C_{10}H_8O_4$	192.042	-1.4	Scopoletin	193.0482 [M+H]+ , 178.0255, 150.0303, 133.0278, 137.0593, 122.0357, 94.0412, 77.0386
3	2.8	341.085	$C_{15}H_{16}O_9$	340.079	-1.7	Esculin	341.085 [M+H]+, 179.0333 [M-Glc+H]+, 153.0906, 123.0409, 87.0441

SUPPLEMENTAL FIGURE S4. MS/MS confirmation of the identity of metabolite features corresponding to the selected coumarins shown in Supplemental Figure S3C. Retention times (RT), exact mass-to-charge ratios (m/z), molecular formula, calculated mass (Da) and error (accuracy of single reading) of a selected group of compound standards. Identification was achieved with MS/MS fragmentation in root extracts of Col-0, *myb72* and *bglu42* plants grown under iron-sufficient or iron-deficient conditions.

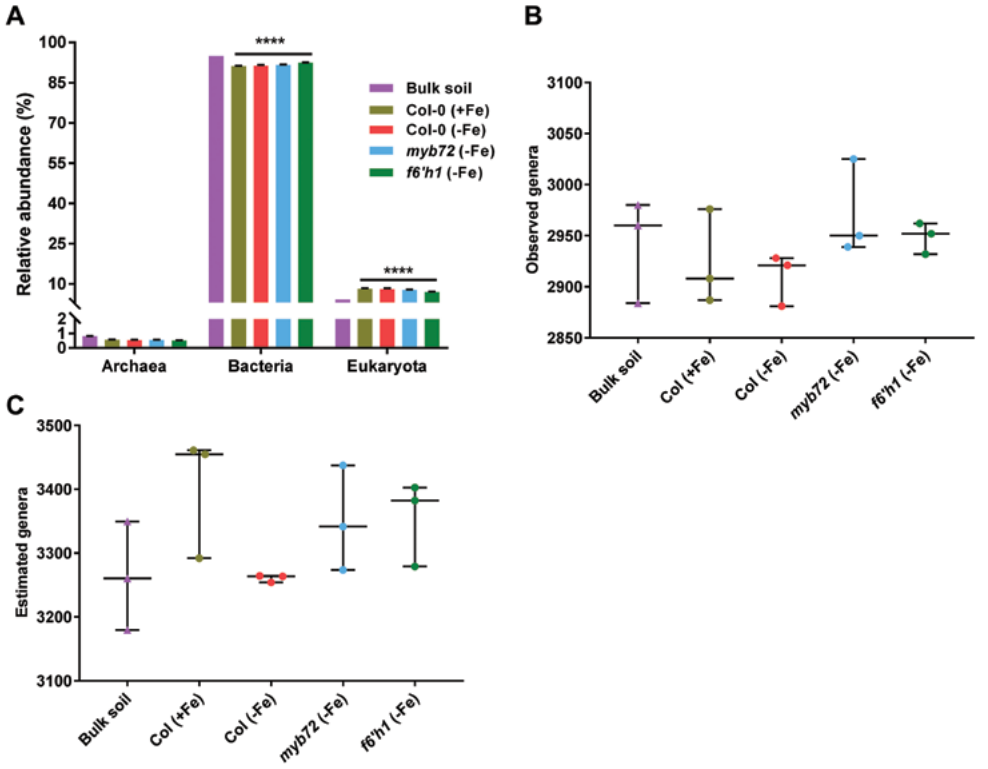

SUPPLEMENTAL FIGURE S5. Domain relative abundance and α-diversity estimates of the communities in soil and roots of different genotypes.

(**A**) Average relative abundance of Archaea, Bacteria and Eukaryota domains in bulk soil and root-associated microbial communities. Bar correspond to the average of 3 replicates and error bars represent the standard error of the mean. Stars indicate statistically significant differences of root samples compared to bulk soil (Two-way ANOVA, Tukey's test; ****$P < 0.0001$). (**B**) Total number of observed genera and (**C**) number of estimated genera based on Chao1 index. Shapes with same color indicate samples of one treatment. Horizontal bars correspond to median, the first (25%) and third (75%) and maximum and minimum values of each treatment.

SUPPLEMENTAL TABLE S1. List of primers used in this study

Primer name	Primer sequence (5'→3')
*At1g13320*_Fw (PP2AA3)	TAACGTGGCCAAAATGATGC
*At1g13320*_Rev (PP2AA3)	GTTCTCCACAACCGCTTGGT
*MYB72*_Fw	ACGAGATCAAAAACGTGTGGAAC
MYB72 _Rev	TCATGATCTGCTTTTGTGCTTTG
*IRT1*_Fw	ACCCGTGCGTCAACAAAGCTAAAG
*IRT1*_Rev	TCCCGGAGGCGAAACACTTAATGA
*FRO2*_Fw	TGTGGCTCTTCTTCTCTGGTGCTT
*FRO2*_Rev	TGCCACAAAGATTCGTCATGTGCG
F6'H1 _Fw	TGATATCTGCAGGAATGAAACG
*F6'H1*_Rev	GGGTAGTAGTTAAGGTTGACTC

SUPPLEMENTAL TABLE S2. Shotgun metagenomic sequencing of samples and classification of obtained reads by Kaiju. Samples analyzed come from two different compartments (bulk soil and root-rhizosphere). The root-rhizosphere samples are sampled from 3 different genotypes (Col-0, *myb72*, *f6'h1*) and 2 different conditions of iron availability (yes= sufficient iron; no=iron deficiency) are tested. Paired-end sequencing reads (in millions (M)) were classified with Kaiju (Menzel et al., 2016) using a database containing protein sequences of Bacteria, Archaea, Viruses, Fungi, microbial eukaryotes and Arabidopsis. Reads classified to Arabidopsis and not classified to genus level were excluded from downstream statistical processing.

Sample characteristics				Reads			
				Sequencing output	Kaiju		
					Classified		Not classified (%)
Sample name	Sample type	Genotype	Iron	Paired-end reads (M)	Microbiome (%)	Arabidopsis (%)	
B 1	bulk soil	n/a	n/a	66.8	65.45	0.03	34.52
B 2	bulk soil	n/a	n/a	65.8	65.97	0.01	34.02
B 3	bulk soil	n/a	n/a	52.4	65.85	0.01	34.14
Col +Fe 1	root-rhizosphere	Col-0	yes	83.6	34.39	29.82	35.79
Col +Fe 2	root-rhizosphere	Col-0	yes	64.5	34.18	30.54	35.28
Col +Fe 3	root-rhizosphere	Col-0	yes	55.6	36.73	28.25	35.02
Col -Fe 1	root-rhizosphere	Col-0	no	63.4	38.56	26.59	34.86
Col -Fe 2	root-rhizosphere	Col-0	no	77.2	34.69	29.87	35.44
Col - Fe 3	root-rhizosphere	Col-0	no	67.6	34.25	32.12	33.63
myb72 - Fe 1	root-rhizosphere	*myb72*	no	76.0	35.15	30.03	34.81
myb72 - Fe 2	root-rhizosphere	*myb72*	no	75.7	32.97	30.11	36.91
myb72 - Fe 3	root-rhizosphere	*myb72*	no	108.7	36.40	28.87	34.73
f6'h1 - Fe 1	root-rhizosphere	*f6'h1*	no	79.0	34.49	29.94	35.58
f6'h1 - Fe 2	root-rhizosphere	*f6'h1*	no	80.3	35.85	30.41	33.75
f6'h1 - Fe 3	root-rhizosphere	*f6'h1*	no	82.0	33.57	31.61	34.82
Total				**1098.6**			

Supplemental Datasets S1-S6 are available upon request.

CHAPTER 5

A forward genetic screen to identify novel regulators of *MYB72* activation in iron deficiency and induced systemic resistance in Arabidopsis

Ioannis A. Stringlis[1], Fabiola Peña Morcom[1], Andrea Manzotti[1], Christos Zamioudis[1,2] and Corné M.J. Pieterse[1]

[1] Plant-Microbe Interactions, Department of Biology, Faculty of Science, Utrecht University, P.O. Box 800.56, 3508 TB, Utrecht, The Netherlands
[2] Present address: Rijk Zwaan Breeding B.V., P.O. Box 40, 2678 ZG De Lier, The Netherlands

Abstract

Selected root-inhabiting beneficial microbes can trigger a systemic form of immunity in their plant hosts, known as induced systemic resistance (ISR). This defense phenomenon provides the plant with resistance against various pathogens and insects. ISR establishment in *Arabidopsis thaliana* (Arabidopsis) by *Pseudomonas simiae* WCS417 (WCS417) is associated with the root-specific activation of the transcription factor gene *MYB72*. MYB72 is required for the onset of ISR, but is also involved in plant responses to iron limitation. In a previous study, a transgenic *MYB72*$_{pro}$*:GFP-GUS* reporter line was developed, which allowed the visualization of tissue-specific *MYB72* expression patterns in roots in response to WCS417 or iron deficiency conditions. In this study, we aimed to identify upstream components of the signaling pathway that regulates the activation of *MYB72* gene expression in Arabidopsis roots. For that we screened EMS-mutagenized seedlings of the transgenic line *MYB72*$_{pro}$*:GFP-GUS* for putative mutants with reduced *MYB72* expression under *MYB72*-inducing iron deficiency conditions. Screening of the M_2 generation of *MYB72*$_{pro}$*:GFP-GUS* seedlings under the fluorescence stereomicroscope yielded 168 putative mutants (putants) with decreased GFP signal. Seeds from these M_2 plants were harvested and next-generation M3 seedlings were rescreened for *MYB72* expression by qRT-PCR, yielding 11 putants with clearly reduced *MYB72* expression levels during growth in iron-limited medium. Sequencing of both the promoter region and the *MYB72* coding sequence of these putants, however, did not yield mutations that could explain their reduced *MYB72* expression phenotype. Future analysis, involving backcrossing with the parental line and whole genome sequencing of the putants should reveal the mutations responsible for the observed reduced *MYB72* expression phenotype and their role in the regulation of MYB72-dependent ISR and iron uptake responses.

Introduction

The soil layer surrounding roots that is strongly affected by plant secretions, known as the rhizosphere, harbors a complex microbial community referred to as the root microbiome (Bulgarelli et al., 2013; Philippot et al., 2013). A multitude of microorganisms in the root microbiome depends on root secretions for their survival and proliferation (Badri et al., 2009a). Most of these rhizosphere microbes need to compete with other organisms for the colonization of exudate-rich niches. The outcome of such microbe-microbe interactions can have a great impact on plant fitness and longevity (Berendsen et al., 2012). The microbiome can contain plant pathogens, but also beneficial microorganisms that aid plants in nutrient uptake, growth, and overcoming different biotic and abiotic stresses. When achieving sufficiently high numbers in the rhizosphere, selected members of the root microbiome can trigger a systemic form of immunity in their host (Raaijmakers et al., 1995; Pieterse et al., 2014). This phenomenon is called induced systemic resistance (ISR) and provides plants with increased resistance against a broad range of pathogens and insects (Pieterse et al., 2014). A characteristic of ISR is that it is dependent on functional ethylene (ET) and jasmonic acid (JA) signaling pathways (Pieterse et al., 1998; Pieterse et al., 2000). Studies on the interaction between *Arabidopsis thaliana* (hereafter Arabidopsis) and *Pseudomonas simiae* WCS417 (previously *P. fluorescens* WCS417; (Berendsen et al., 2015)) revealed several of the molecular components required for the establishment of ISR. One key finding is that the root-specific transcription factor gene *MYB72* is required locally in the roots for the onset of ISR (Van der Ent et al., 2008; Segarra et al., 2009). In a microarray study on the transcriptional changes in Arabidopsis roots in response to colonization by WCS417, *MYB72* was identified as one of the induced genes (Verhagen et al., 2004). Subsequently, mutant *myb72* plants were shown to be incapable of mounting ISR in response to colonization of the roots by ISR-inducing *Pseudomonas* spp. strains (Van der Ent et al., 2008) or by ISR-inducing *Trichoderma* spp. strains (Segarra et al., 2009). In another microarray study with wild-type Col-0, mutant *myb72,* and *MYB72*-overexpressing plants, Zamioudis et al. (2014) identified the β-glucosidase gene *BGLU42* as a major downstream target of MYB72. Mutant *bglu42* plants were unable to mount ISR in response to colonization of the roots by ISR-inducing WCS417, while overexpression of *BGLU42* resulted in constitutive resistance against various foliar pathogens (Zamioudis et al., 2014), indicating that MYB72-regulated *BGLU42* expression is important for the onset and expression of ISR.

A number of studies have observed that MYB72 is additionally involved in plant responses to iron limitation (Van de Mortel et al., 2008; Buckhout et al., 2009). Together with MYB10, MYB72 was shown to be required for plant survival in alkaline substrates where iron availability is extremely low (Palmer et al., 2013). These findings, suggest a role of MYB72 in linking ISR and the iron uptake response in plants. In roots of dicotyledonous plants, iron deficiency activates a set of iron uptake-promoting processes described as Strategy I (Kobayashi and Nishizawa, 2012). In this iron uptake response, acidification of the rhizosphere by membrane-localized H^+-ATPases results in enhanced solubility of Fe^{3+}, that is reduced to Fe^{2+} through the activity of FERRIC REDUCTION OXIDASE 2 (FRO2). Finally, IRON-REGULATED TRANSPORTER 1 (IRT1) is responsible for the transport of Fe^{2+} from the rhizosphere into the root interior (Walker and Connolly, 2008). A key regulatory role in these processes was demonstrated for FER-LIKE IRON DEFICIENCY TRANSCRIPTION

FACTOR (FIT) (Colangelo and Guerinot, 2004). A link between ISR and the iron deficiency response was provided by Zamioudis et al. (2015), who showed that a significant proportion of root transcriptomic changes in response to WCS417 is shared with root responses to iron limitation (Dinneny et al., 2008; Zamioudis et al., 2015). ISR-inducing rhizobacteria appeared to simultaneously trigger the expression of *MYB72* and the iron uptake genes *FRO2* and *IRT1* in Arabidopsis roots in a FIT-dependent manner, while ISR-non-inducing rhizobacteria did not. Volatile organic compounds produced by the beneficial rhizobacteria emerged as important elicitors of this response (Zamioudis et al., 2015). Finally, it was shown that MYB72 has a central regulatory role in the biosynthesis of iron-mobilizing phenolic compounds produced via the phenylpropanoid pathway in plant roots, and that BGLU42 plays a role in their secretion into the rhizosphere (Fourcroy et al., 2014; Schmid et al., 2014; Zamioudis et al., 2014; Fourcroy et al., 2016; Verbon et al., 2017).

Using the transgenic line *MYB72*$_{pro}$*:GFP-GUS*, which expresses a GFP-GUS fusion protein under control of the promoter of *MYB72*, Zamioudis et al. (2015) studied the expression pattern of *MYB72* in Arabidopsis roots in response to WCS417 volatiles (VOCs) and iron deficiency. Employment of this *MYB72*-reporter line revealed that WCS417 VOCs induce *MYB72* expression in epidermal and cortical cells of the late maturation zone, while iron deficiency induced the expression of *MYB72* in a larger root area, including the elongation and early and late maturation zone. Using grafts of VOCs-exposed and non-exposed Arabidopsis rootstocks and scions, Martinez-Medina et al. (2017) provided evidence that the microbial VOCs are perceived by the roots, resulting in priming of shoot tissues for enhanced JA-dependent defenses and ISR. Although VOCs are perceived in the roots, activation of *MYB72* in root epidermal and cortical cells requires a systemic photosynthesis-related signal from the shoots, as decapitated roots or exposure of the roots to VOCs in the dark, renders the roots incapable of activating *MYB72* and the iron uptake marker genes *FRO2* and *IRT1* (Zamioudis et al., 2015).

Despite this knowledge on the regulation of *MYB72* in Arabidopsis roots in response to ISR-inducing rhizobacteria and the essential role of MYB72 in downstream ISR and iron uptake responses, it still remains elusive what signals function between VOCs perception and *MYB72* activation in plant roots. In this study, we aimed to shed light on this issue. To this end, we performed EMS mutagenesis on seeds of transgenic line *MYB72*$_{pro}$*:GFP-GUS* and screened for mutants with reduced *MYB72* expression in the roots under *MYB72*-inducing conditions. Here, we describe the screening and the initial characterization of 11 putants.

Results

EMS mutagenesis and screening conditions

In order to identify signaling components that act upstream of *MYB72* activation in Arabidopsis roots, we performed an EMS mutagenesis screen using *MYB72*$_{pro}$*:GFP-GUS* as parental line. The strategy and main steps of this screen are presented in Figure 1. In the initial screen, we managed to screen 60,000 M_2 seedlings derived from 50 M_1 pools, representing ~2250 M_1 plants. As an independent measure for the successfulness of the EMS mutagenesis, we determined the percentage of lethality and chlorophyll

mutations (albino) in the M_2 generation (Kim et al., 2006). Both characteristics are indicators of the successfulness of EMS mutagenesis (Pollock and Larkin, 2004). The M_1 seeds showed a reduction of 20-30% in the outgrowth of viable seedlings. Moreover, of the 60,000 M_2 seedlings tested, 12 seedlings displayed a visible albino phenotype which is equal to a ratio of 1 albino per 5000 seedlings (0.02% of the population) (Figure 3B). These figures are in the range of what others have found before with similar EMS mutagenesis approaches (Jander et al., 2003; Micol-Ponce et al., 2014).

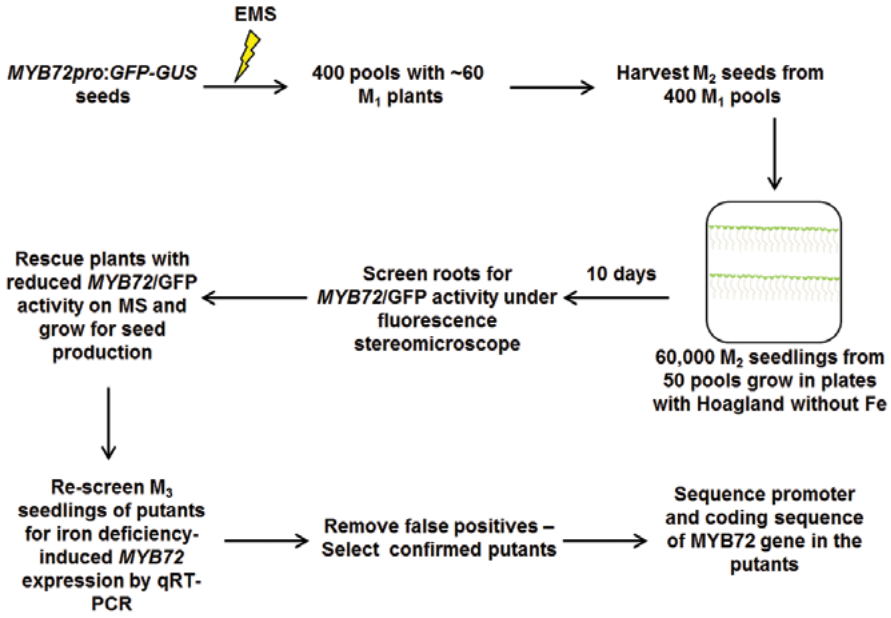

FIGURE 1. Workflow of EMS mutagenesis screen for regulators of *MYB72* gene expression in Arabidopsis roots.
A total of ~25,000 EMS-mutagenized M_1 seeds of parental line *MYB72pro:GFP-GUS* were divided into 400 pools with ~60 M_1 seeds each. M_1 plants were grown to maturity, after which M_2 seeds were harvested from each of the 400 pools. Of 50 M_1 pools, M_2 descendants (~1200 per pool) were grown on iron-deficient Hoagland medium to screen their roots for *MYB72*-dependent GFP activity under a fluorescence stereomicroscope. Putants with visibly reduced *MYB72*/GFP activity were rescued on MS medium with iron and grown to maturity, after which M_3 seeds were harvested. Roots of M_3 seedlings were re-screened for iron deficiency-induced *MYB72* gene expression by qRT-PCR. Positive putants were sequenced for mutations in the *MYB72* promoter region and coding sequence.

To determine the most optimal conditions for the mutant screening, we first tested GFP activity in the parental line *MYB72$_{pro}$:GFP-GUS* in response to WCS417 VOCs exposure and in response to iron starvation. As a negative control, we used wild-type Col-0 plants. The screening for *MYB72*/GFP activity was carried out by individually inspecting the roots of WCS417 VOCs- or iron starvation-treated *MYB72$_{pro}$:GFP-GUS* seedlings under a fluorescence stereomicroscope in situ on the agar plate. Figure 2 shows that exposure of the *MYB72$_{pro}$:GFP-GUS* seedlings to WCS417 VOCs or iron starvation conditions resulted in enhanced accumulation of the GFP fluorophore, while in the seedlings that were not treated with the VOCs or were growing under sufficient iron conditions, no or very low GFP activity was detectable. As expected in Col-0, no GFP activity was detected in any of the tested conditions (data not shown). Although *MYB72*-driven

GFP activity was detected in *MYB72$_{pro}$:GFP-GUS* roots exposed to WCS417 VOCs, it was not apparent in all roots tested. By contrast, GFP activity was detected in the majority of the *MYB72$_{pro}$:GFP-GUS* roots when the seedlings were grown in iron-limited medium. Hence, we decided to use iron starvation as the screening condition for the EMS mutagenesis screen for mutants with impaired inducible *MYB72* expression.

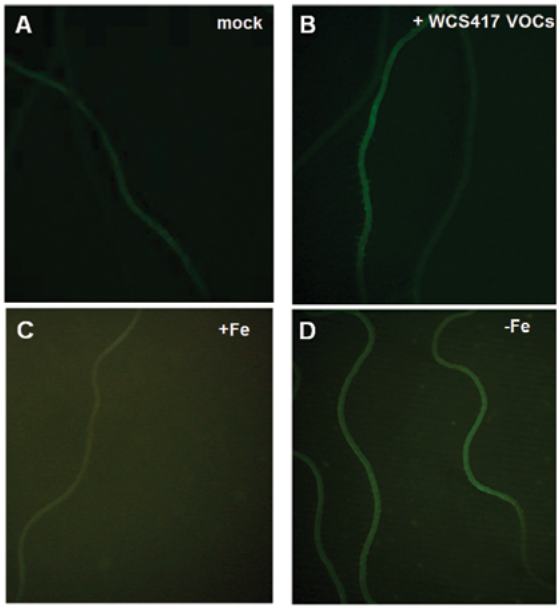

FIGURE 2. Visualization of GFP fluorophore in *MYB72pro:GFP-GUS* seedlings after WCS417-VOCs exposure or iron starvation.
Photographs show representative images of roots from 10-day-old *MYB72pro:GFP-GUS* seedlings grown (A) without *P. simiae* WCS417 VOCs, (B) in the presence of WCS417 VOCs, (C) in Hoagland medium with iron (+Fe) and (D) in Hoagland medium without iron (-Fe). Pictures were taken under a fluorescence stereomicroscope (Leica MZ16 FA) with a GFP3 filter (excitation: 450-490 nm, emission: 500-550 nm).

Identification of putative mutants with impaired *MYB72* expression

Approximately 70-80% of the *MYB72$_{pro}$:GFP-GUS* M_1 seeds produced viable seedlings. Hence, the 400 pools of M_2 seeds were each collectively descendants of ~45 M_1 plants. In this initial screen, we screened 50 of the 400 pools, and for each pool we screened 1200 M_2 seedlings (~60,000 seedlings in total from ~2250 mutagenized M_1 plants). As described above, all mutagenized seedlings were grown under iron deficiency conditions (as in Figure 2D). On each plate, ~60 mutagenized seedlings were grown. Plates with parental *MYB72$_{pro}$:GFP-GUS* seedlings were also included. After 10 d of growth in long-day growth chambers, M_2 seedlings were individually inspected under a fluorescence stereomicroscope for reduced or lack of GFP fluorophore accumulation in roots in comparison to the parental line (Figure 3A). Of the 60,000 seedlings tested, 183 putants with decreased or no GFP fluorescence in the roots were identified. Putant seedlings were transferred to MS agar plates with sufficient iron and allowed to recover from iron deficiency for 1 week before being transplanted into pots containing soil. In the soil, putants were grown to maturity and seed set (M_3 seeds). The putants showed differences in flowering time and displayed various growth phenotypes (data not shown), indicating that the EMS mutagenesis had affected various life processes. In total 15 of the 183 M_2 putants didn't survive after transplanting, resulting in a final number of 168 M_2 putants from the initial screen.

A.

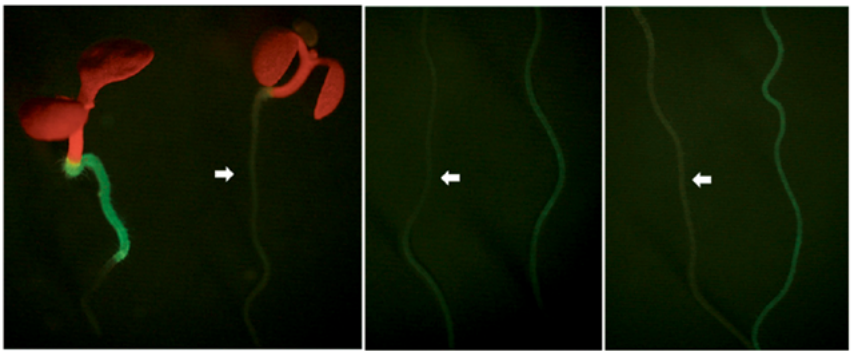

B.

Number of pools screened	Number of M_2 plants screened	Number of albino plants	Number of putants	Number of dead putants after transplanting	Final number of M_2 putants
50/400	60,000	12	183	15	168

FIGURE 3. Selection of putants with altered induced *MYB72* expression patterns in roots of mutagenized *MYB72pro:GFP-GUS* seedlings.

(A) Representative images of putants from 10-d-old *MYB72pro:GFP-GUS* M_2 seedlings grown on Hoagland medium without iron. White arrows point to roots of putants with reduced MYB72-driven GFP fluorophore accumulation. Pictures were taken under a fluorescence stereomicroscope (Leica MZ16 FA) with a GFP3 filter (excitation: 450-490 nm, emission: 500-550 nm). (B) Summary of the results of the initial EMS mutagenesis screen.

Secondary screening and selection of positive putants

To validate the putants selected in the initial screening, we tested the expression of their endogenous *MYB72* gene in response to iron starvation. To this end, M_3 seedlings of the putants were grown on plates containing modified Hoagland medium with or without iron. First, the parental *MYB72*$_{pro}$*:GFP-GUS* line was tested to make sure that at harvesting time (10 d of growth under iron deficient or iron sufficient conditions), expression of *MYB72* and the iron deficiency marker genes *FRO2* and *IRT1* were induced by iron starvation. Figure 4 shows that iron starvation indeed induced the expression of all three genes in roots of the parental line. Next, the expression of *MYB72* was tested in the roots of 108 of the initial 168 putants (representing all M_2 putants from M_1 pool numbers 1-24). This rescreening resulted in 11 positive putants with significantly reduced *MYB72* gene expression levels in the roots in response to iron starvation (Figure 5).

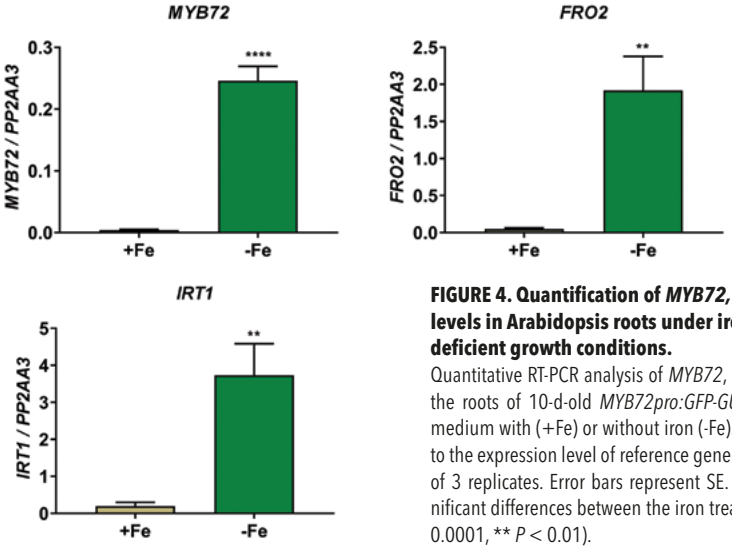

FIGURE 4. Quantification of *MYB72*, *FRO2*, and *IRT1* transcript levels in Arabidopsis roots under iron sufficient and iron deficient growth conditions.

Quantitative RT-PCR analysis of *MYB72*, *FRO2* and *IRT1* transcript levels in the roots of 10-d-old *MYB72pro:GFP-GUS* seedlings grown in Hoagland medium with (+Fe) or without iron (-Fe). Gene expression was normalized to the expression level of reference gene *At1g13320*. The values are means of 3 replicates. Error bars represent SE. Asterisks indicate statistically significant differences between the iron treatments (Student's *t* test; ****$P <$ 0.0001, ** $P < 0.01$).

Sequencing of the *MYB72* gene of the positive putants

The fact that both the transgene *MYB72*$_{pro}$*:GFP-GUS* and the endogenous *MYB72* gene are impaired in their responsiveness to iron starvation makes it very unlikely that the mutant phenotypes of the 11 putants are caused by mutations in the *MYB72*$_{pro}$*:GFP-GUS* transgene or the endogenous *MYB72* gene itself. Nevertheless, we checked the genomic sequence of the *MYB72* gene of the 11 positive putants for the presence of mutations in the *MYB72* promoter or coding sequence. To this end, genomic DNA from the putants was isolated after which the promoter region (1900 bp upstream from the ATG start codon) and the coding sequence of *MYB72* were PCR-amplified. Sequencing of the PCR fragments confirmed that none of the 11 putants had a mutation in the amplified promoter or coding region of the *MYB72* gene (data not shown), indicating that the mutant phenotype of the putants is not caused by mutations in the *MYB72* gene itself. Hence, mutations elsewhere in the genome of these putants are likely responsible for the impaired iron-starvation induced expression of *MYB72* induction.

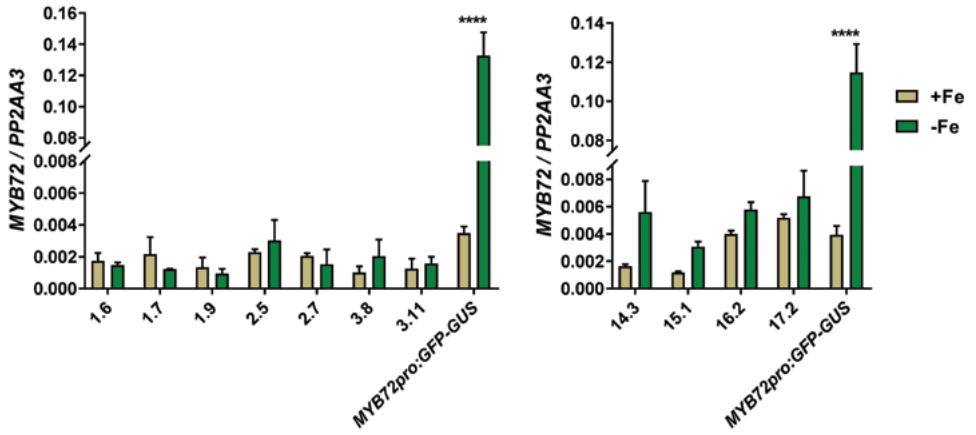

FIGURE 5. Quantification of *MYB72* transcript levels in roots of confirmed putants under iron sufficient and iron deficient growth conditions.

Quantitative RT-PCR analysis of *MYB72* transcript levels in the roots of 10-d-old M_3 putants grown in Hoagland medium with (+Fe) or without iron (-Fe). Expression of *MYB72* in the parental *MYB72pro:GFP-GUS* line was tested as a positive control. Code numbers of the putants refer to the M_1 pool number, followed by the number of the putant that was selected in that pool (e.g. 1.6 = putant number 6 in pool number 1). Gene expression was normalized to the expression level of reference gene *At1g13320*. The values are means of 2 replicates. Error bars represent SE. Asterisks indicate statistically significant differences between the iron treatments (Two-way ANOVA, Sidak's test; ****$P < 0.0001$).

Discussion

Evidence is accumulating for a dual role of the root-specific transcription factor MYB72 in both the onset of ISR and the iron deficiency response in Arabidopsis (Van der Ent et al., 2008; Palmer et al., 2013; Zamioudis et al., 2015; Martinez-Medina et al., 2017). While ISR- and iron uptake-related processes acting downstream of MYB72 are relatively well studied (Zamioudis et al., 2014; Zamioudis et al., 2015), knowledge of the signaling pathway that leads to the activation of *MYB72* remained limited. The generation of transgenic reporter line *$MYB72_{pro}$:GFP-GUS* allowed the study of cell type-specific expression of *MYB72* in response to ISR-inducing rhizobacteria and iron starvation (Zamioudis et al., 2015). Using this reporter line, it was shown that VOCs of *P. simiae* WCS417, as well as conditions of iron deficiency, activate *MYB72* in the epidermal and cortex cells of Arabidopsis roots (Zamioudis et al., 2015). Using the characteristics of this line in the visualization of *MYB72* expression in Arabidopsis roots, we performed an EMS forward genetic screen aiming to find components that have a role upstream of *MYB72* activation (Figure 1).

EMS mutagenesis is a commonly used chemical method that induces mutations that lead to base pair substitutions such as GC→AT (Greene et al., 2003). This form of mutagenesis can generate random mutations distributed throughout the plant genome (Koornneef, 2002), which allows the screening for mutants with a phenotype of interest. An important aspect to consider before performing this kind of genetic screens is the nature of the parental line, as this can define the screening method necessary to identify mutants of interest (Page and Grossniklaus, 2002). In this study, we performed EMS mutagenesis on the transgenic line *$MYB72_{pro}$:GFP-GUS*, which allows visualization of *MYB72* expression in stimulated roots with two

different approaches: detection of GFP fluorescence under the fluorescence microscope or measurement of GUS activity by GUS staining. We chose detection of GFP activity by fluorescence microscopy, because this approach is non-destructive and makes the recovery of putants after the selection relatively easy (Figures 2 and 3). The best condition for the mutant screen appeared to be iron starvation, because this treatment lead to a more robust activation of *MYB72*/GFP in the roots of the reporter line than treatment of the roots with WCS417 VOCs (Figure 2).

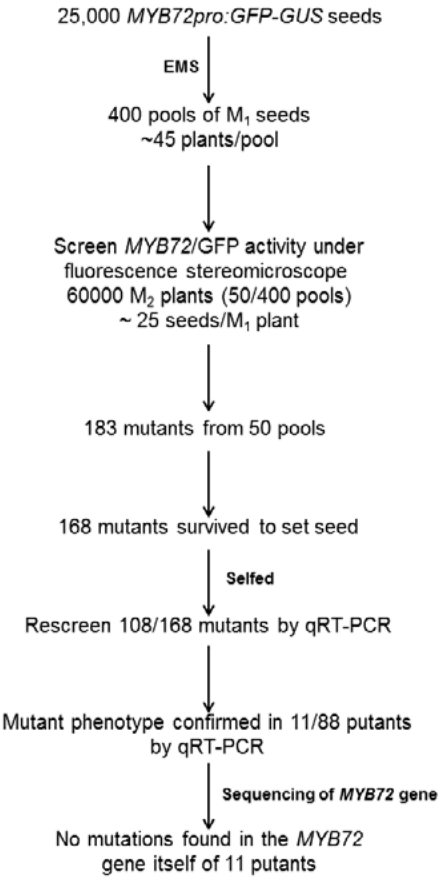

FIGURE 6. Schematic overview of the current status of the EMS mutagenesis screen for mutants with impaired *MYB72* activation in Arabidopsis roots.

An indication of successful EMS mutagenesis is the presence of albino plants and effects on growth or embryonic lethality (Pollock and Larkin, 2004). Indeed, after the sowing of M_1 seeds, we roughly estimated that 20-30% didn't germinate, while during the screening of M_2 seedlings we observed 12 albino seedlings. We managed to screen 60,000 M_2 seedlings deriving from 50 M_1 pools, consisting of ~45 plants each (M_2 progeny of in total ~2250 M_1 plants). The initial screen for impaired iron starvation-induced *MYB72* expression in the roots yielded 168 M_2 putants.

Assuming that all of them are positive putants resulting in *MYB72* repression then we estimated the mutation frequency according to Gaul method (Gaul, 1957, 1960). The formula for the calculation is m=m′/n x f, where m′ is the number of mutants found per number of screened M_2 plants (n), while f is the average mutant frequency in the progeny of a heterozygote (0.25 for recessive mutants) (Koornneef et al., 1982; Koornneef, 2002). Based on the putants we found in the number of M_2 plants we screened then "m" in our case should be 168/60,000*0.25, that is equal to a mutation frequency per locus per cell of $7x10^{-4}$.

After rescreening the M_3 progeny of 108 of the 168 primary M_2 putants for impaired iron starvation-induced *MYB72* expression, the mutant phenotype was confirmed for 11 putants (Figure 5 and 6). From these putants, three were isolated from pool 1, two from pool 2 and two from pool 3, making it possible that they originate from the same M_1 plant (Jander et al., 2003). The other four confirmed putants were single putants from pools 14, 15, 16 and 17. Sequencing of the *MYB72* gene in the 11 confirmed putants showed that the *MYB72* gene was fully intact. Because both the expression of the endogenous *MYB72* gene and the *MYB72*$_{pro}$*:GFP-GUS* transgene were impaired in the putants, it is likely that the mutations responsible for the impaired *MYB72* promoter activity is caused by mutations elsewhere in the genome. Future research will be aimed at identifying the nature of the mutant phenotype of the 11 selected putants. First the responsible genes should be identified. For that, the putants will undergo several rounds of backcrossing with the non-mutated parental line and selfing to reduce the number of non-relevant EMS mutations. Subsequently, after confirming by quantitative RT-PCR (qRT-PCR) that the mutated phenotype is still stable, whole genome sequencing of the parental line and the putants should lead to the identification of the mutations responsible for the repression of *MYB72* (Zuryn et al., 2010; Austin et al., 2011; Nordström et al., 2013). Ideally, the expected mutations in these putants are located in a gene that codes for a protein that regulates the activation of *MYB72* in Arabidopsis roots during conditions of iron starvation and in response to exposure to VOCs of ISR-inducing microbes, as this would provide further insight into the signaling steps that act upstream of *MYB72* activation during these processes.

Materials and methods

Plant material and EMS mutagenesis

Arabidopsis thaliana accession Col-0 and transgenic line *MYB72*$_{pro}$*:GFP-GUS* (in Col-0 background) were used in this study. Reporter line *MYB72*$_{pro}$*:GFP-GUS* was generated in a previous study by Zamioudis et al. (2015). Ethyl methanesulfonate (EMS) mutagenesis was performed on *MYB72*$_{pro}$*:GFP-GUS* seeds as described (Weigel and Glazebrook, 2006). Generation M_0 seeds were placed in 50-ml Falcon tubes containing 0.1% TWEEN® 20 (Sigma-Aldrich, St. Louis, MO, USA) on a roller bench for 15 min, after which they were washed twice with milliQ water and kept immersed in milliQ water for 5 d at 4°C on a roller bench in the dark. Subsequently, EMS was added to the tube with seeds to a final concentration of 0.2% (w/v). The tube was fully covered in aluminum foil and placed on a roller bench for 18 h at room temperature. After the 18-h EMS treatment, seeds were transferred to filter paper in a Buchner funnel and washed 8 times with dH_2O. Flow through dH2O was diluted with same volume of 1M NaOH to inactivate EMS. Washed seeds

were then dried on filter paper for 45 min, after which they were suspended in 0.1% agarose (Hispanagar, Burgos, Spain). Since EMS is a mutagen, the mutagenesis procedure was performed in a fume hood and the procedure was performed with particular care (double gloves, masks, lab coat).

Plant growth conditions

After EMS mutagenesis approximately 25,000 mutagenized *MYB72$_{pro}$:GFP-GUS* seeds (M_1) that were suspended in 0.1% agarose were sown in 400 pots, with each pot containing ~60 M_1 seeds. Pots were subsequently placed in a plant growth chamber under long day-conditions (21°C; 16 h light, 8 h dark; light intensity 100 µmol $m^{-2}.s^{-1}$). M_2 generation seeds of M_1 plants were harvested per pot and kept separately in 400 pools. Because ~70-80% of the M_1 seeds produced viable seedlings, each pool of M_2 seeds consisted of ~45 mutagenized M_1 generation plants each.

To test the best *MYB72*-inducing condition for the mutant screen, *MYB72$_{pro}$:GFP-GUS* seedlings were exposed to VOCs of *P. simiae* WCS417 or grown under iron deficiency conditions. Col-0 plants were used as a negative control for GFP fluorescence. For WCS417-VOCs exposure, seeds were sown on 1 x Murashige and Skoog (MS; (Murashige and Skoog, 1962)) agar-solidified medium supplemented with 0.5% sucrose, and pH adjusted to 6.0 with KOH. For growth under iron deficiency conditions, seeds were sown on agar-solidified Hoagland medium (Hoagland and Arnon, 1938) consisting of KNO_3 (3 mM), $MgSO_4$ (0.5 mM), $CaCl_2$ (1.5 mM), K_2SO_4 (1.5 mM), NaH_2PO_4 (1.5 mM), H_3BO_3 (25 µM), $MnSO_4$ (1 µM), $ZnSO_4$ (0.5 µM), $(NH_4)_6Mo_7O_{24}$ (0.05 µM), and $CuSO_4$ (0.3 µM) without added iron. For the iron-amended control, Fe(III)-EDTA was added to a final concentration of 50 µM. The pH was adjusted to 5.8 with KOH. After 2 d of stratification at 4°C, the Petri dishes were positioned vertically and transferred to a growth chamber (21°C; 16 h light, 8 h dark; light intensity 100 µmol m^{-2} s^{-1}).

Cultivation of *Pseudomonas simiae* WCS417 and treatment

P. simiae WCS417 was cultured at 28°C on King's medium B (KB; (King et al., 1954)) agar plates, supplemented with 50 µg ml^{-1} of rifampicin. After 24 h of growth, cells were collected in 10 mM $MgSO_4$, washed twice by centrifugation for 5 min at 5000 *g* and finally resuspended in 10 mM $MgSO_4$. For the VOCs experiment, 10 µl of WCS417 bacteria with OD_{600} of 0.1 (10^8 CFU.ml^{-1}) were added 5 cm below the root tip of 8-day-old seedlings growing in MS agar.

Microscopic inspection of *MYB72$_{pro}$:GFP-GUS* expression levels

For bacterial VOCs-treated seedlings, the accumulation of the GFP fluorophore corresponding to *MYB72* expression in the *MYB72$_{pro}$:GFP-GUS* reporter line was monitored under a fluorescence stereomicroscope (Leica MZ16 FA, Wetzlar, Germany), 2 d after VOCs exposure (GFP3 filter: excitation: 450-490 nm, emission: 500-550 nm). For seedlings grown under iron deficiency conditions, *MYB72*-driven GFP fluorescence levels were tested under the fluorescence stereomicroscope at 10 d after sowing.

Mutant screening conditions

For the mutant screening, mutagenized *MYB72$_{pro}$:GFP-GUS* M_2 seeds were surface-sterilized (Van Wees et al., 2013), after which they were sown on square (120 x 120 x 17 mm) Petri dishes containing modified Hoagland medium without iron. For each of the 400 M_2 seed pools (each consisting of the seeds from ~45 mutagenized M_1 generation plants), 1200 seedlings were screened, corresponding to ~25 M_2 seedlings per M_1 plant. The 1200 M_2 seeds per M_1 pool were distributed over 20 plates, with each plate containing 2 rows of ~30 seeds each. In each screening round a plate sown with seeds of the *MYB72$_{pro}$:GFP-GUS* parental line was included as a positive control. After sowing, the plates were placed at 4°C for 2 d, after which they were transferred for 10 d in vertical position under long-day conditions in the plant growth chamber. At day 10, seedlings were screened for *MYB72* induction by monitoring GFP fluorescence levels under the fluorescence stereomicroscope. Putants with visually reduced levels of GFP fluorescence in comparison to the non-mutagenized control were transplanted to a square MS-agar plate to recover from the iron-limiting condition. After 1 week of growth on MS-agar medium, putants were transplanted into pots containing soil and further cultivated to maturity after which M_3 seeds from these M_2 generation putants were collected.

Validation of putants by quantitative RT-PCR (qRT-PCR)

To validate *MYB72* gene expression in the putants, total RNA was extracted from roots of 10-d-old M_3 seedlings and the *MYB72$_{pro}$:GFP-GUS* parental line. RNA extraction was performed according to Oñate-Sánchez and Vicente-Carbajosa (2008) and DNase-treated following the manufacturer's instructions (Thermo Scientific, Waltham, MA USA). Synthesis of cDNA was performed by using SuperScript™ III Reverse Transcriptase according to the Thermo Scientific protocol. To identify the most optimal time of sampling, *MYB72*, *IRT1* and *FRO2* expression levels were determined by qRT-PCR in the *MYB72$_{pro}$:GFP-GUS* parental line growing under iron deficient and iron sufficient conditions. Subsequently, *MYB72* expression levels were determined in the putants by qRT-PCR, using the *MYB72* mRNA levels of unmutagenized *MYB72$_{pro}$:GFP-GUS* as a control. qRT-PCR analysis was performed in a ViiA7 Real-Time PCR System (Applied Biosystems, Foster City, CA, USA). *MYB72, FRO2,* and *IRT1* expression levels were normalized to that of the reference gene *At1g13320* (Czechowski et al., 2005) using the $2^{-\Delta Ct}$ method (Livak and Schmittgen, 2001; Schmittgen and Livak, 2008). Primers used for the qRT-PCR analysis are given in Supplemental Table S1.

Sequencing of putants for *MYB72* mutations

The genomic DNA of *MYB72$_{pro}$:GFP-GUS* putants was extracted from one leaf per putant. Each leaf was snap frozen in liquid nitrogen and ground to a fine powder. Subsequently, ~100 mg of the ground leaf tissue was transferred into a 1.5-ml Eppendorf tube containing 500 µl of extraction buffer (200 mM Tris, 250 mM NaCl, 25 mM EDTA, and 0.5% SDS). Next, the tube was vortexed for 5 sec, incubated for 10 min at 65°C, and centrifuged for 5 min at 18,000 *g*. A volume of 400 µl of the supernatant was transferred to a new 1.5-ml tube after which 400 µl of isopropanol was added to the tube. After gentle shaking and 5 min incubation at room temperature, the tube was centrifuged for 10 min at 18,000 *g*. The supernatant was then carefully removed, after which the pellet was washed with 750 µl of 70% EtOH, and allowed to air dry for 15 min. Finally, the DNA pellet was resuspended in 50 µL of milliQ water.

The genomic DNA was used as a template for the PCR amplification of the *MYB72* promoter and coding region using the primers given in Supplemental Table S1. The PCRs were performed in a Biorad C1000 Touch Thermal Cycler (Biorad, Veenendaal, The Netherlands). The PCR program included 30 sec at 98°C (initial denaturation), 34 cycles at 98°C for 8 sec (denaturation), 52°C at 30 sec (annealing) and 72°C for 30 sec/kb and a final extension at 72°C for 8 min. Purified *MYB72* PCR fragments were sequenced by MACROGEN using Ez-seq DNA sequencing service (Amsterdam, The Netherlands). The primers used for sequencing are listed in Supplemental Table S1. The sequences were analysed by aligning the sequenced genomic regions with reference *MYB72* promoter and coding regions with CLC Main Workbench 6 (Qiagen, Hilden, Germany). The sequences used as reference for *MYB72* promoter and coding regions were downloaded from Arabidopsis Information Resource (TAIR) database (https://www.arabidopsis.org/).

Acknowledgements

This work was supported by ERC Advanced Grant no. 269072 of the European Research Council (to CMJP).

Supplemental data

SUPPLEMENTAL TABLE S1. List of primers used in this study for qRT-PCR, gene amplification and sequencing

Primer name	Primer sequence (5'→3')
Primers used for qRT-PCR:	
*MYB72*_Fw	ACGAGATCAAAAACGTGTGGAAC
*MYB72*_Rev	TCATGATCTGCTTTTGTGCTTTG
*FRO2*_Fw	TGTGGCTCTTCTTCTCTGGTGCTT
*FRO2*_Rev	TGCCACAAAGATTCGTCATGTGCG
*IRT1*_Fw	ACCCGTGCGTCAACAAAGCTAAAG
*IRT1*_Rev	TCCCGGAGGCGAAACACTTAATGA
*At1g13320*_Fw (*PP2AA3*)	TAACGTGGCCAAAATGATGC
*At1g13320*_Rev (*PP2AA3*)	GTTCTCCACAACCGCTTGGT
Primers used to amplify promoter and coding region of MYB72:	
Prom MYB72_Fw (promoter)	TTACTTAGACCCACACATGCT
Prom MYB72_Rev (promoter)	TTCCAAGGGTTTGATGGTAG
MYB72 Gene_Fw (coding region)	TGACGTAAAGAGCCGGGTTA
MYB72 Gene_Rev (coding region)	GCCATCAACCTGCGACCTGT
Primers used to sequence the promoter and coding region of MYB72:	
Prom MYB72_Fw (promoter Fw 1)	TTACTTAGACCCACACATGCT
Seq PromMYB72 II_Fw (promoter Fw 2)	TGTCTGAAAACTGAACTTAATG
Seq Promot MYB72_Rev (promoter Rev 1)	AAAACTCAACCCACATCATCA
Prom MYB72_Rev (promoter Rev 2)	TTCCAAGGGTTTGATGGTAG
MYB72 Gene_Fw (coding region Fw 1)	TGACGTAAAGAGCCGGGTTA
Seq Gene MYB72 II_Fw (coding region Fw 2)	GAAAAGTTGCCGACTAAGATGG
MYB72 Gene Down II_Rev (coding region Rev 1)	GCCATCAACCTGCGACCTGT

CHAPTER 6

Summarizing discussion

Partly adapted from:

Verbon, E., Trapet, P., Stringlis, I. A., Kruijs, S., Bakker, P. A. H. M., and Pieterse, C. M. J.

Iron and immunity

Annual Review of Phytopathology 55: 255-375 (2017)

Early molecular dialogue in root/microbe interactions

Due to their sessile lifestyle, plants need to quickly adapt to the continuous abiotic and biotic challenges they encounter. Plant roots mediate key functions for plant longevity including anchoring the plant in a fixed position, soil exploration for nutrients and water, and maintenance of a healthy state. Members of the rhizosphere-inhabiting microbiome can provide their plant hosts with beneficial effects on these key functions as they can promote plant growth, induce changes in the root architecture, and potentiate the plant body for enhanced defense against pathogen attack. One of them, *Pseudomonas simiae* WCS417, is well studied for its ability to trigger induced systemic resistance (ISR), to improve root architecture and to promote plant growth during its interaction with Arabidopsis (Zamioudis et al., 2013; Pieterse et al., 2014).

The demonstration that roots have the potential to respond to different microbial elicitors, similarly to leaves, and that receptors of MAMPs are active in this plant organ (Millet et al., 2010; Jacobs et al., 2011; Beck et al., 2014; Wyrsch et al., 2015) generated questions about how potential beneficial microbes and their MAMPs can be distinguished from pathogens locally in the roots. In Chapter 2 of this thesis, we aimed to characterize the early molecular events following recognition of *P. simiae* WCS417 in Arabidopsis roots. To understand how recognition of WCS417 compares to the recognition of immune-eliciting MAMPs, we studied in a time-series experiment root transcriptional changes to the MAMPs flg22^{417} (from *P. simiae* WCS417), flg22^{Pa} (from the pathogen *P. aeruginosa*), and fungal chitin. We observed that independent of the MAMP trigger, roots mount a core transcriptional response, as was previously observed in Arabidopsis leaves and seedlings (Thilmony et al., 2006; Zipfel et al., 2006; Denoux et al., 2008). Furthermore, we identified distinct patterns in the root transcriptional response to the bacterial elicitors and chitin. Interestingly, flg22^{417} of beneficial P. simiae WCS417 displayed a very similar immune-eliciting potential as flg22^{Pa} from the pathogen *P. aeruginosa*. MAMPs of other beneficial microbes were previously found to trigger mild defense responses as a result of their coevolution with their host (Lopez-Gomez et al., 2012; Trda et al., 2014). Interestingly, despite the strong contribution of flg22^{417} in the recognition of WCS417, the rhizobacterium suppressed about half of the transcriptional changes inflicted by flg22^{417}. This indicates that WCS417 cannot avoid its recognition, but can quickly dampen the MAMP-elicited transcriptional program in the roots, possibly to establish its beneficial association with the host, as was also shown for beneficial fungi *Piriformospora indica* (Jacobs et al., 2011) and *Trichoderma* spp. (Brotman et al., 2013).

Activation of plant defenses has a negative impact on plant growth (Huot et al. 2014), so beneficial microbes need to wisely circumvent the induction of growth-retarding immune responses (Zamioudis and Pieterse, 2012). Our findings in Chapter 2 suggest that live WCS417 cells have a much milder and more transient effect on the induction of immune-related processes than that induced by the MAMP elicitors (Figure 1A). Moreover, the MAMPs strongly downregulated growth-related processes, while this was much milder when roots were exposed to live WCS417 cells. Hence, although WCS417 MAMPs, such as its flagellin, are recognized by the plant immune system in a similar manner as those of pathogens, a large proportion of the downstream transcriptional response is dampened, possibly to accommodate the beneficial microbe and to prevent plant growth repression that is typically associated with MAMP recognition.

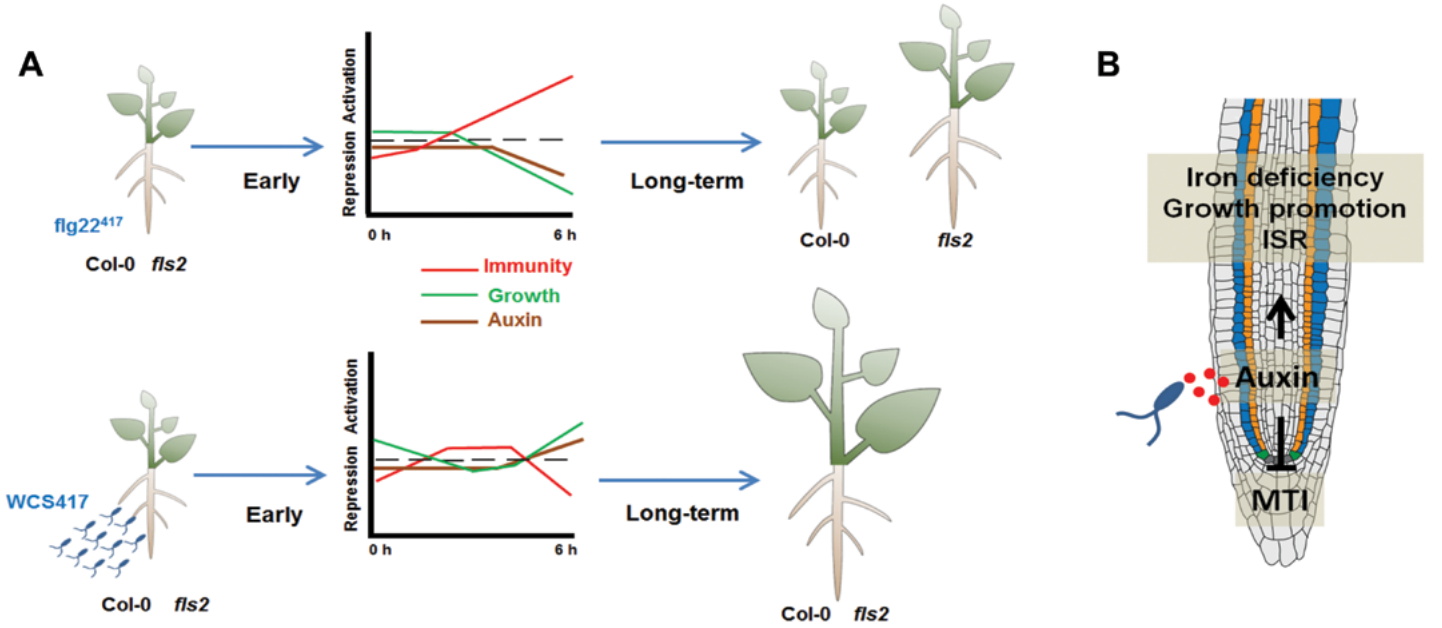

FIGURE 1. Early transcriptional signatures of roots to *P. simiae* WCS417 and flg22^{417} and simplified model linking early responses to known beneficial phenotypes.
(A) During the first steps of recognition, WCS417 and flg22^{417} affect the root transcriptome in a distinct manner. Flg22^{417} triggers a stronger and more durable activation of genes and processes related to plant defense, and its effect on growth- and auxin-related genes and processes is repressing. In contrast, WCS417 recognition results in milder and transient activation of genes related to immunity. Moreover, the rhizobacterium suppresses the initial negative effect on growth- and auxin-related genes, as colonization progresses. In the long-term, this results in growth-inhibition of plants treated with flg22^{417}, while plants colonized by WCS417 do not display this MAMP-mediated growth reduction. Because the flagellin receptor mutant *fls2* shows a similar growth promotion in response to WCS417 as Col-0, it is likely that WCS417 suppresses also the negative effect of other MAMPs. **(B)** Increased auxin-related gene activity observed following recognition of WCS417 could be the result of effector activity (red dots) that stimulate auxin signaling and consequently suppress MAMP-triggered immunity (MTI). At the same time, this increased auxin activity links the recognition of the rhizobacterium with iron-deficiency responses and the onset of ISR (Chapter 2) and the later observed growth promotion and root phenotypic plasticity (Zamioudis et al. 2013).

Auxin is a hormone with an established role in plant growth and development (Santner et al., 2009) and has a well-documented role in plant-microbe interactions (Kazan and Manners, 2009; Naseem et al., 2015). Increased auxin activity in roots following colonization coincides with root phenotypic changes triggered by WCS417 (Zamioudis et al., 2013) and other beneficial bacteria and fungi (Contreras-Cornejo et al., 2009; Felten et al., 2009; Breakspear et al., 2014; Cheng et al., 2017). Pathogenic microbes exploit auxin as well to suppress either salicylic acid (SA) or MTI/ETI responses (Naseem et al., 2015). When activated, auxin signaling has a repressive effect on SA accumulation (Robert-Seilaniantz et al., 2011). Additionally, exogenous application of the auxin analog IAA can block the activation of an MTI marker in Arabidopsis roots treated with flg22 (Zhang et al., 2015b). A number of root-infecting microbes depend on auxin to cause disease (Kidd et al., 2011; Denance et al., 2013; Evangelisti et al., 2013; Lyons et al., 2015), and effectors from pathogenic *Pseudomonas* bacteria, the oomycete *Peronospora parasitica* and the beneficial fungus *Laccaria bicolor* can target auxin signaling and activity to facilitate host colonization (Chen et al., 2007; Plett et al., 2011; Cui et al., 2013; Evangelisti et al., 2013). As we show in Chapter 3, beneficial rhizobacteria able to induce ISR in different hosts possess gene clusters coding for proteins with a structural role in T3SSs, but also for T3SS effector proteins with unknown function. One of the identified effectors in the WCS417 genome is RopE, which shows a high degree of sequence similarity with AvrE effectors. Effectors of the AvrE family were previously found to suppress SA-dependent basal immunity and to promote infection of plants by plant pathogenic bacteria (DebRoy et al., 2004; Ham et al., 2009). A possible scenario could involve the release of effectors by WCS417 to manipulate auxin activity, early during colonization, therewith promoting plant growth and at the same time suppressing root-defense responses that could restrict its colonization (Figure 1B). Genes encoding effectors are also present in the genomes of many other root-associated beneficial *Pseudomonas* spp. (Preston et al., 2001; Mavrodi et al., 2011; Loper et al., 2012; Berendsen et al., 2015). Studies involving agroinfiltration to deliver effectors inside plant cells or heterologous expression of "beneficial" effectors in host plants could shed light on the elusive role that effector molecules have in the establishment of colonization locally in the roots.

Auxin has also role in the regulation of the iron deficiency response in Arabidopsis roots (Chen et al., 2010; Hindt and Guerinot, 2012). In Chapter 2, we observed that activation of marker genes of the iron deficiency response and ISR initiation in roots upon WCS417-colonization both require intact auxin signaling. The increased auxin activity following recognition of WCS417 could be a prelude for the observed activation of the iron deficiency response during the onset of ISR, even under conditions in which plants have plenty of iron available (Zamioudis et al., 2015). This could be the one side of the "coin" where the plant benefits: enhanced protection and increased iron uptake. On the other side, the bacterium needs to benefit from the interaction as well. In beneficial symbiotic interactions, like those of rhizobia or mycorrhizal fungi, the microbes provide the plants with their services and in return they have privileged access to plant photosynthates (Parniske, 2008; Oldroyd et al., 2011). There is no evidence so far that WCS417 can colonize Arabidopsis endophytically. Hence, the rhizobacterium needs to find alternative ways to acquire nutrients from its host. Two breakthrough methodologies, microfluidic-based devices to track root-bacteria interactions and bacterial *lux* fusion bioreporters, provided evidence that the elongation zone and the lateral roots constitute important sites for root exudation and niches for preferential colonization (Massalha et al.,

2017; Pini et al., 2017). Cross-sectional imaging of roots reveals their organization in concentric circles, with each circle corresponding to a different cell type (Wachsman et al., 2015). Endodermis is the root layer surrounding the xylem, characterized for the presence of endodermal barriers like the Casparian strip and suberin lamellae (Geldner, 2013). Interestingly, both the elongation zone and the sites of lateral root emergence lack the endodermal barriers suberin and the Casparian strip, that block the free diffusion of water and nutrients from the xylem to the outer cell types of the root (Barberon, 2017). Previously, WCS417 colonization was shown to increase the emergence of lateral roots in Arabidopsis (Zamioudis et al., 2013). However, the effect of this rhizobacterium on the activity of endodermal barriers and nutrient availability is still largely unknown. Indirect evidence comes from Barberon et al. (2016) showing that iron-starved Arabidopsis roots accumulate less suberin in the endodermis, allowing as such enhanced nutrient flow through the apoplast. It is probable that triggering of the iron-deficiency response in the root by WCS417 (Zamioudis et al., 2015) could increase nutrient availability for the rhizobacterium by locally and transiently reducing suberization (Figure 2).

Colonization of nutrient-rich niches is not straightforward as a microbe needs to confront with other microbes and the plant itself to gain access to them. The elongation zone is a root tissue with potent defense responses including generation of Ca^{2+} signals, expression of MTI- genes and callose deposition (Millet et al., 2010; Jacobs et al., 2011; Keinath et al., 2015). Nevertheless, bacteria preferably colonize this root part (Massalha et al., 2017; Pini et al., 2017). Work by Beck et al. (2014) demonstrated that outgrowing lateral roots and the xylem display increased promoter activity of the flg22 receptor gene *FLS2*. This suggests that beneficial microbes that colonize roots need to have an arsenal of effectors to suppress local immune responses (Millet et al., 2010; Jacobs et al., 2011) or have machineries installed to evade the recognition of their MAMPs (Bardoel et al., 2011; Pel and Pieterse, 2013). The effectors identified in Chapter 3, are candidates that may have a function in the early attachment of beneficial rhizobacteria onto the root surface (Figure 1B).

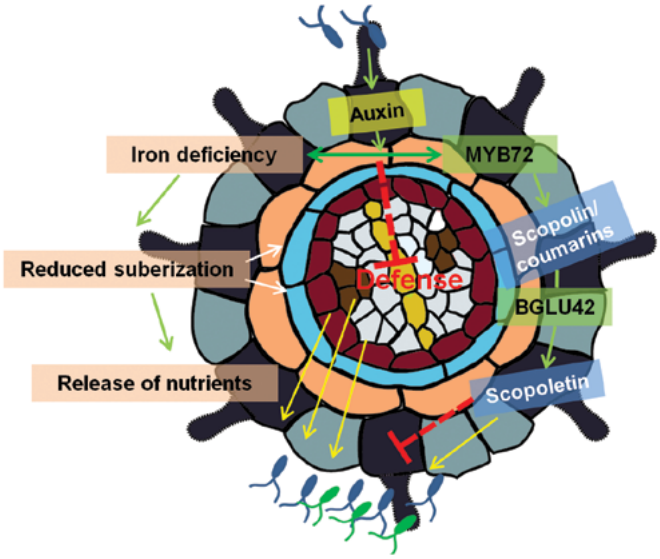

FIGURE 2. Possible model showing how colonizing beneficial rhizobacteria can affect locally root iron homeostasis and establish an association with its host plant.
Increased auxin activity following colonization by WCS417, leads to local iron deficiency responses and upregulation of *MYB72*. Activation of the iron deficiency response might lead to repression of local plant defenses. At the same time, iron deficiency triggered by the rhizobacteria can lead to reduced suberization and subsequently to localized and transient increase in the availability of nutrients for the colonizing beneficial microbes. In parallel, the increased MYB72 activity affects phenylpropanoid metabolism and more specifically coumarin accumulation inside the roots. The MYB72-regulated β-glucosidase BGLU42 controls the deglycosylation of scopolin to scopoletin before its release into the rhizosphere. Coumarins can act as a carbon source for putative beneficial microbes. Moreover, because of their differential antimicrobial activity, coumarins could function in the microbial population in the rhizosphere. Solid lines indicate established processes; dashed lines represent predicted processes. Yellow lines indicate positive effect, red lines negative effect and green lines indicate steps during processes.

In the future, emerging novel methodologies, such as microfluidics tracking root interaction system, microfluidics organ-on-a-chip approaches and lux biosensors (Massalha et al., 2017; Pini et al., 2017; Stanley et al., 2017) will aid in increasing our understanding of the function of different root cell types during nutrient deficiencies and microbial recognition (Walker et al., 2017). Moreover, they can provide insight into the role of preformed or dynamic root-barriers during colonization of beneficial microbes on the root system (Barberon et al., 2016). Ultimately, this will shed new light on root-beneficial microbe interactions and foster the identification of bacterial and plant traits that can help to improve plant growth and yield in agriculture.

Different shades of MYB72, from iron deficiency and ISR to microbiome assembly

R2R3-MYB-like transcription factor gene *MYB72* is among the genes activated following colonization of Arabidopsis roots by WCS417 (Verhagen et al., 2004). Moreover, *myb72* mutant studies show that MYB72 is required for the onset of ISR triggered by beneficial rhizobacteria and fungi (Van der Ent et al., 2008; Segarra et al., 2009). MYB72 also emerged as an important player during the iron deficiency response, which is activated when plants are grown under iron limited conditions (Colangelo and Guerinot, 2004; Buckhout et al., 2009; Palmer et al., 2013). Recently, Zamioudis et al. (2015) provided a mechanistic link between the iron deficiency responses in roots and the onset of ISR by demonstrating that the iron deficiency response regulator FIT (Colangelo and Guerinot, 2004) also controls the upregulation of *MYB72* in response to WCS417, even under conditions where plants had excess of iron available and thus did not physically experience iron deficiency (Zamioudis et al., 2015). In dicot plants like Arabidopsis, sensing of iron-limitation in the root vicinity activates a set of iron deficiency responses (also known as Strategy I), that aim to increase iron availability and uptake in roots (Kobayashi and Nishizawa, 2012; Verbon et al., 2017). Plants respond to iron deficiency by altering the composition of their exudates and release coumarins in the rhizosphere to mobilize iron and integrate it in Strategy I (Jin et al., 2007; Fourcroy et al., 2014; Schmid et al., 2014; Schmidt et al., 2014; Fourcroy et al., 2016). MYB72 is required for the production of fluorescent iron-mobilizing compounds and MYB72-regulated β-glucosidase BGLU42, a novel ISR signaling component, has a role in their release into the rhizosphere (Zamioudis et al., 2014). In Chapter 4, we performed untargeted metabolomic analysis on exudates and the root interior of Col-0, *myb72* and *bglu42* plants and demonstrated that MYB72 is required for the production of coumarins, while BGLU42 is involved in the deglycosylation of the coumarin scopolin to scopoletin, before its subsequent release into the rhizosphere by the iron deficiency–regulated ABC transporter PDR9 (Fourcroy et al., 2014). Scopoletin is a antimicrobial compound with the potential to limit growth of plant pathogens in different plant species (Gnonlonfin et al., 2012). Previous studies have shown that scopoletin together with the glycosylated form scopolin are prominent coumarins in roots and exudates of Arabidopsis (Bednarek et al., 2005; Kai et al., 2006; Strehmel et al., 2014). However, the role of scopoletin in root-microbiome interactions is not clear. In Chapter 4, we observed that different scopoletin concentrations displayed an unspecific suppressive effect on the growth of two soil-borne phytopathogenic fungi, while growth of two ISR-inducing rhizobacteria was not affected. Additionally, using the chemotropism assay developed by Turrà et al. (2015) we observed that scopoletin had a deterrent effect on the orientation of fungal hyphae. These findings demonstrate that scopoletin can have a differential effect on different soil-inhabiting microbes upon its release from roots. The fact that ISR mutants *myb72* and *bglu42* produce no or very low levels of scopoletin into the rhizosphere and that the ISR-inducing microbes *P. simiae* WCS41 and *P. capeferrum* WCS358 can grow in the presence of this toxic coumarin suggests a positive role of coumarins in favoring beneficial microbes over pathogenic ones in the rhizosphere.

To study the role of scopoletin in the assembly of the root microbiome, we studied the composition of the root-associated microbiome of wild-type Col-0 and compared it with that of *myb72* and the scopoletin

biosynthesis mutant *f6'h1*. *F6'H1* encodes a key enzyme in the ortho-hydroxylation of feruloyl CoA and the production of scopoletin and relative coumarins (Kai et al., 2008). Like *MYB72,* the expression of *F6'H1* is regulated by the iron deficiency response regulator FIT (Schmid et al., 2014). Upon colonization of Arabidopsis roots by WCS417, we observed accumulation of fluorescent compounds in Col-0 roots but not in the mutant *f6'h1*, indicating that the compounds produced are coumarins. Other studies have also shown scopoletin accumulation or production of fluorescent compounds following root colonization by the beneficial rhizobacteria *P. fluorescens* SS101 and *Paenibacillus polymyxa* BFKC01 (Van de Mortel et al., 2012; Zhou et al., 2016). These observations raise questions about the role that this coumarin accumulation might have for plant health and fitness, except their profound role in iron mobilization during iron limitation (Fourcroy et al., 2016). Previously, Kai et al. (2006) observed scopolin and scopoletin accumulation in response to Arabidopsis treatment with 2,4-dichlorophenoxyacetic acid, which mimics auxin activity. The coumarin-inducing bacteria WCS417, SS101 and BFKC01 also affect auxin homeostasis in roots. Moreover, they promote plant growth and increase the formation of lateral roots resulting in a more-developed root system. Interestingly, previous studies have shown that the interplay between coumarins and auxin activity plays a role in root growth and morphology. In these studies, coumarin application in media where Arabidopsis grow, results in inhibition of primary root growth, increased emergence of lateral root, and longer root hairs and their findings suggest that coumarin affects positively auxin transport but not biosynthesis (Li et al., 2011; Lupini et al., 2014). Nevertheless, deglycosylated coumarins, such as scopoletin, are toxic and unstable, for that plants have acquired glucosyltransferases to convert the aglycone coumarins to their stable form and subsequently store them in the vacuoles (Chong et al., 2002; Le Roy et al., 2016). Involvement of auxin is also suggested in this process, since this hormone increases the activity of glucosyltransferases in Arabidopsis and tobacco (Taguchi et al., 2001; Grubb et al., 2004; Li et al., 2011). Hence, the modulation of auxin-responsive processes in roots by beneficial microbes seems to be intrinsically connected to changes in secondary metabolism and subsequent effects on plant performance. On the one hand, a concerted action of auxin and coumarins could contribute to enhanced root growth and on the other hand control excessive accumulation of toxic aglycone coumarins. This fine balance between secondary metabolism, microbial colonization and benefits for the plant could also function in an extra direction. Hiruma et al. (2016) demonstrated that products of the phenylpropanoid metabolism produced under phosphate starvation (Pant et al., 2015) are necessary to control the growth of the beneficial endophytic fungus *Colletotrichum tofieldiae*. This fungus developed a pathogenic lifestyle in mutant plants not producing these compounds, indicating that secondary metabolites produced under phosphate starvation determine the lifestyle of specific microbiota. Promoter activity of *MYB72*, *BGLU42* and *F6'H1* is observed in the outer root layers (Schmid et al., 2014; Zamioudis et al., 2014; Zamioudis et al., 2015) and coincides with the root layers where coumarins accumulate (Schmid et al., 2014). Hence, accumulation of coumarins, following *MYB72* activation could be involved in maintaining microbial densities on the root surface. By controlling the PGPR population, a fine balance between delivery of beneficial effects and prevention of overexploitation of plant-derived nutrients can be achieved (Figure 2).

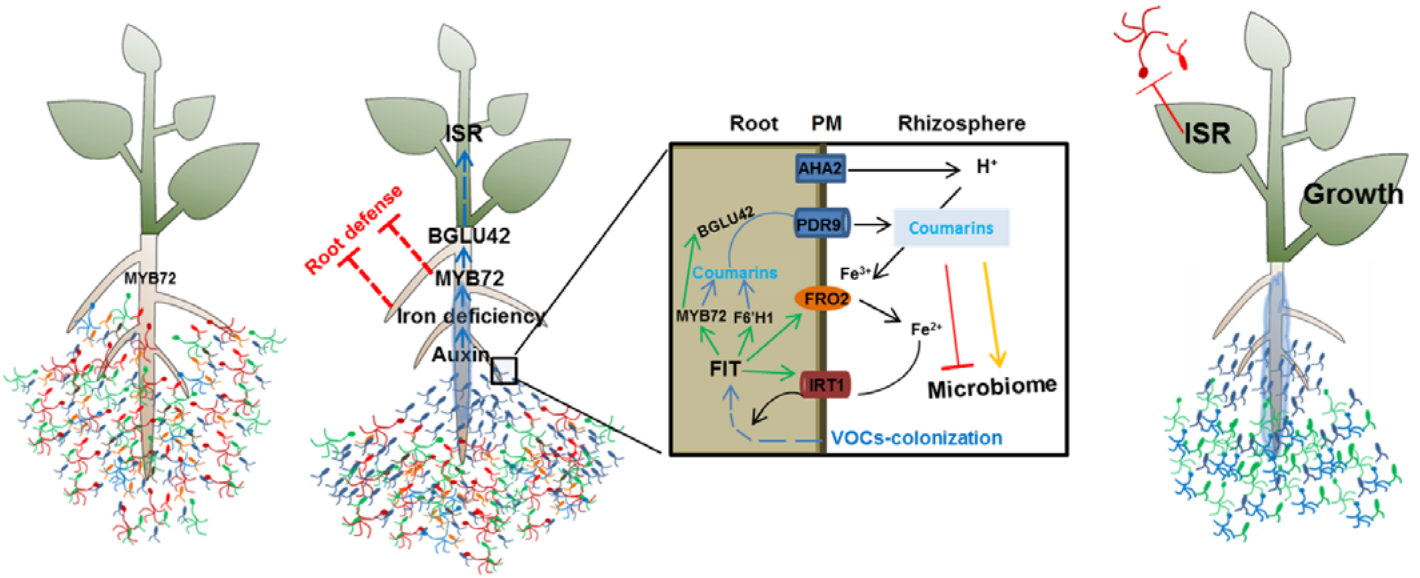

FIGURE 3. Microbiome assembly following recognition of beneficial rhizobacteria, release of coumarins and proposed effect on plant fitness.
(A) A plant growing in soil with low number of ISR-inducing rhizobacteria, showing basal *MYB72* expression levels and moderate plant growth. **(B)** Following root colonization by ISR-inducing microbes or perception of their VOCs, there is activation of a set of molecular changes locally in the roots. Initially, there is FIT-dependent activation of transcription factor gene *MYB72* and iron-uptake genes *FRO2* and *IRT1*. MYB72 is involved, together or in parallel with F6'H1, in the biosynthesis of coumarins. MYB72-regulated gene *BGLU42*, encoding a β-glucosidase, is involved in the deglycosylation of coumarin scopolin to its toxic form scopoletin, which is released together with other coumarins into the rhizosphere via the ABC transporter PDR9. Coumarins in the rhizosphere mobilize Fe^{3+} and make it available for reduction by FRO2 and uptake in the root through IRT1. Concerted activation of MYB72 and iron deficiency might lead to local suppression of root defenses. That in turn could facilitate root colonization by beneficial microbes. On the other hand, exudation of coumarins exerts a selective pressure in the rhizosphere, repelling coumarin-intolerant microbes and attracting coumarin-tolerant microbes. BGLU42 is a novel ISR component and its overexpression results in constitutive resistance against various plant pathogens. Thus involvement of BGLU42 in the generation of a signal linking root colonization with ISR is possible. **(C)** After established colonization by selected root-inhabiting microbes, the plant body is showing stronger immune responses against foliar pathogens and increased growth. Solid lines indicate established processes; dashed lines represent predicted processes. Red lines indicate negative effect, green lines transcriptional activation, orange lines positive effect and blue lines steps during processes. Abbreviations: PM, plasma membrane; VOCs, volatile organic compounds. (Part of the figure is adapted from Verbon et al. 2017).

Recently, Martinez-Medina et al. (2017) demonstrated that VOCs from beneficial *Trichoderma* fungi are perceived by roots, activate local iron-deficiency responses and subsequently trigger JA-dependent priming in shoots of Arabidopsis and tomato. Interestingly, using grafting they showed that a signal from roots to shoots is required for the expression of ISR in leaves. Previously, Zamioudis et al. (2014) found that *bglu42* mutants cannot develop ISR, while plants overexpressing BGLU42 have constitutive resistance against different pathogens. In Chapter 4, we found that *BGLU42* specifically catalyzes the hydrolysis of scopolin to its aglycone form scopoletin. It is probable that the activity of BGLU42 on specific coumarins or the interaction of coumarins with hormones, e.g. auxin, could generate a mobile signal that travels from the root to the shoots and prime systemic tissues for enhanced defense against a subsequent pathogen attack (Verbon et al., 2017). However, this scenario requires further study using mutants defected in coumarin accumulation, approaches to trace the activity and movement of coumarins inside the plant, and grafting techniques to establish the role of coumarins in systemic ISR signaling.

In Chapter 4, using the chemotropism assay, we observed that pure scopoletin or as part of exudate mixes can negatively affect the orientation of growth of phytopathogen *F. oxysporum* towards the roots. This finding, combined with the accumulation of coumarins during colonization by ISR-inducing microbes (Van de Mortel et al., 2012; Zhou et al., 2016) suggests that scopoletin-insensitive microbes could be favored by the exudation of coumarins in the rhizosphere. To test this hypothesis, we performed shotgun metagenomic analysis of the root microbiomes of Col-0, *myb72* and *f6'h1*. The analysis showed a pronounced rhizosphere effect between bulk soil and the rhizosphere samples already at 3 d after transplanting the seedlings into the soil. The term "rhizosphere effect" characterizes the impact of root exudation on microbial abundance and activity in the rhizosphere compared to bulk soil (Raaijmakers et al., 2009). Moreover, between the rhizosphere samples, *f6'h1* assembled the most distinct rhizosphere microbiome, suggesting a role for scopoletin in shaping the microbial communities established in the rhizosphere. This is in line with previous studies showing that perturbation on the exudation rates of phenolic compounds alters microbial composition (Badri et al., 2009b; Badri et al., 2013). In Chapter 4, a closer look on the genera with differential abundance between the different rhizospheres revealed that exudation of *myb72* and *f6'h1* plants (both pre-grown under iron limitation) affected microbial abundance in a similar manner. On the other hand, the rich-in-coumarin exudates of Col-0 (pre-grown under iron limitation) increased the abundance of a number of microbes compared to their abundance in rhizospheres of plants not producing coumarins. A literature search suggested that some of these microbes can use coumarins as carbon sources or have been found to provide plants with benefits such as antibiosis, growth-promotion and facilitation of metal uptake. Previous studies have also shown that exudation of plants can change due to biotic and abiotic stresses (Jin et al., 2007; Rudrappa et al., 2008; Jin et al., 2010). Plants experiencing a stress attract microbes either in the rhizosphere or inside the roots that could subsequently aid in stress amelioration (Rudrappa et al., 2008; Almario et al., 2017; Berendsen et al., 2017; Zhang et al., 2017). In future research, microbes insensitive to scopoletin found in our study should be isolated from the soil samples and tested for their possible role in iron deficiency, plant growth promotion or ISR (Figure 3). Until recently, there was no study characterizing both the microbiome and the root metabolome in soil (Pétriacq et al., 2017). Hence, methodologies like the one developed by Pétriaq et al. (2017) could allow us to study root-microbiome interactions in situ. Even

more, the shotgun metagenomic sequencing methodology employed in Chapter 4, will allow us to recover whole genome sequences and metatranscriptomics of the same samples will allow the identification of functions activated by different members of the microbiome. Detailed information collected by such analyses will enrich our knowledge on the mechanisms governing microbiome assemblage in roots and also direct us to the characterization of an "active" fraction of the microbiome whose traits could be used to improve plant health and fitness.

Entering the labyrinth of *MYB72* regulation

There is a dynamic crosstalk between different nutrient deficiencies and the outcome of that crosstalk can define plant fitness and development in the changing environments where plants grow (Briat et al., 2015). Recent findings indicate that exudation during iron deficiency has similarities with root exudation of phosphate-starved plants (Fourcroy et al., 2014; Schmid et al., 2014; Schmidt et al., 2014; Ziegler et al., 2016). While different components of iron deficiency like *F6'H1* and ferritin gene *FER1* are positively regulated by both iron and phosphate deficiency (Lan et al., 2012; Bournier et al., 2013), other key components like *IRT1* and *FIT* are negatively regulated or not affected by phosphate deficiency (Hoehenwarter et al., 2016; Tsai and Schmidt, 2017). Similarly, *MYB72* is strongly upregulated during iron deficiency (Colangelo and Guerinot, 2004; Dinneny et al., 2008; Palmer et al., 2013), but its expression during phosphate starvation is not affected, or increased only when phosphate-starved plants are transferred to phosphate-replete conditions (Bustos et al., 2010; Woo et al., 2012; Hoehenwarter et al., 2016). As already mentioned, *MYB72* has a dual role in both iron deficiency (Colangelo and Guerinot, 2004; Palmer et al., 2013) and ISR, while hijacking of the iron deficiency signaling pathway by beneficial microbes results in defense priming (Van der Ent et al., 2008; Zamioudis et al., 2015; Martinez-Medina et al., 2017). Recently, a synthetic community of microbes was shown to induce phosphate starvation response in Arabidopsis that in turn partly suppressed immune responses through the activity of the regulator of phosphate starvation responses PHR1 (Castrillo et al., 2017). During later stages of colonization, this could be a strategy of the microbes, to turn the focus of the plant to the amelioration of the abiotic stress (e.g. iron deficiency or phosphate starvation) instead of activating defense responses, therewith facilitating colonization (Figure 2). These data highlight the complexity behind the regulation of genes with specific functions under a given stress and also how the delicate balance between the activation and repression of a gene could affect the outcome of root-microbe interactions. Only a few genes are known to function upstream in the regulation of MYB72, including *FIT*, *bHLH38* and *bHLH39* (Zamioudis et al., 2015; Verbon et al., 2017). In Chapter 5, we initiated a forward genetic screen to identify novel signaling components upstream of *MYB72* that regulate its activity during ISR and iron deficiency. EMS mutagenesis was performed on reporter line *MYB72*$_{pro}$*:GFP-GUS* that has allowed the visualization of *MYB72* promoter activity in a tissue-specific manner in response to VOCs from beneficial rhizobacteria and iron deficiency (Zamioudis et al., 2015; Martinez-Medina et al., 2017). This screening yielded mutant Arabidopsis plants in which no *MYB72* induction is observed during iron stress. Following this finding, the nature of the mutation affecting *MYB72* activity needs to be elucidated. After, the initial confirmation with qRT-PCR and sequencing that none of the known regulators of *MYB72* is affected

by a mutation induced by EMS, subsequent back-crossing with the non-mutagenized parental line will reduce unwanted mutations. After back-crossing and selfing, whole genome sequencing of the parental line and the putants should lead to the targeting of the mutations responsible for the repression of *MYB72* under iron limitation and exposure to VOCs produced by beneficial microbes (Zuryn et al., 2010; Austin et al., 2011; Nordström et al., 2013).

Concluding remarks

In conclusion, with the results presented in this thesis, we demonstrate that a beneficial rhizobacterium, at the early stages of root colonization, circumvents recognition of its MAMPs and activates auxin responses that are needed for the initiation of the iron-deficiency response and the onset of ISR. Additionally, we found a role for MYB72 in the production of coumarins and BGLU42 in the deglycosylation of scopolin to scopoletin. We demonstrate differential activity of scopoletin towards different root-inhabiting microbes and a role in microbiome assembly in the rhizosphere. Finally, with the identification of putative effectors in the genomes of the beneficial rhizobacteria and the selection of putative MYB72-impaired mutants, we provide a firm basis for future research that can reveal novel insights into the molecular mechanisms that play a role at the interface between plant roots and beneficial members of the root microbiome.

Acknowledgements

The author would like to thank the curators of figshare Plant Illustations profile for the plant and root illustrations used to prepare the figures (Illustrations, 2017)

References

Ahn, I.P., Lee, S.W., and Suh, S.C. (2007). Rhizobacteria-induced priming in Arabidopsis is dependent on ethylene, jasmonic acid, and NPR1. Mol. Plant-Microbe Interact. **20,** 759-768.

Ahn, Y.O., Shimizu, B., Sakata, K., Gantulga, D., Zhou, C., Bevan, D.R., and Esen, A. (2010). Scopolin-hydrolyzing beta-glucosidases in roots of Arabidopsis. Plant and Cell Physiology **51,** 132-143.

Akiyama, K., Matsuzaki, K., and Hayashi, H. (2005). Plant sesquiterpenes induce hyphal branching in arbuscular mycorrhizal fungi. Nature **435,** 824-827.

Akum, F.N., Steinbrenner, J., Biedenkopf, D., Imani, J., and Kogel, K.H. (2015). The *Piriformospora indica* effector PIIN_08944 promotes the mutualistic Sebacinalean symbiosis. Front. Plant Sci. **6,** 906.

Alfano, J.R., and Collmer, A. (2004). Type III secretion system effector proteins: double agents in bacterial disease and plant defense. Annu. Rev. Phytopathol. **42,** 385-414.

Aliotta, G., De Feo, V., Pinto, G., and Pollio, A. (1999). In vitro inhibition of algal growth by *Ruta graveolens* L. extracts: biological and chemical aspects. Plant Biosystem **133,** 185-191.

Alizadeh, H., Behboudi, K., Ahmadzadeh, M., Javan-Nikkhah, M., Zamioudis, C., Pieterse, C.M.J., and Bakker, P.A.H.M. (2013). Induced systemic resistance in cucumber and *Arabidopsis thaliana* by the combination of T*richoderma harzianum* Tr6 and *Pseudomonas* sp. Ps14. Biological Control **65,** 14-23.

Almario, J., Jeena, G., Wunder, J., Langen, G., Zuccaro, A., Coupland, G., and Bucher, M. (2017). Root-associated fungal microbiota of nonmycorrhizal *Arabis alpina* and its contribution to plant phosphorus nutrition. Proc. Natl. Acad. Sci. U S A.

Anders, S., Pyl, P.T., and Huber, W. (2015). HTSeq--a Python framework to work with high-throughput sequencing data. Bioinformatics **31,** 166-169.

Anderson, J.C., Wan, Y., Kim, Y.M., Pasa-Tolic, L., Metz, T.O., and Peck, S.C. (2014). Decreased abundance of type III secretion system-inducing signals in Arabidopsis *mkp1* enhances resistance against *Pseudomonas syringae*. Proc. Natl. Acad. Sci. U S A **111,** 6846-6851.

Antolin-Llovera, M., Petutsching, E.K., Ried, M.K., Lipka, V., Nurnberger, T., Robatzek, S., and Parniske, M. (2014). Knowing your friends and foes-plant receptor-like kinases as initiators of symbiosis or defence. New Phytol. **204,** 791-802.

Asai, T., Tena, G., Plotnikova, J., Willmann, M.R., Chiu, W.L., Gomez-Gomez, L., Boller, T., Ausubel, F.M., and Sheen, J. (2002). MAP kinase signalling cascade in Arabidopsis innate immunity. Nature **415,** 977-983.

Austin, R.S., Vidaurre, D., Stamatiou, G., Breit, R., Provart, N.J., Bonetta, D., Zhang, J., Fung, P., Gong, Y., Wang, P.W., McCourt, P., and Guttman, D.S. (2011). Next-generation mapping of Arabidopsis genes. Plant J. **67,** 715-725.

Badri, D.V., Weir, T.L., Van der Lelie, D., and Vivanco, J.M. (2009a). Rhizosphere chemical dialogues: plant-microbe interactions. Curr Opin Biotechnol **20,** 642-650.

Badri, D.V., Chaparro, J.M., Zhang, R., Shen, Q., and Vivanco, J.M. (2013). Application of natural blends of phytochemicals derived from the root exudates of Arabidopsis to the soil reveal that phenolic-related compounds predominantly modulate the soil microbiome. J. Biol. Chem. **288,** 4502-4512.

Badri, D.V., Quintana, N., El Kassis, E.G., Kim, H.K., Choi, Y.H., Sugiyama, A., Verpoorte, R., Martinoia, E., Manter, D.K., and Vivanco, J.M. (2009b). An ABC transporter mutation alters root exudation of phytochemicals that provoke an overhaul of natural soil microbiota. Plant. Physiol. **151,** 2006-2017.

Bai, Y., Muller, D.B., Srinivas, G., Garrido-Oter, R., Potthoff, E., Rott, M., Dombrowski, N., Munch, P.C., Spaepen, S., Remus-Emsermann, M., Huttel, B., McHardy, A.C., Vorholt, J.A., and Schulze-Lefert, P. (2015). Functional overlap of the Arabidopsis leaf and root microbiota. Nature **528,** 364-369.

Bais, H.P., Walker, T.S., Schweizer, H.P., and Vivanco, J.M. (2002). Root specific elicitation and antimicrobial activity of rosmarinic acid in hairy root cultures of *Ocimum basilicum*. Plant Physiology and Biochemistry **40,** 983-995.

Bais, H.P., Weir, T.L., Perry, L.G., Gilroy, S., and Vivanco, J.M. (2006). The role of root exudates in rhizosphere interactions with plants and other organisms. Annu. Rev. Plant Biol. **57,** 233-266.

Bakker, P.A.H.M., Berendsen, R.L., Doornbos, R.F., Wintermans, P.C., and Pieterse, C.M.J. (2013). The rhizosphere revisited: root microbiomics. Front. Plant Sci. **4,** 165.

Barberon, M. (2017). The endodermis as a checkpoint for nutrients. New Phytol. **213,** 1604-1610.

Barberon, M., Vermeer, J.E., De Bellis, D., Wang, P., Naseer, S., Andersen, T.G., Humbel, B.M., Nawrath, C., Takano, J., Salt, D.E., and Geldner, N. (2016). Adaptation of root function by nutrient-induced plasticity of endodermal differentiation. Cell **164,** 447-459.

Bardoel, B.W., Van der Ent, S., Pel, M.J., Tommassen, J., Pieterse, C.M.J., Van Kessel, K.P., and Van Strijp, J.A. (2011). *Pseudomonas* evades immune recognition of flagellin in both mammals and plants. PLoS Pathog. **7,** e1002206.

Beck, M., Wyrsch, I., Strutt, J., Wimalasekera, R., Webb, A., Boller, T., and Robatzek, S. (2014). Expression patterns of *FLAGELLIN SENSING 2* map to bacterial entry sites in plant shoots and roots. J. Exp. Bot. **65,** 6487-6498.

Bednarek, P., Schneider, B., Svatos, A., Oldham, N.J., and Hahlbrock, K. (2005). Structural complexity, differential response to infection, and tissue specificity of indolic and phenylpropanoid secondary metabolism in Arabidopsis roots. Plant. Physiol. **138,** 1058-1070.

Berendsen, R.L., Pieterse, C.M.J., and Bakker, P.A.H.M. (2012). The rhizosphere microbiome and plant health. Trends. Plant. Sci. **17,** 478-486.

Berendsen, R.L., Van Verk, M.C., Stringlis, I.A., Zamioudis, C., Tommassen, J., Pieterse, C.M.J., and Bakker, P.A.H.M. (2015). Unearthing the genomes of plant-beneficial *Pseudomonas* model strains WCS358, WCS374 and WCS417. BMC Genomics **16,** 539.

Berendsen, R.L., Vismans, G., Yu, K., Song, Y., De Jonge, R., Burgman, W.P., Burmølle, M., Herschend, J., Bakker, P.A.H.M., and Pieterse, C.M.J. (2017). Disease-induced assemblage of a plant-beneficial bacterial consortium. *Submitted*.

Boller, T., and Felix, G. (2009). A renaissance of elicitors: perception of microbe-associated molecular patterns and danger signals by pattern-recognition receptors. Annu. Rev. Plant Biol. **60,** 379-406.

Bournier, M., Tissot, N., Mari, S., Boucherez, J., Lacombe, E., Briat, J.F., and Gaymard, F. (2013). Arabidopsis ferritin 1 (*AtFer1*) gene regulation by the phosphate starvation response 1 (AtPHR1) transcription factor reveals a direct molecular link between iron and phosphate homeostasis. J. Biol. Chem. **288,** 22670-22680.

Boyle, E.I., Weng, S., Gollub, J., Jin, H., Botstein, D., Cherry, J.M., and Sherlock, G. (2004). GO::TermFinder--open source software for accessing Gene Ontology information and finding significantly enriched Gene Ontology terms associated with a list of genes. Bioinformatics **20,** 3710-3715.

Bozsoki, Z., Cheng, J., Feng, F., Gysel, K., Vinther, M., Andersen, K.R., Oldroyd, G., Blaise, M., Radutoiu, S., and Stougaard, J. (2017). Receptor-mediated chitin perception in legume roots is functionally separable from Nod factor perception. Proc. Natl. Acad. Sci. U S A**,** 10.1073/pnas.1706795114

Breakspear, A., Liu, C., Roy, S., Stacey, N., Rogers, C., Trick, M., Morieri, G., Mysore, K.S., Wen, J., Oldroyd, G.E., Downie, J.A., and Murray, J.D. (2014). The root hair "infectome" of *Medicago truncatula* uncovers changes in cell cycle genes and reveals a requirement for auxin signaling in rhizobial infection. Plant Cell **26,** 4680-4701.

Briat, J.F., Rouached, H., Tissot, N., Gaymard, F., and Dubos, C. (2015). Integration of P, S, Fe, and Zn nutrition signals in *Arabidopsis thaliana*: potential involvement of PHOSPHATE STARVATION RESPONSE 1 (PHR1). Front. Plant Sci. **6,** 290.

Brotman, Y., Briff, E., Viterbo, A., and Chet, I. (2008). Role of swollenin, an expansin-like protein from *Trichoderma*, in plant root colonization. Plant. Physiol. **147,** 779-789.

Brotman, Y., Landau, U., Cuadros-Inostroza, A., Tohge, T., Fernie, A.R., Chet, I., Viterbo, A., and Willmitzer, L. (2013). *Trichoderma*-plant root colonization: escaping early plant defense responses and activation of the antioxidant machinery for saline stress tolerance. PLoS Pathog. **9,** e1003221.

Bruckhoff, V., Haroth, S., Feussner, K., Konig, S., Brodhun, F., and Feussner, I. (2016). Functional characterization of CYP94-genes and identification of a novel jasmonate catabolite in flowers. PLoS One **11,** e0159875.

Buckhout, T.J., Yang, T.J., and Schmidt, W. (2009). Early iron-deficiency-induced transcriptional changes in Arabidopsis roots as revealed by microarray analyses. BMC Genomics **10,** 147.

Bulgarelli, D., Schlaeppi, K., Spaepen, S., Ver Loren van Themaat, E., and Schulze-Lefert, P. (2013). Structure and functions of the bacterial microbiota of plants. Annu. Rev. Plant Biol. **64,** 807-838.

Bulgarelli, D., Garrido-Oter, R., Munch, P.C., Weiman, A., Droge, J., Pan, Y., McHardy, A.C., and Schulze-Lefert, P. (2015). Structure and function of the bacterial root microbiota in wild and domesticated barley. Cell Host Microbe **17,** 392-403.

Bulgarelli, D., Rott, M., Schlaeppi, K., Ver Loren van Themaat, E., Ahmadinejad, N., Assenza, F., Rauf, P., Huettel, B., Reinhardt, R., Schmelzer, E., Peplies, J., Gloeckner, F.O., Amann, R., Eickhorst, T., and Schulze-Lefert, P. (2012). Revealing structure and assembly cues for Arabidopsis root-inhabiting bacterial microbiota. Nature **488,** 91-95.

Bustos, R., Castrillo, G., Linhares, F., Puga, M.I., Rubio, V., Perez-Perez, J., Solano, R., Leyva, A., and Paz-Ares, J. (2010). A central regulatory system largely controls transcriptional activation and repression responses to phosphate starvation in Arabidopsis. PLoS Genet. **6,** e1001102.

Cao, Y., Liang, Y., Tanaka, K., Nguyen, C.T., Jedrzejczak, R.P., Joachimiak, A., and Stacey, G. (2014). The kinase LYK5 is a major chitin receptor in Arabidopsis and forms a chitin-induced complex with related kinase CERK1. eLife **3**.

Carotenuto, G., Chabaud, M., Miyata, K., Capozzi, M., Takeda, N., Kaku, H., Shibuya, N., Nakagawa, T., Barker, D.G., and Genre, A. (2017). The rice LysM receptor-like kinase *Os*CERK1 is required for the perception of short-chain chitin oligomers in arbuscular mycorrhizal signaling. New Phytol. **214,** 1440-1446.

Carvalhais, L.C., Dennis, P.G., Badri, D.V., Tyson, G.W., Vivanco, J.M., and Schenk, P.M. (2013). Activation of the jasmonic acid plant defence pathway alters the composition of rhizosphere bacterial communities. PLoS One **8,** e56457.

Carvalhais, L.C., Dennis, P.G., Badri, D.V., Kidd, B.N., Vivanco, J.M., and Schenk, P.M. (2015). Linking jasmonic acid signaling, root exudates, and rhizosphere microbiomes. Mol. Plant-Microbe Interact. **28,** 1049-1058.

Castrillo, G., Teixeira, P.J., Paredes, S.H., Law, T.F., De Lorenzo, L., Feltcher, M.E., Finkel, O.M., Breakfield, N.W., Mieczkowski, P., Jones, C.D., Paz-Ares, J., and Dangl, J.L. (2017). Root microbiota drive direct integration of phosphate stress and immunity. Nature **543,** 513-518.

Chaiwanon, J., and Wang, Z.Y. (2015). Spatiotemporal brassinosteroid signaling and antagonism with auxin pattern stem cell dynamics in Arabidopsis roots. Curr. Biol. **25,** 1031-1042.

Chaparro, J.M., Badri, D.V., and Vivanco, J.M. (2014). Rhizosphere microbiome assemblage is affected by plant development. ISME J. **8,** 790-803.

Chaparro, J.M., Badri, D.V., Bakker, M.G., Sugiyama, A., Manter, D.K., and Vivanco, J.M. (2013). Root exudation of phytochemicals in Arabidopsis follows specific patterns that are developmentally programmed and correlate with soil microbial functions. PLoS One **8,** e55731.

Chapelle, E., Mendes, R., Bakker, P.A., and Raaijmakers, J.M. (2016). Fungal invasion of the rhizosphere microbiome. ISME J. **10,** 265-268.

Chatterjee, A., Cui, Y., and Chatterjee, A.K. (2002). Regulation of *Erwinia carotovora hrpL*(Ecc) (sigma-L(Ecc)), which encodes an extracytoplasmic function subfamily of sigma factor required for expression of the HRP regulon. Mol. Plant-Microbe Interact. **15,** 971-980.

Chen, W.W., Yang, J.L., Qin, C., Jin, C.W., Mo, J.H., Ye, T., and Zheng, S.J. (2010). Nitric oxide acts downstream of auxin to trigger root ferric-chelate reductase activity in response to iron deficiency in Arabidopsis. Plant. Physiol. **154,** 810-819.

Chen, Z., Agnew, J.L., Cohen, J.D., He, P., Shan, L., Sheen, J., and Kunkel, B.N. (2007). *Pseudomonas syringae* type III effector AvrRpt2 alters *Arabidopsis thaliana* auxin physiology. Proc. Natl. Acad. Sci. U S A **104,** 20131-20136.

Cheng, X., Etalo, D.W., van de Mortel, J.E., Dekkers, E., Nguyen, L., Medema, M.H., and Raaijmakers, J.M. (2017). Genome-wide analysis of bacterial determinants of plant growth promotion and induced systemic resistance by *Pseudomonas fluorescens*. Environ. Microbiol.**,** in press.

Chong, J., Baltz, R., Schmitt, C., Beffa, R., Fritig, B., and Saindrenan, P. (2002). Downregulation of a pathogen-responsive tobacco UDP-Glc:phenylpropanoid glucosyltransferase reduces scopoletin glucoside accumulation, enhances oxidative stress, and weakens virus resistance. Plant Cell **14,** 1093-1107.

Colangelo, E.P., and Guerinot, M.L. (2004). The essential basic helix-loop-helix protein FIT1 is required for the iron deficiency response. Plant Cell **16,** 3400-3412.

Contreras-Cornejo, H.A., Macias-Rodriguez, L., Cortes-Penagos, C., and Lopez-Bucio, J. (2009). *Trichoderma virens*, a plant beneficial fungus, enhances biomass production and promotes lateral root growth through an auxin-dependent mechanism in Arabidopsis. Plant. Physiol. **149,** 1579-1592.

Coolen, S., Proietti, S., Hickman, R., Davila Olivas, N.H., Huang, P.P., Van Verk, M.C., Van Pelt, J.A., Wittenberg, A.H., De Vos, M., Prins, M., Van Loon, J.J., Aarts, M.G., Dicke, M., Pieterse, C.M.J., and Van Wees, S.C.M. (2016). Transcriptome dynamics of Arabidopsis during sequential biotic and abiotic stresses. Plant J. **86,** 249-267.

Cooley, M.B., Miller, W.G., and Mandrell, R.E. (2003). Colonization of *Arabidopsis thaliana* with *Salmonella enterica* and enterohemorrhagic *Escherichia coli* O157:H7 and competition by *Enterobacter asburiae*. Appl. Environ. Microbiol. **69,** 4915-4926.

Cornelis, G.R. (2010). The type III secretion injectisome, a complex nanomachine for intracellular 'toxin' delivery. Biol. Chem. **391,** 745-751.

Couto, D., and Zipfel, C. (2016). Regulation of pattern recognition receptor signalling in plants. Nat. Rev. Immunol. **16,** 537-552.

Cui, F., Wu, S., Sun, W., Coaker, G., Kunkel, B., He, P., and Shan, L. (2013). The *Pseudomonas syringae* type III effector AvrRpt2 promotes pathogen virulence via stimulating Arabidopsis auxin/indole acetic acid protein turnover. Plant. Physiol. **162,** 1018-1029.

Czechowski, T., Stitt, M., Altmann, T., Udvardi, M.K., and Scheible, W.R. (2005). Genome-wide identification and testing of superior reference genes for transcript normalization in Arabidopsis. Plant. Physiol. **139,** 5-17.

Dakora, F.D., and Phillips, D.A. (2002). Root exudates as mediators of mineral acquisition in low-nutrient environments. Plant and Soil **245,** 35-47.

Danhorn, T., and Fuqua, C. (2007). Biofilm formation by plant-associated bacteria. Annu. Rev. Microbiol. **61,** 401-422.

Darling, A.E., Mau, B., and Perna, N.T. (2010). progressiveMauve: multiple genome alignment with gene gain, loss and rearrangement. PLoS One **5,** e11147.

Dastager, S.G., Deepa, C.K., and Pandey, A. (2011). Plant growth promoting potential of *Pontibacter niistensis* in cowpea (*Vigna unguiculata* (L.) Walp.). Appl. Soil Ecol. **49,** 250-255.

De Nys, R., and Steinberg, P.D. (2002). Linking marine biology and biotechnology. Curr Opin Biotechnol **13,** 244-248.

DebRoy, S., Thilmony, R., Kwack, Y.B., Nomura, K., and He, S.Y. (2004). A family of conserved bacterial effectors inhibits salicylic acid-mediated basal immunity and promotes disease necrosis in plants. Proc. Natl. Acad. Sci. U S A **101,** 9927-9932.

Denance, N., Ranocha, P., Oria, N., Barlet, X., Riviere, M.P., Yadeta, K.A., Hoffmann, L., Perreau, F., Clement, G., Maia-Grondard, A., van den Berg, G.C., Savelli, B., Fournier, S., Aubert, Y., Pelletier, S., Thomma, B.P., Molina, A., Jouanin, L., Marco, Y., and Goffner, D. (2013). Arabidopsis *wat1* (walls are thin1)-mediated resistance to the bacterial vascular pathogen, *Ralstonia solanacearum*, is accompanied by cross-regulation of salicylic acid and tryptophan metabolism. Plant J. **73,** 225-239.

Denoux, C., Galletti, R., Mammarella, N., Gopalan, S., Werck, D., De Lorenzo, G., Ferrari, S., Ausubel, F.M., and Dewdney, J. (2008). Activation of defense response pathways by OGs and Flg22 elicitors in Arabidopsis seedlings. Mol. Plant **1,** 423-445.

Deslandes, L., and Rivas, S. (2012). Catch me if you can: bacterial effectors and plant targets. Trends. Plant. Sci. **17,** 644-655.

Dinneny, J.R., Long, T.A., Wang, J.Y., Jung, J.W., Mace, D., Pointer, S., Barron, C., Brady, S.M., Schiefelbein, J., and Benfey, P.N. (2008). Cell identity mediates the response of Arabidopsis roots to abiotic stress. Science **320,** 942-945.

Dodds, P.N., and Rathjen, J.P. (2010). Plant immunity: towards an integrated view of plant-pathogen interactions. Nat. Rev. Genet. **11,** 539-548.

Dombrowski, N., Schlaeppi, K., Agler, M.T., Hacquard, S., Kemen, E., Garrido-Oter, R., Wunder, J., Coupland, G., and Schulze-Lefert, P. (2017). Root microbiota dynamics of perennial *Arabis alpina* are dependent on soil residence time but independent of flowering time. ISME J. **11,** 43-55.

Driouich, A., Follet-Gueye, M.L., Vicre-Gibouin, M., and Hawes, M. (2013). Root border cells and secretions as critical elements in plant host defense. Curr. Opin. Plant Biol. **16,** 489-495.

Dubos, C., Stracke, R., Grotewold, E., Weisshaar, B., Martin, C., and Lepiniec, L. (2010). MYB transcription factors in Arabidopsis. Trends. Plant. Sci. **15,** 573-581.

Duijff, B.J., Dekogel, W.J., Bakker, P.A.H.M., and Schippers, B. (1994). Influence of pseudobactin-358 on the iron nutrition of barley. Soil Biol. Biochem. **26,** 1681-1688.

Edwards, J., Johnson, C., Santos-Medellin, C., Lurie, E., Podishetty, N.K., Bhatnagar, S., Eisen, J.A., and Sundaresan, V. (2015). Structure, variation, and assembly of the root-associated microbiomes of rice. Proc. Natl. Acad. Sci. U S A **112,** 911-920.

Eide, D., Broderius, M., Fett, J., and Guerinot, M.L. (1996). A novel iron-regulated metal transporter from plants identified by functional expression in yeast. Proc. Natl. Acad. Sci. U S A **93,** 5624-5628.

El Oirdi, M., Trapani, A., and Bouarab, K. (2010). The nature of tobacco resistance against *Botrytis cinerea* depends on the infection structures of the pathogen. Environ. Microbiol. **12,** 239-253.

Evangelisti, E., Govetto, B., Minet-Kebdani, N., Kuhn, M.L., Attard, A., Ponchet, M., Panabieres, F., and Gourgues, M. (2013). The *Phytophthora parasitica* RXLR effector penetration-specific effector 1 favours *Arabidopsis thaliana* infection by interfering with auxin physiology. New Phytol. **199,** 476-489.

Federhen, S. (2012). The NCBI Taxonomy database. Nucleic Acids Res. **40,** 136-143.

Felix, G., Duran, J.D., Volko, S., and Boller, T. (1999). Plants have a sensitive perception system for the most conserved domain of bacterial flagellin. Plant J. **18,** 265-276.

Felten, J., Kohler, A., Morin, E., Bhalerao, R.P., Palme, K., Martin, F., Ditengou, F.A., and Legue, V. (2009). The ectomycorrhizal fungus *Laccaria bicolor* stimulates lateral root formation in poplar and Arabidopsis through auxin transport and signaling. Plant. Physiol. **151,** 1991-2005.

Finck-Barbancon, V., Goranson, J., Zhu, L., Sawa, T., Wiener-Kronish, J.P., Fleiszig, S.M., Wu, C., Mende-Mueller, L., and Frank, D.W. (1997). ExoU expression by *Pseudomonas aeruginosa* correlates with acute cytotoxicity and epithelial injury. Mol. Microbiol. **25,** 547-557.

Floerl, S., Majcherczyk, A., Possienke, M., Feussner, K., Tappe, H., Gatz, C., Feussner, I., Kues, U., and Polle, A. (2012). *Verticillium longisporum* infection affects the leaf apoplastic proteome, metabolome, and cell wall properties in *Arabidopsis thaliana*. PLoS One **7,** e31435.

Fourcroy, P., Tissot, N., Gaymard, F., Briat, J.F., and Dubos, C. (2016). Facilitated Fe nutrition by phenolic compounds excreted by the Arabidopsis ABCG37/PDR9 transporter requires the IRT1/FRO2 high-affinity root Fe(2+) transport system. Mol. Plant **9,** 485-488.

Fourcroy, P., Siso-Terraza, P., Sudre, D., Saviron, M., Reyt, G., Gaymard, F., Abadia, A., Abadia, J., Alvarez-Fernandez, A., and Briat, J.F. (2014). Involvement of the ABCG37 transporter in secretion of scopoletin and derivatives by Arabidopsis roots in response to iron deficiency. New Phytol. **201,** 155-167.

Fradin, E.F., Zhang, Z., Juarez Ayala, J.C., Castroverde, C.D., Nazar, R.N., Robb, J., Liu, C.M., and Thomma, B.P.H.J. (2009). Genetic dissection of *Verticillium* wilt resistance mediated by tomato Ve1. Plant. Physiol. **150,** 320-332.

Fries, L.L.M., Pacovsky, R.S., Safir, G.R., and Siqueira, J.O. (1997). Plant growth and arbuscular mycorrhizal fungal colonization affected by exogenously applied phenolic compounds. J. Chem. Ecol. **23,** 1755-1767.

Galan, J.E., and Collmer, A. (1999). Type III secretion machines: bacterial devices for protein delivery into host cells. Science **284,** 1322-1328.

Galan, J.E., Lara-Tejero, M., Marlovits, T.C., and Wagner, S. (2014). Bacterial type III secretion systems: specialized nanomachines for protein delivery into target cells. Annu. Rev. Microbiol. **68,** 415-438.

Gaspar, Y.M., Nam, J., Schultz, C.J., Lee, L.Y., Gilson, P.R., Gelvin, S.B., and Bacic, A. (2004). Characterization of the Arabidopsis lysine-rich arabinogalactan-protein *AtAGP17* mutant (*rat1*) that results in a decreased efficiency of agrobacterium transformation. Plant. Physiol. **135,** 2162-2171.

Gaul, H. (1957). Die bestimmungder frequenz von punktmutationen bei pflanzen. Z. Naturforsch. Pt. B. **12,** 557-559.

Gaul, H. (1960). Critical analysis of the methods for determining the mutation frequency after seed treatment with mutagens. Genet. Agr. **12,** 297-318.

Geldner, N. (2013). The endodermis. Annu. Rev. Plant Biol. **64,** 531-558.

Gkarmiri, K., Mahmood, S., Ekblad, A., Alstrom, S., Hogberg, N., and Finlay, R. (2017). Identifying the active microbiome associated with roots and rhizosphere soil of oilseed rape. Appl. Environ. Microbiol. **in press**.

Gnonlonfin, G.J.B., Sanni, A., and Brimer, L. (2012). Review scopoletin - A coumarin phytoalexin with medicinal properties. Crit. Rev. Plant Sci. **31,** 47-56.

Gomez-Gomez, L., and Boller, T. (2000). FLS2: an LRR receptor-like kinase involved in the perception of the bacterial elicitor flagellin in Arabidopsis. Mol. Cell **5,** 1003-1011.

Gomez-Gomez, L., Felix, G., and Boller, T. (1999). A single locus determines sensitivity to bacterial flagellin in *Arabidopsis thaliana*. Plant J. **18,** 277-284.

Gourion, B., Berrabah, F., Ratet, P., and Stacey, G. (2015). Rhizobium-legume symbioses: the crucial role of plant immunity. Trends. Plant. Sci. **20,** 186-194.

Greenberg, J.T., and Vinatzer, B.A. (2003). Identifying type III effectors of plant pathogens and analyzing their interaction with plant cells. Curr. Opin. Microbiol. **6,** 20-28.

Greene, E.A., Codomo, C.A., Taylor, N.E., Henikoff, J.G., Till, B.J., Reynolds, S.H., Enns, L.C., Burtner, C., Johnson, J.E., Odden, A.R., Comai, L., and Henikoff, S. (2003). Spectrum of chemically induced mutations from a large-scale reverse-genetic screen in Arabidopsis. Genetics **164,** 731-740.

Grubb, C.D., Zipp, B.J., Ludwig-Muller, J., Masuno, M.N., Molinski, T.F., and Abel, S. (2004). Arabidopsis glucosyltransferase UGT74B1 functions in glucosinolate biosynthesis and auxin homeostasis. Plant J. **40,** 893-908.

Guan, S., Ji, C., Zhou, T., Li, J.X., Ma, Q.G., and Niu, T.G. (2008). Aflatoxin B-1 degradation by *Stenotrophomonas maltophilia* and other microbes selected using coumarin medium. Int. J. Mol. Sci. **9,** 1489-1503.

Gutierrez-Barranquero, J.A., Reen, F.J., McCarthy, R.R., and O'Gara, F. (2015). Deciphering the role of coumarin as a novel quorum sensing inhibitor suppressing virulence phenotypes in bacterial pathogens. Appl. Microbiol. Biotechnol. **99,** 3303-3316.

Guttman, D.S., Vinatzer, B.A., Sarkar, S.F., Ranall, M.V., Kettler, G., and Greenberg, J.T. (2002). A functional screen for the type III (Hrp) secretome of the plant pathogen *Pseudomonas syringae*. Science **295,** 1722-1726.

Guzman-Guzman, P., Aleman-Duarte, M.I., Delaye, L., Herrera-Estrella, A., and Olmedo-Monfil, V. (2017). Identification of effector-like proteins in *Trichoderma* spp. and role of a hydrophobin in the plant-fungus interaction and mycoparasitism. BMC Genet. **18,** 16.

Hacquard, S., Spaepen, S., Garrido-Oter, R., and Schulze-Lefert, P. (2017). Interplay between innate immunity and the plant microbiota. Annu. Rev. Phytopathol. **55,** in press (10.1146/annurev-phyto-080516-035623).

Hacquard, S., Garrido-Oter, R., Gonzalez, A., Spaepen, S., Ackermann, G., Lebeis, S., McHardy, A.C., Dangl, J.L., Knight, R., Ley, R., and Schulze-Lefert, P. (2015). Microbiota and host nutrition across plant and animal kingdoms. Cell Host Microbe **17,** 603-616.

Ham, J.H., Majerczak, D.R., Nomura, K., Mecey, C., Uribe, F., He, S.Y., Mackey, D., and Coplin, D.L. (2009). Multiple activities of the plant pathogen type III effector proteins WtsE and AvrE require WxxxE motifs. Mol. Plant-Microbe Interact. **22,** 703-712.

Han, J.I., Choi, H.K., Lee, S.W., Orwin, P.M., Kim, J., Laroe, S.L., Kim, T.G., O'Neil, J., Leadbetter, J.R., Lee, S.Y., Hur, C.G., Spain, J.C., Ovchinnikova, G., Goodwin, L., and Han, C. (2011). Complete genome sequence of the metabolically versatile plant growth-promoting endophyte *Variovorax paradoxus* S110. J. Bacteriol. **193,** 1183-1190.

Heard, N.A., Holmes, C.C., and Stephens, D.A. (2006). A quantitative study of gene regulation involved in the immune response of anopheline mosquitoes: An application of Bayesian hierarchical clustering of curves. J. Am. Stat. Assoc. **101,** 18-29.

Hickman, R.J., Van Verk, M.C., Van Dijken, A.J.H., Mendes, M.P., Vroegop-Vos, I.A., Caarls, L., Steenbergen, M., Van der Nagel, I., Jan Wesselink, G., Jironkin, A., Talbot, A., Rhodes, J., De Vries, M., Schuurink, R.C., Denby, K., Pieterse, C.M.J., and Van Wees, S.C.M. (2017). Architecture and dynamics of the jasmonic acid gene regulatory network. Plant Cell**,** in press.

Hiltner, L. (1904). Uber neure Erfahrungen und probleme aufdem gebeit der bodenbackteriologie und unter besonderer berucksichtigung der grundungung und brache. **98,** 59–78.

Hindt, M.N., and Guerinot, M.L. (2012). Getting a sense for signals: regulation of the plant iron deficiency response. Biochim. Biophys. Acta **1823,** 1521-1530.

Hiruma, K., Gerlach, N., Sacristan, S., Nakano, R.T., Hacquard, S., Kracher, B., Neumann, U., Ramirez, D., Bucher, M., O'Connell, R.J., and Schulze-Lefert, P. (2016). Root endophyte *Colletotrichum tofieldiae* confers plant fitness benefits that are phosphate status dependent. Cell **165,** 464-474.

Hoagland, D.R., and Arnon, D.I. (1938). The water-culture method for growing plants without soil. Calif. Agric. Exp. Stn. Bull. **347,** 36-39.

Hoehenwarter, W., Monchgesang, S., Neumann, S., Majovsky, P., Abel, S., and Muller, J. (2016). Comparative expression profiling reveals a role of the root apoplast in local phosphate response. BMC Plant Biol. **16,** 106.

Hoffland, E., Pieterse, C.M.J., Bik, L., and Van Pelt, J.A. (1995). Induced systemic resistance in radish is not associated with accumulation of pathogenesis-related proteins. Physiological and Molecular Plant Pathology **46,** 309-320.

Hossain, M.M., Sultana, F., Kubota, M., and Hyakumachi, M. (2008). Differential inducible defense mechanisms against bacterial speck pathogen in *Arabidopsis thaliana* by plant-growth-promoting-fungus *Penicillium* sp. GP16-2 and its cell free filtrate. Plant and Soil **304,** 227-239.

Huot, B., Yao, J., Montgomery, B.L., and He, S.Y. (2014). Growth-defense tradeoffs in plants: a balancing act to optimize fitness. Mol. Plant **7,** 1267-1287.

Iavicoli, A., Boutet, E., Buchala, A., and Metraux, J.P. (2003). Induced systemic resistance in *Arabidopsis thaliana* in response to root inoculation with *Pseudomonas fluorescens* CHA0. Mol. Plant-Microbe Interact. **16,** 851-858.

Illustrations, P. (2017). Shoot illustrations. figshare**,** https://doi.org/10.6084/m6089.figshare.c.3701035.v3701037.

Inceoglu, O., Salles, J.F., Van Overbeek, L., and Van Elsas, J.D. (2010). Effects of plant genotype and growth stage on the betaproteobacterial communities associated with different potato cultivars in two fields. Appl. Environ. Microbiol. **76,** 3675-3684.

Jackson, R.W., Preston, G.M., and Rainey, P.B. (2005). Genetic characterization of *Pseudomonas fluorescens* SBW25 *rsp* gene expression in the phytosphere and in vitro. J. Bacteriol. **187,** 8477-8488.

Jacobs, S., Zechmann, B., Molitor, A., Trujillo, M., Petutschnig, E., Lipka, V., Kogel, K.H., and Schafer, P. (2011). Broad-spectrum suppression of innate immunity is required for colonization of Arabidopsis roots by the fungus *Piriformospora indica*. Plant. Physiol. **156,** 726-740.

Jander, G., Baerson, S.R., Hudak, J.A., Gonzalez, K.A., Gruys, K.J., and Last, R.L. (2003). Ethylmethanesulfonate saturation mutagenesis in Arabidopsis to determine frequency of herbicide resistance. Plant. Physiol. **131,** 139-146.

Jiang, C.H., Fan, Z.H., Xie, P., and Guo, J.H. (2016). *Bacillus cereus* AR156 extracellular polysaccharides served as a novel micro-associated molecular pattern to induced systemic immunity to *Pst* DC3000 in Arabidopsis. Front. Microbiol. **7,** 664.

Jiang, Y., Wang, W., Xie, Q., Liu, N., Liu, L., Wang, D., Zhang, X., Yang, C., Chen, X., Tang, D., and Wang, E. (2017). Plants transfer lipids to sustain colonization by mutualistic mycorrhizal and parasitic fungi. Science **356,** 1172-1175.

Jimenez-Guerrero, I., Perez-Montano, F., Monreal, J.A., Preston, G.M., Fones, H., Vioque, B., Ollero, F.J., and Lopez-Baena, F.J. (2015). The *Sinorhizobium (Ensifer) fredii* HH103 type 3 secretion system suppresses early defense responses to effectively nodulate soybean. Mol. Plant-Microbe Interact. **28,** 790-799.

Jin, C.W., Li, G.X., Yu, X.H., and Zheng, S.J. (2010). Plant Fe status affects the composition of siderophore-secreting microbes in the rhizosphere. Ann. Bot. **105,** 835-841.

Jin, C.W., He, Y.F., Tang, C.X., Wu, P., and Zheng, S.J. (2006). Mechanisms of microbially enhanced Fe acquisition in red clover (*Trifolium pratense* L.). Plant Cell Environ. **29,** 888-897.

Jin, C.W., You, G.Y., He, Y.F., Tang, C., Wu, P., and Zheng, S.J. (2007). Iron deficiency-induced secretion of phenolics facilitates the reutilization of root apoplastic iron in red clover. Plant. Physiol. **144,** 278-285.

Jones, D.L., Nguyen, C., and Finlay, R.D. (2009). Carbon flow in the rhizosphere: carbon trading at the soil–root interface. Plant and Soil **321,** 5-33.

Jones, J.D., and Dangl, J.L. (2006). The plant immune system. Nature **444,** 323-329.

Jones, P., and Vogt, T. (2001). Glycosyltransferases in secondary plant metabolism: tranquilizers and stimulant controllers. Planta **213,** 164-174.

Jovanovic, M., James, E.H., Burrows, P.C., Rego, F.G., Buck, M., and Schumacher, J. (2011). Regulation of the co-evolved HrpR and HrpS AAA+ proteins required for *Pseudomonas syringae* pathogenicity. Nat. Commun. **2,** 177.

Kaever, A., Lingner, T., Feussner, K., Gobel, C., Feussner, I., and Meinicke, P. (2009). MarVis: a tool for clustering and visualization of metabolic biomarkers. BMC Bioinformatics **10,** 92.

Kaever, A., Landesfeind, M., Feussner, K., Mosblech, A., Heilmann, I., Morgenstern, B., Feussner, I., and Meinicke, P. (2015). MarVis-Pathway: integrative and exploratory pathway analysis of non-targeted metabolomics data. Metabolomics **11,** 764-777.

Kai, K., Shimizu, B., Mizutani, M., Watanabe, K., and Sakata, K. (2006). Accumulation of coumarins in *Arabidopsis thaliana*. Phytochemistry **67,** 379-386.

Kai, K., Mizutani, M., Kawamura, N., Yamamoto, R., Tamai, M., Yamaguchi, H., Sakata, K., and Shimizu, B. (2008). Scopoletin is biosynthesized via ortho-hydroxylation of feruloyl CoA by a 2-oxoglutarate-dependent dioxygenase in *Arabidopsis thaliana*. Plant J. **55,** 989-999.

Katari, M.S., Nowicki, S.D., Aceituno, F.F., Nero, D., Kelfer, J., Thompson, L.P., Cabello, J.M., Davidson, R.S., Goldberg, A.P., Shasha, D.E., Coruzzi, G.M., and Gutierrez, R.A. (2010). VirtualPlant: a software platform to support systems biology research. Plant. Physiol. **152,** 500-515.

Kawaharada, Y., Nielsen, M.W., Kelly, S., James, E.K., Andersen, K.R., Rasmussen, S.R., Fuchtbauer, W., Madsen, L.H., Heckmann, A.B., Radutoiu, S., and Stougaard, J. (2017). Differential regulation of the *Epr3* receptor coordinates membrane-restricted rhizobial colonization of root nodule primordia. Nat. Commun. **8,** 14534.

Kazan, K., and Manners, J.M. (2009). Linking development to defense: auxin in plant-pathogen interactions. Trends. Plant. Sci. **14,** 373-382.

Keinath, N.F., Waadt, R., Brugman, R., Schroeder, J.I., Grossmann, G., Schumacher, K., and Krebs, M. (2015). Live cell imaging with R-GECO1 shedslight on flg22- and chitin-induced transient [Ca(2+)]cyt patterns in Arabidopsis. Mol. Plant **8,** 1188-1200.

Kelly, S., Radutoiu, S., and Stougaard, J. (2017). Legume LysM receptors mediate symbiotic and pathogenic signalling. Curr. Opin. Plant Biol. **39,** 152-158.

Kidd, B.N., Kadoo, N.Y., Dombrecht, B., Tekeoglu, M., Gardiner, D.M., Thatcher, L.F., Aitken, E.A., Schenk, P.M., Manners, J.M., and Kazan, K. (2011). Auxin signaling and transport promote susceptibility to the root-infecting fungal pathogen *Fusarium oxysporum* in Arabidopsis. Mol. Plant-Microbe Interact. **24,** 733-748.

Kim, K.K., Kim, M.K., Lim, J.H., Park, H.Y., and Lee, S.T. (2005). Transfer of *Chryseobacterium meningosepticum* and *Chryseobacterium miricola* to *Elizabethkingia* gen. nov. as *Elizabethkingia meningoseptica* comb. nov. and *Elizabethkingia miricola* comb. nov. Int. J. Syst. Evol. Microbiol. **55,** 1287-1293.

Kim, Y.H., Schumaker, K.S., and Zhu, J.K. (2006). EMS mutagenesis of Arabidopsis. Arabidopsis Protocols**,** 101-103.

Kim, Y.H., Choi, D.I., Yeo, W.H., Kim, Y.S., Chae, S.Y., Park, E.K., and Kim, S.S. (2000). Scopoletin production related to induced resistance of tobacco plants against Tobacco mosaic virus. The Plant Pathology Journal **16,** 264-268.

King, E.O., Ward, M.K., and Raney, D.E. (1954). Two simple media for the demonstration of pyocyanin and fluorescin. J. Lab. Clin. Med. **44,** 301-307.

Kloppholz, S., Kuhn, H., and Requena, N. (2011). A secreted fungal effector of *Glomus intraradices* promotes symbiotic biotrophy. Curr. Biol. **21,** 1204-1209.

Kobayashi, T., and Nishizawa, N.K. (2012). Iron uptake, translocation, and regulation in higher plants. Annu. Rev. Plant Biol. **63,** 131-152.

König, S., Feussner, K., Kaever, A., Landesfeind, M., Thurow, C., Karlovsky, P., Gatz, C., Polle, A., and Feussner, I. (2014). Soluble phenylpropanoids are involved in the defense response of Arabidopsis against *Verticillium longisporum*. New Phytol. **202,** 823-837.

Koornneef, M. (2002). Classical mutagenesis in higher plants. In 'Molecular plant biology. Vol. 1. A practical approach'.(Eds PM Gilmartin, C Bowler) (Oxford University Press: Oxford, UK), pp. 1-11.

Koornneef, M., Dellaert, L.W.M., and Van der Veen, J.H. (1982). EMS- and radiation-induced mutation frequencies at individual loci in *Arabidopsis thaliana* (L) Heynh. Mutat. Res. **93,** 109-123.

Korolev, N., David, D.R., and Elad, Y. (2008). The role of phytohormones in basal resistance and *Trichoderma*-induced systemic resistance to *Botrytis cinerea* in *Arabidopsis thaliana*. BioControl **53,** 667-683.

Krishnamurthi, S., Ruckmani, A., Pukall, R., and Chakrabarti, T. (2010). *Psychrobacillus* gen. nov. and proposal for reclassification of *Bacillus insolitus* Larkin & Stokes, 1967, *B. psychrotolerans* Abd-El Rahman et al., 2002 and *B. psychrodurans* Abd-El Rahman et al., 2002 as *Psychrobacillus insolitus* comb. nov., *Psychrobacillus psychrotolerans* comb. nov. and *Psychrobacillus psychrodurans* comb. nov. Syst. Appl. Microbiol. **33,** 367-373.

Kuijken, R.C.P., Snel, J.F.H., Heddes, M.M., Bouwmeester, H.J., and Marcelis, L.F.M. (2015). The importance of a sterile rhizosphere when phenotyping for root exudation. Plant and Soil **387,** 131-142.

Kunze, G., Zipfel, C., Robatzek, S., Niehaus, K., Boller, T., and Felix, G. (2004). The N terminus of bacterial elongation factor Tu elicits innate immunity in Arabidopsis plants. Plant Cell **16,** 3496-3507.

Kyselkova, M., Kopecky, J., Frapolli, M., Defago, G., Sagova-Mareckova, M., Grundmann, G.L., and Moenne-Loccoz, Y. (2009). Comparison of rhizobacterial community composition in soil suppressive or conducive to tobacco black root rot disease. ISME J. **3,** 1127-1138.

Lakshmanan, V., Castaneda, R., Rudrappa, T., and Bais, H.P. (2013). Root transcriptome analysis of *Arabidopsis thaliana* exposed to beneficial *Bacillus subtilis* FB17 rhizobacteria revealed genes for bacterial recruitment and plant defense independent of malate efflux. Planta **238,** 657-668.

Lakshmanan, V., Kitto, S.L., Caplan, J.L., Hsueh, Y.H., Kearns, D.B., Wu, Y.S., and Bais, H.P. (2012). Microbe-associated molecular patterns-triggered root responses mediate beneficial rhizobacterial recruitment in Arabidopsis. Plant. Physiol. **160,** 1642-1661.

Lan, P., Li, W., Wen, T.N., and Schmidt, W. (2012). Quantitative phosphoproteome profiling of iron-deficient Arabidopsis roots. Plant. Physiol. **159,** 403-417.

Larousse, M., Rancurel, C., Syska, C., Palero, F., Etienne, C., Industri, B., Nesme, X., Bardin, M., and Galiana, E. (2017). Tomato root microbiota and *Phytophthora parasitica*-associated disease. Microbiome **5,** 56.

Le Roy, J., Huss, B., Creach, A., Hawkins, S., and Neutelings, G. (2016). Glycosylation is a major regulator of phenylpropanoid availability and biological activity in plants. Front. Plant Sci. **7,** 735.

Lebeis, S.L., Paredes, S.H., Lundberg, D.S., Breakfield, N., Gehring, J., McDonald, M., Malfatti, S., Glavina del Rio, T., Jones, C.D., Tringe, S.G., and Dangl, J.L. (2015). Salicylic acid modulates colonization of the root microbiome by specific bacterial taxa. Science **349,** 860-864.

Lee, J.H., Kim, Y.G., Cho, H.S., Ryu, S.Y., Cho, M.H., and Lee, J. (2014). Coumarins reduce biofilm formation and the virulence of *Escherichia coli* O157:H7. Phytomedicine **21,** 1037-1042.

Leeman, M., Den Ouden, E.M., Van Pelt, J.A., Dirkx, F.P.M., Steijl, H., Bakker, P.A.H.M., and Schippers, B. (1996). Iron availability affects induction of systemic resistance to Fusarium wilt of radish by *Pseudomonas fluorescens*. Phytopathology **86,** 149-155.

Li, X., Gruber, M.Y., Hegedus, D.D., Lydiate, D.J., and Gao, M.J. (2011). Effects of a coumarin derivative, 4-methylumbelliferone, on seed germination and seedling establishment in Arabidopsis. J. Chem. Ecol. **37,** 880-890.

Limon, M.C., Rodriguez-Ortiz, R., and Avalos, J. (2010). Bikaverin production and applications. Appl. Microbiol. Biotechnol. **87,** 21-29.

Lindeberg, M., Stavrinides, J., Chang, J.H., Alfano, J.R., Collmer, A., Dangl, J.L., Greenberg, J.T., Mansfield, J.W., and Guttman, D.S. (2005). Proposed guidelines for a unified nomenclature and phylogenetic analysis of type III Hop effector proteins in the plant pathogen *Pseudomonas syringae*. Mol. Plant-Microbe Interact. **18,** 275-282.

Liu, H., Carvalhais, L.C., Schenk, P.M., and Dennis, P.G. (2017). Effects of jasmonic acid signalling on the wheat microbiome differ between body sites. Sci. Rep. **7,** 41766.

Liu, J., Osbourn, A., and Ma, P. (2015a). MYB transcription factors as regulators of phenylpropanoid metabolism in plants. Mol. Plant **8,** 689-708.

Liu, P., Zhang, W., Zhang, L.Q., Liu, X., and Wei, H.L. (2015b). Supramolecular structure and functional analysis of the type III secretion system in *Pseudomonas fluorescens* 2P24. Front. Plant Sci. **6,** 1190.

Livak, K.J., and Schmittgen, T.D. (2001). Analysis of relative gene expression data using real-time quantitative PCR and the 2(-Delta Delta C(T)) Method. Methods **25,** 402-408.

Loper, J.E., Hassan, K.A., Mavrodi, D.V., Davis, E.W., II, Lim, C.K., Shaffer, B.T., Elbourne, L.D., Stockwell, V.O., Hartney, S.L., Breakwell, K., Henkels, M.D., Tetu, S.G., Rangel, L.I., Kidarsa, T.A., Wilson, N.L., van de Mortel, J.E., Song, C., Blumhagen, R., Radune, D., Hostetler, J.B., Brinkac, L.M., Durkin, A.S., Kluepfel, D.A., Wechter, W.P., Anderson, A.J., Kim, Y.C., Pierson, L.S., III, Pierson, E.A., Lindow, S.E., Kobayashi, D.Y., Raaijmakers, J.M., Weller, D.M., Thomashow, L.S., Allen, A.E., and Paulsen, I.T. (2012). Comparative genomics of plant-associated *Pseudomonas* spp.: insights into diversity and inheritance of traits involved in multitrophic interactions. PLoS Genet. **8,** e1002784.

Lopez-Gomez, M., Sandal, N., Stougaard, J., and Boller, T. (2012). Interplay of flg22-induced defence responses and nodulation in *Lotus japonicus*. J. Exp. Bot. **63,** 393-401.

Love, M.I., Huber, W., and Anders, S. (2014). Moderated estimation of fold change and dispersion for RNA-seq data with DESeq2. Genome Biol. **15,** 550.

Lugtenberg, B., and Kamilova, F. (2009). Plant-growth-promoting rhizobacteria. Annu. Rev. Microbiol. **63,** 541-556.

Lugtenberg, B.J., Dekkers, L., and Bloemberg, G.V. (2001). Molecular determinants of rhizosphere colonization by *Pseudomonas*. Annu. Rev. Phytopathol. **39,** 461-490.

Lundberg, D.S., Lebeis, S.L., Paredes, S.H., Yourstone, S., Gehring, J., Malfatti, S., Tremblay, J., Engelbrektson, A., Kunin, V., Del Rio, T.G., Edgar, R.C., Eickhorst, T., Ley, R.E., Hugenholtz, P., Tringe, S.G., and Dangl, J.L. (2012). Defining the core *Arabidopsis thaliana* root microbiome. Nature **488,** 86-90.

Lupini, A., Araniti, F., Sunseri, F., and Abenavoli, M.R. (2014). Coumarin interacts with auxin polar transport to modify root system architecture in *Arabidopsis thaliana*. Plant Growth Regul. **74,** 23-31.

Lyons, R., Stiller, J., Powell, J., Rusu, A., Manners, J.M., and Kazan, K. (2015). *Fusarium oxysporum* triggers tissue-specific transcriptional reprogramming in *Arabidopsis thaliana*. PLoS One **10,** e0121902.

Macho, A.P., and Zipfel, C. (2014). Plant PRRs and the activation of innate immune signaling. Mol. Cell **54,** 263-272.

Maillet, F., Poinsot, V., Andre, O., Puech-Pages, V., Haouy, A., Gueunier, M., Cromer, L., Giraudet, D., Formey, D., Niebel, A., Martinez, E.A., Driguez, H., Becard, G., and Denarie, J. (2011). Fungal lipochitooligosaccharide symbiotic signals in arbuscular mycorrhiza. Nature **469,** 58-63.

Martinez-Medina, A., Van Wees, S.C.M., and Pieterse, C.M.J. (2017). Airborne signals by *Trichoderma* fungi stimulate iron uptake responses in roots resulting in priming of jasmonic acid-dependent defences in shoots of *Arabidopsis thaliana* and *Solanum lycopersicum*. Plant Cell Environ.**,** in press (10.1111/pce.13016).

Martinez-Medina, A., Flors, V., Heil, M., Mauch-Mani, B., Pieterse, C.M.J., Pozo, M.J., Ton, J., Van Dam, N.M., and Conrath, U. (2016). Recognizing plant defense priming. Trends. Plant. Sci. **21,** 818-822.

Masalha, J., Kosegarten, H., Elmaci, Ö., and Mengel, K. (2000). The central role of microbial activity for iron acquisition in maize and sunflower. Biology and Fertility of Soils **30,** 433-439.

Massalha, H., Korenblum, E., Malitsky, S., Shapiro, O.H., and Aharoni, A. (2017). Live imaging of root-bacteria interactions in a microfluidics setup. Proc. Natl. Acad. Sci. U S A **114,** 4549-4554.

Matyash, V., Liebisch, G., Kurzchalia, T.V., Shevchenko, A., and Schwudke, D. (2008). Lipid extraction by methyl-tert-butyl ether for high-throughput lipidomics. J. Lipid Res. **49,** 1137-1146.

Maunoury, N., Redondo-Nieto, M., Bourcy, M., Van de Velde, W., Alunni, B., Laporte, P., Durand, P., Agier, N., Marisa, L., Vaubert, D., Delacroix, H., Duc, G., Ratet, P., Aggerbeck, L., Kondorosi, E., and Mergaert, P. (2010). Differentiation of symbiotic cells and endosymbionts in *Medicago truncatula* nodulation are coupled to two transcriptome-switches. PLoS One **5,** e9519.

Mavrodi, D.V., Joe, A., Mavrodi, O.V., Hassan, K.A., Weller, D.M., Paulsen, I.T., Loper, J.E., Alfano, J.R., and Thomashow, L.S. (2011). Structural and functional analysis of the type III secretion system from *Pseudomonas fluorescens* Q8r1-96. J. Bacteriol. **193,** 177-189.

Mazurier, S., Corberand, T., Lemanceau, P., and Raaijmakers, J.M. (2009). Phenazine antibiotics produced by fluorescent pseudomonads contribute to natural soil suppressiveness to *Fusarium* wilt. ISME J. **3,** 977-991.

McBride, M.J. (2001). Bacterial gliding motility: multiple mechanisms for cell movement over surfaces. Annu. Rev. Microbiol. **55,** 49-75.

McBride, M.J., Liu, W., Lu, X., Zhu, Y., and Zhang, W. (2014). The family *Cytophagaceae*. In The Prokaryotes (Springer), pp. 577-593.

McMurdie, P.J., and Holmes, S. (2013). phyloseq: an R package for reproducible interactive analysis and graphics of microbiome census data. PLoS One **8,** e61217.

Medentsev, A.G., Arinbasarova, A.Y., and Akimenko, V.K. (2005). Biosynthesis of naphthoquinone pigments by fungi of the genus *Fusarium*. Appl. Biochem. Microbiol. **41,** 503-507.

Mendes, R., Kruijt, M., De Bruijn, I., Dekkers, E., Van der Voort, M., Schneider, J.H., Piceno, Y.M., DeSantis, T.Z., Andersen, G.L., Bakker, P.A.H.M., and Raaijmakers, J.M. (2011). Deciphering the rhizosphere microbiome for disease-suppressive bacteria. Science **332,** 1097-1100.

Menzel, P., Ng, K.L., and Krogh, A. (2016). Fast and sensitive taxonomic classification for metagenomics with Kaiju. Nat. Commun. **7,** 11257.

Meziane, H., Van Der Sluis, I., Van Loon, L.C., Hofte, M., and Bakker, P.A.H.M. (2005). Determinants of *Pseudomonas putida* WCS358 involved in inducing systemic resistance in plants. Mol. Plant Pathol. **6,** 177-185.

Micol-Ponce, R., Aguilera, V., and Ponce, M.R. (2014). A genetic screen for suppressors of a hypomorphic allele of Arabidopsis ARGONAUTE1. Sci. Rep. **4,** 5533.

Millet, Y.A., Danna, C.H., Clay, N.K., Songnuan, W., Simon, M.D., Werck-Reichhart, D., and Ausubel, F.M. (2010). Innate immune responses activated in Arabidopsis roots by microbe-associated molecular patterns. Plant Cell **22,** 973-990.

Mimmo, T., Del Buono, D., Terzano, R., Tomasi, N., Vigani, G., Crecchio, C., Pinton, R., Zocchi, G., and Cesco, S. (2014). Rhizospheric organic compounds in the soil-microorganism-plant system: their role in iron availability. Eur. J. Soil Sci. **65,** 629-642.

Miya, A., Albert, P., Shinya, T., Desaki, Y., Ichimura, K., Shirasu, K., Narusaka, Y., Kawakami, N., Kaku, H., and Shibuya, N. (2007). CERK1, a LysM receptor kinase, is essential for chitin elicitor signaling in Arabidopsis. Proc. Natl. Acad. Sci. U S A **104,** 19613-19618.

Morant, A.V., Jorgensen, K., Jorgensen, C., Paquette, S.M., Sanchez-Perez, R., Moller, B.L., and Bak, S. (2008). beta-Glucosidases as detonators of plant chemical defense. Phytochemistry **69,** 1795-1813.

Mudgett, M.B. (2005). New insights to the function of phytopathogenic bacterial type III effectors in plants. Annu. Rev. Plant Biol. **56,** 509-531.

Mulet, M., Lalucat, J., and Garcia-Valdes, E. (2010). DNA sequence-based analysis of the *Pseudomonas* species. Environ. Microbiol. **12,** 1513-1530.

Muller, D.B., Vogel, C., Bai, Y., and Vorholt, J.A. (2016). The plant microbiota: systems-level insights and perspectives. Annu. Rev. Genet. **50,** 211-234.

Mur, L.A., Kenton, P., Lloyd, A.J., Ougham, H., and Prats, E. (2008). The hypersensitive response; the centenary is upon us but how much do we know? J. Exp. Bot. **59,** 501-520.

Murashige, T., and Skoog, F. (1962). A revised medium for rapid growth and bio assays with tobacco tissue cultures. Physiologia plantarum **15,** 473-497.

Nagata, T., Oobo, T., and Aozasa, O. (2013). Efficacy of a bacterial siderophore, pyoverdine, to supply iron to *Solanum lycopersicum* plants. J. Biosci. Bioeng. **115,** 686-690.

Naito, K., Taguchi, F., Suzuki, T., Inagaki, Y., Toyoda, K., Shiraishi, T., and Ichinose, Y. (2008). Amino acid sequence of bacterial microbe-associated molecular pattern flg22 is required for virulence. Mol. Plant-Microbe Interact. **21,** 1165-1174.

Naseem, M., Kaltdorf, M., and Dandekar, T. (2015). The nexus between growth and defence signalling: auxin and cytokinin modulate plant immune response pathways. J. Exp. Bot. **66,** 4885-4896.

Nazina, T.N., Tourova, T.P., Poltaraus, A.B., Novikova, E.V., Grigoryan, A.A., Ivanova, A.E., Lysenko, A.M., Petrunyaka, V.V., Osipov, G.A., Belyaev, S.S., and Ivanov, M.V. (2001). Taxonomic study of aerobic thermophilic bacilli: descriptions of *Geobacillus subterraneus* gen. nov., sp. nov. and *Geobacillus uzenensis* sp. nov. from petroleum reservoirs and transfer of *Bacillus stearothermophilus*, *Bacillus thermocatenulatus*, *Bacillus thermoleovorans*, *Bacillus kaustophilus*, *Bacillus thermodenitrificans* to *Geobacillus* as the new combinations *G. stearothermophilus*, *G. thermocatenulatus*, *G. thermoleovorans*, *G. kaustophilus*, *G. thermoglucosidasius* and *G. thermodenitrificans*. Int. J. Syst. Evol. Microbiol. **51,** 433-446.

Nishizawa, T., Quan, A.H., Kai, A., Tago, K., Ishii, S., Shen, W.S., Isobe, K., Otsuka, S., and Senoo, K. (2014). Inoculation with N_2-generating denitrifier strains mitigates N_2O emission from agricultural soil fertilized with poultry manure. Biology and Fertility of Soils **50,** 1001-1007.

Niu, D., Wang, X., Wang, Y., Song, X., Wang, J., Guo, J., and Zhao, H. (2016). *Bacillus cereus* AR156 activates PAMP-triggered immunity and induces a systemic acquired resistance through a NPR1-and SA-dependent signaling pathway. Biochem. Biophys. Res. Commun. **469,** 120-125.

Nordström, K.J., Albani, M.C., James, G.V., Gutjahr, C., Hartwig, B., Turck, F., Paszkowski, U., Coupland, G., and Schneeberger, K. (2013). Mutation identification by direct comparison of whole-genome sequencing data from mutant and wild-type individuals using k-mers. Nat. Biotechnol. **31,** 325-330.

Okazaki, S., Kaneko, T., Sato, S., and Saeki, K. (2013). Hijacking of leguminous nodulation signaling by the rhizobial type III secretion system. Proc. Natl. Acad. Sci. U S A **110,** 17131-17136.

Okazaki, S., Tittabutr, P., Teulet, A., Thouin, J., Fardoux, J., Chaintreuil, C., Gully, D., Arrighi, J.F., Furuta, N., Miwa, H., Yasuda, M., Nouwen, N., Teaumroong, N., and Giraud, E. (2016a). Rhizobium-legume symbiosis in the absence of Nod factors: two possible scenarios with or without the T3SS. ISME J. **10,** 64-74.

Okazaki, S., Tittabutr, P., Teulet, A., Thouin, J., Fardoux, J., Chaintreuil, C., Gully, D., Arrighi, J.F., Furuta, N., Miwa, H., Yasuda, M., Nouwen, N., Teaumroong, N., and Giraud, E. (2016b). Rhizobium-legume symbiosis in the absence of Nod factors: two possible scenarios with or without the T3SS. ISME Journal **10,** 64-74.

Oldroyd, G.E. (2013). Speak, friend, and enter: signalling systems that promote beneficial symbiotic associations in plants. Nat. Rev. Microbiol. **11,** 252-263.

Oldroyd, G.E., Murray, J.D., Poole, P.S., and Downie, J.A. (2011). The rules of engagement in the legume-rhizobial symbiosis. Annu. Rev. Genet. **45,** 119-144.

Onate-Sanchez, L., and Vicente-Carbajosa, J. (2008). DNA-free RNA isolation protocols for *Arabidopsis thaliana*, including seeds and siliques. BMC Res. Notes **1,** 93.

Page, D.R., and Grossniklaus, U. (2002). The art and design of genetic screens: *Arabidopsis thaliana*. Nat. Rev. Genet. **3,** 124-136.

Palmer, C.M., Hindt, M.N., Schmidt, H., Clemens, S., and Guerinot, M.L. (2013). *MYB10* and *MYB72* are required for growth under iron-limiting conditions. PLoS Genet. **9,** e1003953.

Pant, B.D., Pant, P., Erban, A., Huhman, D., Kopka, J., and Scheible, W.R. (2015). Identification of primary and secondary metabolites with phosphorus status-dependent abundance in Arabidopsis, and of the transcription factor PHR1 as a major regulator of metabolic changes during phosphorus limitation. Plant Cell Environ **38,** 172-187.

Parniske, M. (2008). Arbuscular mycorrhiza: the mother of plant root endosymbioses. Nat. Rev. Microbiol. **6,** 763-775.

Peiffer, J.A., Spor, A., Koren, O., Jin, Z., Tringe, S.G., Dangl, J.L., Buckler, E.S., and Ley, R.E. (2013). Diversity and heritability of the maize rhizosphere microbiome under field conditions. Proc. Natl. Acad. Sci. U S A **110,** 6548-6553.

Pel, M.J., and Pieterse, C.M.J. (2013). Microbial recognition and evasion of host immunity. J. Exp. Bot. **64,** 1237-1248.

Perez Rodriguez, N., Langella, F., Rodushkin, I., Engstrom, E., Kothe, E., Alakangas, L., and Ohlander, B. (2014). The role of bacterial consortium and organic amendment in Cu and Fe isotope fractionation in plants on a polluted mine site. Environ. Sci. Pollut. Res. Int. **21,** 6836-6844.

Peters, J., Wilson, D.P., Myers, G., Timms, P., and Bavoil, P.M. (2007). Type III secretion à la *Chlamydia*. Trends Microbiol. **15,** 241-251.

Petnicki-Ocwieja, T., Schneider, D.J., Tam, V.C., Chancey, S.T., Shan, L., Jamir, Y., Schechter, L.M., Janes, M.D., Buell, C.R., Tang, X., Collmer, A., and Alfano, J.R. (2002). Genome wide identification of proteins secreted by the Hrp type III protein secretion system of *Pseudomonas syringae* pv. *tomato* DC3000. Proc. Natl. Acad. Sci. U S A **99,** 7652-7657.

Pétriacq, P., Williams, A., Cotton, A., McFarlane, A.E., Rolfe, S.A., and Ton, J. (2017). Metabolite profiling of non-sterile rhizosphere soil. Plant J. **92,** 147-162.

Philippot, L., Raaijmakers, J.M., Lemanceau, P., and Van der Putten, W.H. (2013). Going back to the roots: the microbial ecology of the rhizosphere. Nat. Rev. Microbiol. **11,** 789-799.

Pieterse, C.M.J., De Jonge, R., and Berendsen, R.L. (2016). The soil-borne supremacy. Trends. Plant. Sci. **21,** 171-173.

Pieterse, C.M.J., Van Wees, S.C.M., Hoffland, E., Van Pelt, J.A., and Van Loon, L.C. (1996). Systemic resistance in Arabidopsis induced by biocontrol bacteria is independent of salicylic acid accumulation and pathogenesis-related gene expression. Plant Cell **8,** 1225-1237.

Pieterse, C.M.J., Van der Does, D., Zamioudis, C., Leon-Reyes, A., and Van Wees, S.C.M. (2012). Hormonal modulation of plant immunity. Annu. Rev. Cell Dev. Biol. **28,** 489-521.

Pieterse, C.M.J., Zamioudis, C., Berendsen, R.L., Weller, D.M., Van Wees, S.C.M., and Bakker, P.A.H.M. (2014). Induced systemic resistance by beneficial microbes. Annu. Rev. Phytopathol. **52,** 347-375.

Pieterse, C.M.J., Van Wees, S.C.M., Van Pelt, J.A., Knoester, M., Laan, R., Gerrits, H., Weisbeek, P.J., and Van Loon, L.C. (1998). A novel signaling pathway controlling induced systemic resistance in Arabidopsis. Plant Cell **10,** 1571-1580.

Pieterse, C.M.J., Van Pelt, J.A., Ton, J., Parchmann, S., Mueller, M.J., Buchala, A.J., Metraux, J.P., and Van Loon, L.C. (2000). Rhizobacteria-mediated induced systemic resistance (ISR) in Arabidopsis requires sensitivity to jasmonate and ethylene but is not accompanied by an increase in their production. Physiological and Molecular Plant Pathology **57,** 123-134.

Pini, F., East, A.K., Appia-Ayme, C., Tomek, J., Karunakaran, R., Mendoza-Suarez, M., Edwards, A., Terpolilli, J.J., Roworth, J., Downie, J.A., and Poole, P.S. (2017). Bacterial biosensors for in vivo spatiotemporal mapping of root secretion. Plant. Physiol. **174,** 1289-1306.

Plancot, B., Santaella, C., Jaber, R., Kiefer-Meyer, M.C., Follet-Gueye, M.L., Leprince, J., Gattin, I., Souc, C., Driouich, A., and Vicre-Gibouin, M. (2013). Deciphering the responses of root border-like cells of Arabidopsis and flax to pathogen-derived elicitors. Plant. Physiol. **163,** 1584-1597.

Plett, J.M., Khachane, A., Ouassou, M., Sundberg, B., Kohler, A., and Martin, F. (2014a). Ethylene and jasmonic acid act as negative modulators during mutualistic symbiosis between *Laccaria bicolor* and Populus roots. New Phytol. **202,** 270-286.

Plett, J.M., Kemppainen, M., Kale, S.D., Kohler, A., Legue, V., Brun, A., Tyler, B.M., Pardo, A.G., and Martin, F. (2011). A secreted effector protein of *Laccaria bicolor* is required for symbiosis development. Curr. Biol. **21,** 1197-1203.

Plett, J.M., Daguerre, Y., Wittulsky, S., Vayssieres, A., Deveau, A., Melton, S.J., Kohler, A., Morrell-Falvey, J.L., Brun, A., Veneault-Fourrey, C., and Martin, F. (2014b). Effector MiSSP7 of the mutualistic fungus *Laccaria bicolor* stabilizes the Populus JAZ6 protein and represses jasmonic acid (JA) responsive genes. Proc. Natl. Acad. Sci. U S A **111,** 8299-8304.

Pollock, D.D., and Larkin, J.C. (2004). Estimating the degree of saturation in mutant screens. Genetics **168,** 489-502.

Poncini, L., Wyrsch, I., Denervaud Tendon, V., Vorley, T., Boller, T., Geldner, N., Metraux, J.P., and Lehmann, S. (2017). In roots of *Arabidopsis thaliana*, the damage-associated molecular pattern AtPep1 is a stronger elicitor of immune signalling than flg22 or the chitin heptamer. PLoS One **12,** e0185808.

Pozo, M.J., Van Der Ent, S., Van Loon, L.C., and Pieterse, C.M.J. (2008). Transcription factor MYC2 is involved in priming for enhanced defense during rhizobacteria-induced systemic resistance in *Arabidopsis thaliana*. New Phytol. **180,** 511-523.

Preston, G.M., Bertrand, N., and Rainey, P.B. (2001). Type III secretion in plant growth-promoting *Pseudomonas fluorescens* SBW25. Mol. Microbiol. **41,** 999-1014.

Pryor, S.W., Gibson, D.M., Bergstrom, G.C., and Walker, L.P. (2007). Minimization of between-well sample variance of antifungal activity using a high-throughput screening microplate bioassay. Biotechniques **42,** 168-172.

Qiang, X., Zechmann, B., Reitz, M.U., Kogel, K.H., and Schafer, P. (2012). The mutualistic fungus *Piriformospora indica* colonizes Arabidopsis roots by inducing an endoplasmic reticulum stress-triggered caspase-dependent cell death. Plant Cell **24,** 794-809.

Quince, C., Walker, A.W., Simpson, J.T., Loman, N.J., and Segata, N. (2017). Shotgun metagenomics, from sampling to sequencing and analysis. Nat Biotechnol. **35,** 833–844.

Raaijmakers, J.M., and Mazzola, M. (2016). Soil immune responses. Science **352,** 1392-1393.

Raaijmakers, J.M., Paulitz, T.C., Steinberg, C., Alabouvette, C., and Moenne-Loccoz, Y. (2009). The rhizosphere: a playground and battlefield for soilborne pathogens and beneficial microorganisms. Plant and Soil **321,** 341-361.

Raaijmakers, J.M., Leeman, M., Van Oorschot, M.M.P., Van der Sluis, I., Schippers, B., and Bakker, P.A.H.M. (1995). Dose-response relationships in biological-control of *Fusarium*-wilt of radish by *Pseudomonas* spp. Phytopathology **85,** 1075-1081.

Rainey, P.B. (1999). Adaptation of *Pseudomonas fluorescens* to the plant rhizosphere. Environ. Microbiol. **1,** 243-257.

Reinhold-Hurek, B., Bunger, W., Burbano, C.S., Sabale, M., and Hurek, T. (2015). Roots shaping their microbiome: global hotspots for microbial activity. Annu. Rev. Phytopathol. **53,** 403-424.

Rezzonico, F., Binder, C., Defago, G., and Moenne-Loccoz, Y. (2005). The type III secretion system of biocontrol *Pseudomonas fluorescens* KD targets the phytopathogenic Chromista *Pythium ultimum* and promotes cucumber protection. Mol. Plant-Microbe Interact. **18,** 991-1001.

Robatzek, S., Chinchilla, D., and Boller, T. (2006). Ligand-induced endocytosis of the pattern recognition receptor FLS2 in Arabidopsis. Genes Dev. **20,** 537-542.

Robert-Seilaniantz, A., MacLean, D., Jikumaru, Y., Hill, L., Yamaguchi, S., Kamiya, Y., and Jones, J.D. (2011). The microRNA miR393 re-directs secondary metabolite biosynthesis away from camalexin and towards glucosinolates. Plant J. **67,** 218-231.

Robinson, N.J., Procter, C.M., Connolly, E.L., and Guerinot, M.L. (1999). A ferric-chelate reductase for iron uptake from soils. Nature **397,** 694-697.

Rodriguez-Celma, J., Lin, W.D., Fu, G.M., Abadia, J., Lopez-Millan, A.F., and Schmidt, W. (2013). Mutually exclusive alterations in secondary metabolism are critical for the uptake of insoluble iron compounds by Arabidopsis and *Medicago truncatula*. Plant. Physiol. **162,** 1473-1485.

Rosenzweig, N., Tiedje, J.M., Quensen III, J.F., Meng, Q., and Hao, J.J. (2012). Microbial communities associated with potato common scab-suppressive soil determined by pyrosequencing analyses. Plant Disease **96,** 718-725.

Rudrappa, T., Czymmek, K.J., Pare, P.W., and Bais, H.P. (2008). Root-secreted malic acid recruits beneficial soil bacteria. Plant. Physiol. **148,** 1547-1556.

Ryu, C.M., Farag, M.A., Hu, C.H., Reddy, M.S., Kloepper, J.W., and Pare, P.W. (2004). Bacterial volatiles induce systemic resistance in Arabidopsis. Plant. Physiol. **134,** 1017-1026.

Sanguin, H., Sarniguet, A., Gazengel, K., Moenne-Loccoz, Y., and Grundmann, G.L. (2009). Rhizosphere bacterial communities associated with disease suppressiveness stages of take-all decline in wheat monoculture. New Phytol. **184,** 694-707.

Santi, S., and Schmidt, W. (2009). Dissecting iron deficiency-induced proton extrusion in Arabidopsis roots. New Phytol. **183,** 1072-1084.

Santner, A., Calderon-Villalobos, L.I., and Estelle, M. (2009). Plant hormones are versatile chemical regulators of plant growth. Nat. Chem. Biol. **5,** 301-307.

Sauder, L.A., Albertsen, M., Engel, K., Schwarz, J., Nielsen, P.H., Wagner, M., and Neufeld, J.D. (2017). Cultivation and characterization of *Candidatus* Nitrosocosmicus exaquare, an ammonia-oxidizing archaeon from a municipal wastewater treatment system. ISME J. **11,** 1142-1157.

Schlaeppi, K., Dombrowski, N., Garrido-Oter, R., Ver Loren van Themaat, E., and Schulze-Lefert, P. (2014). Quantitative divergence of the bacterial root microbiota in *Arabidopsis thaliana* relatives. Proc. Natl. Acad. Sci. U S A **111,** 585-592.

Schmid, N.B., Giehl, R.F., Doll, S., Mock, H.P., Strehmel, N., Scheel, D., Kong, X., Hider, R.C., and Von Wiren, N. (2014). Feruloyl-CoA 6'-Hydroxylase1-dependent coumarins mediate iron acquisition from alkaline substrates in Arabidopsis. Plant. Physiol. **164,** 160-172.

Schmidt, H., Gunther, C., Weber, M., Sporlein, C., Loscher, S., Bottcher, C., Schobert, R., and Clemens, S. (2014). Metabolome analysis of *Arabidopsis thaliana* roots identifies a key metabolic pathway for iron acquisition. PLoS One **9,** e102444.

Schmittgen, T.D., and Livak, K.J. (2008). Analyzing real-time PCR data by the comparative C(T) method. Nat Protoc **3,** 1101-1108.

Segarra, G., Van der Ent, S., Trillas, I., and Pieterse, C.M.J. (2009). MYB72, a node of convergence in induced systemic resistance triggered by a fungal and a bacterial beneficial microbe. Plant Biol. **11,** 90-96.

Shimizu, B., Fujimori, A., Miyagawa, H., Ueno, T., Watanabe, K., and Ogawa, K. (2000). Resistance against fusarium wilt induced by non-pathogenic *Fusarium* in *Ipomoea tricolor*. J. Pestic. Sci. **25,** 365-372.

Siegwald, L., Touzet, H., Lemoine, Y., Hot, D., Audebert, C., and Caboche, S. (2017). Assessment of common and emerging bioinformatics pipelines for targeted metagenomics. PLoS One **12,** e0169563.

Simon, C., Langlois-Meurinne, M., Bellvert, F., Garmier, M., Didierlaurent, L., Massoud, K., Chaouch, S., Marie, A., Bodo, B., Kauffmann, S., Noctor, G., and Saindrenan, P. (2010). The differential spatial distribution of secondary metabolites in Arabidopsis leaves reacting hypersensitively to *Pseudomonas syringae* pv. *tomato* is dependent on the oxidative burst. J. Exp. Bot. **61,** 3355-3370.

Sinha, A.K., and Wood, R.K.S. (1968). Studies on nature of resistance in tomato plants to *Verticillium albo-atrum*. Ann. Appl. Biol. **62,** 319-327.

Son, S.W., Kim, H.Y., Choi, G.J., Lim, H.K., Jang, K.S., Lee, S.O., Lee, S., Sung, N.D., and Kim, J.C. (2008). Bikaverin and fusaric acid from *Fusarium oxysporum* show antioomycete activity against *Phytophthora infestans*. J. Appl. Microbiol. **104,** 692-698.

Srinivasan, S., Kim, M.K., Joo, E.S., Lee, S.Y., Lee, D.S., and Jung, H.Y. (2015). Complete genome sequence of *Rufibacter* sp. DG31D, a bacterium resistant to gamma and UV radiation toxicity. Mol. Cell. Toxicol. **11,** 415-421.

Stanley, C.E., Shrivastava, J., Brugman, R., Van Swaay, D., and Grossmann, G. (2017). An organ-on-a-chip approach for investigating root-environment interactions in heterogeneous conditions. bioRxiv**,** 126987.

Stein, E., Molitor, A., Kogel, K.H., and Waller, F. (2008). Systemic resistance in Arabidopsis conferred by the mycorrhizal fungus *Piriformospora indica* requires jasmonic acid signaling and the cytoplasmic function of NPR1. Plant Cell Physiol. **49,** 1747-1751.

Strehmel, N., Bottcher, C., Schmidt, S., and Scheel, D. (2014). Profiling of secondary metabolites in root exudates of *Arabidopsis thaliana*. Phytochemistry **108,** 35-46.

Stringlis, I.A., Proietti, S., Hickman, R., Van Verk, M.C., Zamioudis, C., and Pieterse, C.M.J. (2017). Root transcriptional dynamics induced by beneficial rhizobacteria and microbial immune elicitors reveal signatures of adaptation to mutualists. Plant J., in press.

Subramanian, S., Stacey, G., and Yu, O. (2007). Distinct, crucial roles of flavonoids during legume nodulation. Trends. Plant. Sci. **12,** 282-285.

Sun, H., Wang, L., Zhang, B., Ma, J., Hettenhausen, C., Cao, G., Sun, G., Wu, J., and Wu, J. (2014). Scopoletin is a phytoalexin against *Alternaria alternata* in wild tobacco dependent on jasmonate signalling. J. Exp. Bot. **65,** 4305-4315.

Sun, J., Miller, J.B., Granqvist, E., Wiley-Kalil, A., Gobbato, E., Maillet, F., Cottaz, S., Samain, E., Venkateshwaran, M., Fort, S., Morris, R.J., Ane, J.M., Denarie, J., and Oldroyd, G.E. (2015). Activation of symbiosis signaling by arbuscular mycorrhizal fungi in legumes and rice. Plant Cell **27,** 823-838.

Sun, W., Dunning, F.M., Pfund, C., Weingarten, R., and Bent, A.F. (2006). Within-species flagellin polymorphism in *Xanthomonas campestris* pv *campestris* and its impact on elicitation of Arabidopsis *FLAGELLIN SENSING2*-dependent defenses. Plant Cell **18,** 764-779.

Taguchi, G., Yazawa, T., Hayashida, N., and Okazaki, M. (2001). Molecular cloning and heterologous expression of novel glucosyltransferases from tobacco cultured cells that have broad substrate specificity and are induced by salicylic acid and auxin. Eur. J. Biochem. **268,** 4086-4094.

Tampakaki, A.P., Fadouloglou, V.E., Gazi, A.D., Panopoulos, N.J., and Kokkinidis, M. (2004). Conserved features of type III secretion. Cell. Microbiol. **6,** 805-816.

Tampakaki, A.P., Skandalis, N., Gazi, A.D., Bastaki, M.N., Sarris, P.F., Charova, S.N., Kokkinidis, M., and Panopoulos, N.J. (2010). Playing the "Harp": evolution of our understanding of *hrp/hrc* genes. Annu. Rev. Phytopathol. **48,** 347-370.

Thilmony, R., Underwood, W., and He, S.Y. (2006). Genome-wide transcriptional analysis of the *Arabidopsis thaliana* interaction with the plant pathogen *Pseudomonas syringae* pv. *tomato* DC3000 and the human pathogen *Escherichia coli* O157:H7. Plant J. **46,** 34-53.

Tjamos, S.E., Flemetakis, E., Paplomatas, E.J., and Katinakis, P. (2005). Induction of resistance to *Verticillium dahliae* in *Arabidopsis thaliana* by the biocontrol agent K-165 and pathogenesis-related proteins gene expression. Mol. Plant-Microbe Interact. **18,** 555-561.

Ton, J., Pieterse, C.M.J., and Van Loon, L.C. (1999). Identification of a locus in Arabidopsis controlling both the expression of rhizobacteria-mediated induced systemic resistance (ISR) and basal resistance against *Pseudomonas syringae* pv. *tomato*. Mol. Plant-Microbe Interact. **12,** 911-918.

Ton, J., Davison, S., Van Wees, S.C.M., Van Loon, L.C., and Pieterse, C.M.J. (2001). The Arabidopsis ISR1 locus controlling rhizobacteria-mediated induced systemic resistance is involved in ethylene signaling. Plant. Physiol. **125,** 652-661.

Trantas, E.A., Licciardello, G., Almeida, N.F., Witek, K., Strano, C.P., Duxbury, Z., Ververidis, F., Goumas, D.E., Jones, J.D., Guttman, D.S., Catara, V., and Sarris, P.F. (2015). Comparative genomic analysis of multiple strains of two unusual plant pathogens: *Pseudomonas corrugata* and *Pseudomonas mediterranea*. Front. Microbiol. **6,** 811.

Trapnell, C., Pachter, L., and Salzberg, S.L. (2009). TopHat: discovering splice junctions with RNA-Seq. Bioinformatics **25,** 1105-1111.

Trda, L., Boutrot, F., Claverie, J., Brule, D., Dorey, S., and Poinssot, B. (2015). Perception of pathogenic or beneficial bacteria and their evasion of host immunity: pattern recognition receptors in the frontline. Front. Plant Sci. **6,** 219.

Trda, L., Fernandez, O., Boutrot, F., Heloir, M.C., Kelloniemi, J., Daire, X., Adrian, M., Clement, C., Zipfel, C., Dorey, S., and Poinssot, B. (2014). The grapevine flagellin receptor VvFLS2 differentially recognizes flagellin-derived epitopes from the endophytic growth-promoting bacterium *Burkholderia phytofirmans* and plant pathogenic bacteria. New Phytol. **201,** 1371-1384.

Tsai, H.H., and Schmidt, W. (2017). One way. Or another? Iron uptake in plants. New Phytol. **214,** 500-505.

Turner, T.R., Ramakrishnan, K., Walshaw, J., Heavens, D., Alston, M., Swarbreck, D., Osbourn, A., Grant, A., and Poole, P.S. (2013). Comparative metatranscriptomics reveals kingdom level changes in the rhizosphere microbiome of plants. ISME J. **7,** 2248-2258.

Turrà, D., El Ghalid, M., Rossi, F., and Di Pietro, A. (2015). Fungal pathogen uses sex pheromone receptor for chemotropic sensing of host plant signals. Nature **527,** 521-524.

Valle, T., Lopez, J.L., Hernandez, J.M., and Corchete, P. (1997). Antifungal activity of scopoletin and its differential accumulation in Ulmus pumila and *Ulmus campestris* cell suspension cultures infected with *Ophiostoma ulmi* spores. Plant Sci. **125,** 97-101.

Van de Mortel, J.E., Schat, H., Moerland, P.D., Ver Loren van Themaat, E., Van der Ent, S., Blankestijn, H., Ghandilyan, A., Tsiatsiani, S., and Aarts, M.G. (2008). Expression differences for genes involved in lignin, glutathione and sulphate metabolism in response to cadmium in *Arabidopsis thaliana* and the related Zn/Cd-hyperaccumulator *Thlaspi caerulescens*. Plant Cell Environ **31,** 301-324.

Van de Mortel, J.E., De Vos, R.C., Dekkers, E., Pineda, A., Guillod, L., Bouwmeester, K., Van Loon, J.J., Dicke, M., and Raaijmakers, J.M. (2012). Metabolic and transcriptomic changes induced in Arabidopsis by the rhizobacterium *Pseudomonas fluorescens* SS101. Plant. Physiol. **160,** 2173-2188.

Van der Ent, S., Verhagen, B.W., Van Doorn, R., Bakker, D., Verlaan, M.G., Pel, M.J., Joosten, R.G., Proveniers, M.C., Van Loon, L.C., Ton, J., and Pieterse, C.M.J. (2008). *MYB72* is required in early signaling steps of rhizobacteria-induced systemic resistance in Arabidopsis. Plant. Physiol. **146,** 1293-1304.

Van Loon, L.C., Bakker, P.A.H.M., Van der Heijdt, W.H., Wendehenne, D., and Pugin, A. (2008). Early responses of tobacco suspension cells to rhizobacterial elicitors of induced systemic resistance. Mol. Plant-Microbe Interact. **21,** 1609-1621.

Van Oosten, V.R., Bodenhausen, N., Reymond, P., Van Pelt, J.A., Van Loon, L.C., Dicke, M., and Pieterse, C.M.J. (2008). Differential effectiveness of microbially induced resistance against herbivorous insects in Arabidopsis. Mol. Plant-Microbe Interact. **21,** 919-930.

Van Verk, M.C., Hickman, R., Pieterse, C.M.J., and Van Wees, S.C.M. (2013). RNA-Seq: revelation of the messengers. Trends. Plant. Sci. **18,** 175-179.

Van Wees, S.C.M., Van der Ent, S., and Pieterse, C.M.J. (2008). Plant immune responses triggered by beneficial microbes. Curr. Opin. Plant Biol. **11,** 443-448.

Van Wees, S.C.M., Van Pelt, J.A., Bakker, P.A.H.M., and Pieterse, C.M.J. (2013). Bioassays for assessing jasmonate-dependent defenses triggered by pathogens, herbivorous insects, or beneficial rhizobacteria. Methods Mol. Biol. **1011,** 35-49.

Van Wees, S.C.M., Luijendijk, M., Smoorenburg, I., Van Loon, L.C., and Pieterse, C.M.J. (1999). Rhizobacteria-mediated induced systemic resistance (ISR) in Arabidopsis is not associated with a direct effect on expression of known defense-related genes but stimulates the expression of the jasmonate-inducible gene Atvsp upon challenge. Plant Mol. Biol. **41,** 537-549.

Van Wees, S.C.M., Pieterse, C.M.J., Trijssenaar, A., Van't Westende, Y.A.M., Hartog, F., and Van Loon, L.C. (1997a). Differential induction of systemic resistance in Arabidopsis by biocontrol bacteria. Mol. Plant-Microbe Interact. **10,** 716-724.

Van Wees, S.C.M., Pieterse, C.M.J., Trijssenaar, A., Van 't Westende, Y.A.M., Hartog, F., and Van Loon, L.C. (1997b). Differential induction of systemic resistance in Arabidopsis by biocontrol bacteria. Mol. Plant-Microbe Interact. **10,** 716-724.

Vasse, J., Genin, S., Frey, P., Boucher, C., and Brito, B. (2000). The *hrpB* and *hrpG* regulatory genes of *Ralstonia solanacearum* are required for different stages of the tomato root infection process. Mol. Plant-Microbe Interact. **13,** 259-267.

Venturi, V., and Keel, C. (2016). Signaling in the rhizosphere. Trends. Plant. Sci. **21,** 187-198.

Verbon, E.H., Trapet, P.L., Stringlis, I.A., Kruijs, S., Bakker, P.A.H.M., and Pieterse, C.M.J. (2017). Iron and immunity. Annu. Rev. Phytopathol. **55,** 355-375.

Verhagen, B.W., Glazebrook, J., Zhu, T., Chang, H.S., Van Loon, L.C., and Pieterse, C.M.J. (2004). The transcriptome of rhizobacteria-induced systemic resistance in Arabidopsis. Mol. Plant-Microbe Interact. **17,** 895-908.

Vicre, M., Santaella, C., Blanchet, S., Gateau, A., and Driouich, A. (2005). Root border-like cells of Arabidopsis. Microscopical characterization and role in the interaction with rhizobacteria. Plant. Physiol. **138,** 998-1008.

Viollet, A., Corberand, T., Mougel, C., Robin, A., Lemanceau, P., and Mazurier, S. (2011). Fluorescent pseudomonads harboring type III secretion genes are enriched in the mycorrhizosphere of *Medicago truncatula*. FEMS Microbiol. Ecol. **75,** 457-467.

Viollet, A., Pivato, B., Mougel, C., Cleyet-Marel, J.C., Gubry-Rangin, C., Lemanceau, P., and Mazurier, S. (2017). *Pseudomonas fluorescens* C7R12 type III secretion system impacts mycorrhization of *Medicago truncatula* and associated microbial communities. Mycorrhiza **27,** 23-33.

Vogt, T. (2010). Phenylpropanoid biosynthesis. Mol. Plant **3,** 2-20.

Vos, I.A., Pieterse, C.M.J., and van Wees, S.C.M. (2013). Costs and benefits of hormone-regulated plant defences. Plant Pathol. **62,** 43-55.

Wachsman, G., Sparks, E.E., and Benfey, P.N. (2015). Genes and networks regulating root anatomy and architecture. New Phytol. **208,** 26-38.

Walker, E.L., and Connolly, E.L. (2008). Time to pump iron: iron-deficiency-signaling mechanisms of higher plants. Curr. Opin. Plant Biol. **11,** 530-535.

Walker, L., Boddington, C., Jenkins, D., Wang, Y., Gronlund, J.T., Hulsmans, J., Kumar, S., Patel, D., Moore, J.D., Carter, A., Samavedam, S., Bomono, G., Hersh, D.S., Coruzzi, G.M., Burroughs, N.J., and Gifford, M.L. (2017). Root architecture shaping by the environment is orchestrated by dynamic gene expression in space and time. Plant Cell**,** in press.

Wan, J., Zhang, X.C., Neece, D., Ramonell, K.M., Clough, S., Kim, S.Y., Stacey, M.G., and Stacey, G. (2008). A LysM receptor-like kinase plays a critical role in chitin signaling and fungal resistance in Arabidopsis. Plant Cell **20,** 471-481.

Wang, E., Schornack, S., Marsh, J.F., Gobbato, E., Schwessinger, B., Eastmond, P., Schultze, M., Kamoun, S., and Oldroyd, G.E. (2012). A common signaling process that promotes mycorrhizal and oomycete colonization of plants. Curr. Biol. **22,** 2242-2246.

Wang, L., Albert, M., Einig, E., Furst, U., Krust, D., and Felix, G. (2016). The pattern-recognition receptor CORE of Solanaceae detects bacterial cold-shock protein. Nat. Plants **2,** 16185.

Warmink, J.A., and Van Elsas, J.D. (2008). Selection of bacterial populations in the mycosphere of *Laccaria proxima*: is type III secretion involved? ISME J. **2,** 887-900.

Weigel, D., and Glazebrook, J. (2006). EMS mutagenesis of Arabidopsis seed. Cold Spring Harbor Protocols**,** pdb. prot4621.

Weller, D.M., Raaijmakers, J.M., Gardener, B.B., and Thomashow, L.S. (2002). Microbial populations responsible for specific soil suppressiveness to plant pathogens. Annu. Rev. Phytopathol. **40,** 309-348.

Weller, D.M., Mavrodi, D.V., Van Pelt, J.A., Pieterse, C.M.J., Van Loon, L.C., and Bakker, P.A.H.M. (2012). Induced systemic resistance in *Arabidopsis thaliana* against *Pseudomonas syringae* pv. *tomato* by 2,4-diacetylphloroglucinol-producing *Pseudomonas fluorescens*. Phytopathology **102,** 403-412.

Wickham, H. (2009). ggplot2: Elegant graphics for data analysis Springer-Verlag, New York.

Woo, J., MacPherson, C.R., Liu, J., Wang, H., Kiba, T., Hannah, M.A., Wang, X.J., Bajic, V.B., and Chua, N.H. (2012). The response and recovery of the *Arabidopsis thaliana* transcriptome to phosphate starvation. BMC Plant Biol. **12,** 62.

Worrall, L.J., Lameignere, E., and Strynadka, N.C. (2011). Structural overview of the bacterial injectisome. Curr. Opin. Microbiol. **14,** 3-8.

Wyrsch, I., Dominguez-Ferreras, A., Geldner, N., and Boller, T. (2015). Tissue-specific FLAGELLIN-SENSING 2 (FLS2) expression in roots restores immune responses in Arabidopsis *fls2* mutants. New Phytol. **206,** 774-784.

Xiao, Y., and Hutcheson, S.W. (1994). A single promoter sequence recognized by a newly identified alternate sigma factor directs expression of pathogenicity and host range determinants in *Pseudomonas syringae*. J. Bacteriol. **176,** 3089-3091.

Xiao, Y., Heu, S., Yi, J., Lu, Y., and Hutcheson, S.W. (1994). Identification of a putative alternate sigma factor and characterization of a multicomponent regulatory cascade controlling the expression of *Pseudomonas syringae* pv. *syringae* Pss61 *hrp* and *hrmA* genes. J. Bacteriol. **176,** 1025-1036.

Xie, F., Williams, A., Edwards, A., and Downie, J.A. (2012). A plant arabinogalactan-like glycoprotein promotes a novel type of polar surface attachment by *Rhizobium leguminosarum*. Mol. Plant-Microbe Interact. **25,** 250-258.

Xu, Z., Escamilla-Trevino, L., Zeng, L., Lalgondar, M., Bevan, D., Winkel, B., Mohamed, A., Cheng, C.L., Shih, M.C., Poulton, J., and Esen, A. (2004). Functional genomic analysis of *Arabidopsis thaliana* glycoside hydrolase family 1. Plant Mol. Biol. **55,** 343-367.

Yahr, T.L., and Wolfgang, M.C. (2006). Transcriptional regulation of the *Pseudomonas aeruginosa* type III secretion system. Mol. Microbiol. **62,** 631-640.

Yang, C.H., and Crowley, D.E. (2000). Rhizosphere microbial community structure in relation to root location and plant iron nutritional status. Appl. Environ. Microbiol. **66,** 345-351.

Yoneyama, K., Yoneyama, K., Takeuchi, Y., and Sekimoto, H. (2007). Phosphorus deficiency in red clover promotes exudation of orobanchol, the signal for mycorrhizal symbionts and germination stimulant for root parasites. Planta **225,** 1031-1038.

Yoneyama, K., Xie, X., Kim, H.I., Kisugi, T., Nomura, T., Sekimoto, H., Yokota, T., and Yoneyama, K. (2012). How do nitrogen and phosphorus deficiencies affect strigolactone production and exudation? Planta **235,** 1197-1207.

Zamioudis, C., and Pieterse, C.M.J. (2012). Modulation of host immunity by beneficial microbes. Mol. Plant-Microbe Interact. **25,** 139-150.

Zamioudis, C., Hanson, J., and Pieterse, C.M.J. (2014). β-Glucosidase BGLU42 is a MYB72-dependent key regulator of rhizobacteria-induced systemic resistance and modulates iron deficiency responses in Arabidopsis roots. New Phytol. **204,** 368-379.

Zamioudis, C., Mastranesti, P., Dhonukshe, P., Blilou, I., and Pieterse, C.M.J. (2013). Unraveling root developmental programs initiated by beneficial *Pseudomonas* spp. bacteria. Plant. Physiol. **162,** 304-318.

Zamioudis, C., Korteland, J., Van Pelt, J.A., Van Hamersveld, M., Dombrowski, N., Bai, Y., Hanson, J., Van Verk, M.C., Ling, H.Q., Schulze-Lefert, P., and Pieterse, C.M.J. (2015). Rhizobacterial volatiles and photosynthesis-related signals coordinate *MYB72* expression in Arabidopsis roots during onset of induced systemic resistance and iron-deficiency responses. Plant J. **84,** 309-322.

Zeidler, D., Zahringer, U., Gerber, I., Dubery, I., Hartung, T., Bors, W., Hutzler, P., and Durner, J. (2004). Innate immunity in *Arabidopsis thaliana*: lipopolysaccharides activate nitric oxide synthase (NOS) and induce defense genes. Proc. Natl. Acad. Sci. U S A **101,** 15811-15816.

Zgadzaj, R., Garrido-Oter, R., Jensen, D.B., Koprivova, A., Schulze-Lefert, P., and Radutoiu, S. (2016). Root nodule symbiosis in *Lotus japonicus* drives the establishment of distinctive rhizosphere, root, and nodule bacterial communities. Proc. Natl. Acad. Sci. U S A **113,** 7996-8005.

Zhang, H., Sun, Y., Xie, X., Kim, M.S., Dowd, S.E., and Pare, P.W. (2009). A soil bacterium regulates plant acquisition of iron via deficiency-inducible mechanisms. Plant J. **58,** 568-577.

Zhang, L., Shen, X., Liu, Y., and Li, S. (2013). *Nafulsella turpanensis* gen. nov., sp. nov., a member of the phylum *Bacteroidetes* isolated from soil. Int. J. Syst. Evol. Microbiol. **63,** 1639-1645.

Zhang, N., Wang, D., Liu, Y., Li, S., Shen, Q., and Zhang, R. (2014). Effects of different plant root exudates and their organic acid components on chemotaxis, biofilm formation and colonization by beneficial rhizosphere-associated bacterial strains. Plant and Soil **374,** 689-700.

Zhang, X., Dong, W., Sun, J., Feng, F., Deng, Y., He, Z., Oldroyd, G.E., and Wang, E. (2015a). The receptor kinase *CERK1* has dual functions in symbiosis and immunity signalling. Plant J. **81,** 258-267.

Zhang, X.C., Millet, Y.A., Cheng, Z., Bush, J., and Ausubel, F.M. (2015b). Jasmonate signalling in Arabidopsis involves SGT1b-HSP70-HSP90 chaperone complexes. Nat. Plants **1,** 15049.

Zhang, Y., Xu, J., Riera, N., Jin, T., Li, J., and Wang, N. (2017). Huanglongbing impairs the rhizosphere-to-rhizoplane enrichment process of the citrus root-associated microbiome. Microbiome **5,** 97.

Zhou, C., Guo, J., Zhu, L., Xiao, X., Xie, Y., Zhu, J., Ma, Z., and Wang, J. (2016). *Paenibacillus polymyxa* BFKC01 enhances plant iron absorption via improved root systems and activated iron acquisition mechanisms. Plant Physiology and Biochemistry **105,** 162-173.

Ziegler, J., Schmidt, S., Chutia, R., Muller, J., Bottcher, C., Strehmel, N., Scheel, D., and Abel, S. (2016). Non-targeted profiling of semi-polar metabolites in Arabidopsis root exudates uncovers a role for coumarin secretion and lignification during the local response to phosphate limitation. J. Exp. Bot. **67,** 1421-1432.

Zipfel, C., Robatzek, S., Navarro, L., Oakeley, E.J., Jones, J.D., Felix, G., and Boller, T. (2004). Bacterial disease resistance in Arabidopsis through flagellin perception. Nature **428,** 764-767.

Zipfel, C., Kunze, G., Chinchilla, D., Caniard, A., Jones, J.D., Boller, T., and Felix, G. (2006). Perception of the bacterial PAMP EF-Tu by the receptor EFR restricts Agrobacterium-mediated transformation. Cell **125,** 749-760.

Zum Felde, T., Baumert, A., Strack, D., Becker, H.C., and Mollers, C. (2007). Genetic variation for sinapate ester content in winter rapeseed (*Brassica napus* L.) and development of NIRS calibration equations. Plant Breeding **126,** 291-296.

Zuryn, S., Le Gras, S., Jamet, K., and Jarriault, S. (2010). A strategy for direct mapping and identification of mutations by whole-genome sequencing. Genetics **186,** 427-430.

Zwiesler-Vollick, J., Plovanich-Jones, A.E., Nomura, K., Bandyopadhyay, S., Joardar, V., Kunkel, B.N., and He, S.Y. (2002). Identification of novel *hrp*-regulated genes through functional genomic analysis of the *Pseudomonas syringae* pv. *tomato* DC3000 genome. Mol. Microbiol. **45,** 1207-1218.

Summary

The interface between roots and their adjacent soil layer, the rhizosphere, constitutes a hotspot of microbial activity and represents one of the most diverse ecosystems on Earth. The root-associated microbial community, the microbiome, contains rhizobacteria that can change the phenotypic plasticity of their hosts and trigger a broad-spectrum form of systemic immunity, known as induced systemic resistance (ISR). Although the effect of beneficial rhizobacteria on plant growth and plant health is relatively well studied, very little is known about the early molecular processes that occur at the root-microbiome interface. In this thesis, we investigated early changes in the root transcriptome and metabolome of plant roots in response to colonization of the roots by beneficial ISR-inducing *Pseudomonas* rhizobacteria. We discovered that ISR-inducing rhizobacteria suppress host immune responses that are triggered by their general microbial elicitors to subsequently allow root colonization and promotion of plant growth and protection. Moreover, we uncovered the iron-mobilizing coumarin scopoletin as a major player in the chemical dialogue between plants roots and ISR-inducing members in the root microbiome.

The discovery that roots possess an immune system indicates that even beneficial root-inhabiting microbes need to overcome plant defenses to achieve colonization. To gain insight in this, a time-series RNA-seq transcriptomic analysis was designed to test early Arabidopsis root responses to the beneficial rhizobacterium *Pseudomonas simiae* WCS417 and compare this response with those of elicitors of bacterial and fungal pathogens. We demonstrate that elicitors of the beneficial rhizobacterium WCS417 have the same immune-eliciting potential as those of pathogenic bacteria. However, live beneficial WCS417 bacteria suppress a significant proportion of the growth-retarding immune responses that are triggered by their elicitors, possibly to allow these plant growth-promoting rhizobacteria to colonize the roots and subsequently stimulate plant growth and health. Additionally, we observed a strong transcriptional auxin signature in the root transcriptome following recognition of WCS417. This auxin response in the roots could be linked to the onset of ISR following colonization. The suppression of defense-related processes suggests that beneficial WCS417 bacteria have a mechanism in place that manipulates early plant root responses in order to establish an intimate association with their host.

In phytopathogenic bacteria, type III secretion system (T3SS) activity is associated with suppression of host immunity. Previously, genes encoding T3SS proteins were also identified in the genomes of the ISR-inducing rhizobacteria WCS417 and *Pseudomonas defensor* WCS374. Here, we characterized the T3SS gene clusters in the genomes of these rhizobacteria. Phylogenetic analysis revealed their similarity with the T3SSs of other beneficial pseudomonads and their evolutionary distance from those of pathogenic bacteria. Additionally, we discovered genes coding for putative effector proteins with a potential role in the suppression of immunity and microbial competence in the rhizosphere. These findings facilitate future investigations towards the role of effector proteins of beneficial rhizobacteria in plant-microbe interactions.

In Arabidopsis, successful colonization by ISR-inducing rhizobacteria and fungi leads to the upregulation of the root-specific transcription factor gene *MYB72*. Previously, MYB72 was demonstrated to be an essential early, root-specific regulator of the onset of ISR in the leaves. MYB72 and MYB72-regulated β-glucosidase

BGLU42 were previously found to regulate biosynthesis and release of fluorescent phenolic compounds that are secreted by plant roots during conditions of iron limitation to mobilize iron from the rhizosphere. To study the nature and role of these compounds in the context of ISR and root-microbiome interactions, we performed an untargeted metabolomic analysis of the root exudates and root extracts of wild-type Col-0 and mutant *myb72* and *bglu42* Arabidopsis plants. We discovered that the compounds produced in the roots in a MYB72-dependent manner are coumarins. Moreover, we showed that BGLU42 activity is involved in the processing of the coumarin scopolin into scopoletin before its release into the rhizosphere. Scopoletin possesses antimicrobial activity. Interestingly, we observed that the ISR-inducing rhizobacteria WCS417 and WCS358 are tolerant to high concentrations of scopoletin, while scopoletin negatively impacted the performance of the soil-borne pathogens *Fusarium oxysporum* and *Verticillium dahliae*. This differential sensitivity to the antimicrobial activity of scopoletin suggests that MYB72-dependent production and excretion of this coumarin plays a role in shaping the composition of the microbiome in the rhizosphere. To investigate the role of scopoletin in microbiome assembly, we performed shotgun metagenomic sequencing of the rhizospheres of Arabidopsis plants with differential coumarin exudation patterns. This microbiome analysis revealed that scopoletin biosynthesis mutant *f6'h1* forms a similar root-associated microbial community as mutant *myb72*. However, the root-associated microbiome of *f6'h1* was significantly different from that of wild-type, coumarin-exuding Col-0 plants. Collectively, our data point to a role for coumarins and scopoletin in microbiome assembly.

Activation of the root-specific transcription factor gene *MYB72* by ISR-inducing rhizobacteria is not only important for the onset of ISR, it is also contributing to the capacity of plants to take up iron when growing under iron-limiting conditions. However, little is known about the molecular events that play a role in the activation of *MYB72* in roots. To gain insight into the regulation of *MYB72* activation, we performed an EMS mutagenesis screen with the transgenic reporter line of $MYB72_{pro}$*:GFP-GUS*. This screening yielded eleven putants with abolished *MYB72* expression following iron-limiting condition and no mutations could be found following sequencing of *MYB72* gene, suggesting that mutation(s) in other genomic regions are responsible for this phenotype. These findings form the basis for future research on the regulation of *MYB72* gene transcription.

Collectively, our results show that beneficial rhizobacteria are capable of suppressing root immune responses that are activated by their general elicitors, possibly via the action of immune-suppressive effectors. This paves the way to colonize the roots and provide beneficial functions to the host plant, such as enhanced growth and protection. Within the root, the transcription factor MYB72 regulates the biosynthesis of coumarins, such as scopolin. Due to the action of the MYB72-regulated β-glucosidase BGLU42, scopolin is hydrolyzed into scopoletin, which facilitates the excretion of this metabolite into the rhizosphere. Scopoletin has a differential antimicrobial activity to which ISR-inducing rhizobacteria WCS417 and WCS358 are insensitive, but which impacts the performance of selected soil-borne pathogens. Analysis of the root-associated microbiomes of Arabidopsis roots with different scopoletin exudation patterns demonstrated a role for scopoletin in microbiome assembly. Knowledge on the molecular mechanisms that play a role in the interaction between plant roots and beneficial members of the root microbiome is essential for the development of durable biological control strategies and crops with traits that can maximize the profitable functions the root microbiome.

Samenvatting

Micro-organismen maken een belangrijk deel uit van het "sociale netwerk" van planten. Op en in de plantenwortels leven miljarden bacteriën en schimmels. Deze microbiële gemeenschap in de rhizosfeer wordt het wortelmicrobioom genoemd. Het microbioom wordt gevormd en gevoed door voedingsstoffen die worden uitgescheiden door de plantenwortels. Planten scheiden tot wel 20% van de suikers die zij via fotosynthese hebben vastgelegd weer uit via de wortels om deze rijke microbiële gemeenschap te voeden. Planten krijgen daarvoor een aantal belangrijke functies terug die ze zelf niet of niet goed kunnen uitvoeren. Het microbioom verbetert de opname van nutriënten uit de bodem, verbetert de architectuur van het wortelstelsel, stimuleert de groei van de plant, biedt bescherming tegen bodempathogenen, en versterkt het immuunsysteem van de plant. Dit laatste fenomeen wordt "induced systemic resistance" (ISR) genoemd. ISR wordt geactiveerd indoor specifieke micro-organismen in het microbioom en biedt bescherming tegen een breed scala aan ziekteverwekkers, ook in bovengrondse delen van de plant. In dit proefschrift is onderzoek gedaan naar de vroege moleculaire communicatie tussen plantenwortels en goedaardige ISR-inducerende bodembacteriën.

In het onderzoek is gebruik gemaakt van de modelplant *Arabidopsis thaliana* (zandraket) en de ISR-inducerende gewasbeschermingsbacterie *Pseudomonas simiae* WCS417. Met behulp van RNA-seq is de vroege reactie van plantenwortels op herkenning door WCS417 onderzocht. We ontdekten dat WCS417 net als een pathogeen herkend kan worden door algemene "microbe-associated molecular patterns" (MAMPs), zoals flagelline. De afweerreactie die in de plantenwortel wordt geïnduceerd is vrijwel identiek aan de afweerreactie die in gang wordt gezet door flagelline van een pathogene *Pseudomonas* stam. Echter, WCS417 bacteriën blijken een groot deel van deze algemene afweerreactie te onderdrukken. Dit stelt deze bacterie in staat om de wortels te koloniseren en zijn groei-bevorderende en resistentie-inducerende functies uit te voeren.

Pathogene micro-organismen hebben speciale eiwitten, effectoren, die ingrijpen in het immuunsysteem van de plant waardoor ze beter in staat zijn de gastheer te koloniseren en ziekte te veroorzaken. Veel pathogene bacteriën gebruiken hiervoor een zogenaamd type III secretiesysteem (T3SS). De ISR-inducerende en plantengroeibevorderende bacteriën *P. simiae* WCS417 en *Pseudomonas defensor* WCS374 hebben ook een dergelijk T3SS. In dit onderzoek hebben we het T3SS systeem van deze twee goedaardige micro-organismen vergeleken met dat van andere bacteriesoorten. We ontdekten dat het T3SS van WCS417 en WCS374 meer overeenkomsten heeft met het T3SS van andere goedaardige bacteriën dan met dat van pathogene bacteriën. Bovendien ontdekten we in de genomen van WCS417 en WCS374 een aantal genen die mogelijk coderen voor effectoren. Toekomstig onderzoek moet uitwijzen of deze effectoren een rol spelen in het onderdrukken van het afweersysteem in de wortels waardoor het mogelijk wordt voor deze micro-organismen om de wortels te koloniseren en hun goedaardige functies uit te oefenen.

In dit proefschrift is ook uitgebreid onderzoek gedaan naar de metabolieten die door de plantenwortels worden uitgescheiden en die een rol spelen in de communicatie met goedaardige micro-organismen in het microbioom. Hierbij hebben we gebruik gemaakt van de transcriptiefactor MYB72. Eerder onderzoek heeft

aangetoond dat MYB72 een essentiële moleculaire schakel is in de communicatie tussen de plantenwortel en ISR-inducerende micro-organismen. Kolonisatie van de wortels door *P. simiae* WCS417 induceert het *MYB72* gen in de wortel. Hierdoor wordt een transcriptioneel netwerk geactiveerd wat uiteindelijk resulteert in systemische ziekteresistentie in de gehele plant. Een belangrijke speler in het MYB72 transcriptionele netwerk is het β-glucosidase gen *BGLU42*. β-glucosidases zijn enzymen die glycosiden (chemische stoffen die zijn opgebouwd uit een suiker en een niet-suiker zoals secundaire metabolieten) hydrolyseren. Net als MYB72, is BGLU42 ook noodzakelijk is voor ISR. Uit de gedetailleerde analyse van het metaboloom van de wortels van wild-type Arabidopsis planten en dat van de mutanten *myb72* en *bglu42* kwam scopoletin naar voren als de belangrijkste chemische stof in de communicatie tussen de ISR-inducerende micro-organismen en de plant. Uit het onderzoek bleek dat de biosynthese van scopoletin in de wortel wordt gereguleerd door MYB72. Door de activiteit van BGLU42 wordt scopoletin vervolgens uitgescheiden waar het in contact komt met het microbioom in de rhizosfeer.

Van scopoletin is bekend dat het de plant helpt bij de opname van ijzer uit de bodem. Bovendien heeft het een selectieve antimicrobiële werking. We onderzochten daarom of scopoletin de samenstelling van het wortelmicrobioom kan beïnvloeden. Metagenoomanalyse van het wortelmicrobioom van scopoletin-producerende wild-type Arabidopsis planten en scopoletin-deficiënte mutanten liet zien dat scopoletin inderdaad een invloed heeft op de compositie van het microbioom. Sommige micro-organismen namen in aantal af door toedoen van scopoletin, terwijl anderen in aantal toenamen. De ISR-inducerende *Pseudomonas* stammen WCS417 en WCS358 bleken ongevoelig te zijn voor de anti-microbiële werking van scopoletin, terwijl de bodempathogenen *Fusarium oxysporum* en *Verticillium dahliae* heel gevoelig waren voor scopoletin. Deze resultaten laten zien dat scopoletin een belangrijke rol speelt in de samenwerking tussen plantenwortels en goedaardige micro-organismen in het microbioom.

Het inzetten van goedaardige bodembacteriën bij het bestrijden van plantenziekten is sterk in opkomst. Grote multinationals uit de agro-industrie zijn geïnteresseerd in het ontwikkelen van nieuwe biologische producten die de groei en weerbaarheid van de plant kunnen bevorderen waardoor er minder gebruik gemaakt hoeft te worden van kunstmest en toxische gewasbeschermingsmiddelen. Het tot in detail begrijpen van de moleculaire en biologische mechanismen waarbij planten voordeel halen uit de microbiële functies die worden uitgeoefend door goedaardige bodembacteriën in het microbioom is van groot belang voor de ontwikkeling van nieuwe strategieën voor deze duurzame vorm van gewasbescherming.

Σύνοψη

Σήματα που προέρχονται από το «υπόγειο» μέρος των φυτών και η αλληλεπίδραση τους με το ανοσοποιητικό σύστημα των φυτών

Η ριζόσφαιρα, που ορίζεται ως η ενδιάμεση ζώνη ανάμεσα στο ριζικό σύστημα των φυτών και το περιβάλλων έδαφος είναι μια περιοχή με έντονη μικροβιακή δραστηριότητα και αποτελεί ένα από τα οικοσυστήματα με την μεγαλύτερη ποικιλομορφία στη Γη. Η μικροβιακή κοινότητα που αλληλεπιδρά με τη ρίζα, το μικροβίωμα, περιέχει ριζοβακτήρια που μπορούν να επηρεάσουν το φαινότυπο των ξενιστών τους και να ενεργοποιήσουν μια ευρέως φάσματος διασυστηματική ανθεκτικότητα (induced systemic resistance; ISR). Μολονότι η επίδραση των ωφέλιμων ριζοβακτηρίων στην ανάπτυξη και την υγεία των φυτών εχει μελετηθεί εκτενώς, τα αρχικά στάδια της αλληλεπίδρασης μεταξύ της ρίζας και αυτών των βακτηρίων δεν είναι επαρκώς μελετημένα. Στην παρούσα διατριβή, διερευνήσαμε τις πρώιμες αλλαγές που συμβαίνουν τοπικά στις ρίζες σε μεταγραφικό και μεταβολομικό επιπεδο, όταν αυτές αλληλεπιδρούν με το ωφέλιμο ριζοβακτήριο *Pseudomonas simiae* WCS417 που επάγει την ISR, και εξετάσαμε πως οι αλλαγές αυτές μπορούν να επηρεάσουν το σχηματισμό μικροβιακών κοινοτήτων στη ριζόσφαιρα.

Η ανακάλυψη της ύπαρξης και λειτουργίας ανοσοποιητικού συστήματος τοπικά στη ρίζα υποδεικνύει ότι ακόμα και οι ωφέλιμοι μικροοργανισμοί του εδάφους πρέπει να ξεπεράσουν τους αμυντικούς μηχανισμούς του φυτού για να επιτύχουν τον αποικισμό του. Για να κατανοήσουμε πως επιτυγχάνεται αυτό, πραγματοποιήσαμε αλληλούχιση του μεταγραφικού RNA της ρίζας του φυτού Arabidopsis σε διάφορα πρώιμα χρονικά σημεία μετά την αναγνώριση του ωφέλιμου ριζοβακτηρίου WCS417 και συγκρίναμε τις αποκρίσεις των ριζών με αυτές που επάγονται από διεγέρτες βακτηριακής ή μυκητολογικής προέλευσης. Αποδεικνύουμε ότι οι διεγέρτες του ωφέλιμου ριζοβακτηρίου ενεργοποιούν τους αμυντικούς μηχανισμούς στη ρίζα σε ανάλογο επίπεδο με αυτούς από παθογόνα βακτήρια. Παρ' όλα αυτά, τα ριζοβακτήρια WCS417 καταστέλλουν ένα σημαντικό ποσοστό της αμυντικής ενεργοποίησης που επάγουν μέσω των διεγερτών τους με συνέπεια να αποικίζουν τη ρίζα και να συμβάλλουν στην αύξηση του μεγέθους του φυτού αλλά και στην διατήρηση της υγείας του. Επιπλέον, παρατηρηρούμε ότι η αναγνώριση του WCS417 προκαλεί στις ρίζες μεταγραφικές αποκρίσεις που είναι ανάλογες σε μεγάλο ποσοστό με αυτές που παρατηρούνται μετά την εφαρμογή της ορμόνης αυξίνης στη ρίζα. Αυτές οι αποκρίσεις φαίνεται να συνδέονται με την εγκαθίδρυση της ISR, μετα τον αποικισμό των ριζών. Η καταστολή των διαδικασιών που σχετίζονται με την άμυνα του φυτού υποδηλώνει ότι τα ριζοβακτήρια WCS417 διαθέτουν ένα μηχανισμό χειραγώγησης των πρώιμων αποκρίσεων της ρίζας των φυτών ώστε να εξασφαλίσουν μια στενή σχέση με τον ξενιστή τους.

Στην περίπτωση των φυτοπαθογόνων βακτηρίων, η δραστηριότητα του εκκριτικού συστήματος τύπου III (type III secretion system; T3SS) σχετίζεται με την καταστολή της άμυνας των φυτών. Σε προηγούμενη μελέτη, αναγνωρίστηκαν γονίδια που κωδικοποιούν πρωτεΐνες του T3SS στα γονιδιώματα των ριζοβακτηρίων WCS417 και *Pseudomonas defensor* WCS374, που επάγουν την ISR. Στην παρούσα διατριβή χαρακτηρίζουμε τη συστάδα γονιδίων του T3SS που βρίσκεται στα γονιδιώματα αυτών των ριζοβακτηρίων. Η φυλογενετική τους ανάλυση καταδεικνύει την ομοιότητά τους με τις συστάδες T3SS άλλων ωφέλιμων βακτηρίων και τη διαφοροποίησή τους από αυτές των φυτοπαθογόνων. Επίσης, εντοπίζουμε γονίδια που κωδικοποιούν υποθετικές πρωτεΐνες τελεστές

με πιθανό ρόλο στην καταστολή του ανασοποιητικού συτήματος αλλά και στην ανταγωνιστική ικανότητα των ριζοβακτηρίων στη ριζόσφαιρα.

Στο φυτό Arabidopsis, ο επιτυχής αποικισμός της ρίζας από ριζοβακτήρια και μύκητες που επάγουν την ISR οδηγεί στην υπερέκφραση του γονιδίου που κωδικοποιεί το μεταγραφικό παράγοντα MYB72, ο οποίος είναι απαραίτητος για την έκφραση της ISR στο υπέργειο τμήμα των φυτών. Προηγουμένως είχε βρεθεί ότι ο MYB72 και η β-γλυκοσιδάση BGLU42, της οποίας η έκφραση ελέγχεται από το MYB72, εμπλέκονται στη βιοσύνθεση και απελευθέρωση φθοριζουσών φαινολικών ενώσεων, που εκκρίνονται από τις ρίζες σε συνθήκες έλλειψης σιδήρου, με σκοπό να κινητοποιήσουν σίδηρο από τη ριζόσφαιρα. Στην παρούσα μελέτη, επιδιώκουμε να ταυτοποιήσουμε αυτές τις ενώσεις καθώς και να μελετήσουμε το ρόλο τους στην ISR αλλά στις αλληλεπιδράσεις ρίζας-μικροβιώματος. Για το λόγο αυτό πραγματοποιήσαμε μη στοχευμένη μεταβολομική ανάλυση σε ριζικές εκκρίσεις και εκχυλίσματα ριζών από φυτά Arabidopsis του αγρίου τύπου Col-0 και των μεταλλαγμένων σειρών *myb72* and *bglu42*. Μέσω αυτής της ανάλυσης βρίσκουμε ότι οι κουμαρίνες είναι οι ενώσεις που παράγονται στις ρίζες μέσω ενός μηχανισμού ελεγχόμενου από το MYB72. Επιπλέον, δείχνουμε ότι η δραστηριότητα του BGLU42 σχετίζεται με την επεξεργασία της κουμαρίνης σκοπολίνης για την παραγωγή σκοπολετίνης, πριν η τελευταία απελευθερωθεί στη ριζόσφαιρα. Παρά το γεγονός ότι η σκοπολετίνη διαθέτει αντιμικροβιακές ιδιότητες, τα πειράματά μας δείχνουν ότι τα ριζοβακτήρια WCS417 και *Pseudomonas capeferrum* WCS358, που επάγουν την ISR, είναι ανεκτικά σε υψηλές συγκεντρώσεις σκοπολετίνης, ενώ η σκοπολετίνη επηρεάζει αρνητικά την ανάπτυξη των εδαφογενών φυτοπαθογόνων μυκήτων *Fusarium oxysporum* και *Verticillium dahliae*. Για να μελετήσουμε περαιτέρω αν η σκοπολετίνη μπορεί να επηρεάσει τη συγκρότηση του μικροβιώματος στη ρίζα, πραγματοποιήσαμε μεταγονιδιωματική αλληλούχιση (shotgun metagenomic sequencing) στη ριζόσφαιρα φυτών Arabidopsis με διαφορετικά μοτίβα απέκκρισης κουμαρινών. Τα αποτελέσματα καταδεικνύουν ότι η μεταλλαγμένη σειρά φυτών στη βιοσύνθεση σκοπολετίνης *f6'h1* σχηματίζει παρόμοια ριζική μικροβιακή κοινότητα με τη μεταλλαγμένη σειρά *myb72*, ενώ διαφοροποιείται από αυτή των φυτών αγρίου τύπου Col-0, που απεκκρίνουν κουμαρίνες. Συλλογικά τα δεδομένα μας υποδεικνύουν ότι οι κουμαρίνες και η σκοπολετίνη παίζουν σημαντικό ρόλο στη συγκρότηση του μικροβιώματος της ριζόσφαιρας.

Το γονίδιο *MYB72* εκφράζεται στη ρίζα είτε ως απόκριση των ριζών στον αποικισμό ριζοβακτηρίων που επάγουν την ISR, ή σαν συστατικό της αντίδρασης των φυτών σε συνθήκες έλλειψης σιδήρου. Παρ' όλα, αυτά το μονοπάτι μεταγωγής σήματος που οδηγεί στη ενεργοποίηση του *MYB72* δεν είναι αρκετά μελετημένο. Για να κατανοήσουμε καλύτερα το μονοπάτι αυτό, πραγματοποιήσαμε χημική μεταλλαξογένεση με EMS στη διαγονιδιακή σειρά $MYB72_{pro}$*:GFP-GUS*. Η λεπτομερής εξέταση των φυτών που προέκυψαν από αυτή τη μεταλλαξογένεση απέδωσε έντεκα μεταλλαγμένα φυτά στα οποία δεν υπάρχει έκφραση του γονιδίου *MYB72* σε συνθήκες έλλειψης σιδήρου, ενώ μετά από αλληλούχιση του γονιδίου *MYB72* στα φυτά αυτά δε βρέθηκαν μεταλλάξεις. Τα αποτελέσματα αυτά υποδεικνύουν ότι σε μελλοντικά πειράματα πρέπει να εντοπιστούν τα σημεία του γονιδιώματος που έχουν προκληθεί μεταλλάξεις που να εξηγούν την απορρύθμιση της έκφρασης του γονιδίου MYB72 και με αυτό τον τρόπο να βρεθούν νέα συστατικά του μονοπατιού μεταγωγής σήματος με ρόλο στην ενεργοποίηση του γονιδίου.

Συμπερασματικά, τα αποτελέσματα μας δείχνουν ότι τα ωφέλιμα ριζοβακτήρια μπορούν να καταστείλουν τις αμυντικές αποκρίσεις τοπικά στη ρίζα, που ενεργοποιούνται εξαιτίας των δειγερτών που διαθέτουν, πιθανότατα μέσω της δράσης τελεστών. Μέσω αυτού του μηχανισμού επιτυγχάνεται ο αποικισμός απο τα ριζοβακτήρια με

επακόλουθο τις ωφέλιμες επιδράσεις στο φυτό-ξενιστή, όπως η αυξημένη του ανάπτυξη και η προστασία του από παθογόνα. Εντός της ρίζας, ο μεταγραφικός παράγοντας MYB72 ρυθμίζει τη βιοσύνθεση κουμαρινών, όπως η σκοπολίνη. Μέσω της δραστηριότητας της β-γλυκοσιδάσης BGLU42, η σκοπολίνη υδρολύεται και παράγεται σκοπολετίνη, η οποία απελευθερώνεται στη ριζόσφαιρα. Η σκοπολετίνη έχει αντιμικροβιακή δραστηριότητα και ενώ επηρεάζει αρνητικά την ανάπτυξη συγκεκριμένων εδαφογενών παθογόνων, δεν επηρεάζει την ανάπτυξη των ριζοβακτηρίων WCS417 και WCS358 που επάγουν την ISR. Ανάλυση των μικροβιωμάτων της ρίζας φυτών με διαφορετικά επίπεδα έκκρισης σκοπολετίνης δείχνει ότι η σκοπολετίνη παίζει ρόλο στη συγκρότηση του μικροβιώματος. Οι πληροφορίες που συλλέξαμε σε αυτή τη διατριβή εμπλουτίζουν σημαντικά τη γνώση πάνω στους μοριακούς μηχανισμούς που εμπλέκονται στην αλληλεπίδραση μεταξύ των ριζών και των ωφέλιμων μελών του μικροβιώματος. Αυτές οι γνώσεις είναι απαραίτητες για την ανάπτυξη αποτελεσματικών στρατηγικών βιολογικής αντιμετώπισης των παθογόνων καθώς και καλλιεργούμενων φυτών με χαρακτηριστικά που μπορούν να μεγιστοποιήσουν τις επωφελείς λειτουργίες του μικροβιώματος της ρίζας.

Acknowledgments

This is the part of the book dedicated to all those that with numerous ways have contributed in a professional or personal manner in order to accomplish my demanding scientific mission.

Corné thank you for believing in me some years ago when I had an interview with you and giving me the chance to work in PMI group. Thank you also for your supervision, mentoring and your critical approach on things. You helped me realize that having an idea is not enough, but answering a question with small but logical steps is more important. Thank you for allowing me to develop my ideas and for the nice and fruitful collaboration in the last months during the finalization of my thesis. You are a real influence in my scientific development! Thank you for that!

Peter, Saskia and Guido thank you for your advice during my half year reports and for the nice scientific and non-scientific moments all these years. Peter thank you for always being kind and willing to help with my questions, Saskia thank you for your positive energy and "dirty" jokes and Guido thank you for the discussions we had, usually at coffee breaks. Ronnie thank you for your fresh ideas, for giving me the chance to continue with my postdoctoral research in the lab, and for helping me learn bioinformatics (hopefully) that will get me out of my comfort zone…the lab bench! Roeland (aka dr. Berendsen) your mom is responsible for who you are…as part of PMI history you helped me since I arrived to adapt to the Dutch lifestyle (Andre Hazes, beer drinking, etc), moving out from my old house and still helping me with bureaucratic and other life-related issues. Thanks! Hans thank you for your willingness to always solve my problems with orders and consumables but also for taking great pictures of my experiments! Anja, Miek and Joyce thank you for answering my questions about how things run in the lab and about the rules I needed to follow so that nothing will explode or burn! Kirstin and Ivo Feussner, from Goettingen University, thank you for your scientific contribution in my projects and for hosting me one week in your lab to acquire knowledge on the analysis of metabolomic data.

My PMI "family" of W301, Silvia, Ke and Marciel…Words cannot describe my gratitude to you! You were/are always there for me, both inside and outside the lab! You made my life easier and I really feel that you are members of my family…I am pretty sure this is something that will continue in the future! Silvia (aka Italian sister!) thank you for your advice on various matters and for all the fun moments we had in daily "office" life and in the meetings we attended together! I wish you success in both your scientific and personal goals! You deserve it! Ke you are a special person…Thank you for all the moments we shared, discussing science late in the evening, for the huge experiments we did together and for being a "real" friend in good and bad times. Good luck with your upcoming PhD defense and your future steps! Marciel thank you for your positive mentality and way of thinking. In moments of desperation, you were always there to see the "sun behind the clouds"…Thanks also for introducing me to the world of mate, as an alternative for coffee. Good luck with finishing your thesis! I would like also to thank my friends from EVP Elaine and Sara, for being part of the W301 "compagnia" and for the nice time outside the lab, during dinners and trips around Europe!

Dr. Zamioudis thank you for supporting my "first steps" in this lab! **Χρηστάρα σε ευχαριστώ για τις συζητήσεις που κάναμε στο μπαλκόνι και για την ανταλλαγή απόψεων πάνω σε επιστημονικά, και όχι μόνο, ζητήματα. Σου εύχομαι ότι καλύτερο για το μέλλον!** Ivan and Ainhoa, my Spanish friends! You arrived some months after I started and

helped me to overcome difficulties and have nice time out of the lab (parties, dinners and trips together)! Ivan thank you as well for all the nice moments we had together playing for De Basis, the football team of the lab, during the games but mostly after the games…the third half! Richard thank you for your scientific help with bioinformatics and also for your unpredictably good humor. Marcel thank you for your bioinformatic and practical advice in my projects. I would like also to thank the PMI members Alexandra, Aster, Colette, Claudia, Eline, Erqin, Gilles, Hao, Joel, Kim, Manon, Merel, Niels, Pauline, Pim (the new), Sarah, Silvia, Tom, Tijmen, Yang for all the nice interaction we had inside and outside the lab! Good luck with your tasks and projects!

I am also grateful to my students: Andrea, David, Fabiola, Jhon, Sietske and Santiago. Due to your efforts, my projects progressed and you also helped me become better in communicating my ideas and improve my supervision skills. Thank you all and good luck with your future plans!

I also want to thank all the previous PMI members: Annalisa, Chiel, Dieuw, Dima, Dongping, Irene, Joost, Lotte, Marco, Nicole, Nora, Paul, Pim (the old), Stan, Tieme and Yeling for the nice atmosphere in the lab from the start of my PhD till almost its end (since you are not there anymore).

I would also like to thank people from other labs such as Debatosh, Diederik, Lot and Hans (from EVP), Zhilei, Simone and Tianjie (E&B), Jebasingh, Savani and Lennard (from MPP) and Freek (from Microbiology Group) for all the nice discussions and interaction during IEB meetings and other occasions.

Θέλω να ευχαριστήσω τους καθηγητές μου στο Εργαστήριο Φυτοπαθολογίας στην Αθήνα Ελευθέριο Τζάμο και Επαμεινώνδα Παπλωματά που με μύησαν στον κόσμο της Φυτοπαθολογίας και που μαζί με τα υπόλοιπα μέλη του Εργαστηρίου Δρ. Δημήτριο Τσιτσιγιάννη, Δρ. Σωτήρη Τζάμο, Δρ. Αλίκη Τζίμα, Δρ. Πολύμνια Αντωνίου και Δρ. Ελισσάβετ Χατζηβασιλείου με βοήθησαν στα πρώτα μου βήματα στον κόσμο της επιστήμης. Σας ευχαριστώ!

Νιώθω την ανάγκη να ευχαριστήσω όλους τους καλούς μου φίλους στην Ελλάδα που παρά το γεγονός ότι λείπω κάποια χρόνια απο εκεί, δεν έπαψαν να επικοινωνούν μαζί μου, να με επισκέπτονται στην Ολλανδία, να ζητουν τη συμμετοχή μου στις «σημαντικές» στιγμές τους και να με κάνουν να νιώθω ότι δεν έλειψα ποτέ. Σας ευχαριστώ για όλα!

Θέλω να ευχαριστήσω από τα βάθη της καρδιάς μου τους δύο συμπαραστάτες μου κατά τη διάρκεια της εξέτασής μου. Τον βιολογικό μου αδερφό Δημήτρη και τον τον φίλο-αδερφό Ιάκωβο. Δημήτρη, έχουμε περάσει σχεδόν τα πάντα μαζί και πάντα στηρίζαμε ο ένας τον άλλο. Θα είμαι πάντα δίπλα σου σε ότι χρειαστείς εσύ και η οικογένειά σου. Ιάκωβε, υπήρξες για εμένα σημαντική επιρροή στα πρώτα μου βήματα στο εργαστήριο και ταυτόχρονα καλός φίλος. Πλέον είμαστε και κουμπάροι και με τη Μαρία είστε μέλη της οικογένειάς μας. Δημήτρη και Ιάκωβε αποτελεί τιμή για εμένα που θα είστε στο πλευρό μου στις 19 Γενάρη. Σας ευχαριστώ!

Κώστα, Μαντώ και Δέσποινα σας ευχαριστώ για την αγάπη που νιώθω σαν μέλος της οικογένειά σας. Σας ευχαριστώ για όσα κάνετε για εμάς.

Αγαπημένοι μου γονείς, Ανδρέα και Αλίκη. Δεν έχω λόγια για να εκφράσω την εκτίμησή μου στο πρόσωπό σας. Είστε πάντα δίπλα μου από τη στιγμή που γεννήθηκα μέχρι σήμερα και με στηρίζετε στις όποιες αποφάσεις μου, ακόμα και αν αυτές με παίρνουν μακριά σας. Μακάρι να είμαι το ίδιο καλός γονέας με εσάς. Σας ευχαριστώ για όλα!

Χρύσα μου, περάσαμε αυτή τη δοκιμασία μαζί. Ήσουν και είσαι πάντα δίπλα μου στις καλές και στις δύσκολες στιγμές. Είσαι ο άνθρωπός μου. Με εσένα δίπλα μου, βλέπω το μέλλον με αισιοδοξία. Σε ευχαριστώ για όλα!

About the author

Ioannis Stringlis was born the 15th of May 1985 in Pyrgos Ilias, Greece. He received his primary and secondary education in Zacharo Ilias and higher education in Athens. In September 2003, he started his bachelor studies in Agricultural Biotechnology Department of the Agricultural University of Athens, with specialization in Plant Pathology. His bachelor diploma thesis project was performed in the Laboratory of Plant Pathology under the supervision of Professor Epaminondas Paplomatas where he studied the mode of action of a non-pathogenic *Fusarium* against soilborne fungal pathogens. He obtained his Bachelor Degree in 2008 with distinction. In October 2010, he joined the Master Program "Crop Protection and Environment" at the Agricultural University of Athens. During his studies, he received a "Bodossaki Foundation" scholarship. His Master's internship was performed in the Laboratory of Plant Pathology under the supervision of dr. Dimitrios Tsitsigiannis on a project entitled "The role of *VdSteA* G Protein-coupled pheromone receptor in virulence and biology of the vascular wilt pathogen *Verticillium dahliae*". He obtained his Master Diploma in April 2012 with the highest distinction. In May 2012, he joined the Plant-Microbe Interactions group at Utrecht University as a PhD student. He studied the early molecular and chemical dialogue between roots and root-associated microbes under the supervision of Prof. Corné Pieterse. The results of his PhD studies are presented in this thesis. After his graduation, he will continue working in the same group as a postdoctoral researcher.

List of publications

Pantelides, I.S., Tjamos, S.E., **Striglis, I.A**., Chatzipavlidis, I., and Paplomatas, E.J. (2009) Mode of action of a non-pathogenic *Fusarium oxysporum* strain against *Verticillium dahliae* using Real Time QPCR analysis and biomarker transformation. ***Biol. Control***. 50, 30-36.

Schoina, C., **Stringlis, I.A**., Pantelides, I.S., Tjamos, S.E., and Paplomatas, E.J. (2011) Evaluation of application methods and biocontrol efficacy of *Paenibacillus alvei* strain K-165, against the cotton black root rot pathogen *Thielaviopsis basicola*. ***Biol. Control***. 58, 68-73.

Gizi, D., **Stringlis, I.A**., Tjamos, S.E., and Paplomatas, E.J. (2011) Seedling vaccination by stem injecting a conidial suspension of F2, a non-pathogenic *Fusarium oxysporum* strain, suppresses Verticillium wilt of eggplant. ***Biol. Control***. 58, 387-392.

Berendsen, R.L., Van Verk, M.C., **Stringlis, I.A.**, Zamioudis, C., Tommassen, J., Pieterse, C.M.J., and Bakker, P.A.H.M. (2015) Unearthing the genomes of plant-beneficial *Pseudomonas* model strains WCS358, WCS374 and WCS417. ***BMC Genomics***. 16, 539.

Verbon, E.H., Trapet, P.L., **Stringlis, I.A.**, Kruijs, S., Bakker, P.A.H.M., and Pieterse, C.M.J. (2017) Iron and Immunity. ***Annu. Rev. Phytopathol.***, 55, 355-375.

Stringlis, I.A., Proietti, S., Hickman, R., Van Verk, M.C., Zamioudis, C., and Pieterse, C.M.J. (2017) Root transcriptional dynamics induced by beneficial rhizobacteria and microbial immune elicitors reveal signatures of adaptation to mutualists. ***Plant J***. doi: 10.1111/tpj.13741.

Antoniou, A., Tsolakidou, M.D., **Stringlis, I.A.**, and Pantelides, I.S. (2017) Rhizosphere microbiome recruited from a suppressive compost improves plant fitness and increases protection against vascular wilt pathogens of tomato. ***Front Plant Sci***. doi: 10.3389/fpls.2017.02022

Stringlis, I. A., Yu, K., Feussner, K., de Jonge, R., Van Bentum, S., Van Verk, M.C., Berendsen R.L., Bakker, P.A.H.M., Feussner, I., and Pieterse, C.M.J. (2017) The role of MYB72-dependent root exudation of coumarins in microbiome assembly. *Submitted*.

Fernández, I., Cosme, M., **Stringlis, I.A.**, Yu, K., de Jonge, R., Van Wees, S.C.M., Pozo, M.J., Pieterse, C.M.J., and Van der Heijden, M.G.A. The molecular dialogue between arbuscular mycorrhizal fungi and the non-host plant *Arabidopsis thaliana* switches from initial recognition to antagonism. *Submitted.*